EARTHQUAKE ENGINEERING TO EXTREME EVENTS

ISSN 1520-295X

Diagonal Tension Field Inclination Angle in Steel Plate Shear Walls

by

Yushan Fu, Fangbo Wang and Michel Bruneau

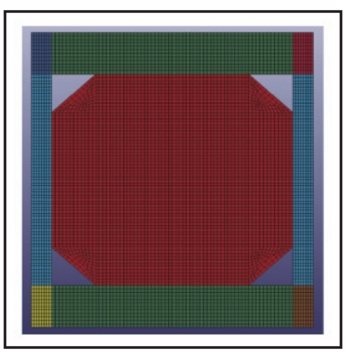
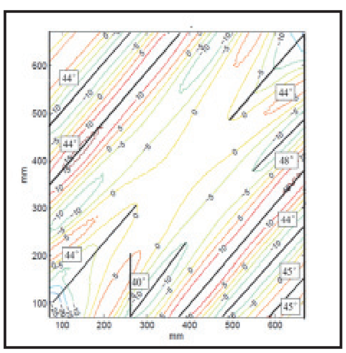
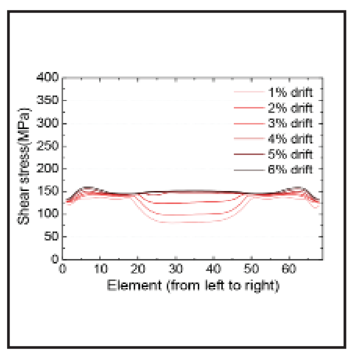

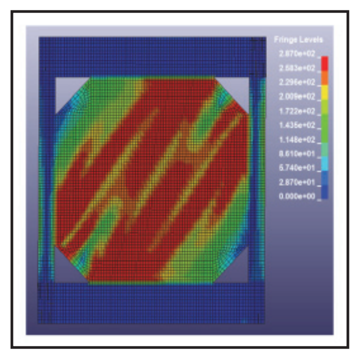

Technical Report MCEER-17-0001

February 10, 2017

This research was conducted at the University at Buffalo, State University of New York, and was supported primarily by MCEER.

NOTICE

Diagonal Tension Field Inclination Angle in Steel Plate Shear Walls

by

Yushan Fu,[1] Fangbo Wang[1] and Michel Bruneau[2]

Publication Date: February 10, 2017
Submittal Date: June 17, 2016

Technical Report MCEER-17-0001

1 Ph.D. Candidate, Department of Civil, Structural and Environmental Engineering, University at Buffalo, State University of New York
2 Professor, Department of Civil, Structural and Environmental Engineering, University at Buffalo, State University of New York

MCEER
University at Buffalo, State University of New York
212 Ketter Hall, Buffalo, NY 14260
E-mail: *mceer@buffalo.edu*; Website: *http://mceer.buffalo.edu*

Preface

MCEER is a national center of excellence dedicated to the discovery and development of new knowledge, tools and technologies that equip communities to become more disaster resilient in the face of earthquakes and other extreme events. MCEER accomplishes this through a system of multidisciplinary, multi-hazard research, in tandem with complimentary education and outreach initiatives.

Headquartered at the University at Buffalo, The State University of New York, MCEER was originally established by the National Science Foundation in 1986, as the first National Center for Earthquake Engineering Research (NCEER). In 1998, it became known as the Multidisciplinary Center for Earthquake Engineering Research (MCEER), from which the current name, MCEER, evolved.

Comprising a consortium of researchers and industry partners from numerous disciplines and institutions throughout the United States, MCEER's mission has expanded from its original focus on earthquake engineering to one which addresses the technical and socio-economic impacts of a variety of hazards, both natural and man-made, on critical infrastructure, facilities, and society.

The Center derives support from several Federal agencies, including the National Science Foundation, Federal Highway Administration, Department of Energy, Nuclear Regulatory Commission, and the State of New York, foreign governments and private industry.

Research was conducted to investigate how the inclination angle of the diagonal tension field action varies in Steel Plate Shear Walls (SPSWs) and to determine the optimum constant angle best matches the demands obtained from finite element (FE) analysis. A FE model was first calibrated against experimental results that showed significant differences in inclination angles at different locations across the web plate. Then, four real SPSWs with varying aspect ratios and number of stories were designed and modeled for FE analyses. The variations in angle in the web plate and along the boundary elements were documented as a function of drift, and showed significant variations. Combined moment-axial force demand ratios in the SPSW boundary elements were calculated and compared for all real SPSWs. Overall, it was found that the demand on the web plate is not sensitive to the variation of inclination angle and using 45° is a reasonable compromise for both HBE and VBE (horizontal and vertical boundary element) design. Consequently, the single angle of 45° is recommended for the design of the entire SPSW.

ABSTRACT

This study focused on investigating how the inclination angle of the diagonal tension field action varied in Steel Plate Shear Walls (SPSWs) and, based on these results, on determining the optimum constant angle to use for the design of SPSWs to best match the demands obtained from finite element analysis. A LS-DYNA model was first developed to replicate the experimental and ABAQUS analysis results obtained by Webster et al. (2014) for a simple tested specimens having pin horizontal boundary elements-to-vertical boundary elements (HBE-to-VBE) connections and cutouts at the web plate corners. It is shown that results from the LS-DYNA model match well with Webster's results with respect to load-drift curve, average inclination angle over the whole web, and stress contour. Then, this validated LS-DYNA finite element model was used to further investigate the changes in inclination angle and their impact on SPSW behavior for SPSWs having a number of different configurations more representative of real SPSWs. SPSWs considered first included modified versions of the Webster specimen, without cutouts at the corner of the webs, then with rigid HBE-to-VBE connections (still without the web cutouts). It is observed that different average inclination angles are obtained at different locations and that the differences are not negligible.

Four real SPSWs with varying aspect ratio and number of stories were subsequently designed and modeled by LS-DYNA (also modeling the HBEs and VBEs). The plastic behavior of HBE was captured by considering the development of plastic hinges at the end of the HBE. Variations in inclination angles are reported for all these cases. Additionally, the demands from actual results obtained from finite element analysis, and demands calculated using various assumed constant inclination angles, were compared for all cases of SPSWs aspect ratio and number of stories considered. For HBEs and VBEs, they were expressed by calculating combined moment-axial force demand ratios. It is found that the aspect ratio has little effect on the conservatism of results obtained using a constant angle for the one-story SPSW, but has a greater influence on those for the three-story SPSWs when using the constant angle of 45° as the basis for comparison. The number of stories also has an impact on the conservatism or results for both HBE and VBE designs using the constant angle of 45°. Overall, using constant angles of 35° and 40° for HBE design and 50° for VBE design were found to be always conservative. It is noted that the demand on the web plate is not sensitive to the variation of inclination angle. Consequently, the single angle of 45° is recommended for the design of the entire SPSW.

TABLE OF CONTENTS

TABLE OF CONTENTS (cont'd)

TABLE OF CONTENTS (cont'd)

LIST OF ILLUSTRATIONS

LIST OF ILLUSTRATIONS (cont'd)

LIST OF ILLUSTRATIONS (cont'd)

LIST OF TABLES

SECTION 1
INTRODUCTION

1.1 General Background

A typical steel plate shear wall (SPSW) consists of horizontal boundary elements (HBEs), vertical boundary elements (VBEs) and web plates. The ultimate strength of SPSWs is reached when the web yield in diagonal tension-field action at an angle α from the vertical and HBEs develop plastic hinging at their ends. Capacity design of a SPSW requires the web plate to have sufficient strength to resist the specified story shear, and the HBE and VBE to be able to resist the diagonal forces applied by the web plate on those boundary elements. Therefore, the inclination angle, denoted as α, is a key parameter in SPSW design. The AISC Seismic Provisions for Structural Steel Buildings (AISC 341-10) provides an equation to calculate the inclination angle (based on research by Timler and Kulak, 1983). Although this approach is generally accepted in design practice, this angle α was derived from an elastic strain energy principle, while seismic design usually expects structures to develop plastic behavior. Alternatively, for simplicity, AISC 341-10 also allows the use of a constant angle of 40° based on work by Dastfan and Driver (2008).

Researchers have observed from experimental or numerical results that the inclination angle typically vary between 38° and 45° for well-designed SPSWs. The quasi-static experiment conducted by Timler and Kulak (1983) showed that the angle of inclination along the vertical center-line of the web plate varied from 44° to 56°. Elgaaly and Caccese (1993) performed finite element analysis using shell elements and reported that the principal tension stress direction in the central area of the plate panel varied between 40° and 50°. In Driver (1997)'s test, the principal stress directions derived from the strain rosette data near the top right corner of a web plate varied from 38° to 64°, as compared with the finite element results varying from 35° to 65°. Lubell (1997) plotted the principal tension strains along the boundary elements and the center of the panel plate at angles of inclination from the vertical, most of which were in the range of 35° to 40°. In Rezai (1999)'s shake table test of a steel plate shear wall with thin unstiffened webs, strain rosettes results showed that the angle of principal strain varied from 35° to 40° near the base, and from 37° to 42° at the center of the panel. Kharrazi (2005) measured the angle of tension field at the crest of the buckle wave from a test, which ranged from 37° to 39°, and compared those to the in-plane principal stress vectors obtained from FE analyses, which were in a similar range of 34° to 40°. Choi et al. (2009) used ABAQUS to perform a parametric study of the inclination angle under different aspect ratio, infill plate thickness and endplate thickness, which showed that the average inclination angle of the tension field in the yielded web varied from 24° to 45°. More recently, Webster et al. (2014) conducted experimental investigations and finite element analyses studying how the inclination angle changes as a function of drift. In particular, two specimens with pin connection and slender VBE were tested, and the experimental results agreed well with results from FE analysis (conducted with ABAQUS). It was also found that the inclination angles, both calculated by averaging values over the whole web and by measuring the orientation of the buckled "corrugations", were different from the value predicted by AISC 341-10. Since the average inclination angle of single panels fixed within an elastic boundary frame at the typical design seismic drifts was found to vary between 43° and 45°, and because a constant angle of 45° was believed to be simpler to implement, Webster et al. recommended using a constant angle of 45° for both capacity design procedure and cyclic analysis of SPSW system. However, the specimens considered by Webster had essentially rigid HBEs, slender VBEs, and pure pin-connections between the boundary frame members, for the sake of experimental purposes, which made them different from real SPSWs. While consideration of a single angle of 45° is appealing for design purposes, it is unknown whether the findings reported by Webster et al. would remain true for real SPSWs with realistic boundary elements, different aspect ratios, and different number of stories. Such information is required to overcome possible (and arguably founded) reservations from code committee members against changing the design requirements for SPSWs. Furthermore, because the forces induced to the HBEs and VBEs by the yielding web are directly related to the inclination angle developed near the boundary elements, additional detailed information of the angle along such boundary element, and information on how these demands compare to those obtained using a constant inclination angle, is also required.

1.2 Scope and objective

The purpose of the study conducted here was to investigate how the inclination angle of the diagonal tension field action varies in Steel Plate Shear Walls (SPSWs) and, based on these results, to determine what optimum constant angle to use for the design of SPSWs best matches the demands obtained from finite element analysis. Ultimately, this is intended to determine whether the constant inclination angle of 40° provided in the AISC Seismic Specifications should continue to be used, or whether it should be replaced by a different value. Also investigated was how the inclination angle of the tension field action changes when different aspect ratios and number of stories are used, considering nonlinear inelastic response and SPSWs designed in compliance with AISC 341 (as opposed to idealized configurations).

The investigation was conducted using the LS-DYNA finite element software to model SPSWs. The LS-DYNA model was first validated by replicating the experimental and ABAQUS analysis results obtained by Webster et al. (2014) for a simple tested specimens having pin HBE-to-VBE connections and cutouts at the web plate corners. Then, this validated LS-DYNA finite element model was used to further investigate the changes in inclination angle and their impact on SPSW behavior for modified versions of the Webster's specimen, without cutouts at the corner of the webs, then with rigid HBE-to-VBE connections (still without the web cutouts).

Two real single SPSWs and two real thee-story SPSWs were subsequently designed, with panel aspect ratios of 1 and 2. Corresponding LS-DYNA models were built also modeling the HBEs and VBEs. The plastic behavior of HBE was captured by considering the development of plastic hinges at the end of the HBEs. This was done to observe how the inclination angle varied as a function of number of stories and panel aspect ratios for SPSWs designed per AISC 341. To determine the appropriate or optimum constant angle to use for SPSW design, demands from real results obtained from finite element analysis, and demands calculated using various assumed constant inclination angles, were compared for all cases of SPSWs aspect ratio and number of stories considered. For HBEs and VBEs, they were expressed by calculating combined moment-axial force demand ratios.

1.3 Overview of this report

The work conducted to accomplish the scope of research described above is presented in this report as follows. Webster's experiment and ABAQUS model results are presented in Section 2. Section 3 describes the LS-DYNA model that was developed here, using the same geometry and model parameters, to analyze Webster's specimen and compare with Webster's ABAQUS results. Expanding on those results, a modified SPSW model, having pin HBE-to-VBE connections (like Webster's specimen) but without cutouts at the corner of the webs (unlike Webster's specimen) was then analyzed, as well as a SPSW model with rigid HBE-to-VBE connections and without the web cutouts. Results and observations from stress analyses, inclination angle variations, and combined moment-axial force demand analyses for the two above modified models are presented in Section 4. Section 5 describes the design procedure of four real SPSWs having different aspect ratios and number of stories, used for further inclination angle investigations. SAP2000 strip models were built to support the design of the VBE. Detailed LS-DYNA modeling of the new real SPSW were also presented. Results obtained from the finite element analyses of the real SPSWs are presented in Section 6 and discussed with respect to aspect ratio and number of stories. Conclusions from this study are provided in Section 7.

Note that in this report, the terms "HBE" and "beam", as well as "VBE" and "column", are used interchangeably, as both terms are commonly used in the literature.

SECTION 2

RESEARCH DONE BY WEBSTER ET AL. (2014)

2.1 Experimental Program

The test specimen used in Section 3 for calibration of the LS-DYNA models is Specimen #2-22 in Webster (2013), which is a single story SPSWs of aspect ratio 1.0 with a linear cutout at each corner of the web. In that specimen, a physical pin was used to connect the HBEs and VBEs together. Detailed dimensions of Specimen #2-22 are shown in Figure 2-1. ASTM A1008 steel sheet (22 Ga) was chosen for the web plate and corresponding coupon test results are presented in Figure 2-2. A displacement control protocol was used in those tests, with target displacement amplitudes of $\pm 0.25\delta y$ for an initial elastic cycle and of $\pm 6.0\delta y$ for three subsequent cycles as shown in Figure 2-3.

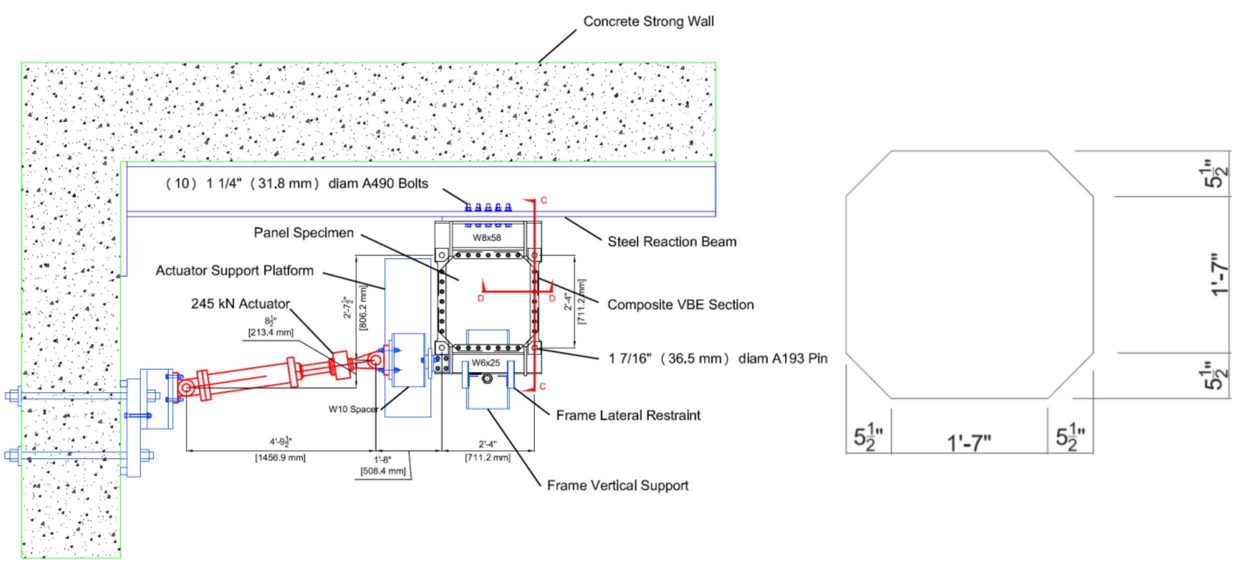

a. Experiment setup **b. Web plate dimension**

Figure 2-1 Dimensions of Specimen #2-22 from Webster (2013) (unit: inch)

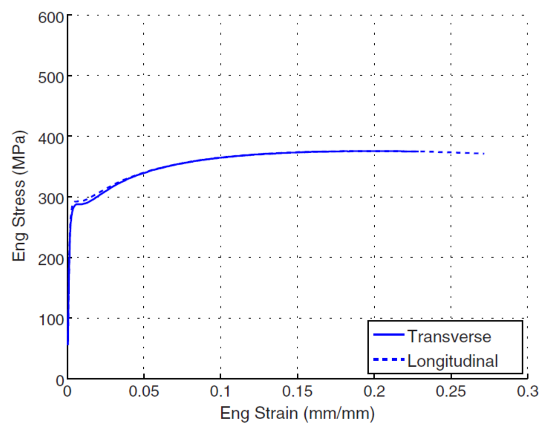

Figure 2-2 Typical 22 Ga A1008 coupon test engineering stress-strain curve

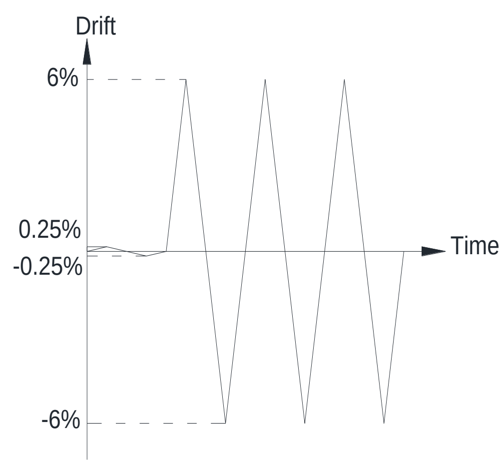

Figure 2-3 Loading Protocol of Specimen #2-22 from Webster (2013)

2.2 ABAQUS Finite-Element Model

An ABAQUS model using explicit analysis was built by Webster to verify the experiment results obtained in that study. An example of the model is shown in Figure 2-4. In all those ABAQUS models, the web plate was meshed into 34×34 elements; material model chosen was the large displacement-finite strain SR4 shell element with enhanced hourglass control. Nine integration points along web thickness were chosen for stress and strain analysis. Initial imperfections were also considered in the web plate simulation. The VBE and top HBE were modeled with B31 shear deformation line elements while the bottom HBE was not explicitly modeled but rather defined as a fixed boundary condition. Elastic material properties were assigned to all the boundary elements. The displacement amplitude history recorded from the experiment was applied at the top HBE of the model to replicate it testing under displacement-control. Note that the steel material properties of the web plate shown in Figure 2-2 were converted into true stress and true strain for ABAQUS analyses.

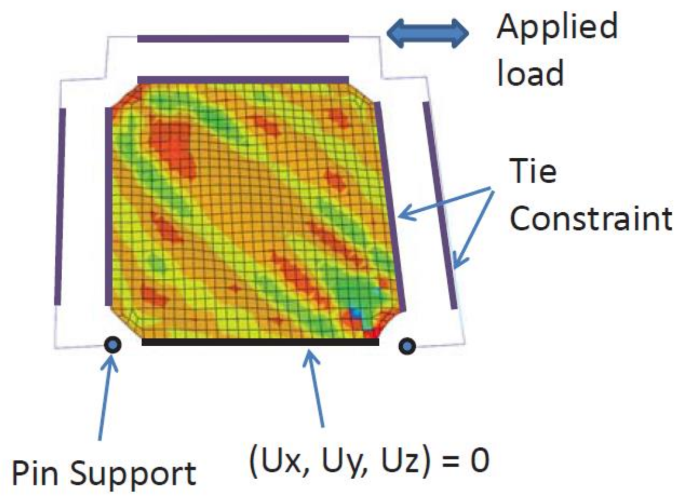

Figure 2-4 The ABAQUS model of Specimen #2-22 from Webster (2013) (unit: mm)

2.3 Comparison between Test and FE Analysis Results

Webster et al. (2014) reported that the hysteric behavior obtained from the ABAQUS numerical analyses agreed well with the experiments result, as shown in Figure 2-5. It was also reported that the average inclination angle varied as a function of drift according to the relationship shown in Figure 2-6. The inclination angle was calculated by taking the average of stresses of all the shell elements first and then by equation 7.7 from Webster (2013). Figure 2-6 shows that the inclination angle migrated from values of less than 40° in the elastic range, up to 44° when drift increased from 0 to 6% drift. Note that at drifts of 2 to 3%, which are typically expected in SPSWs during severe earthquakes, this angle ranged from 42° to 44°. On the basis of those observations, Webster et al. (2014) indicated that a uniform angle of 45° could be adopted in SPSW analyses to obtain more representative results of SPSW inelastic response, and to simplify the analysis of SPSW using strip model (see Bruneau et al, 2011, for a description of the strip model).

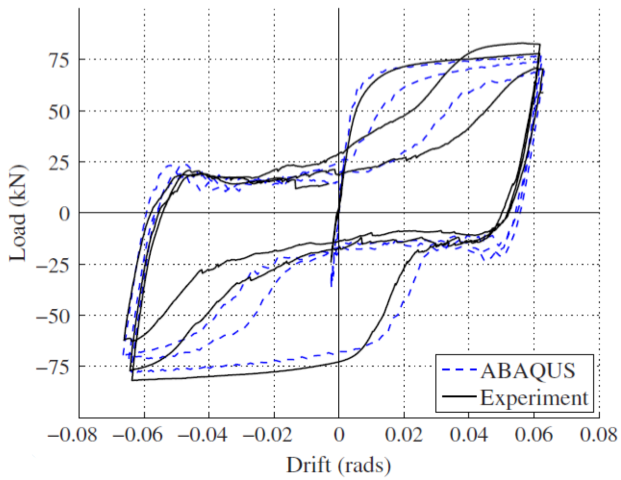

Figure 2-5 Experimental and ABAQUS hysteresis curves from Webster et al. (2014)

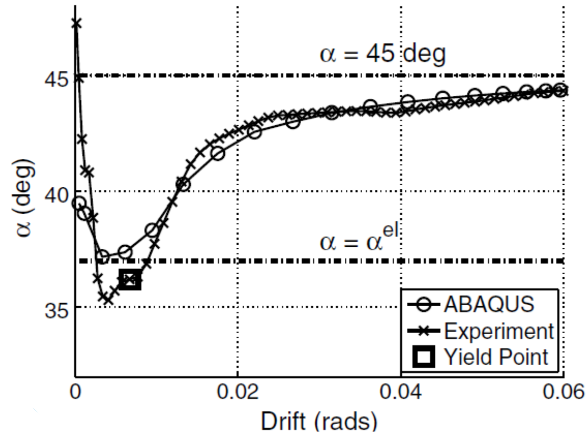

Figure 2-6 Inclination angle versus drift relationship from Webster et al. (2014)

SECTION 3
SPSW MODEL VALIDATION

3.1 General

This section describes the LS-DYNA model developed to replicate the results for one of the single story SPSWs of aspect ratio 1.0 (specimen # 2-22) tested by Webster et al. (2014). The LS-DYNA model is defined here to have the same dimensions, material models, loading and boundary conditions as Webster et al. (2014), with some minor differences described in Section 3.2. Key features of the LS-DYNA model are presented at first in Section 3.2.1 to 3.2.3, and convergence analysis is conducted to verify the model in Section 3.2.4. To validate the LS-DYNA model, resulting load-drift curves of the structure are compared with Webster's experimental and FEM results. Analysis of inclination angle and stress distribution of elements at different locations across the web plate are presented in Section 3.3.

3.2 LS-DYNA Model

3.2.1 Dimensions and Boundary Conditions

In the LS-DYNA model developed to replicate Webster's specimen, dimension of the steel web plate is 762 mm×762 mm×0.71 mm (length×height×thickness). Width of the cutout in each corner of the web plate is 140 mm. Vertical boundary element (VBE) is a 25.4 mm×63.5 mm rectangular section. Horizontal boundary element (HBE) is a 71 mm×150 mm rectangular section, made equivalent to the W6×25 section used by Webster by having the same depth and moment of inertia. Connection between the VBE and HBE in Webster's specimen was achieved by using actual pin, and a point connection was implemented in the LS-DYNA model to achieve the same behavior. Bottom beam is continuously fixed along the wall's base. An initial perturbation was introduced to account for initial imperfections using PERTURBATION CARD. The nodes in the web plate were perturbed using a harmonic field with an amplitude of $t/2=0.035$ mm in the Z direction and a wavelength of 1524 mm in both X and Y directions.

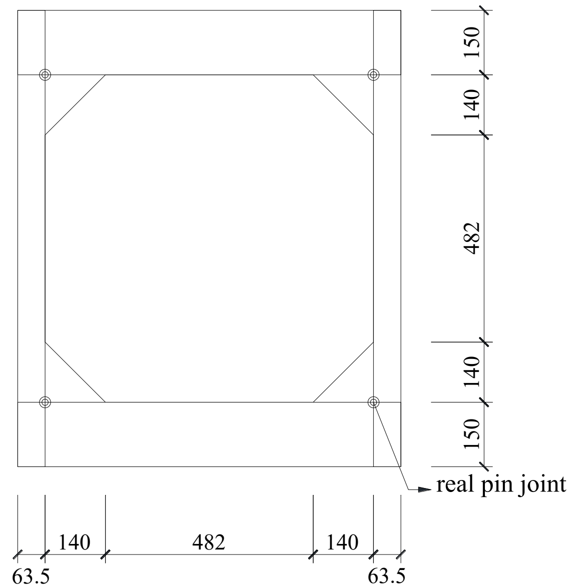

Figure 3-1 Dimensions of SPSW Model (unit: mm)

3.2.2 Material and Element

Here, the constitutive model chosen for the steel web plate was an elastic-plastic model without strain rate effect. (i.e., material MAT024_PIECEWISE_LINEAR_PLASTICITY in LS-DYNA). The material was specified here as having a Young's modulus of 151,000 MPa, a yielding strength of 287 MPa, a Poisson ratio of 0.30, and a density of 7850 Kg/m^3.

Webster et al. (2014) presented coupon test result of the web plate steel in terms of engineering strain versus engineering stress. LS-DYNA requires that non-linear materials be defined in terms of true strain and true stress, which can be obtained by the following conversion formulas, which were used to convert Webster's values into material properties used by LS-DYNA:

$$\varepsilon_{true} = \ln(1 + \varepsilon_{eng}) \tag{3.1}$$

$$\sigma_{true} = \sigma_{eng}(1 + \varepsilon_{eng}) \tag{3.2}$$

Key points defining the steel's material stress-strain curve are presented in Table 3-1.

Table 3-1 Stress-strain relationship of web plate steel reported from Webster et al. (2014)

	Point 1	Point 2	Point 3	Point 4	Point 5	Point 6	Point 7
Eng. Strain	0	0.0014	0.02	0.05	0.165	0.23	0.28
Eng. Stress (MPa)	0	287	300	340	375	381	382
True Strain	0	0.0014	0.0198	0.0488	0.1527	0.2070	0.2469
True Stress (MPa)	0	287.4	306	357	436.9	468.6	489
Effective Plastic Strain	-	0	0.0184	0.0474	0.1513	0.2056	0.2455

Note: effective plastic strain is equal to true strain minus elastic strain.

Beams and columns were modeled as an elastic material (i.e., using LS-DYNA's material MAT001_ ELASTIC), with a Young's modulus of 205,000 MPa and a Poisson ratio of 0.30. To model the actual pin joint of the beam-column connection, beam and column elements in overlapping area are modeled as rigid material (i.e., using LS-DYNA's material MAT020_ RIGID and a Young's modulus 205,000 MPa), and didn't share nodes in the same location. The option JOINT_SPHERICAL in LS-DYNA was employed to the two center nodes (from the beam and column, respectively) in the overlapping area. A SPHERICAL JOINT in LS-DYNA has six degree of freedoms. Only in-plane degrees of freedom (i.e., in the x-y plane) of the joint were needed in the model, therefore, degree of freedom for the z-translation was constrained on peripheral nodes of overlapping area as shown in Figure 3-2.

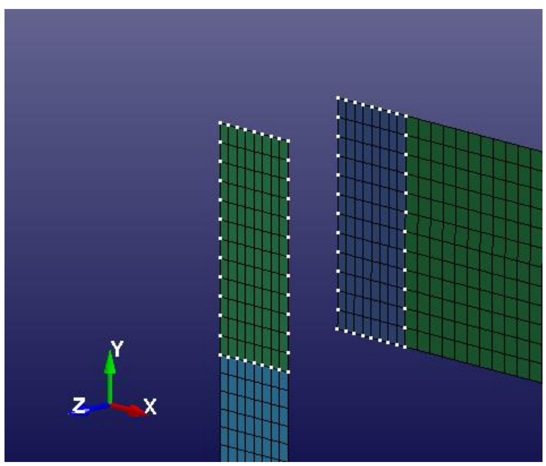

Figure 3-2 Highlighted nodes constrained at z-translation in a beam-column joint

Belytschko-Tsay shell elements were used for the web plate, VBEs and HBEs because of their computational efficiency. The Belytschko-Tsay element is a 4-noded element with reduced integration, having hourglass effect controlled by adding hourglass viscosity stresses to the physical stresses at the local element level (LS-DYNA Theory Manual). The number of through thickness integration points was set to 9, same as Webster (2013).

3.2.3 Loading Protocol

A quasi-static displacement loading history was applied to each node along the middle height of the top beam. Both monotonic loading and cyclic loading scenarios are used. The cyclic loading scenario applied was the same as Webster (2013). The monotonic loading scenario was used to determine the inclination angle and stress amplitude for the distribution analyses reported in Section 3.3. The corresponding load protocols are shown below.

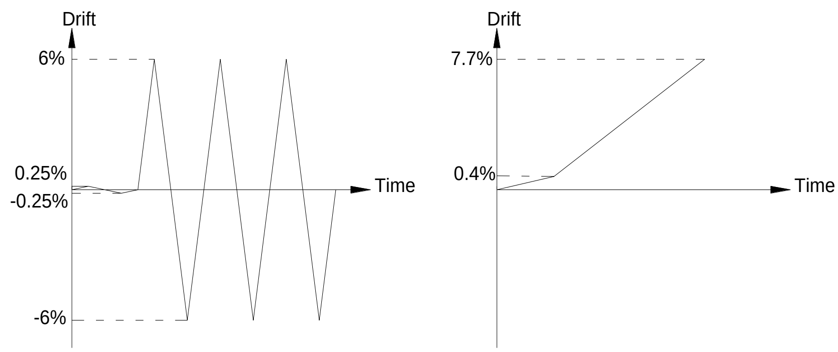

a. Cyclic loading **b. Monotonic loading**

Figure 3-3 Loading Protocol

3.2.4 Convergence Study

To investigate convergence of results for the model described in Section 3.1, as well as to validate the LS-DYNA model, load-versus-drift curves under cyclic loading were compared with Webster's experimental and FEM results. Then, load-versus-drift curves under monotonic loading were also compared with two different mesh refinement levels in LS-DYNA model, to better assess convergence of the results under monotonic displacements. Since stress results are more sensitive than displacements, stress contours of at two different drifts (1% and 6%) under monotonic loading are also compared in Figure 3-7 and Figure 3-8.

Note that a difference between LS-DYNA model and ABAQUS model in Webster et al. (2014) is that the LS-DYNA model here used shell elements to model the HBEs and VBEs, while the ABAQUS model by Webster used line element. Coarse mesh model in LS-DYNA has the same mesh refinement level as the ABAQUS model in Webster et al. (2014).

The coarse mesh configuration considered provided a 34×34 elements web plate (mesh size 22 mm×22 mm), whereas the refined mesh configuration was 68×68 elements (mesh size 11mm×11mm), as shown in Figure 3-4. Both cyclic and monotonic displacement histories described in section 3.2.3 were used to obtain load-versus-drift relationships for the two different mesh sizes considered. LS-DYNA's implicit analysis with single precision executable was adopted to analyze the model because of computational efficiency (e.g., 4 hours per analysis instead of 15 hours using double precision, while identical results were obtained), but results obtained using LS-DYNA's explicit analysis are also presented for comparison. In all implicit analyses (cyclic and monotonic), the analysis time step was 0.001 s, with termination of the analysis at a time of 8.0 s (i.e., after 8000 steps).

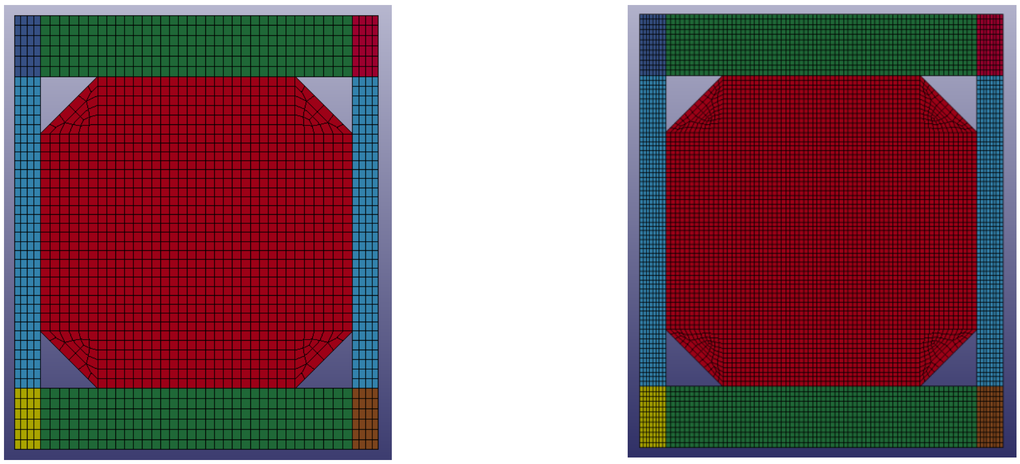

Figure 3-4 Coarse (left) and refined (right) mesh used in LS-DYNA models

Comparing the LS-DYNA model results with the ABAQUS model and experimental results by Webster, cyclic displacement histories show that the load-drift hysteretic curves obtained are similar to each other in Figure 3-5. Peak load difference under the first 6% drift loading cycle is around 5 kN and structural stiffness is slightly smaller than for the ABAQUS model and experimental results. Overall, the results shown in Figure 3-5 were deemed to be in good agreement, and the LS-DYNA model was judged appropriate to predict structural behavior of the system.

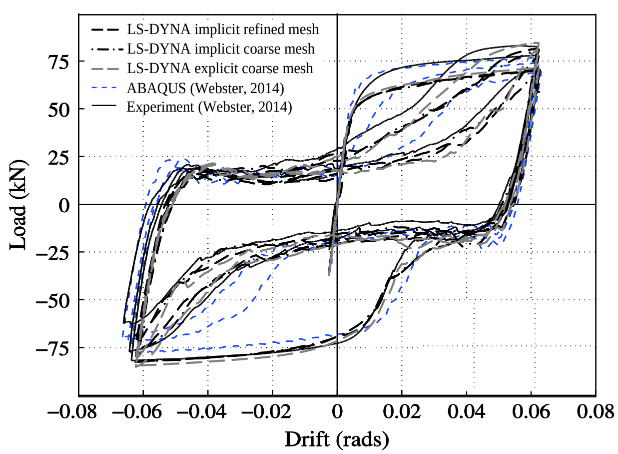

Figure 3-5 Load-drift curves comparison under cyclic loading

Comparing the LS-DYNA coarse mesh and LS-DYNA refined mesh results obtained using the implicit analysis with single precision executable, results were also found to be in good agreement. Peak load in the first 6% drift loading cycle is 72.27 kN with coarse mesh and 70.80 kN with refined mesh, respectively. The difference is only 1.47 kN and 2.08% of the peak load with refined mesh. Additionally, comparing results obtained from the implicit and explicit solvers, the load-drift curves are found to have negligible differences.

For monotonic loading, no data is available in Webster et al. (2014) and only LS-DYNA coarse and refined mesh model are compared. Figure 3-6 shows that the load-drift curves are in good agreement with each other, and the peak difference of the load between refined and coarse mesh is 1 to 2 kN, which is only 1.3% to 2.6% of the total load. The stress contours obtained from the coarse mesh and refined mesh are presented in Figure 3-7 (at 1% drift) and Figure 3-8 (at 6% drift). Under both drifts, stress contours for the coarse mesh model are similar to those for the refined mesh model.

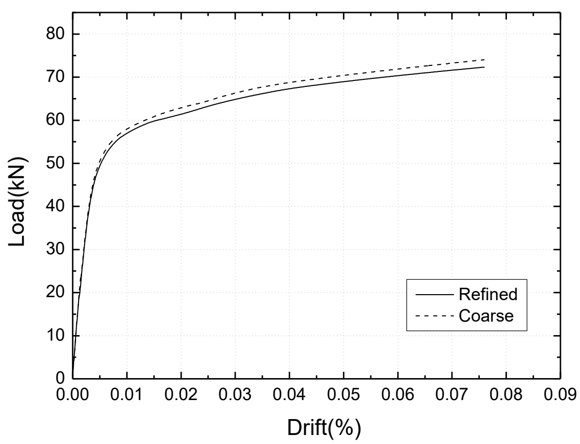

Figure 3-6 Load-drift curves comparison under monotonic loading

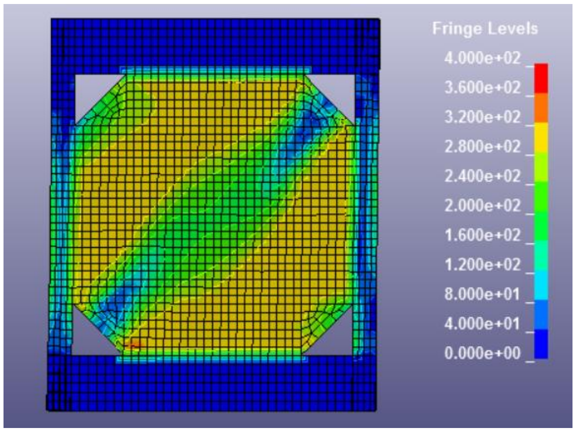

a. Coarse mesh

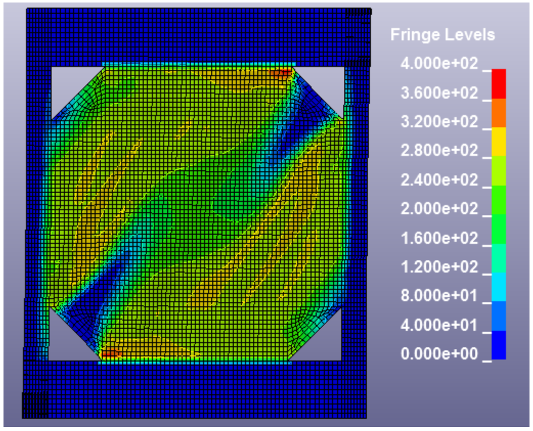

b. Refined mesh

Figure 3-7 Stress contours comparison at 1% drift

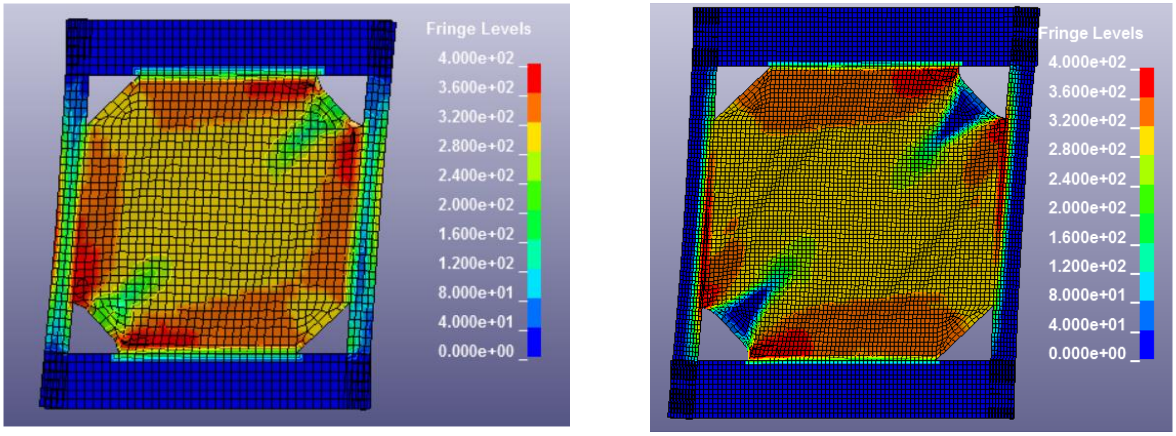

a. Coarse mesh **b. Refined mesh**

Figure 3-8 Stress contours comparison at 6% drift

On the basis of comparisons presented in this section, it was concluded that the LS-DYNA model could adequately capture the structural behavior of the SPSW system, and that the LS-DYNA model results had converged with the refined mesh. As a result, the refined LS-DYNA model with 68×68 mesh configuration (mesh size 11 mm×11 mm) was used in all subsequent monotonic loading inclination angle of the principal stresses and stress distribution in infill plates, described in Section 3.3.

3.3 Inclination angle and VBE, HBE demand analysis

3.3.1 General modeling issues

Stresses at all through thickness Gauss integration points can be outputted by LS-DYNA's post processing tool. However, according to the plane section assumption, stresses at all nine integration points other than at central point are composed of bending and axial components of stresses. Since only the axial stresses in the plate are of interest to analyze the web plate's contribution to story shear resistance and to determine axial demand on boundary elements (which are used for their design), stress results presented in all following sections are taken at the central integration point of the web plate (i.e., using the command History_Element_Stress_Middle layer). In addition, LS-DYNA can only output strains at the lowermost and uppermost integration points, and strains reported here from all for analyses is an average of the results from the lowermost and uppermost integration points (i.e., using the command History_Element_Mean Ipt Strain_Local axis).

Stresses at all through thickness Gauss integration points can be outputted by LS-DYNA's post processing tool. However, according to the plane section assumption, stresses at all nine integration points other than at central point are composed of bending and axial components of stresses. Since only the axial stresses in

the plate are of interest to analyze the web plate's contribution to story shear resistance and to determine axial demand on boundary elements (which are used for their design), stress results presented in all following sections are taken at the central integration point of the web plate (i.e., using the command History_Element_Stress_Middle layer). In addition, LS-DYNA can only output strains at the lowermost and uppermost integration points, and strains reported here from all for analyses is an average of the results from the lowermost and uppermost integration points (i.e., using the command History_Element_Mean Ipt Strain_Local axis).

Note that stress and strain results provided by LS-DYNA are true stress and true strain, respectively. To be able to compare results in the context of design equations (which are all based on engineering stresses and strains), conversion of the LS-DYNA results from true stress to engineering stress was required. The maximum principal true stress and maximum principal true strain are needed to calculate maximum principal engineering strain of an element. Conversion was performed using the following equation:

$$\sigma_{eng} = \sigma_{true}/\exp(\varepsilon_{true}) \tag{3.3}$$

Therefore, all results in this section are presented in terms of engineering stresses and strains.

In SPSWs, determination of the tension field inclination angle from vertical is an important step of the design process. Note that the inclination angle reported in the following sections is taken as the angle from vertical, except when indicated otherwise. The AISC Seismic Provisions for Structural Steel Buildings (AISC 341-10) specifies that the angle is permitted to be taken as 40° or calculated as follows:

$$\tan^4\alpha = \frac{1+\frac{t_w L}{2A_c}}{1+t_w h\left(\frac{1}{A_b}+\frac{h^3}{360 I_c L}\right)} \tag{3.4}$$

where, α =inclination angle from vertical axis; A_b =cross sectional area of the HBE; A_c= cross sectional area of the VBE; t_w=thickness of web plate; I_c= moment of inertia of the VBE; L=length of the plate; h= height of the plate.

To compare with Webster's results, presented earlier in Figure 2-6 (in Section 2 of this report), the average inclination angle across the entire plate was calculated, according to the method outlined by Webster (2013). Results are shown in Figure 3-9. Note that stresses acting in the middle layer (across thickness) of the shell elements used are those that correspond to axial stresses in the web plate. For the ABAQUS model result presented in Webster et al. (2014), it is believed that stresses in the middle layer were used, although this is not documented in the report (Jeffrey Berman, Professor, University of Washington, personal communication, May 2015). The maximum difference between these two curves is within 2°, which means that the average inclination angle across the entire plate obtained from the LS-DYNA model matches well with the Webster's experiment and modeling results.

In the following study, averages of principal stress angles have been performed at three different locations that have an impact on design. First, with respect to the web plate, the average for all web shell elements at mid-height of the wall are calculated, as this is deemed representative of the angle that should be taken to calculate the story shear force resisted by the infill plate (per AISC design equation). Furthermore, because this is significant for the design of VBEs and HBEs, the averages of the web shell elements connected along individual VBEs and HBEs are calculated. This approach is believed to provide a better understanding on the design consequence of varying inclination angles.

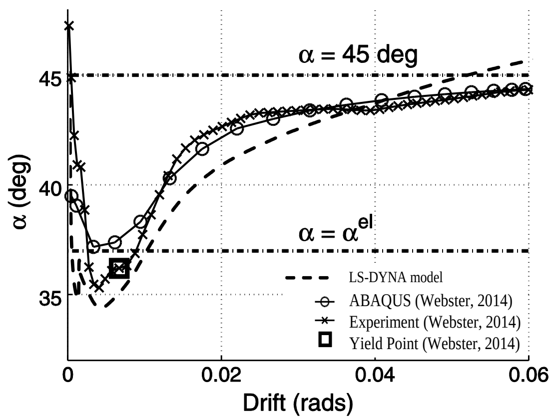

Figure 3-9 Comparison on average inclination angles over the entire web plate for LS-DYNA model, ABAQUS model, and Experiment data in Webster et al. (2014)

3.3.2 Contour analysis

The out-of-plane deformations of the web plate were presented in form of contours by Webster (2013) and inclination angles were also measured using this graphic representation of the buckled "corrugations." To further calibrate the LS-DYNA model, the deformations obtained at $\pm 0.5\%$ drift and $\pm 4\%$ drift, corresponding to cycles #5 and #21 in Webster et al. (2014), were studied. The regions over which the deformation contours are measure in Webster's experiment, and the equivalent region from the LS-DYNA model, are shown in Figure 3-10 and Figure 3-11, respectively.

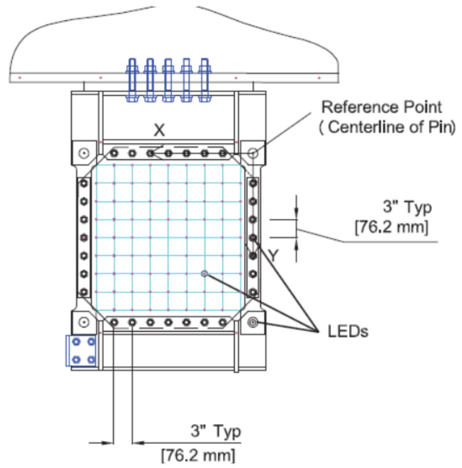

Figure 3-10 OptoTrak LED Locations in Webster (2013)

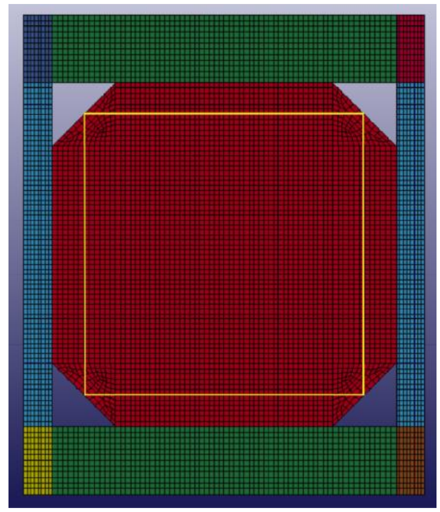

Figure 3-11 Output deformation region in LS-DYNA model

Note that the deformation contours for test #3-22 but not test #2-22 were presented in Webster et al. (2014). Test #3-22 and #2-22 were identical specimens but were subjected to different displacement protocols. For test #3-22, the loading amplitude was gradually increased from ±0.25% to ±1% drift with an increment of 0.25% drift, followed cycles at ±1.5%, ±2%, ±3%, and ±4% drift. Three cycles were applied at each displacement level. A similar displacement protocol was applied to the LS-DYNA model here for the analyses focused on obtaining deformation contours, except that cycles at each displacement amplitude were applied only once. The contours were generated using the contour function in MATLAB.

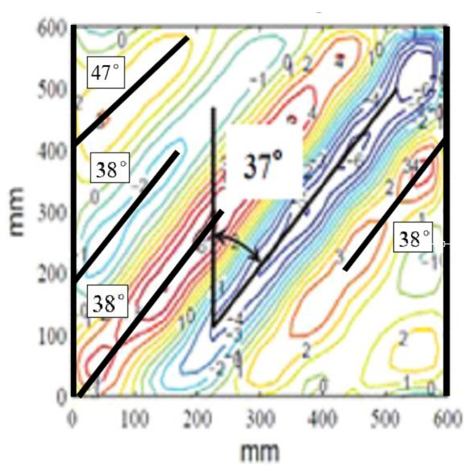

a. Pull stroke of Cycle #5

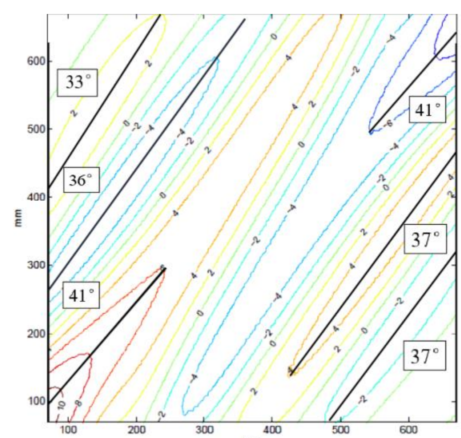

a. Pull stroke of Cycle #5

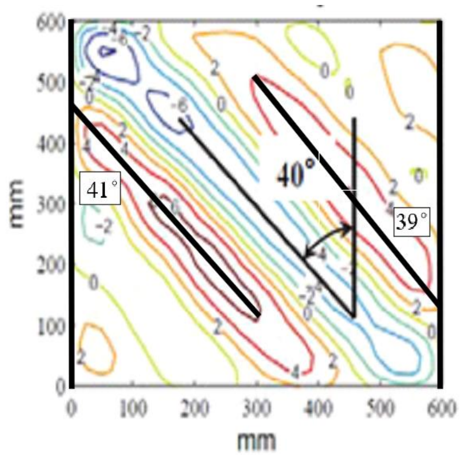

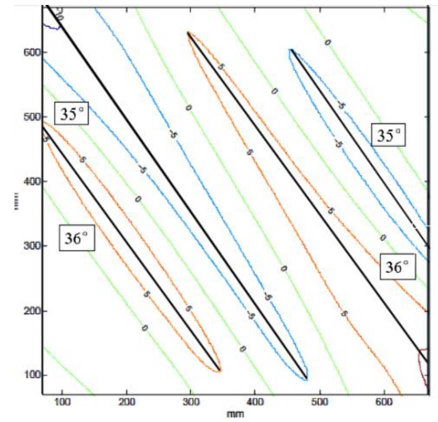

b. Push stroke of Cycle #5 | **b. Push stroke of Cycle #5**

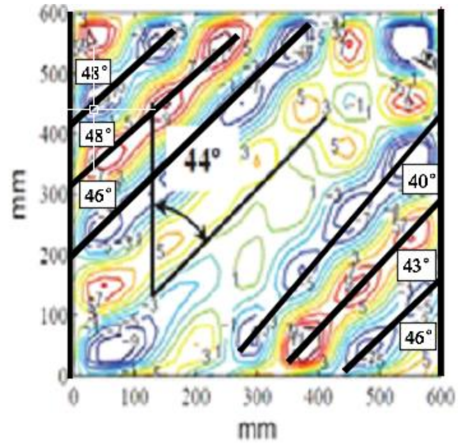

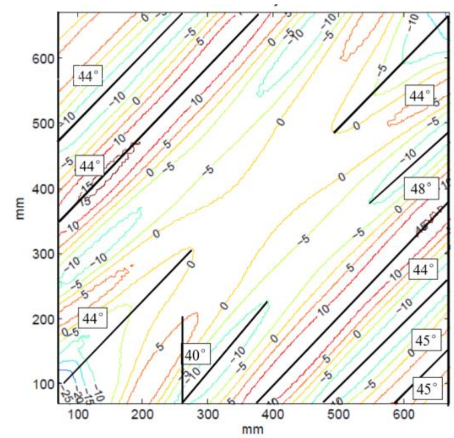

c. Pull stroke of Cycle #21 | **c. Pull stroke of Cycle #21**

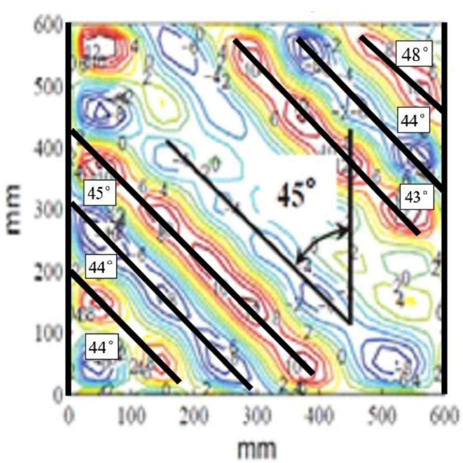

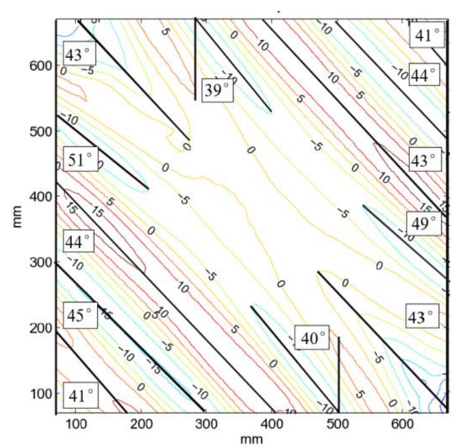

d. Push stroke of Cycle #21 | **d. Push stroke of Cycle #21**

Figure 3-12 Panel deformed shapes in Webster et al. (2014)

Figure 3-13 Panel deformed shapes in LS-DYNA model

Here, in addition to measuring the inclination angles of the buckled corrugations in middle web plate, the inclination angles from other locations of the web plate were also determined, as shown in Figure 3-12 and Figure 3-13. At ±0.5% drift (#5 cycle), the angles of the orientation of the buckled wave in the middle of the panel, obtained from the LS-DYNA model, were 36° and 35° after the pull and push stroke, respectively. The angles across the web plate in the LS-DYNA model varied from 33° to 41°, as compared with the values of 37° to 47° observed in the results reported by Webster et al. (2014). At the drift of ±4%, both the inclination angles from middle buckled corrugations and the range yield a similar result as Webster et al. (2014). Given that that the angles within the elastic range of response (i.e., at 0.5% drift) are less significant, focusing on the larger drift amplitudes, it is found that measured inclination angles based on the out-of-plane deformation contour analysis from the LS-DYNA model are in good agreement with the experimental ones reported by Webster et al..

3.3.3 Inclination angle analysis

Figure 3-14 shows the inclination angle vs. drift relationship of the web plate shell elements located along the top beam, bottom beam, left column, right column, and middle web, identified by the lines in Figure 3-15. Note that the angles presented in Figure 3-14 are the averages for all the elements along each line considered.

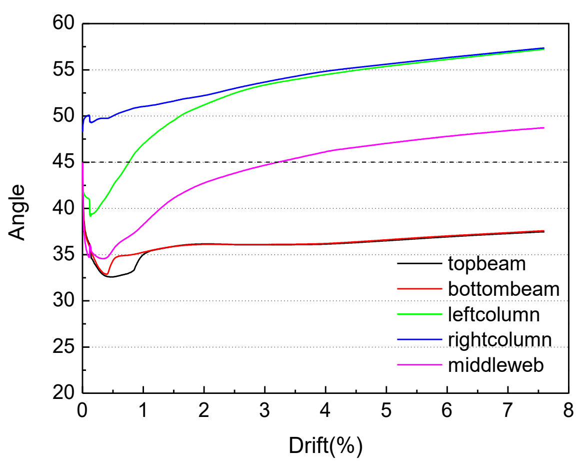

Figure 3-14 Migration of inclination angle of web plate

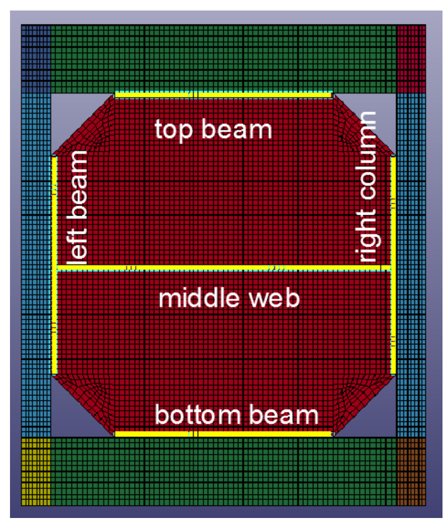

Figure 3-15 Location of shell element groups

In Figure 3-14, all of the curves exhibit a similar trend, in that the angle initially decreases from a relatively high initial value at low stresses, up to nearly 0.5% drift (where some parts of the infill approach their elastic limit as shown in Figure 3-16), and then progressively increase afterwards up to the maximum drift considered.

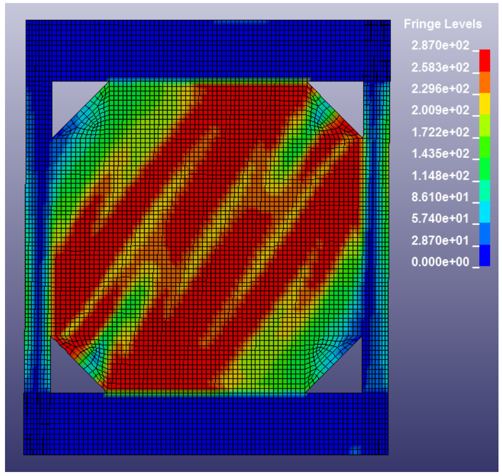

Figure 3-16 Partly yielding state of web plate under 0.5% drift (red color=yielding)

Note that in the earlier stages of elastic response, stresses applied by the steel plate to the boundary elements are not of design concern. Hence, the high values of angle initially observed from 0 to 0.5% drift have no significance on structural design.

However, in spite of this similarity in trend observed in Figure 3-14, quite different angle values are obtained along the different locations considered. Top and bottom beams have approximately the same angle values, starting as low as 33° at 0.5% drift, and reaching an angle of around 37° beyond 3% drift. Similarly, left column and right column have approximately the same angle values, starting as low as 40° for the left column and 50° for the right column at 1% drift, and reaching an angle of around 53° at 3% drift. In addition, the angle across the middle web is approximately 37° at 1% drift, 44° at 3% drift, and 48° at 6% drift.

3.3.4 Web plate, VBE and HBE demand analysis

Design of a SPSW structure shall be based on development of the full tension yielding mechanism of the web plate, and capacity design of the rest of the structure considering forces applied by the yielding web plate. Tension yielding of web plate imposes components of normal and shear stresses on VBEs and HBEs. Their capacity design requires accurate knowledge of the stresses applied by the web plate, which in turns requires an assessment of the inclination angle of the diagonal tension field action acting on the face of the VBEs and HBEs.

In a first step towards this assessment, to compare actual inclination angles against those values considered in design at various drifts values, it is useful to correlate expected stresses with the drifts at which they are likely to occur. Considering rigid VBEs and HBEs with pin connection, assumed to impose uniform diagonal tension strains on the tension strips of a web plate subjected to lateral loading, strain ε at a specific drift can be calculated as (Bruneau, 2011):

$$\varepsilon = \frac{\gamma \cdot sin2\alpha}{2} \tag{3.5}$$

where, γ =drift of structure, and; α =inclination angle from vertical axis.

From this diagonal tension strain, using the known stress-strain relationship for a given material, the principal stresses acting in the web plate can be theoretically determined. To illustrate how demands on HBEs and VBEs due to plate yielding would vary as a function of the inclination angle, normal and shear stresses acting on those members are presented in Table 3-2 for values of the inclination angle of 40° (recommended by AISC 341-10) and 45° (recommended by Webster et al. (2014)). In addition, results at 1% drift considering an average angle of 35° is included for comparison.

Note that at 1% and 6% drift, for the material used by Webster, principal stresses at the strains obtained from Equation 3.5 are 289.5MPa and 313 MPa, respectively. The value of 289.5MPa is close to end of the yielding plateau on the stress-strain curve from coupon testing. It is logical to compare values obtained at 1% drift, even though SPSW could develop a larger drift, because capacity design per AISC 341 assumes that the web plate has fully yielded, and therefore developed yield stress value (sustained by the material, based on coupon tests and Equation 3.5, up to a 1% drift). Comparing results at 6% drift allows to assess demands on the HBEs and VBEs considering strain hardening. In all cases, conversion from design principal stress to design normal and shear stresses were performed using following formulas：

HBE, Web plate:	Normal stress	$\sigma = \sigma_{prin}(cos\alpha)^2$	(3.6)
	Shear stress	$\sigma = (\sigma_{prin} sin2\alpha)/2$	(3.7)
VBE:	Normal stress	$\sigma = \sigma_{prin}(sin\alpha)^2$	(3.8)
	Shear stress	$\sigma = (\sigma_{prin} sin2\alpha)/2$	(3.9)

Table 3-2 Design normal and shear stresses (MPa) on web plate, HBE and VBE at different drifts

Drift	1%						6%			
Inclination angle	35°		40°		45°		40°		45°	
Stress	Normal	Shear	Normal	Shear	Normal	Shear	Normal	Shear	Normal	Shear
Web plate	194.3	136.0	169.9	142.5	144.8	144.8	183.5	154.1	156.5	156.5
HBE	194.3	136.0	169.9	142.5	144.8	144.8	183.5	154.1	156.5	156.5
VBE	95.2	136.0	119.6	142.5	144.8	144.8	129.2	154.1	156.5	156.5

3.3.4.1 Web plate analysis results

The web plate is the main component of SPSW system resisting the story shear force. Seismic provisions for Structural Steel Buildings (AISC 341-10) stipulates that the design shear strength shall be determined as follows:

$$V_n = 0.42 F_y t_w L_{cf} \sin 2\alpha \tag{3.10}$$

where, L_{cf}=clear distance between column flanges.

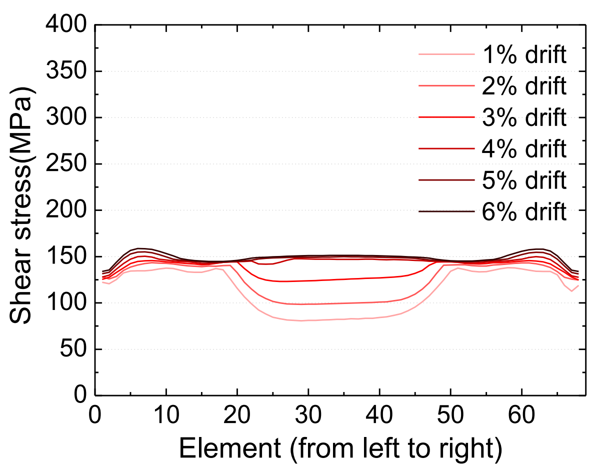

a. Shear stress distribution of six drifts

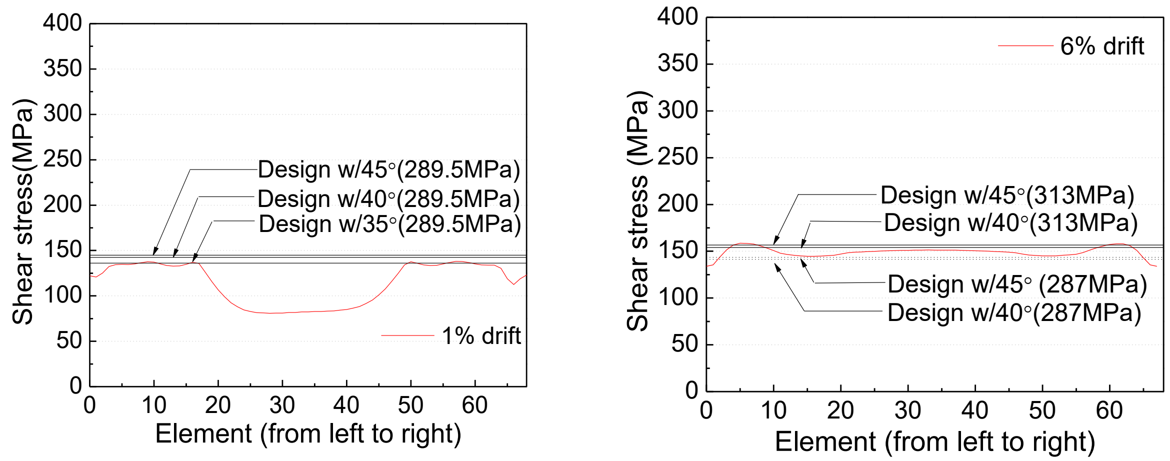

b. Comparison with design shear stress (1%) **c. Comparison with design shear stress (6%)**

Figure 3-17 Shear stress of web plate shell element group (middle web)

Figure 3-17 presents the shear stress distribution from left to right along mid-height of web. It shows that shear stresses increase from 1% to 6% drift. Stresses are less in the middle part of the plate at lower drifts, as a consequence of the web corner cut-outs, which prevents a direct path for diagonal stresses along a corner-to-corner line. Shear stress contours at 1% and 6% drift of the web plate are shown in Figure 3-18.

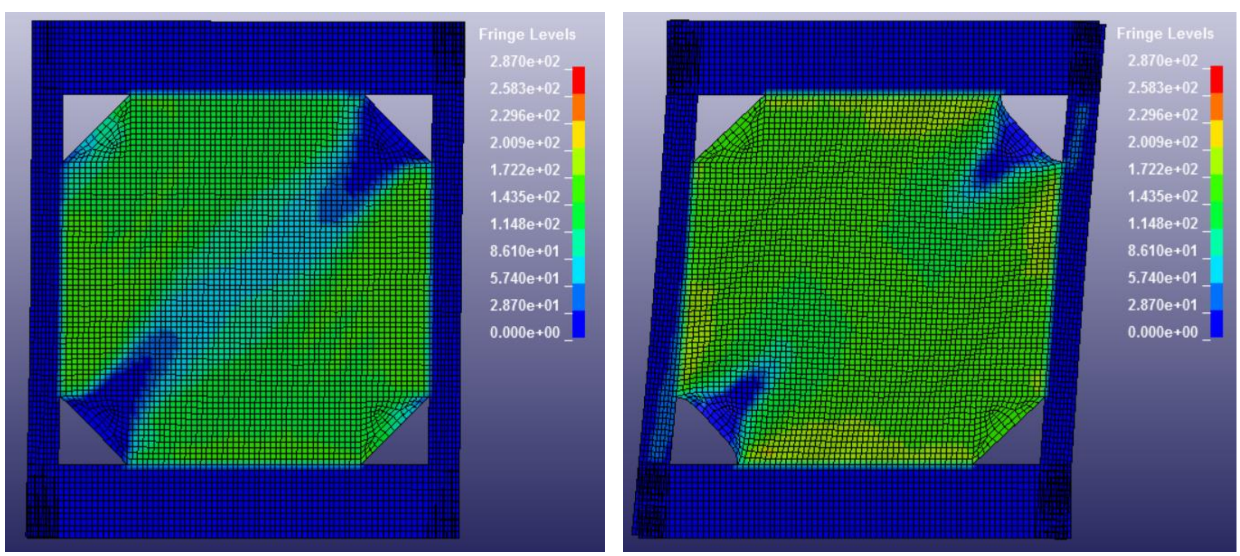

Figure 3-18 Shear stress contours at 1% (left) and 6% drift (right) in web plate

Figure 3-17b and Figure 3-17c compare the above web stresses at 1% and 6% drift with their corresponding AISC-specified stresses (per Equation 3.10) calculated using inclination angles of 35, 40 and 45 degree. These drift levels were selected (as indicated earlier) to compare behavior of the web plate at stresses corresponding to full yielding and ultimate strength, respectively. Results in Figure 3-17b suggest that design-level stresses are apparently higher than actual stresses, but the difference is overall minor, with a difference of approximately 10MPa (except for the middle part of the plate, due to the corner cut-outs, as mentioned earlier). Shear stress at 6% drift is more uniformly distributed than 1% drift and close to design value. Therefore, values predicted by AISC (Equation 10) are conservative in this case.

3.3.4.2VBE demand analysis results

Figure 3-20 and Figure 3-21 show the normal and shear stresses imposed on the left VBE of the SPSW by the adjacent web plate, as obtained from principal stresses in the web elements adjacent to the VBE. It's observed in Figure 3-20 that the normal stress variation along the elements is similar in shape at different drift levels, but the value of normal stresses tend to increase with increasing drift. Fluctuations of normal stress observed from top to bottom of the VBE is due to generation of "strips" of web plates as shown in Figure 3-19. The magnitude of normal stresses in the lower web elements adjacent to the VBE is much higher than upper elements because lower elements are in the region of main tensile "strip". Also, a significant variation in the normal stress distribution is observed from 1% to 2% drift in the upper corner elements. This significant change might be due to geometrical discontinuity, upper elements not lying in the main tensile strips etc.

Figure 3-20b compares actual normal stress distribution under 1% drift with the design strength ones obtained for the same inclination angles considered previously. Figure 3-20c compares actual normal stress distribution under 6% drift with the design strength ones obtained for the same inclination angles considered previously.

For normal stress distribution, Figure 3-20 indicates that it is not necessarily conservative to use α=40°in design, as proposed by AISC 360-10, and that using α=45° is better than α=40° when below 1% drift. More importantly, normal stresses along the elements at 6% drift are much higher than those used for design (calculated with an inclination angle 40°) and hence using 40° is not conservative.

For shear stress distribution, Figure 3-21 shows that design shear stress is not sensitive to inclination angle change as can be explained by Equation 3.9. More importantly, it's higher than actual analysis results and hence using 40° and 45° are both conservative.

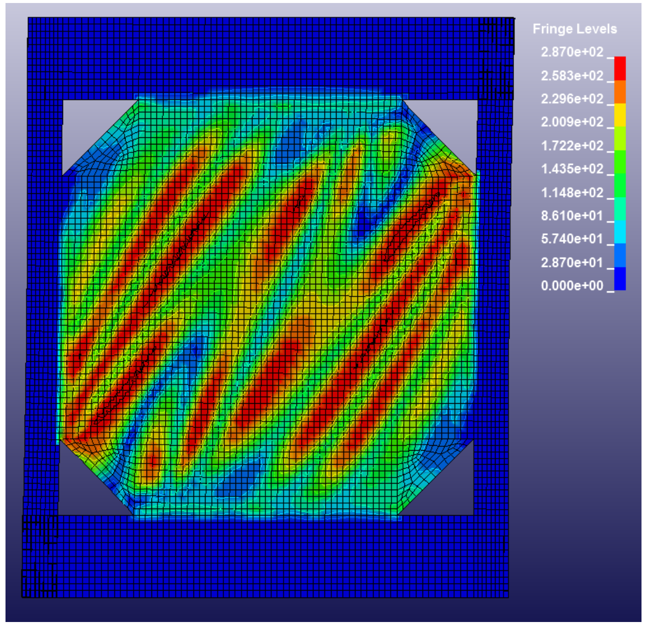

Figure 3-19 "Strips" in web plate under 1% drift

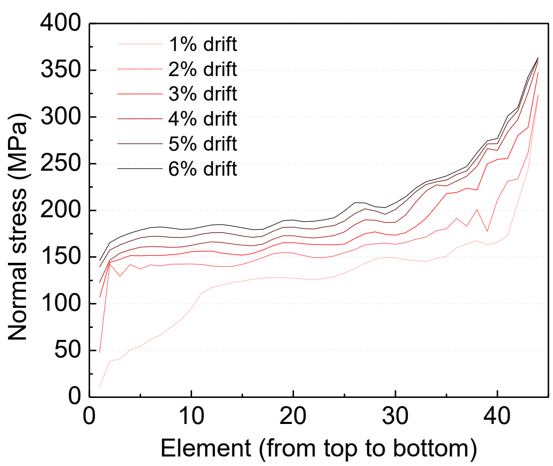

a. Normal stress distribution of six drifts

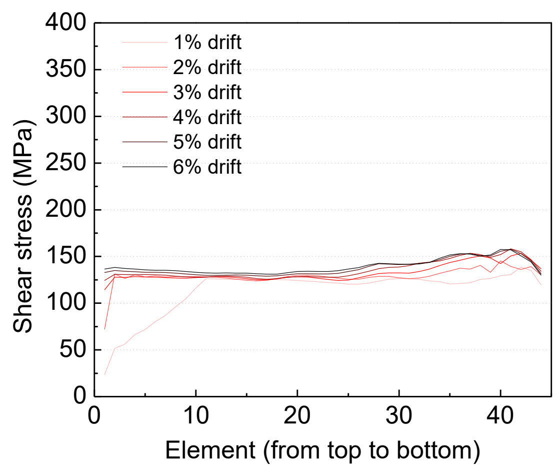

a. Shear stress distribution of six drifts

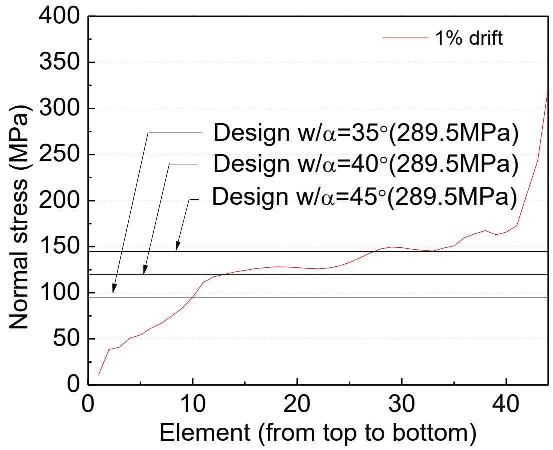

b. Comparison with design normal stress (1%)

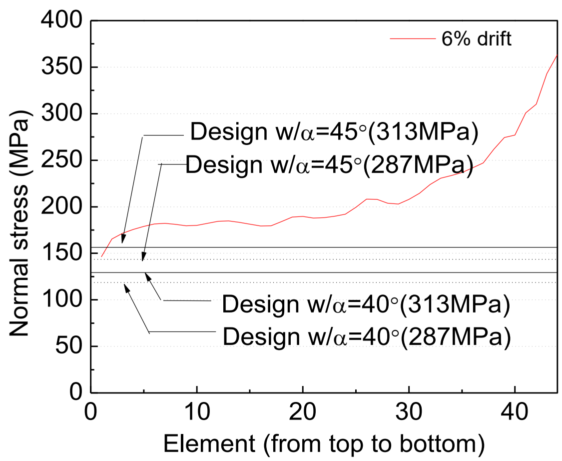

c. Comparison with design normal stress (6%)

Figure 3-20 Normal stress of web plate shell element group (left column)

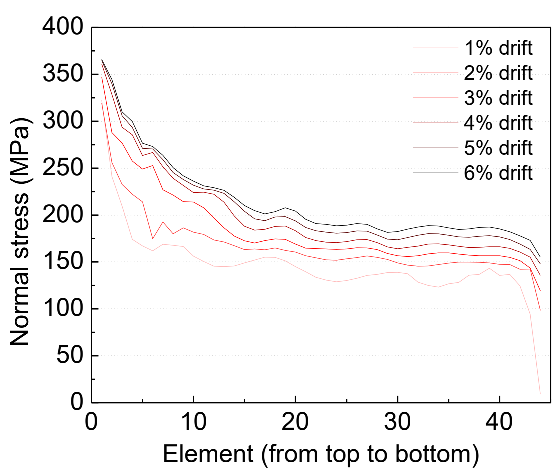

a. Normal stress distribution of six drifts

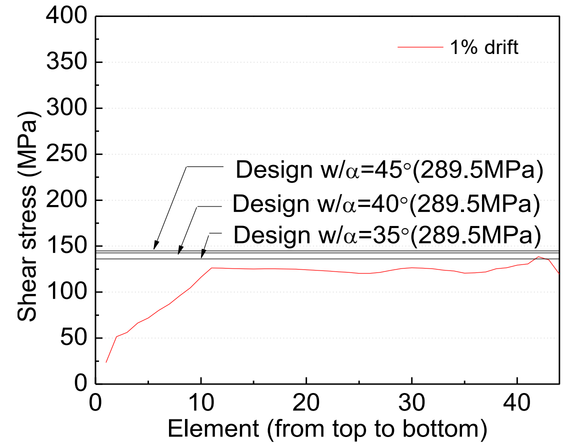

b. Comparison with design shear stress (1%)

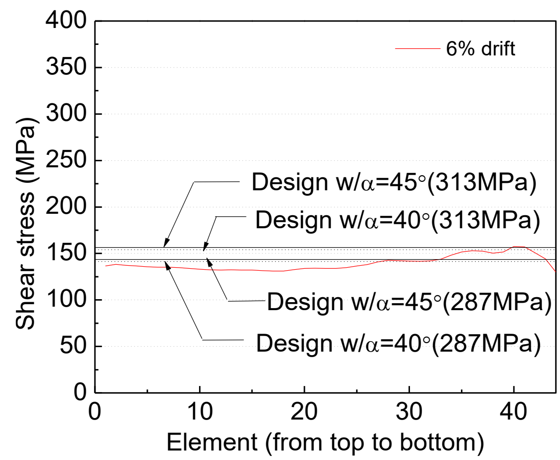

c. Comparison with design shear stress (6%)

Figure 3-21 Shear stress of web plate shell element group (left column)

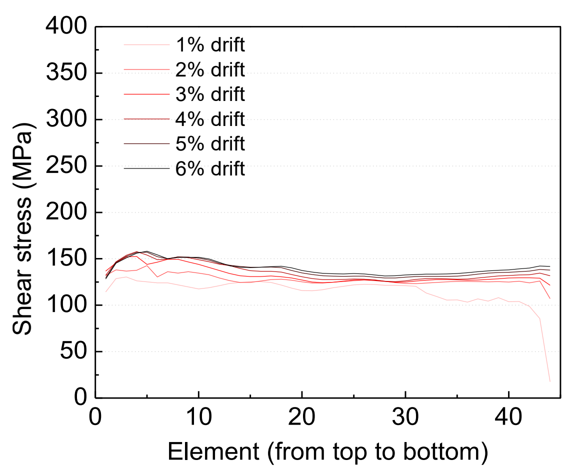

a. Shear stress distribution of six drifts

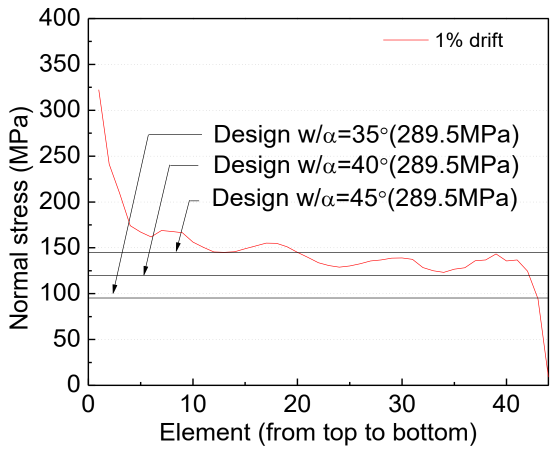

b. Comparison with design normal stress (1%)

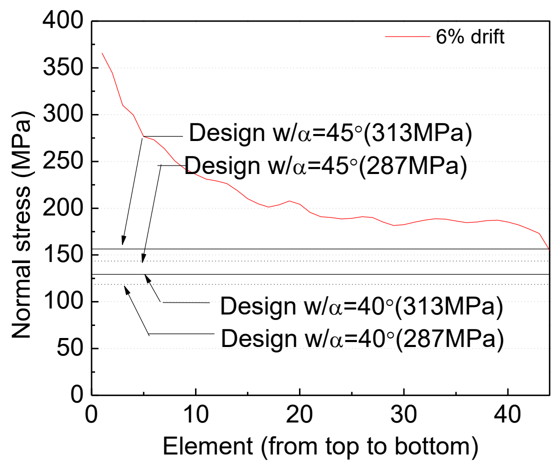

c. Comparison with design normal stress (6%)

Figure 3-22 Normal stress of web plate shell element group (right column)

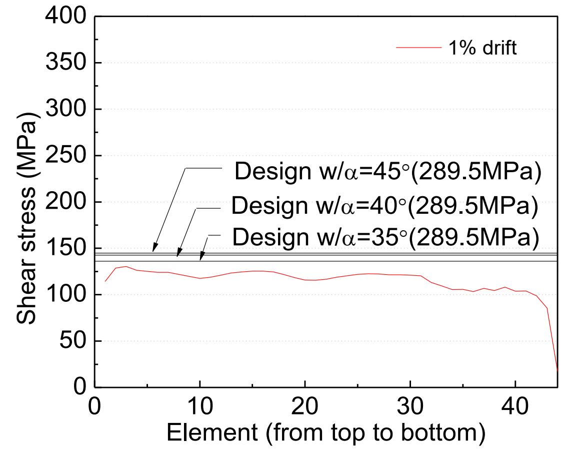

b. Comparison with design shear stress (1%)

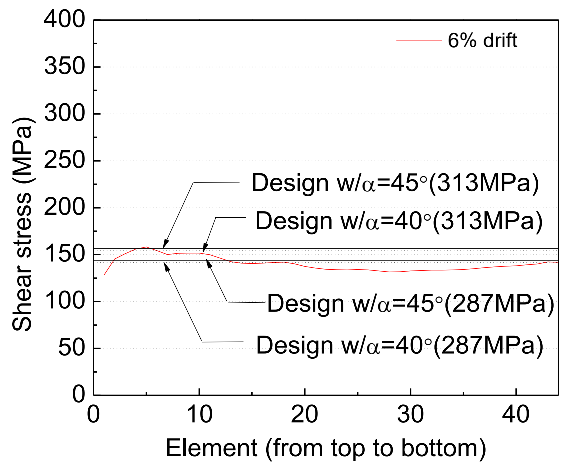

c. Comparison with design shear stress (6%)

Figure 3-23 Shear stress of web plate shell element group (right column)

Figure 3-22 and Figure 3-23 show the normal and shear stresses imposed by adjacent web plate shell elements (right column). It is observed that normal and shear stresses distribution along right column are similar to left column and yield the same conclusion. Since the main tensile "strips" in web plate are located from bottom left to top right as shown in Figure 3-19, the normal stress decreases along elements from top to bottom of right column (Figure 3-22a) in contrast with increasing tendency of that on left column (Figure 3-20a).

3.3.4.3HBE demand analysis results

Figure 3-24 and Figure 3-25 show the normal and shear stresses imposed by adjacent web plate shell elements (top beam). It is observed that the stress distribution along the top beam, for six different drifts considered, are similar to each other. Note that stresses in elements at the left corner of the top beam do not change as significantly as in the corner elements in columns.

Comparing actual stress distribution with specified design stresses, it is observed that normal stresses are much higher than the specified design stresses calculated using both 40° and 45° at 1% and 6% drift. This suggests that using 45° is not necessarily better than using 40°. Hence, it appears to not be necessarily conservative to use 40°, and using 45° would be even less conservative than using 40°. Figure 3-25 shows that the design shear stress (i.e., translating into axial forces in the HBEs and VBEs) is not sensitive to inclination angle change as can be explained by Equation 3.7, and those actual shear stresses are close to the specified design stresses, with some of them a little bit higher than that at 6% drift.

Figure 3-26 and Figure 3-27 show the normal and shear stresses imposed by adjacent web plate shell elements to the bottom beam. It is observed that the stress distribution along bottom beam is similar to that for the top beam, which leads to the same observations made for the top beam.

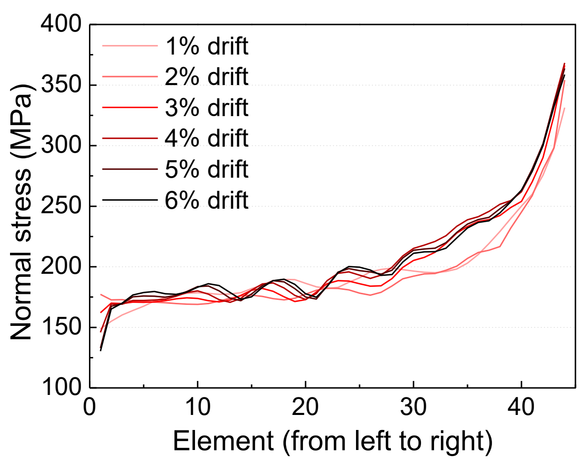

a. Normal stress distribution of six drifts

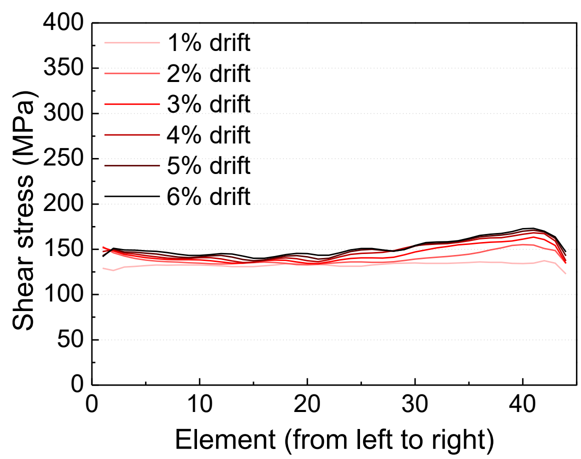

a. Shear stress distribution of six drifts

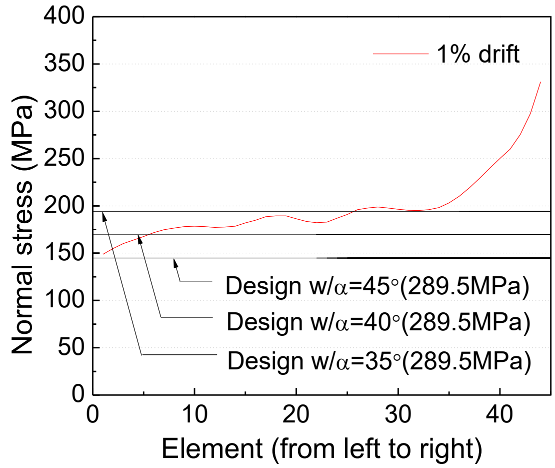

b. Comparison with design normal stress (1%)

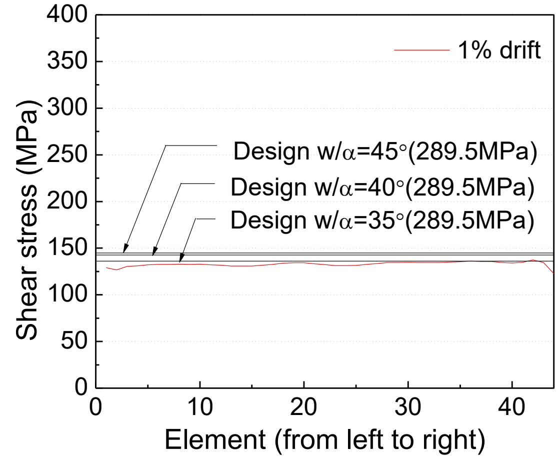

b. Comparison with design shear stress (1%)

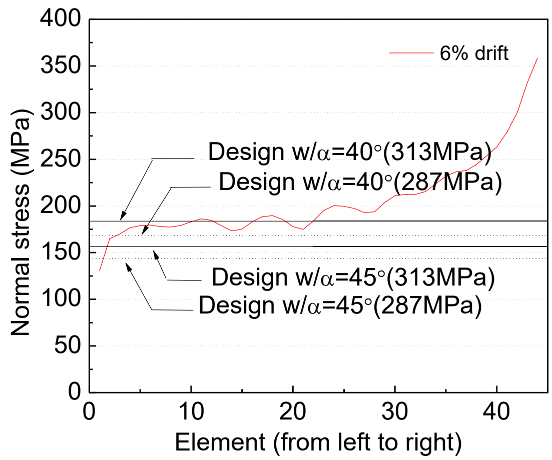

c. Comparison with design normal stress (6%)

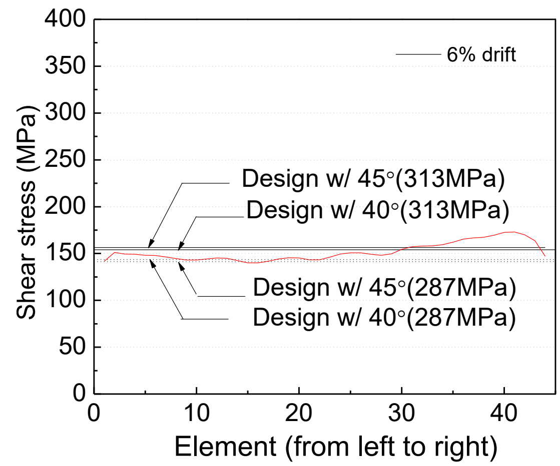

c. Comparison with design shear stress (6%)

Figure 3-24 Normal stress of web plate shell element group (top beam)

Figure 3-25 Shear stress of web plate shell element group (top beam)

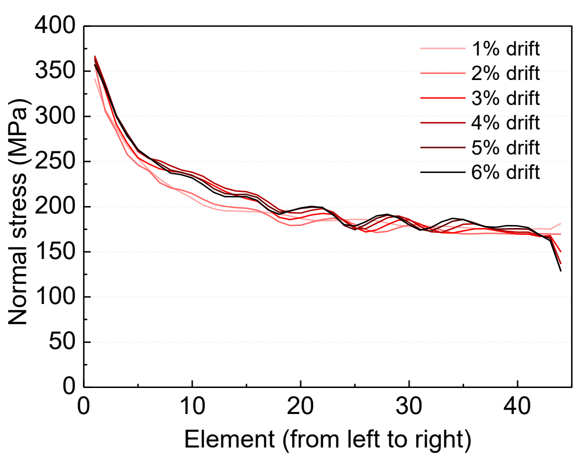

a. **Normal stress distribution of six drifts**

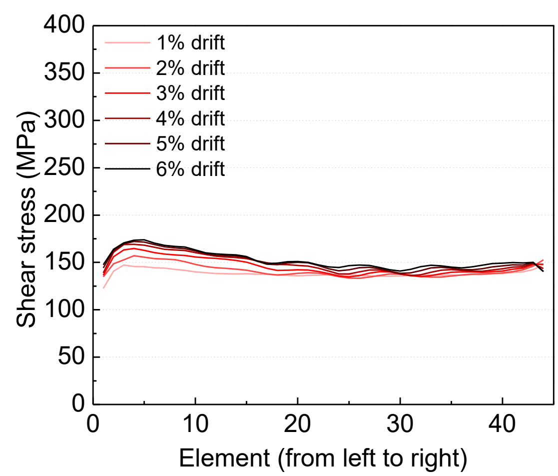

a. Shear stress distribution of six drifts

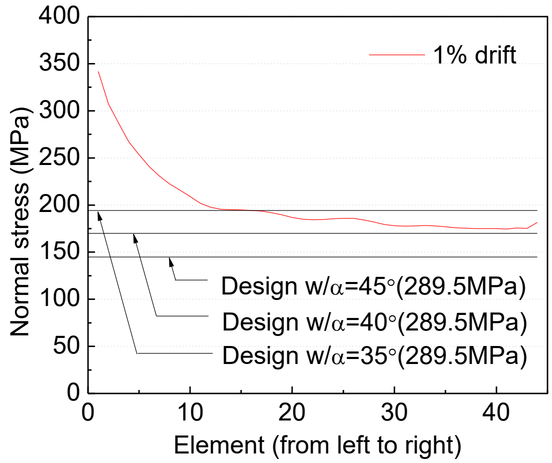

b. Comparison with design normal stress (1%)

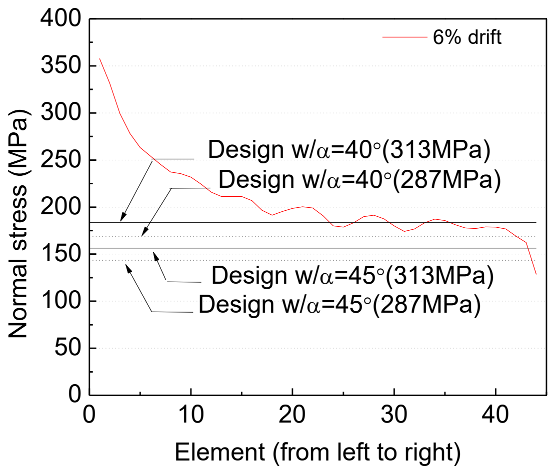

c. Comparison with design normal stress (6%)

Figure 3-26 Normal stress of web plate shell element group (bottom beam)

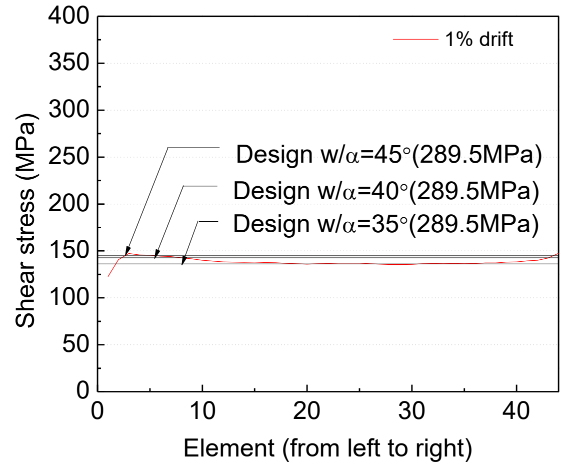

b. Comparison with design shear stress (1%)

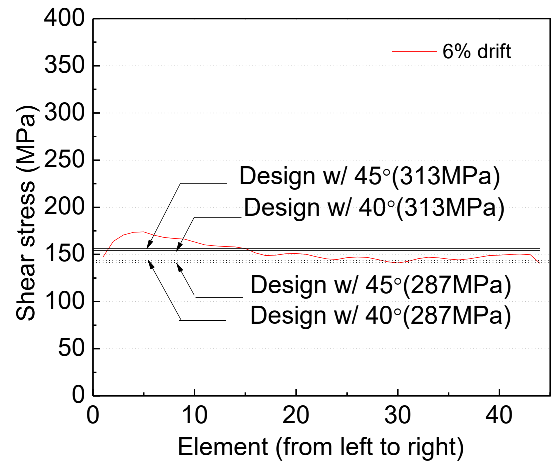

c. Comparison with design shear stress (6%)

Figure 3-27 Shear stress of web plate shell element group (bottom beam)

3.4 Summary

This section described the construction of the LS-DYNA model and compared the results obtained with both the experimental results and the ABAQUS results from Webster et al. (2014). The comparison shows that the load-drift hysteretic curve, the average inclination angle of the web plate, and the out-of-place displacement contours obtained from the LS-DYNA model match well the experimental results obtained by Webster.

Beyond this comparison, the inclination angle and stress distributions at different drifts were also calculated along the middle of the web, and along the left column, right column, top beam and bottom beam (Figure 3-15). Those calculated values were compared against specified design stresses obtained considering various angles of inclinations of the diagonal tension field. It was observed that different average inclination angles were obtained at those different locations (Figure 3-14) and the difference is not negligible.

Shear stresses over the range of 0% to 6% drift at those five locations are typically smaller than design specified values and consequently conservative. As for normal stresses in the left and right columns, results indicate that it is not conservative to use 40°, but conservative to use 45° at 1% drift. At 6% drift, it is not conservative to use either 40° or 45°. Actual normal stresses at 6% drift are approximately 10MPa higher than the design values. For normal stresses in the top and bottom beams, it is not conservative to use either of 40° and 45° at 1% and 6% drift.

Note that the stress distribution obtained along the left and right columns were essentially similar to each other (but mirror images from each other). The same is true comparing results for the top and bottom beams. Hence, in subsequent Chapters, the stress distributions are only reported for the left column and the top beam (in addition to the middle of the web).

SECTION 4
ANALYSIS OF TWO NEW SPSW MODELS

4.1 General

In this section, two new LS-DYNA models were built to further investigate how the inclination angle of the diagonal tension field action varies across the web plate, for a solid web plate and different HBE to VBE connections. Details on the two models considered are presented in detail in Section 4.2. Results in terms of inclination angles, stress distributions, the moment and axial force diagrams, as well as moment-axial force interaction of elements at different locations across the web plate are presented in Section 4.3.

4.2 New LS-DYNA Model Description

The new models were designed with the same material models, loading protocol and boundary conditions as the LS-DYNA model in SECTION 3. The main differences from the LS-DYNA model in SECTION 3 are connection type and absence of cutout. Model A presented below is with pin HBE-to-VBE connections and without web cutouts at the corner of the web plate, and Model B is with rigid HBE-to-VBE connections and also without cutouts. In addition, elasto-plastic HBEs and VBEs were considered in Model B. A summary of these differences is presented in Table 4-1 . To simulate the rigid connection of HBE and VBE, nodes at the end of the HBE were merged to the face of VBE.

Table 4-1 Differences of the three LS-DYNA models

	LS-DYNA model in Section 3	Model A	Model B
Connection Type for HBE to VBE	Pin	Pin	Rigid
Geometry of Web Plate	With Cutout	Without Cutout	Without Cutout
Material Model of VBEs and HBEs	Elastic	Elastic	Elastic-Plastic

4.3 Inclination angle and VBE, HBE demand analysis

4.3.1 Inclination angle analysis

Figure 4-1 shows the change in inclination angle of the tension field action as a function of drift for the web plate in the three models listed in Table 4.1. For Model A, as seen in Figure 4-1, the angle in each location follows a similar trend as the model in SECTION 3 after 2% drift. Up to the maximum drift considered, the average angles are around 55° for VBE, 39° for HBE and 48° for the web plate. Note that the average angle along the right column initially increases to nearly 55° and drops after 0.5% drift, mainly due to localized angle variation at the top and bottom corners of the web, but the amplitude of stress in those corners is not large at those small drifts.

For Model B, the variations in average inclination angle are similar as for the LS-DYNA models from SECTION 3 and Model A above. However, the inclination angle along the left and right columns only increased to around 50° (as opposed to 55°) at large drifts. The implications of those variations of stresses along VBE and HBE is investigated later in this section by comparing the resulting flexural demands on those VBEs and HBEs.

Von-Mises stress contours of Model A and Model B at 1% and 6% drift are presented at Figure 4-2 and Figure 4-3, respectively.

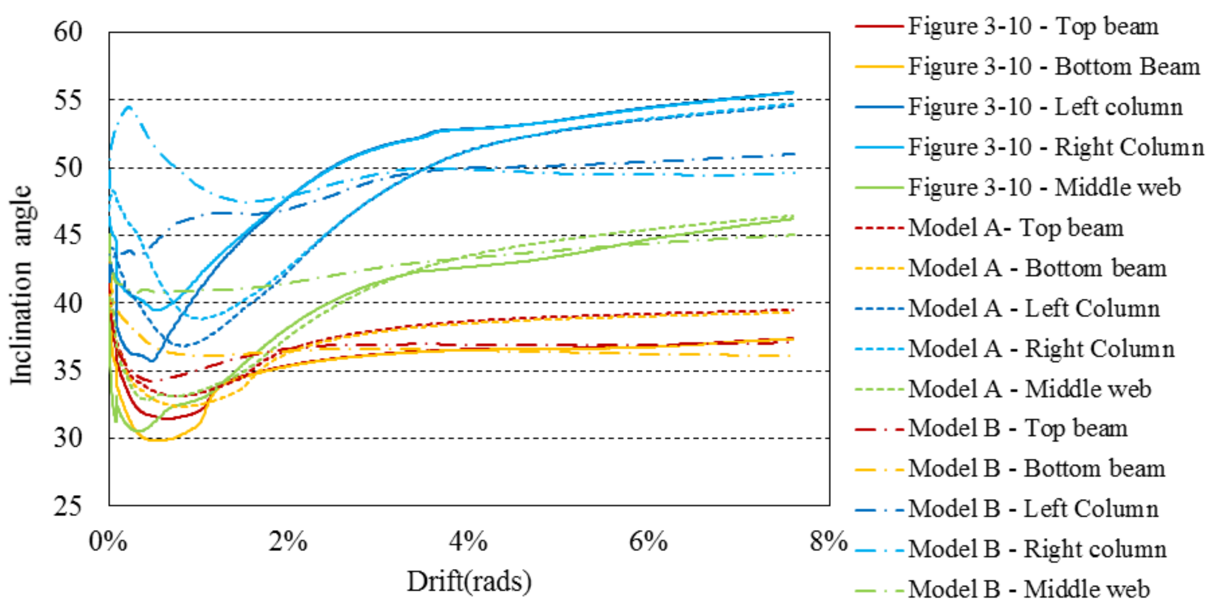

Figure 4-1 Comparison on inclination angle migration of web plate

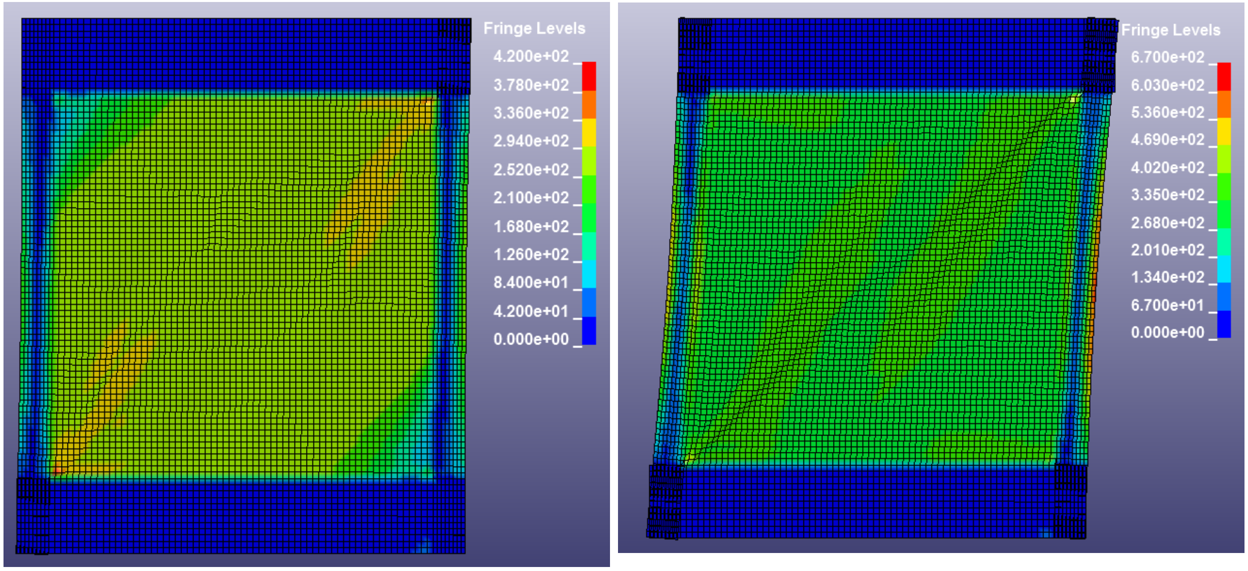

Figure 4-2 Von-Mises stress contours of Model A at 1% (left) and 6% drift (right)

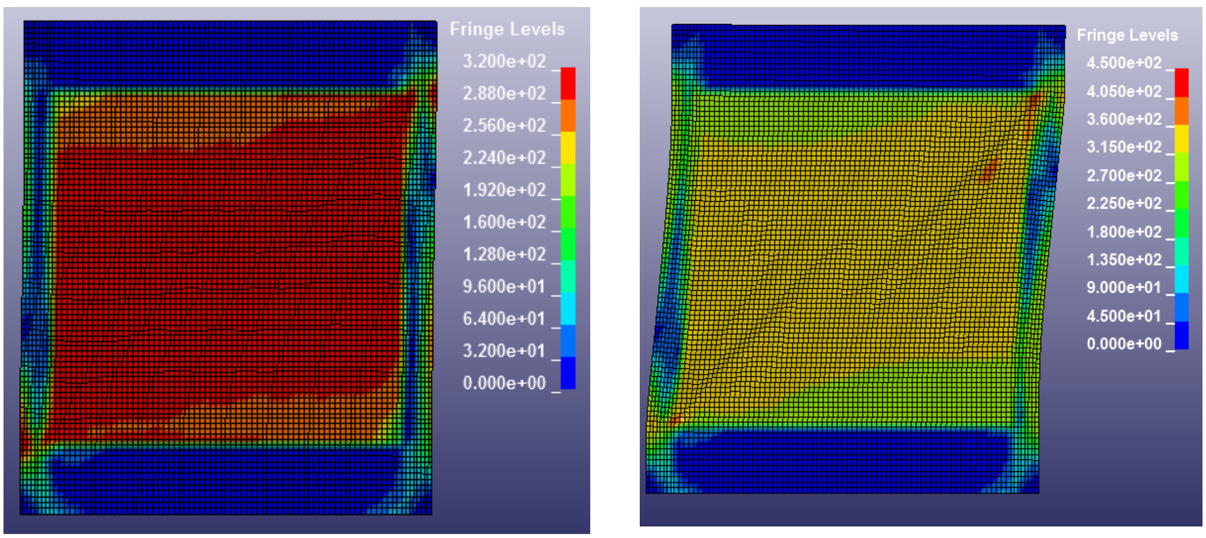

Figure 4-3 Von-Mises stress contours of Model B at 1% (left) and 6% drift (right)

4.3.2 Web plate, VBE and HBE demand analysis

4.3.2.1 Web plate analysis results

Figure 4-4 and 4-5 present the shear stress distribution from left to right along mid-height of the web. As before, shear stresses increase from 1% to 6% drift, however, results here show a more uniform distribution of shear stresses than for the LS-DYNA model in Section 3 (Figure 3-17). This is because the web without cutout allows a diagonal tensile strip developing from bottom left corner to top right corner in the web, and, hence, a more uniform distribution of stresses across the web.

Note that the stress distributions here are compared with the demands considering various design specified yield stress values, as was done in Section 3.3.3. Results show that the actual stresses at 1% drift are pretty close to the design stress while shear stress at 6% drift is slightly higher than the design stress, with a difference of approximately 10MPa. Therefore, using 40° and 45° are both conservative.

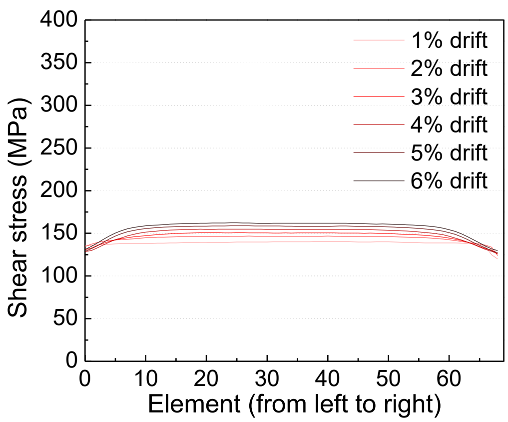

a. Shear stress distribution of six drifts

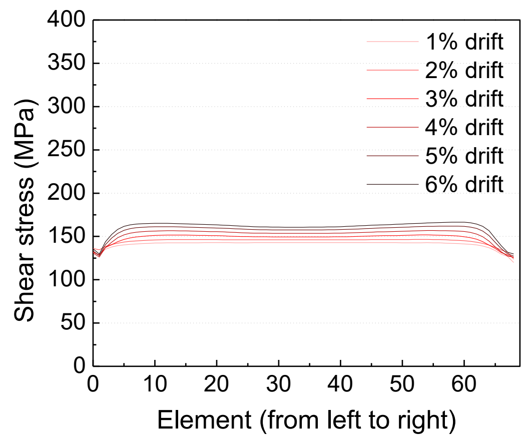

a. Shear stress distribution of six drifts

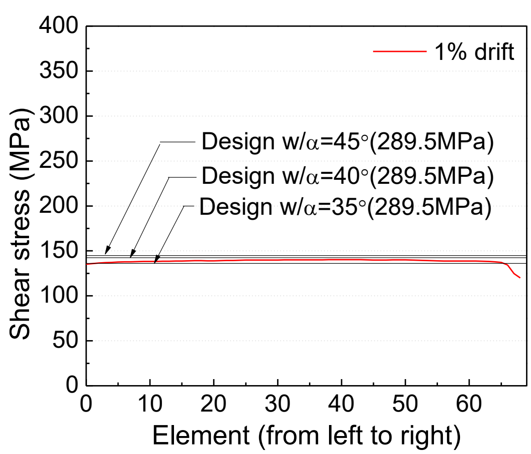

b. Comparison with design shear stress (1%)

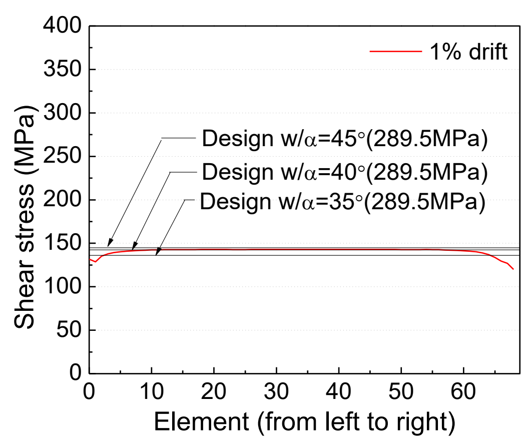

b. Comparison with design shear stress (1%)

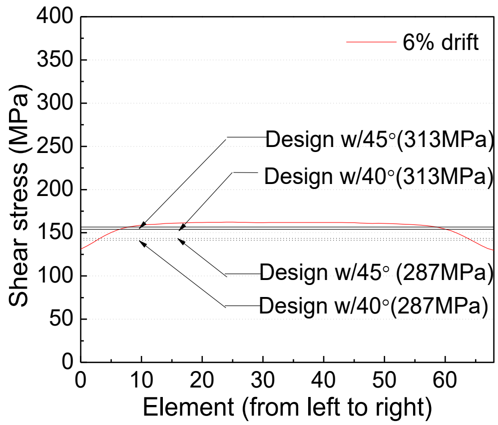

c. Comparison with design shear stress (6%)

Figure 4-4 Shear stress of web plate shell elements (middle web) of model A

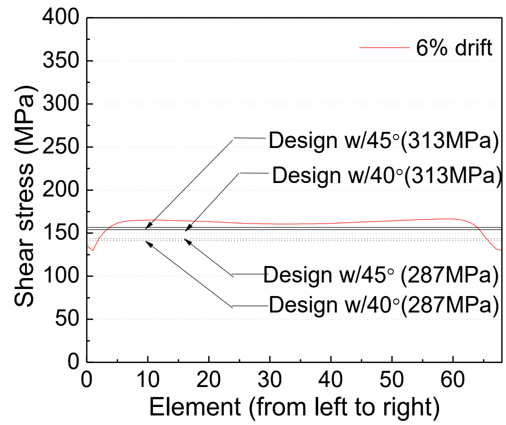

c. Comparison with design shear stress (6%)

Figure 4-5 Shear stress of web plate shell elements (middle web) of model B

4.3.2.2VBE demand analysis results

The normal and shear stresses imposed on the left column of the SPSW by the adjacent web plate are shown in Figure 4-6 to Figure 4-9 for Model A and B. Several significant differences are observed compared to the LS-DYNA model in Section 3.

For Model A, the normal stresses increase with increasing drift and become more uniformly distributed along the left column, as shown in Figure 4-6. Due to large out-of-plane distortion by compression, in plane stresses of the bottom corner elements are very small. Although the stress variation along the left column is different those obtained from the LS-DYNA model in Section 3 (Figure 3-20), the comparison with design specified values leads to the same conclusion. Actual normal stresses are on average lower than the design value at 1% drift (Figure 4-6b) and higher than that at 6% drift (Figure 4-6c) (using 40°). As far as comparing stresses is concerned, it is not conservative to use 40° and conservative to use 45° at 1% drift. At 6% drift, it is not conservative to use either 40° or 45°.

The shear stress distributions of left VBE shown in Figure 4-8 also leads to similar observations as those made for the LS-DYNA model in Section 3, except for the small stresses that develop in the bottom corner region, as explained above.

Based on the actual normal stress and shear stress distribution obtained above, the moment and axial force diagrams are also presented assuming that the columns and beams are rigidly framed as shown in Figure 4-10 and Figure 4-12. Calculated moment and axial force values at column end are listed in Table 4-2. It is observed that the actual moment at the column end is lower than the design values obtained considering α= 45° and 50°.

Table 4-2 Moment and axial force at left column end

		Model A	Model B	Model A	Model B
		Moment (kN·m)	Moment (kN·m)	Axial force (kN)	Axial force (kN)
1% drift	Actual	3.44	4.39	60.92	63.28
	35° with 289.5MPa	3.27	3.27	73.54	73.59
	40° with 289.5MPa	4.11	4.11	77.12	77.12
	45° with 289.5MPa	4.97	4.97	78.31	78.31
	50° with 289.5MPa	5.84	5.84	77.12	78.31
3% drift	Actual	5.43	4.97	69.08	67.47
	35° with 296MPa	3.34	3.34	75.22	75.22
	40° with 287MPa	4.07	4.07	76.46	76.46
	40° with 296MPa	4.21	4.21	78.96	78.96
	45° with 287MPa	4.93	4.93	77.64	77.64
	45° with 296MPa	5.09	5.09	80.21	80.21
	50° with 296MPa	5.98	5.98	78.96	78.96
6% drift	Actual	6.31	5.54	69.51	69.78
	35° with 313MPa	3.51	3.51	79.03	79.03
	40° with 287MPa	4.07	4.07	76.46	76.46
	40° with 313MPa	4.44	4.44	83.38	83.38
	45° with 287MPa	4.93	4.93	77.64	77.64
	45° with 313MPa	5.37	5.37	84.67	84.67
	50° with 313MPa	6.30	6.30	83.30	83.30

However, at 6% drift, the actual moment at the beam's end is substantially higher than the design values. As for the actual axial forces, they are lower than design values obtained considering using both 40° and 45° at 1% and 6% drift, as shown in Figure 4-12. The findings for moments and axial forces analysis are respectively similar to the observations made when comparing normal and shear stresses applied by the web plate in the previous analyses.

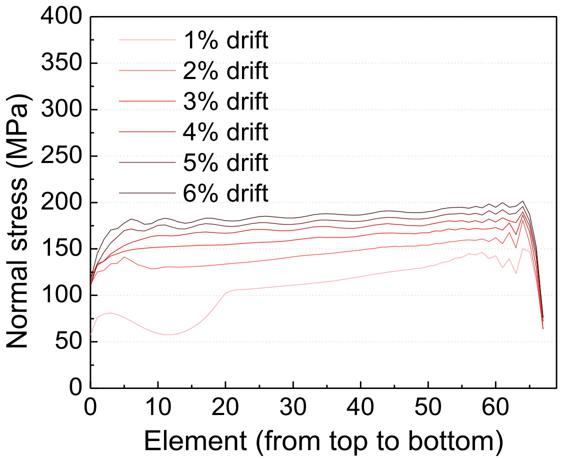

a. Normal stress distribution of six drifts

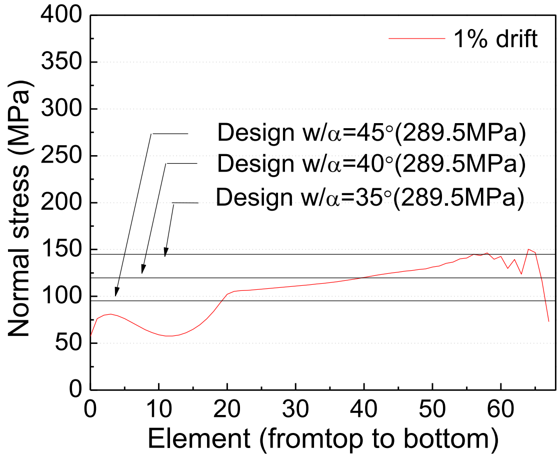

b. Comparison with design normal stress (1%)

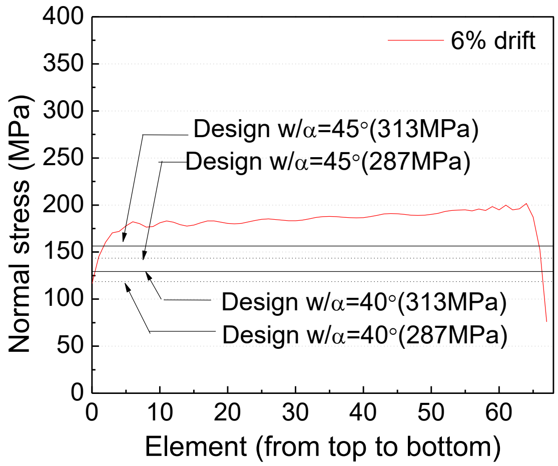

c. Comparison with design normal stress (6%)

Figure 4-6 Normal stress of web plate shell element group (left column) of Model A

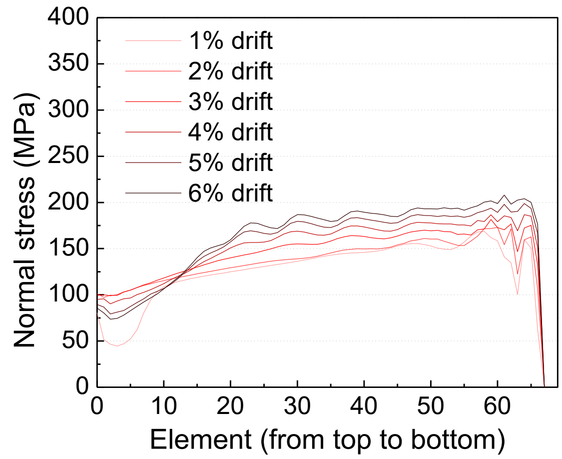

a. Normal stress distribution of six drifts

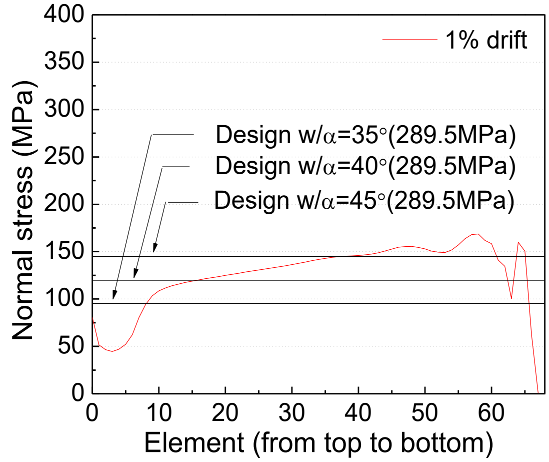

b. Comparison with design normal stress (1%)

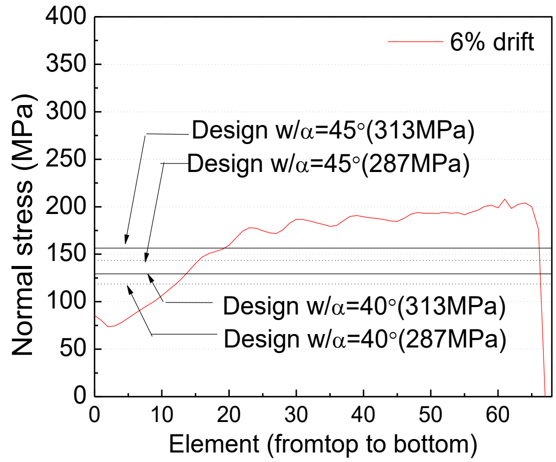

c. Comparison with design normal stress (6%)

Figure 4-7 Normal stress of web plate shell element group (left column) of Model B

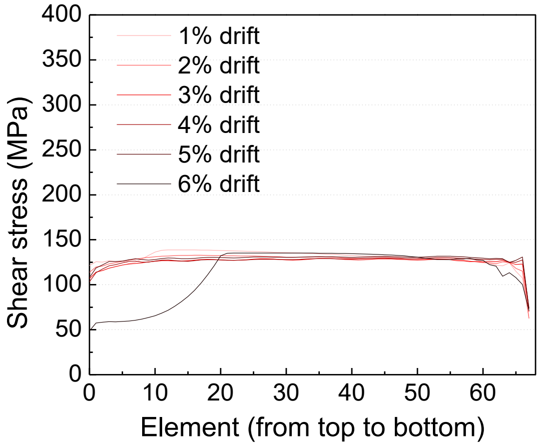

a. Shear stress distribution of six drifts

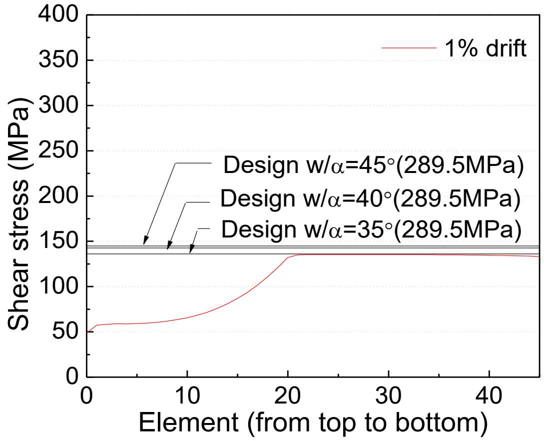

b. Comparison with design shear stress (1%)

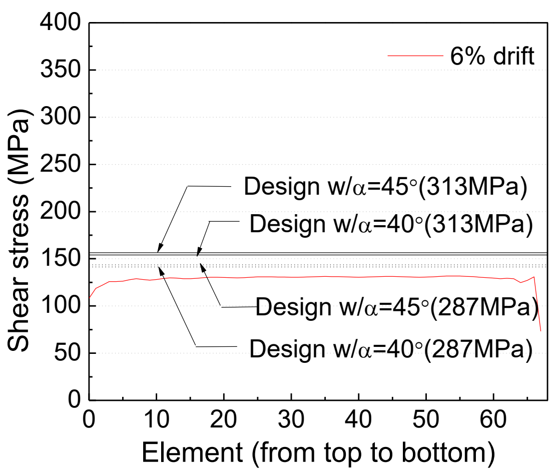

c. Comparison with design shear stress (6%)

Figure 4-8 Shear stress of web plate shell element group (left column) of Model A

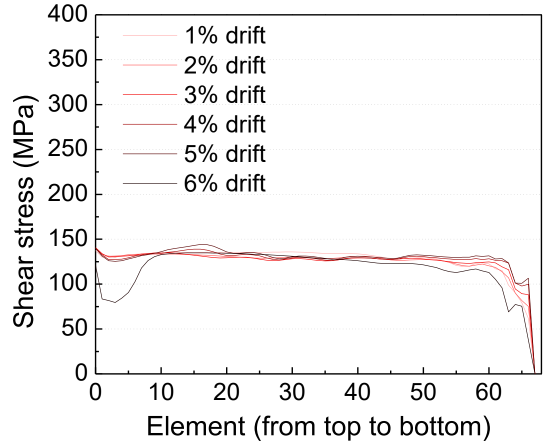

a. Shear stress distribution of six drifts

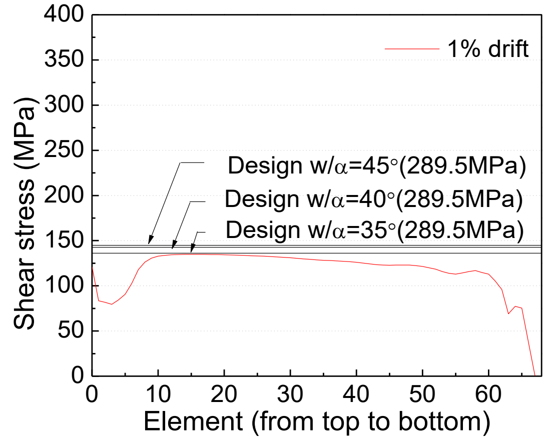

b. Comparison with design shear stress (1%)

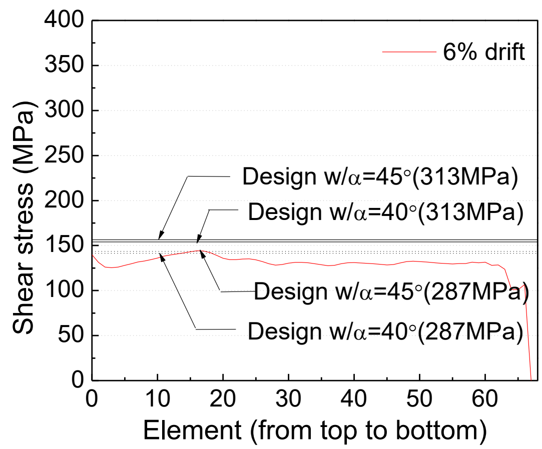

c. Comparison with design shear stress(6%)

Figure 4-9 Shear stress of web plate shell element group (left column) of Model B

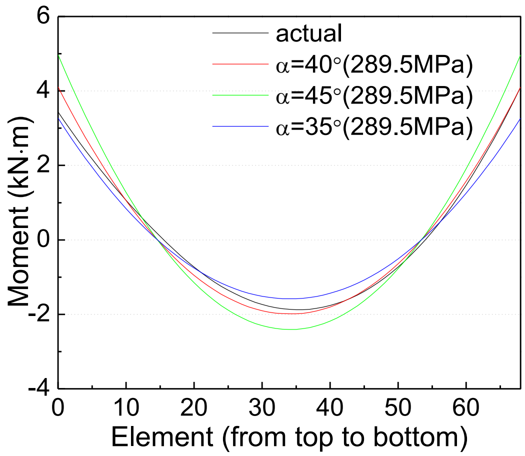

a. 1% drift

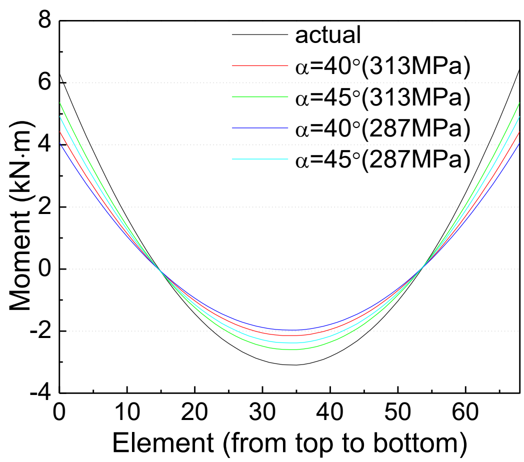

b. 6% drift

Figure 4-10 Moment diagram of web plate shell element group (left column) of Model A

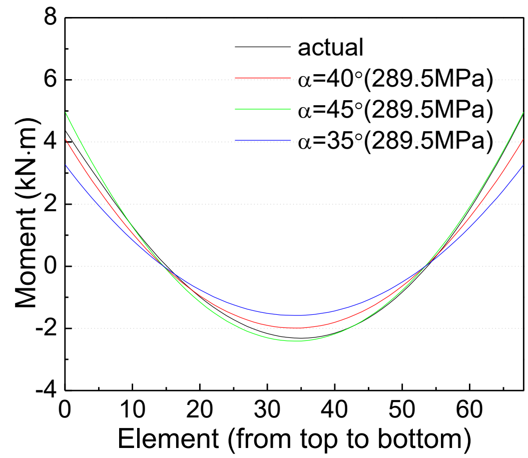

a. 1% drift

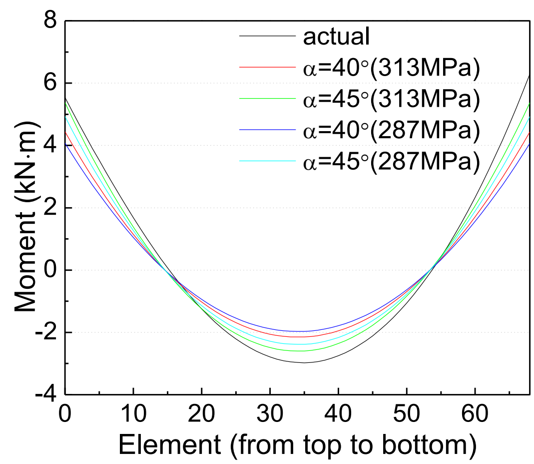

b. 6% drift

Figure 4-11 Moment diagram of web plate shell element group (left column) of Model B

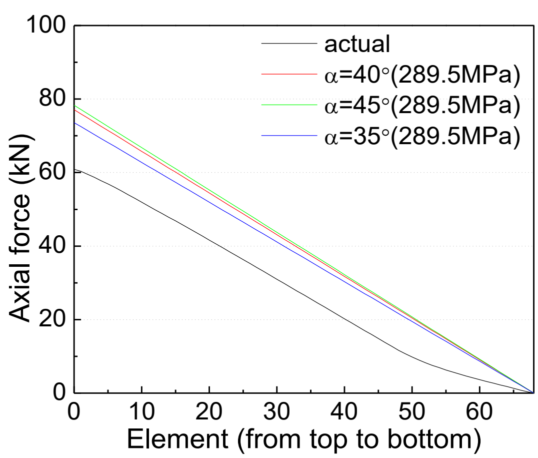

a. 1% drift

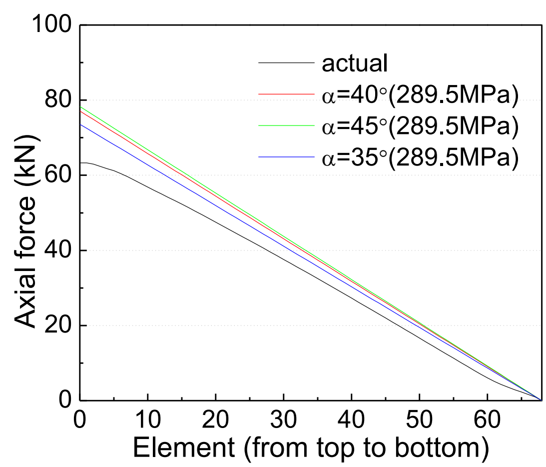

a. 1% drift

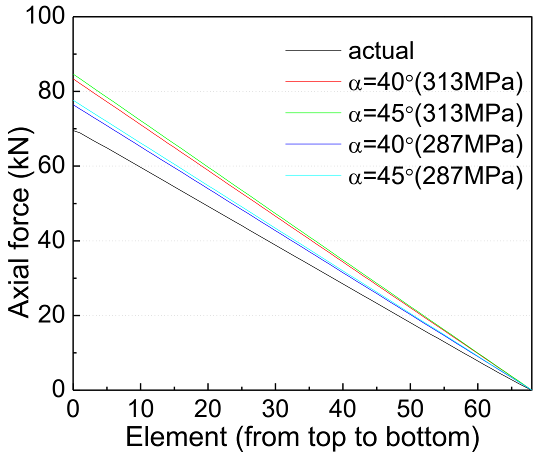

b. 6% drift

Figure 4-12 Axial force of web plate shell element group (left column) of Model A

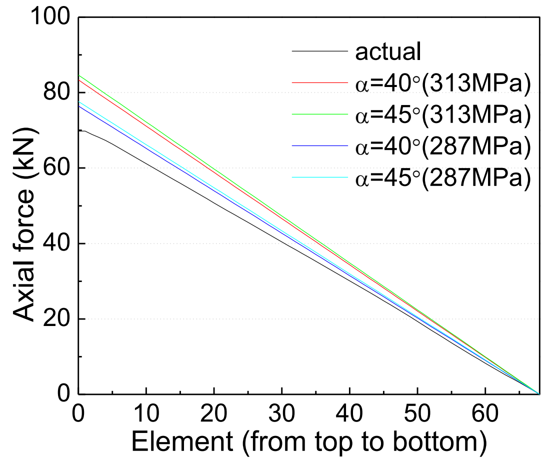

b. 6% drift

Figure 4-13 Axial force of web plate shell element group (left column) of Model B

For Model B, small stresses in the bottom corner elements are also due to large out-of-plane distortion, as observed in Model A. In the top corner elements, stresses lower than in other elements are due to the rigidity of the connection (i.e., the rigid connection of HBE to VBE).

Actual normal stresses are on average lower than the design value at 1% drift (Figure 4-7b) and higher than that at 6% drift (Figure 4-7c) (using 45°). As far as comparing stresses is concerned, it is not conservative to use 40° and conservative to use 45° at 1% drift. At 6% drift, it is not conservative to use either 40° or 45°. The shear stress distributions on left column, shown in Figure 4-8, also leads to similar observations as those made for Model A and for the LS-DYNA model in Section 3, except for the small stresses that develop in the bottom corner region, as explained above.

Calculated moment and axial force values at column end are listed in Table 4-2 and shown in Figure 4-11 and Figure 4-13. It is observed that the actual moment at the column end is higher than the design values obtained considering α=35° and 40°; they are actually close to the value (4.97kN·m) obtained considering α=45° at 1% drift. However, at 6% drift, the actual moment at the column's end is substantially higher than the design values. As for the actual axial forces, they are lower than the design values obtained considering using both 40° and 45° at 1% and 6% drift, as shown in Figure 4-13. The findings for moments and axial forces analysis are respectively similar to the observations made when comparing normal and shear stresses in the previous analyses.

4.3.2.3 HBE demand analysis results

The normal and shear stresses imposed on the top beam of the SPSW by the adjacent web plate are shown in Figure 4-14 to Figure 4-17 for Model A and B.

For Model A, actual normal stresses are on average higher than the design value using 45° and approximately equal to the design value using 40° at 1% and 6% drift. As far as comparing stresses is concerned, it is not conservative to use 45° and conservative to use 40° at both 1% and 6% drift. The shear stress distributions of top beam shown in Figure 4-16 also leads to similar observations as those made for left column in Model A and the LS-DYNA model in Section 3, except for the small stresses that develop in the right corner region, as explained above.

Calculated moment and axial force values at column end are listed in Table 4-3 and shown in Figure 4-18 and Figure 4-20. It is observed that the actual moment at the beam end is higher than the design values obtained considering α=40° and 45°; they are actually close to the value (6.67kN·m) obtained considering α=35° at 1% drift. At 6% drift, the actual moment at the column's end is also higher than the design values using 45° and approximately equal to that using 40°. As for the actual axial forces, they are lower than design values obtained considering using both 40° and 45° at 1% and 6% drift, as shown in Figure 4-20. The findings for moments and axial forces analysis are respectively similar to the observations made when comparing normal and shear stresses in the previous analyses.

For Model B, based on results shown in Figure 4-15, normal stresses are generally higher than design normal stresses obtained using 40° and 45° at 1% and 6% drift. Hence, it is not conservative to use either 40° or 45° for the design of beams in SPSW with rigid connection. Moment diagrams in Figure 4-21 also lead to the same conclusion as reached for the normal stress results.

The shear stress distributions and corresponding axial forces of the top beam shown in Figure 4-16 and Figure 4-20 for Models A and B, again lead to the same conclusion as were made for the LS-DYNA model in SECTION 3.

Table 4-3 Moment and axial force at top beam end

		Model A	Model B	Model A	Model B
		Moment (kN·m)	Moment (kN·m)	Axial force (kN)	Axial force (kN)
1% drift	Actual	6.05	6.06	62.26	64.13
	35° with 289.5MPa	6.67	6.67	73.54	73.59
	40° with 289.5MPa	5.84	5.84	77.12	77.12
	45° with 289.5MPa	4.97	4.97	78.30	78.31
	50° with 289.5MPa	4.11	4.97	77.12	78.31
3% drift	Actual	5.85	6.17	69.82	69.88
	35° with 296MPa	6.82	6.82	75.22	75.22
	40° with 287MPa	5.79	5.79	76.46	76.46
	40° with 296MPa	5.98	5.98	78.96	78.96
	45° with 287MPa	4.93	4.93	77.64	77.64
	45° with 296MPa	5.09	5.09	80.21	80.21
	50° with 296MPa	4.21	4.21	78.96	78.96
6% drift	Actual	5.97	6.32	72.55	71.39
	35° with 313MPa	7.17	7.17	79.03	79.03
	40° with 287MPa	5.79	5.79	76.46	76.46
	40° with 313MPa	6.31	6.31	83.38	83.38
	45° with 287MPa	4.93	4.93	77.64	77.64
	45° with 313MPa	5.38	5.38	84.67	84.67
	50° with 313MPa	4.44	4.44	83.30	83.30

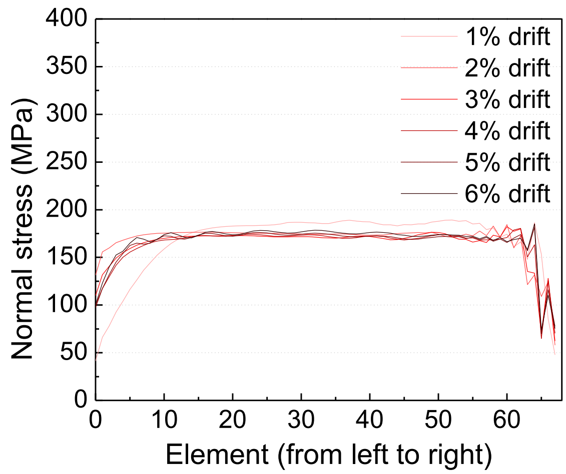

a. Normal stress distribution of six drifts

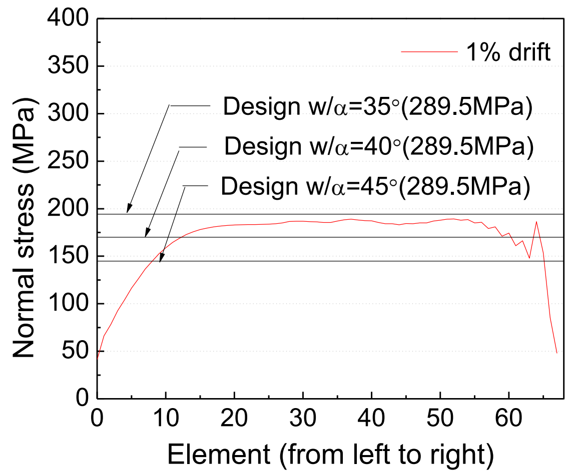

b. Comparison with design normal stress (1%)

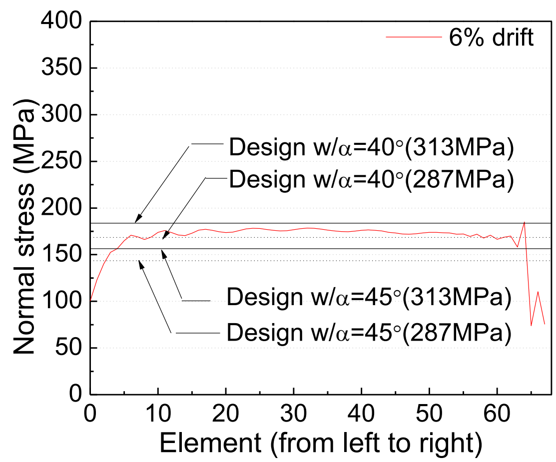

c. Comparison with design normal stress (6%)

Figure 4-14 Normal stress of web plate shell element group (top beam) of Model A

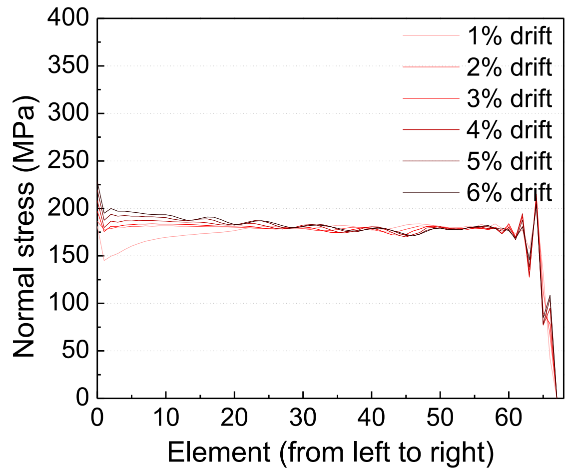

a. Normal stress distribution of six drifts

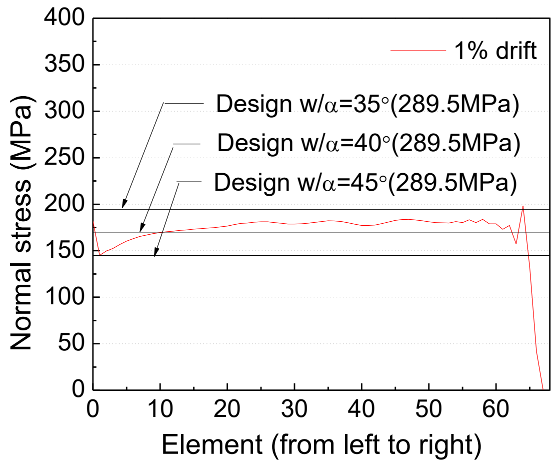

b. Comparison with design normal stress (1%)

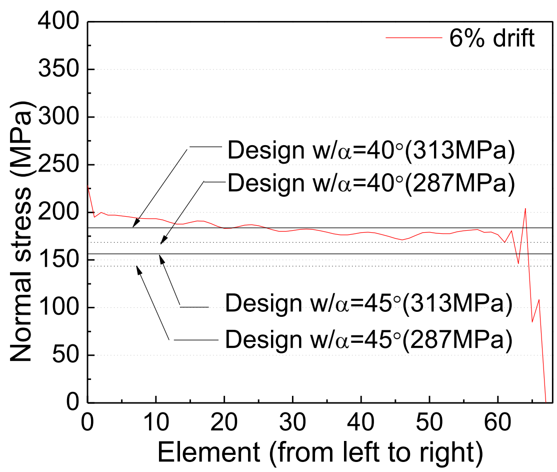

c. Comparison with design normal stress (6%)

Figure 4-15 Normal stress of web plate shell element group (top beam) of Model B

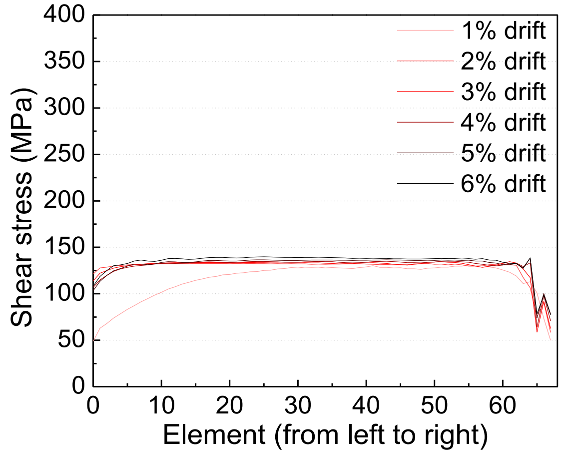

a. Shear stress distribution of six drifts

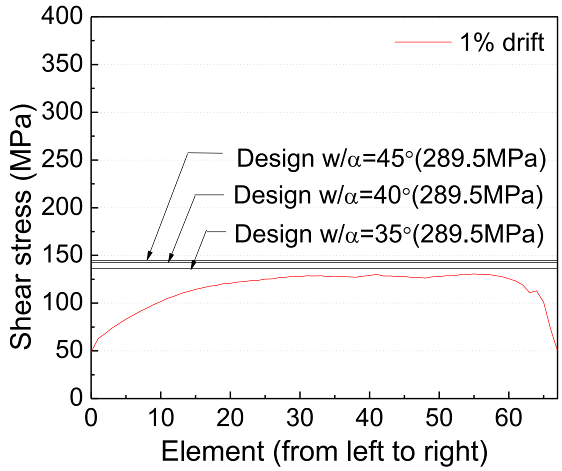

b. Comparison with design shear stress (1%)

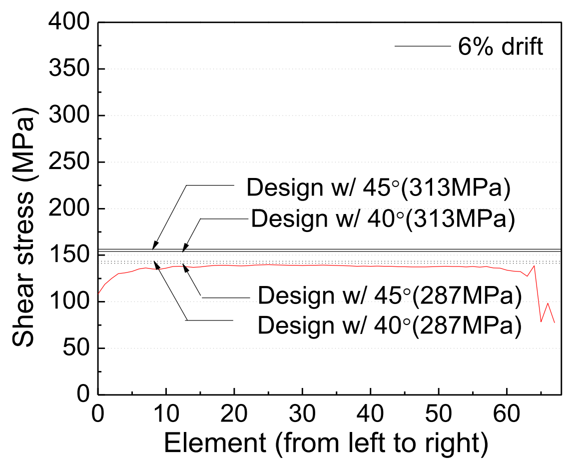

c. Comparison with design shear stress (6%)

Figure 4-16 Shear stress of web plate shell element group (top beam) of Model A

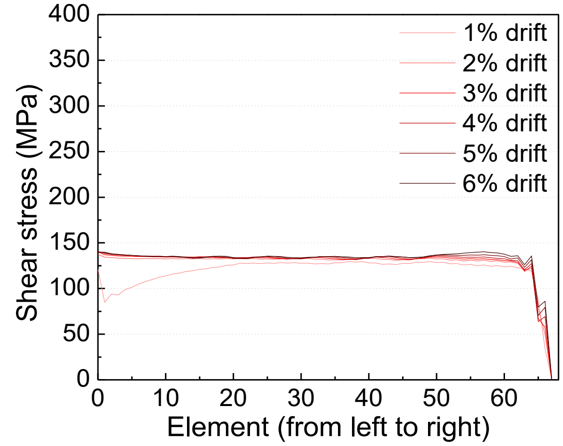

a. Shear stress distribution of six drifts

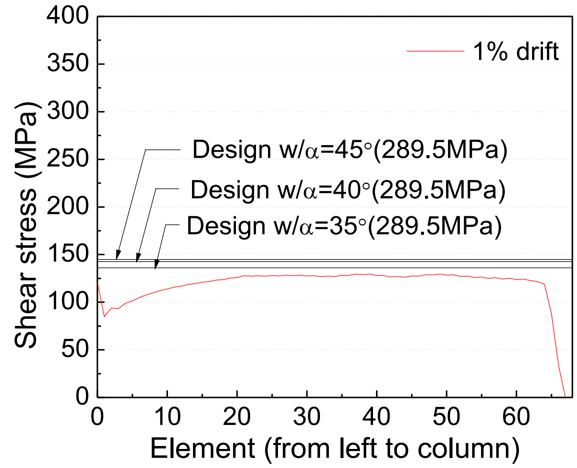

b. Comparison with design shear stress (1%)

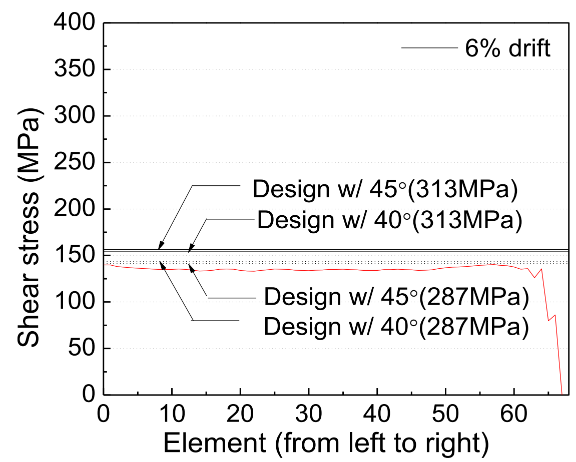

c. Comparison with design shear stress (6%)

Figure 4-17 Shear stress of web plate shell element group (top beam) of Model B

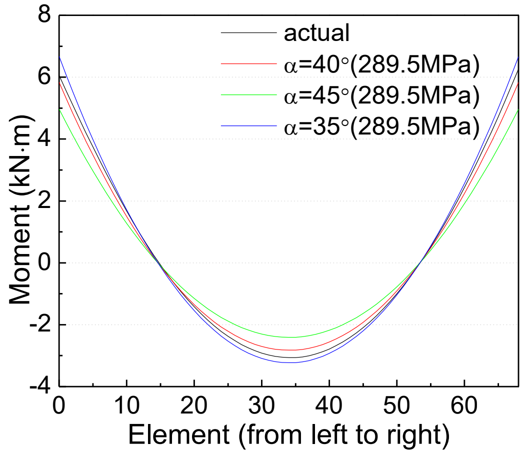

a. 1% drift

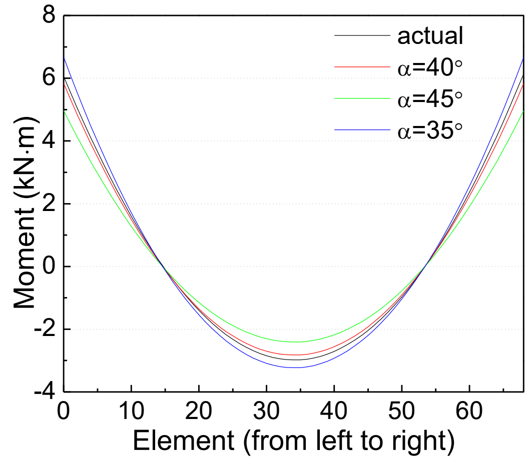

a. 1% drift

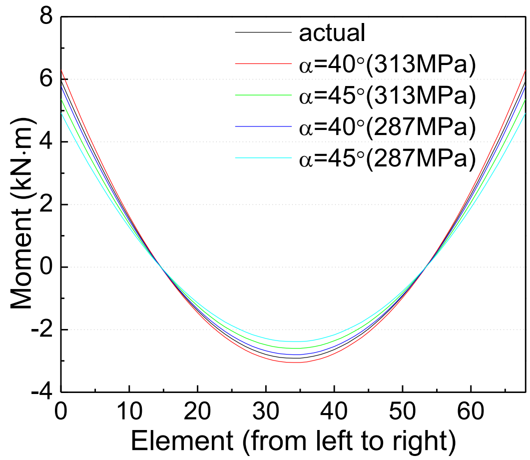

b. 6% drift

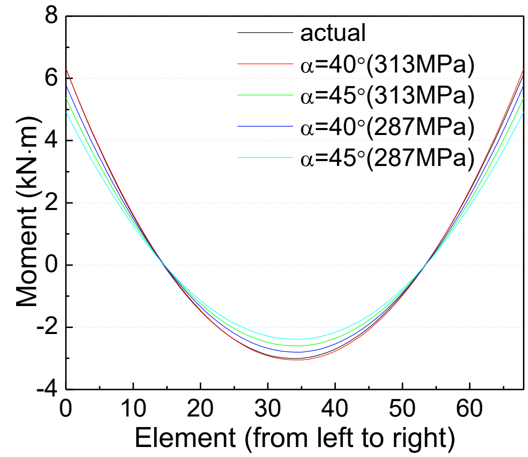

b. 6% drift

Figure 4-18 Moment of web plate shell element group (top beam)

Figure 4-19 Moment of web plate shell element group (top beam)

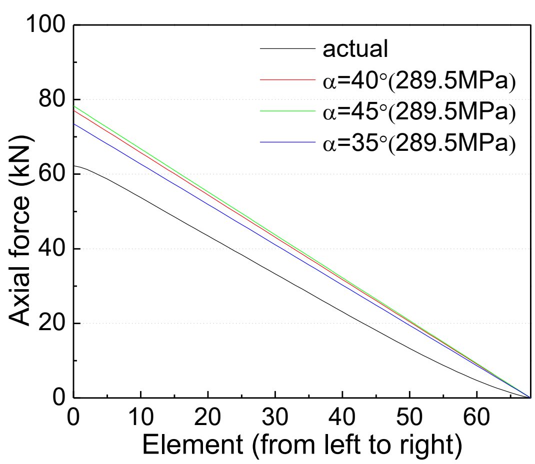

a. 1% drift

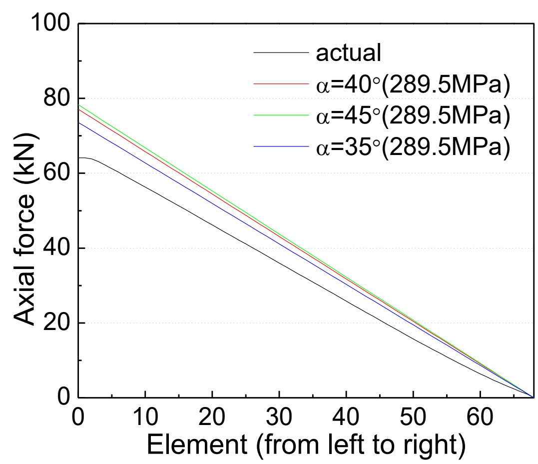

a. 1% drift

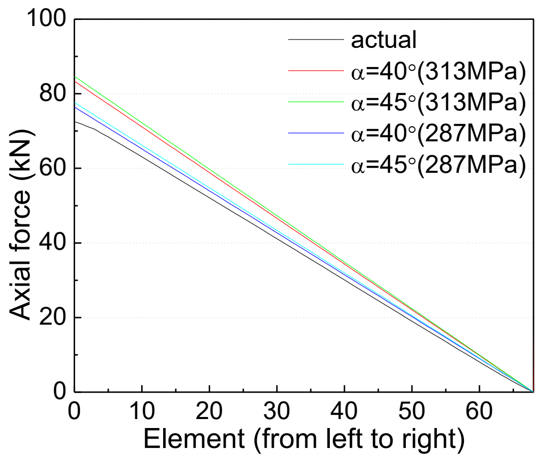

b. 6% drift

Figure 4-20 Axial force of web plate shell element group (top beam) of Model A

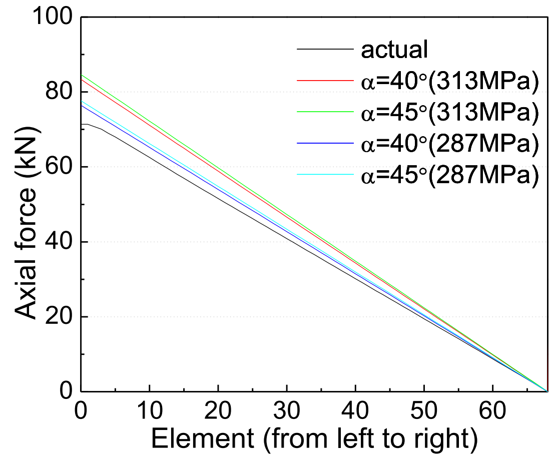

b. 6% drift

Figure 4-21 Axial force of web plate shell element group (top beam) of Model B

4.3.2.4 Combined moment-axial force demand analysis

Since the boundary elements are subjected to combined axial and flexural loading, moment-axial force interaction is considered in their design. To compare the forces obtained from the finite element analyses with those calculated using constant angle models, it is necessary to perform that comparison considering both the effect of axial and flexural demands. Based on the results in Table 4-2 and Table 4-3 for the HBE and VBE demands, this comparison was done using the following relationship:

$$\frac{M_u}{M_{u\_\alpha}} + \frac{P_u}{P_{u\_\alpha}} \leq 2 \tag{4-1}$$

where M_u and P_u are the moment and axial demands obtained from the LS-DYNA, and M_{u_α} and P_{u_α} are the moment and axial demands calculated with 35°, 40°, 45° and 50°, respectively, assuming that the columns and beams are rigidly framed and infinitely rigid (giving uniform forces applied at uniform angles along the VBEs and HBEs). For safety, the force demands calculated using a constant angle should not be less than those obtained from LS-DYNA. Ideally, the ratios of M_u/M_{u_α} and P_u/P_{u_α} should be less than or equal to 1 and their sum should be less than or equal to 2, but an acceptable solution could be also obtained if one of those two ratios is greater than one provided that the sum is less than 2. Note that a comparison of demands using actual interaction diagrams would also be possible, but the approach proposed above more explicitly illustrate the discrepancies in flexural and axial demands and how an underestimated demand for one can compensate for an overestimated demand for another.

The resulting ratios are listed in the Table 4-4. Note that the maximum moment reported in that table may occur at the ends or within the span of the boundary element; both cases are checked, with results corresponding to the latter case being represented by the italicized text in the Table 4-4. The percentage reported indicate by how much the results obtained with Equation 4-1 differ from the value of 2.

For example, for the top beam of Model A at 1% drift for example, when comparing the finite elements with the results obtained for a constant angle of 35°, results in Table 4-4 show that the maximum moment ratios at the beam ends and within the span are 0.908 and 0.950, respectively. Similarly, the maximum axial force ratios at the beam ends and within the span are 0.847 and 0.789. The sums of the ratios are 1.755 and 1.739, which are 12.260% and 13.015% smaller than 2, respectively.

Results in Table 4-4 also show that the results obtained for Model A and B are not significantly different from each other, with the difference being generally less than 4%, with some notable exceptions where the difference was more significant and reached 25.2%. Focusing on the results for Model B, which has rigid HRB to VBE connections and is deemed more representative of actual SPSWs, results in Table 4-4 indicate that, if a constant angle was to be used in calculations for the design of HBEs, it would be always conservative to use a constant angle of 35°, and generally conservative to use a constant angle of 45°, with a few of the obtained results being unconservative by no more than 5.436% (i.e., results for top beam at 3% drift). Results obtained using a constant angle of 50° are always unconservative, by 12% to 19%. In contrast, it would be always conservative to use a constant angle of 50°for the design of VBEs, and generally conservative to use a constant angle of 45°, with only one value being unconservative by merely 0.178% at 6% drift. Results obtained using a constant angle less than 45° are usually unconservative, by as large as 33.584% using 35° (i.e., results for left column at 6% drift). Therefore, from those results, it is found that while using a constant angle of 45° is sometimes slightly unconservative, designing HBEs and VBEs using this angle of 45° would be a good compromise if one desires to simplify the design process such as to use a single angle. The actual axial and flexural demands on the boundary elements can be individually quite different from the values obtained using this constant angle, but taken together, their relative conservatism and nonconservativeness somewhat cancels out.

Table 4-4 Combined moment-axial force demand analysis

			35°								40°							
		Drift	M_u/M_{u_α}		P_u/P_{u_α}		summary				M_u/M_{u_α}		P_u/P_{u_α}		summary			
Model A	top beam	1%	0.908	0.950	0.847	0.789	1.755	−12.260%	1.739	−13.051%	1.038	1.085	0.807	0.753	1.845	−7.740%	1.838	−8.103%
		3%	0.858	0.863	0.928	0.948	1.786	−10.681%	1.811	−9.473%	0.980	0.985	0.884	0.903	1.864	−6.809%	1.888	−5.613%
		6%	0.833	0.841	0.918	0.929	1.751	−12.448%	1.770	−11.488%	0.946	0.955	0.870	0.881	1.816	−9.189%	1.836	−8.206%
	left column	1%	1.052	1.187	0.828	0.718	1.880	−5.982%	1.905	−4.767%	0.837	0.945	0.790	0.684	1.627	−18.651%	1.629	−18.558%
		3%	1.623	1.659	0.918	0.932	2.542	27.087%	2.592	29.576%	1.290	1.319	0.875	0.888	2.165	8.262%	2.207	10.349%
		6%	1.796	1.821	0.880	0.877	2.676	33.786%	2.698	34.918%	1.421	1.440	0.834	0.831	2.254	12.714%	2.272	13.590%
Model B		**Drift**	M_u/M_{u_α}		P_u/P_{u_α}		summary				M_u/M_{u_α}		P_u/P_{u_α}		summary			
	top beam	1%	0.909	0.924	0.872	0.866	1.781	−10.960%	1.791	−10.473%	1.038	1.056	0.832	0.826	1.870	−6.496%	1.882	−5.886%
		3%	0.905	0.898	0.929	0.967	1.834	−8.298%	1.865	−6.759%	1.033	1.025	0.885	0.921	1.918	−4.096%	1.946	−2.699%
		6%	0.882	0.866	0.903	0.925	1.786	−10.722%	1.792	−10.418%	1.002	0.984	0.856	0.877	1.858	−7.090%	1.861	−6.952%
	left column	1%	1.341	1.466	0.861	0.911	2.202	10.078%	2.377	18.841%	1.067	1.167	0.821	0.868	1.888	−5.618%	2.035	1.750%
		3%	1.487	1.596	0.897	0.947	2.384	19.202%	2.543	27.158%	1.182	1.269	0.854	0.902	2.037	1.826%	2.171	8.547%
		6%	1.577	1.752	0.883	0.920	2.460	22.976%	2.672	33.584%	1.247	1.385	0.837	0.872	2.084	4.192%	2.257	12.872%

			45°								50°							
		Drift	M_u/M_{u_α}		P_u/P_{u_α}		summary				M_u/M_{u_α}		P_u/P_{u_α}		summary			
Model A	top beam	1%	1.218	1.274	0.795	0.741	2.013	0.664%	2.015	0.752%	1.474	1.541	0.807	0.753	2.281	14.061%	2.294	14.690%
		3%	1.149	1.156	0.870	0.889	2.020	0.991%	2.044	2.221%	1.391	1.399	0.884	0.903	2.276	13.777%	2.302	15.090%
		6%	1.110	1.121	0.857	0.868	1.967	−1.635%	1.988	−0.583%	1.345	1.358	0.871	0.882	2.216	10.799%	2.239	11.970%
	left column	1%	0.692	0.780	0.778	0.674	1.470	−26.521%	1.454	−27.280%	0.589	0.665	0.790	0.684	1.379	−31.038%	1.349	−32.534%
		3%	1.066	1.090	0.861	0.874	1.927	−3.638%	1.964	−1.811%	0.909	0.929	0.875	0.888	1.783	−10.829%	1.817	−9.166%
		6%	1.174	1.190	0.821	0.819	1.995	−0.256%	2.009	0.449%	1.001	1.015	0.834	0.832	1.836	−8.219%	1.847	−7.636%
Model B		**Drift**	M_u/M_{u_α}		P_u/P_{u_α}		summary				M_u/M_{u_α}		P_u/P_{u_α}		summary			
	top beam	1%	1.219	1.239	0.819	0.814	2.038	1.893%	2.053	2.660%	1.475	1.500	0.832	0.826	2.306	15.315%	2.326	16.295%
		3%	1.212	1.202	0.871	0.907	2.083	4.166%	2.109	5.463%	1.467	1.456	0.885	0.921	2.352	17.613%	2.377	18.836%
		6%	1.176	1.155	0.843	0.864	2.019	0.960%	2.018	0.925%	1.425	1.399	0.857	0.878	2.282	14.077%	2.277	13.833%
	left column	1%	0.882	0.964	0.808	0.855	1.690	−15.508%	1.819	−9.042%	0.751	0.821	0.821	0.868	1.572	−21.408%	1.690	−15.515%
		3%	0.976	1.048	0.841	0.888	1.818	−9.117%	1.936	−3.185%	0.832	0.893	0.854	0.902	1.687	−15.663%	1.796	−10.222%
		6%	1.030	1.145	0.824	0.859	1.855	−7.272%	2.004	0.178%	0.879	0.976	0.838	0.873	1.716	−14.177%	1.849	−7.540%

4.4 Summary

Analyses performed in this section considered two new LS-DYNA models, investigating how results change in the absence of plate cutout and when rigid HBE-to-VBE connections were used, compared to the results from the LS-DYNA model in Section 3. Details of the differences considered are listed in Table 4-1.

The same stress analyses conducted in Section 3 were repeated here for the new models. Although the two new models exhibited different stress variations compared to results obtained by the LS-DYNA model used in Section 3, comparison with design specified stress values generally led to the same conclusion as with the model in Section 3. For web plate, it was found to be conservative to use either a constant angle of 40° or 45°. For VBEs, it was found not conservative to use 40°, but using 45° would result in less difference between the design and actual stresses. However, using 45° is still not conservative at 6% drift, as shown in Figure 4-6c and Figure 4-7c. For HBEs, it was found that design stress value using 40° were approximately equal to actual stress, and that using 45° would be not conservative. However, those observations are based on comparing either axial force demands or flexural demands individually.

Combined moment-axial force demand analysis was introduced in this section. The combined moment-axial force demand ratio was defined to compare the forces obtained from the finite element analyses with those calculated using constant angle models, and to consider both the effect of axial and flexural demands. It was deemed to be a more reasonable criterion to compare results and investigate the consequence of using a constant inclination angle for boundary element design. Referring to Table 4-4, it is observed that the results obtained for Model A and B are not significantly different from each other. For the design of HBEs, it would be always conservative to use a constant angle of 35°, and generally conservative to use a constant angle of 45°. Results obtained using a constant angle of 50° are always unconservative. In contrast, for the design of VBEs, it would be always conservative to use a constant angle of 50°, and generally conservative to use a constant angle of 45°, with only one value being unconservative. Results obtained using a constant angle less than 45° are usually unconservative. Overall, it is found that using a constant angle of 45° would be a good compromise for the design of both VBEs and HBEs if one desires to simplify the design process such as to use a single angle.

SECTION 5
DESIGN OF REAL SPSWS

5.1 General

For the purpose of broadening the previous findings and studying how the inclination angle varies for SPSWs having different numbers of the story and aspect ratios, four real SPSWs were designed and analyzed. The usual strip model was used for the modeling of SPSWs and SAP2000 was used for analysis and for performing preliminary selection of the VBE sections and checking the sway mechanisms of the whole structure. The real SPSW design procedure and details of SAP2000 modeling are described in Section 5.2. Differences between real SPSW LS-DYNA models considered in this section and the models used in previous sections are compared in Section 5.3. The analysis results will be presented in Section 6.

5.2 Structure description and design of real SPSWs

5.2.1 Design information

Four real SPSWs were designed to have one bay width, 10 ft story height, and an aspect ratio of either 1.0 or 2.0, namely two single story SPSWs, and two three-story tall SPSWs. For simplicity, following the example provided in Purba and Bruneau (2010), irrespectively of the aspect ratio, the three-story SPSWs were subjected the same lateral load as the archetype SW320 described in that example, while the one-story SPSWs were then taken to have the same load as that of the third floor in that example. Story weight and design base shear for each archetypes are shown in Table 5-1.

Table 5-1 Story weight and lateral force

Archetype	Level	Story Weight, W_i (kips)	Lateral Force, F_i (kips)	Story Shear Force, V_i (kips)
SW11	1st Floor	380.83	91.44	91.44
SW12	1st Floor	380.83	91.44	91.44
SW31	3rd Floor(Roof)	380.83	91.44	91.44
	2nd Floor	351.60	56.28	147.73
	1st Floor	351.60	28.14	175.87
SW32	3rd Floor	380.83	91.44	91.44
	2nd Floor	351.60	56.28	147.73
	1st Floor	351.60	28.14	175.87

For the designs considered here, the yield strength of web plate and boundary elements were taken as 30 ksi and 50 ksi, respectively. Per the AISC Seismic Provision (2010), the required web plate thickness to resist story shear forces can be determined as follows:

$$\boldsymbol{t_{wi}} = \frac{\boldsymbol{V_{ni}}}{\boldsymbol{0.42 F_y L_{cf} sin2\alpha}} \tag{5-1}$$

$$tan^4\alpha = \frac{1+\frac{t_w L}{2A_c}}{1+t_w h\left(\frac{1}{A_b}+\frac{h^3}{360 I_c L}\right)} \tag{5-2}$$

where V_{ni} is the i-th shear strength; F_y is the web plate yield stress; L_{cf} is the clear distance between column flanges. α is taken as 40° at the beginning and updated after iterations. Here, no strength resistance factor was considered and the plate thickness calculated to resist 100% of the story shear force was used in subsequent calculations (instead of using actual available plate sizes), such as to not introduce overstrength in the boundary element design.

The web plate yield forces, applied to their boundary elements per capacity design principles, produced axial forces, shear forces, and moments on the VBEs and HBEs. Information on how these forces and moments were calculated, and their values for the various walls considered, is presented in Sections 5.2.2 and 5.2.3 for HBEs and VBEs, respectively.

5.2.2 HBE design

While the design of HBE and VBE sections in SPSWs would normally be accomplished by selecting the lightest members that satisfy demand-to-capacity ratio less than 1.0, here, to minimize overstrength of the boundary elements, members chosen were those that had demand-to-capacity ratio as close as possible to 1.0 without exceeding it. Since the axial force in HBE was not significant in this case, only the moment demand-to-capacity ratio was considered here. The distributed loads applied to the VBEs (ω_{yci} and ω_{xci}) and HBEs (ω_{ybi} and ω_{xbi}) were from the web plate yielding at the i-th story and determined per the following well know equations (Bruneau et al. 2011). Table 5-2 shows the detailed results for those values for the corresponding web plate thicknesses.

$$\omega_{xbi} = 1/2 F_y t_{wi} sin2\alpha \tag{5-3}$$

$$\omega_{ybi} = F_y t_{wi} (cos\alpha)^2 \tag{5-4}$$

$$\omega_{xci} = F_y t_{wi} (sin\alpha)^2 \tag{5-5}$$

$$\omega_{yci} = 1/2 F_y t_{wi} sin2\alpha \tag{5-6}$$

Table 5-2 Distributed loads from yield web plate

	Story	Angle	t_w in	ω_{xbi} kip/in	ω_{ybi} kip/in	ω_{xci} kip/in	ω_{yci} kip/in
SW11	1	42.25	0.071	1.0488	1.2499	0.8801	1.0488
SW12	1	44.57	0.036	0.5318	0.6338	0.4462	0.5318
SW31	3	42.45	0.071	1.0488	1.2499	0.8801	1.0488
	2	40.79	0.115	1.6988	2.0245	1.4255	1.6988
	1	39.25	0.141	2.0829	2.4823	1.7477	2.0829
SW32	3	44.31	0.036	0.5464	0.5598	0.5334	0.5464
	2	43.77	0.059	0.8878	0.9267	0.8505	0.8878
	1	43.89	0.072	1.0792	1.1217	1.0383	1.0792

Here, assuming a symmetric distribution of loads along the HBEs, the axial force from the horizontal component of the web plate yield stress, ω_{xb}, along the HBEs, is calculated as:

$$P_{bli} = -(\omega_{xbi} - \omega_{xbi+1})\frac{L}{2} + P_{si} \tag{5-7}$$

$$P_{bri} = (\omega_{xbi} - \omega_{xbi+1})\frac{L}{2} + P_{si} \tag{5-8}$$

where P_{si} is the HBE axial forces from the horizontal component of web plate yield stress on the VBEs, and estimated as:

$$P_{si} = \omega_{xci}\frac{h_i}{2} + \omega_{xci+1}\frac{h_{i+1}}{2} \tag{5-9}$$

The moment component for each HBE results from the vertical component of the web plate yield stress, ω_{yb}. The reduced plastic moments at the left and right HBE ends, M_{prl} and M_{prr}, are also calculated using the following equations, the detailed results is shown in Table 5-3:

$$M_{ui} = \frac{(\omega_{ybi} - \omega_{ybi+1})L^2}{4} \tag{5-10}$$

$$M_{prri} = Min[1.18\left(1 - \frac{|P_{bri}|}{P_y}\right)M_p, M_p] \tag{5-11}$$

$$M_{prli} = Min[1.18\left(1 - \frac{|P_{bli}|}{P_y}\right)M_p, M_p] \tag{5-12}$$

Table 5-3 HBE end actions and selected sections

	HBE	Section	P_s kips	P_{bl} kips	P_{br} kips	V_{bl} kips	V_{br} kips	Mu kip-ft	A_g in^2	M_p kip-ft	M_{prl} kip-ft	M_{prr} kip-ft	Ratio
SW11	1	W12×65	-57.772	-121.377	5.834	142.628	2.572	350.142	19.1	363.000	363.000	363.000	0.96
SW12	1	W18×86	-31.910	-96.703	32.882	135.530	3.970	657.795	25.3	697.500	697.500	697.500	0.94
SW31	3	W12×65	-63.646	-121.855	5.437	142.191	3.009	347.953	19.1	395.062	363.000	363.000	0.96
	2	W14×48	-146.557	-185.296	-107.818	104.022	5.899	245.309	14.1	299.289	255.739	293.864	0.96
	1	W14×38	-189.931	-211.895	-167.967	69.532	2.404	167.820	11.2	215.645	169.165	190.512	0.99
	0	W18×97	-101.584	124.349	-124.349	310.466	6.034	761.082	28.5	866.363	791.250	791.250	0.96
SW32	3	W18×76	-32.001	-97.569	33.567	135.065	0.713	671.760	22.3	678.889	678.889	678.889	0.99
	2	W14×61	-83.033	-124.001	-42.065	86.584	-1.472	440.280	17.9	425.556	425.556	425.556	1.00
	1	W12×45	-113.331	-136.299	-90.363	49.300	2.500	234.000	13.1	267.778	250.226	267.778	0.94
	0	W24×117	-62.299	129.504	-129.504	271.271	2.063	1346.040	34.4	1366.667	1366.667	1366.667	0.98

5.2.3 VBE design and SAP2000 modeling

The capacity design procedure was applied on the VBE design with the aid of the SAP2000 program. The strip model was adopted to simulate the web plate of SPSW, as shown in Figure 5-1a and b. The model used for this purpose consisted of twelve tension strips, pin-ended and inclined in the alpha direction with vertical axis. Regular frame elements and the idealized elasto-perfectly plastic strain-stress material (See Figure 5-1c) were used for boundary elements and strips. Since the strips were designed to subject tensile force only, compression limit with zero value was assigned to each of them.

Fiber P-M2-M3 hinges were used to capture the plastic behavior of both the strip and the HBEs (but were not used to model the VBEs because the VBEs were intended to remain elastic). Based on findings and recommendations from the case study on the desirable numbers of fibers in boundary elements by Purba and Bruneau (2010), here the W-shaped sections used for HBEs at the plastic hinge locations were sliced into 59 fibers, including 13 fibers in the flange and 33 fibers in the web, as shown in Figure 5-1d. Each HBE had hinges at their ends having a relative hinge length equal to 1% of the beam length. The fiber hinge for the strip model, because they were only subjected to axial loads, consisted of only 9 fiber layers. Each strip had the axial fiber hinge located at its midpoint.

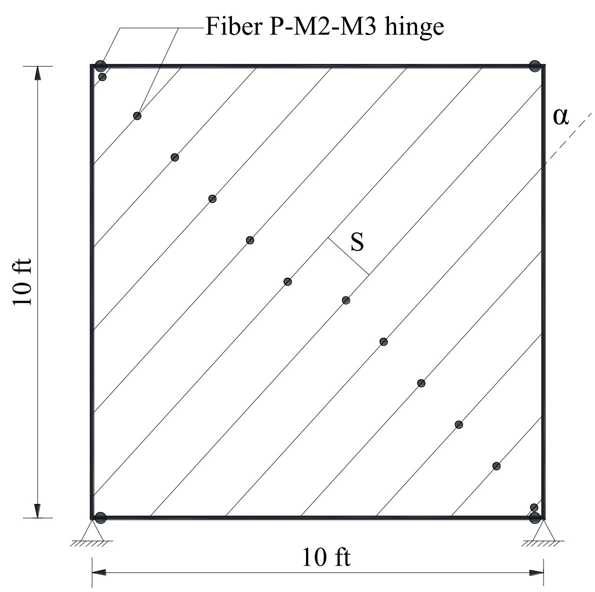

a.

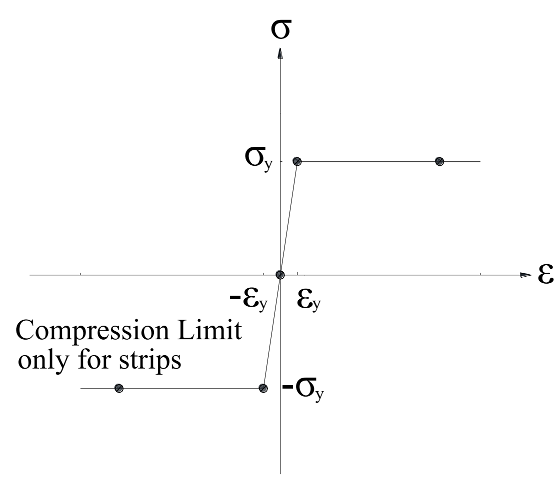

c.

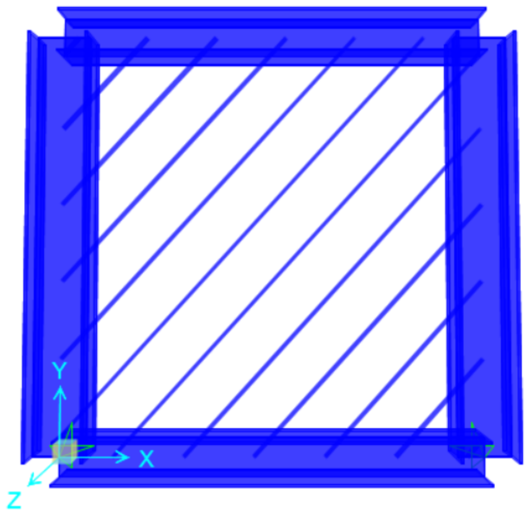

b.

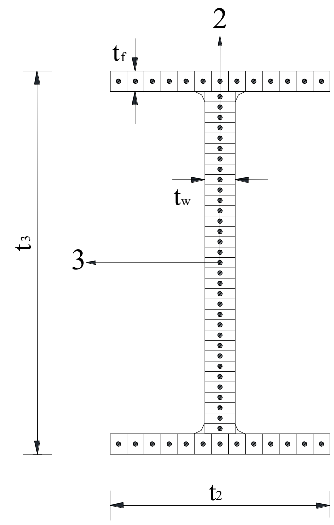

d.

Figure 5-1 Example strip model and material model in SAP2000: (a) 2D strip model; (b) 3D strip model; (c) material model; (d) Fiber hinge of the W-shaped section

In the pushover analysis, the data were obtained from the points of strip yielding and hinge development. The maximum force demands of a VBE may occur at either of its two ends or within the span itself. Since each floor has two VBEs, the force demands and demand-to-capacity ratio of the VBE reported in the subsequent table correspond to the maximum value obtained for these two VBEs. The resulting forces and selected sections are listed in Table 5-4. The detailed information of each SPSW is presented in Figure 5-2 and Figure 5-3.

Table 5-4 VBE end actions and selected sections

	VBE	Section	P_{cl} kips	P_{cr} kips	M_{cl} kip-ft	M_{cr} kip-ft	A_g in^2	P (kip^{-1})	b $(kip\text{-}ft^{-1})$	P_n kip-ft	M_p kip-ft	Ratio
SW11	1	W16×89	180.915	448.234	381.536	389.565	26.2	0.00101	0.00138	990.099	644.122	0.99
SW12	1	W21×111	123.656	394.955	766.588	764.853	32.6	0.000771	0.00085	1297.017	1045.752	0.95
SW31	3	W18×76	180.691	334.244	382.977	396.345	22.3	0.00116	0.00148	862.069	600.601	0.97
	2	W21×111	38.165	952.937	399.260	292.897	32.6	0.000771	0.00085	1297.017	1045.752	0.98
	1	W27×178	41.719	1450.484	867.352	860.065	52.5	0.000473	0.000416	2114.165	2136.752	1.00
SW32	3	W18×106	179.542	324.949	667.225	672.937	31.1	0.000828	0.00104	1207.729	854.701	0.97
	2	W21×122	211.469	754.645	388.568	548.274	35.9	0.000701	0.000772	1426.533	1151.410	0.95
	1	W27×194	255.724	1104.285	1344.978	1342.068	57.2	0.000433	0.000376	2311.896	2364.066	0.98

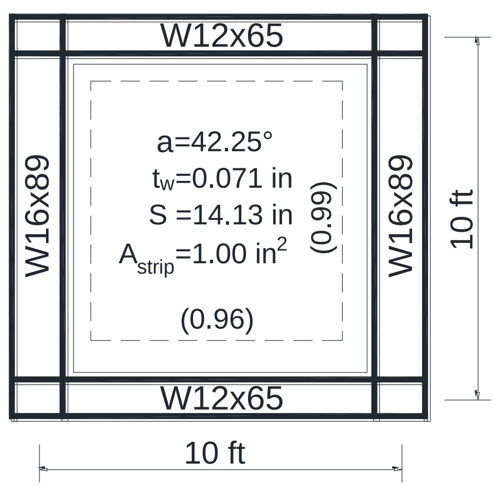

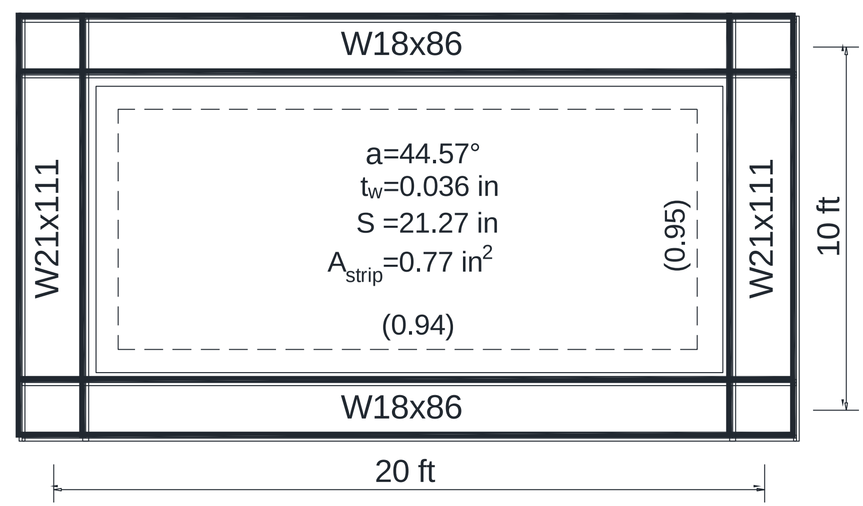

Figure 5-2 One-story SPSW elevations: (a) one-story SPSW w/ aspect ratio of 1.0; (b) one-story SPSW w/ aspect ratio of 2.0

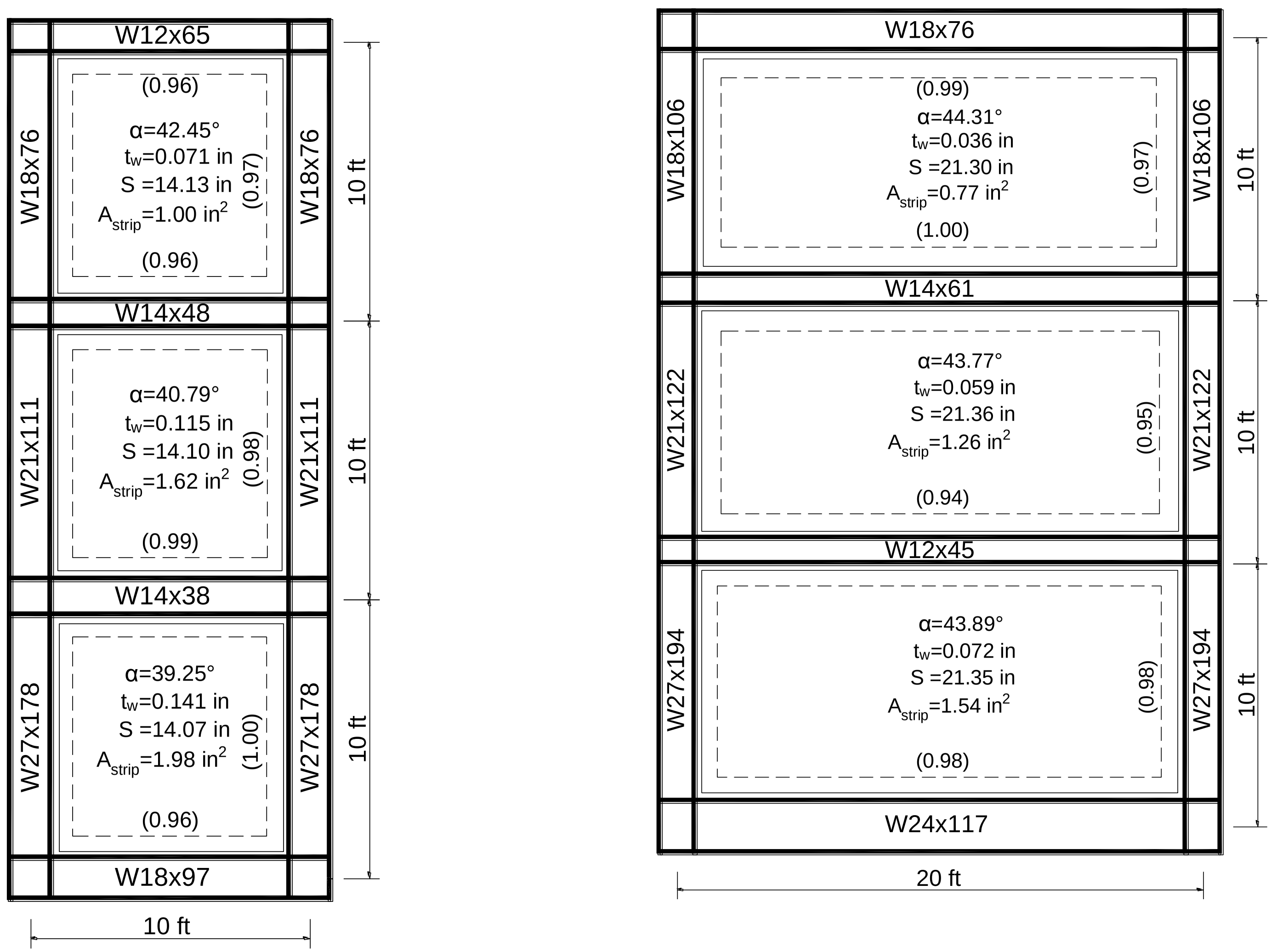

Figure 5-3 Three-story SPSW elevations: (a) three-story SPSW w/ aspect ratio of 1.0; (b) three-story SPSW w/ aspect ratio of 2.0

5.3 LS-DYNA model description of four real SPSWs

New LS-DYNA models were built for the four real SPSWs. Different from the models in SECTION 3 and 4, the new models consisted of three-dimensional boundary elements which is more representative of real SPSWs. The HBEs were rigidly connected with VBEs by merging the nodes at the same coordinate. As seen from Figure 5-4 Figure 5-5, all panel zones were defined as rigid body with respect to a nodal point at their mass centers (e.g., Point A). The nodal points of the two bottom panel zones were pin-supported on the ground by using the NODAL RIGID BODY and BOUNDARY_PRESCRIBED MOTION RIGID. BOUNDARY_PRESCRIBED_MOTION_RIGID was defined with a zero-valued load curve for all translational degrees of freedom, so that the panel zone could only rotate with respect to this point. In addition, z-constraints (z is in the direction normal to the web plate) were applied to the flange plate edge nodes of the upper panel zones, to constrain the SPSW to move within x-y plane. In addition, the HBE ends, over a length equal to approximately one-sixth of the span length, were modeled with a more refined mesh to better capture the non-linear inelastic behavior of the plastic hinges at those locations.

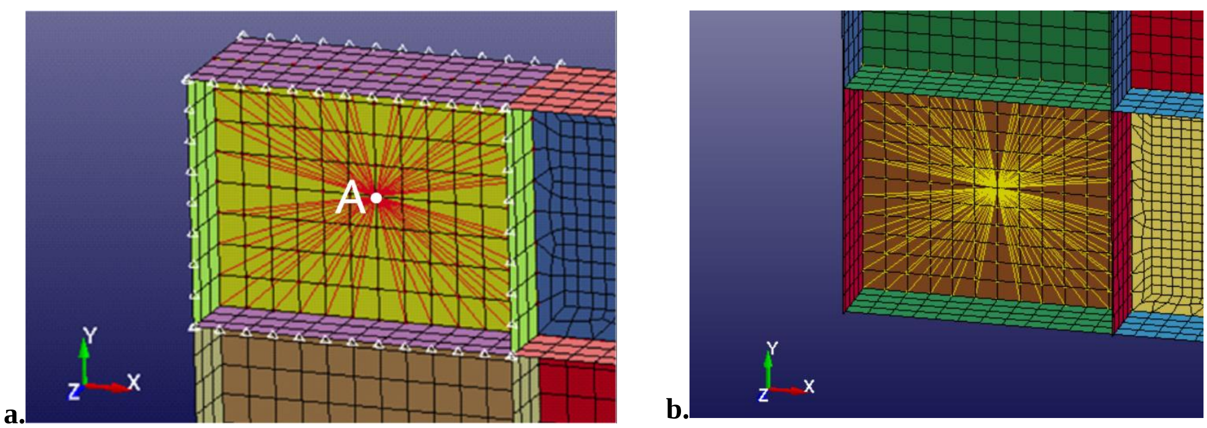

Figure 5-4 Boundary conditions and constraints: (a) The z-constraint; (b) Pin Support

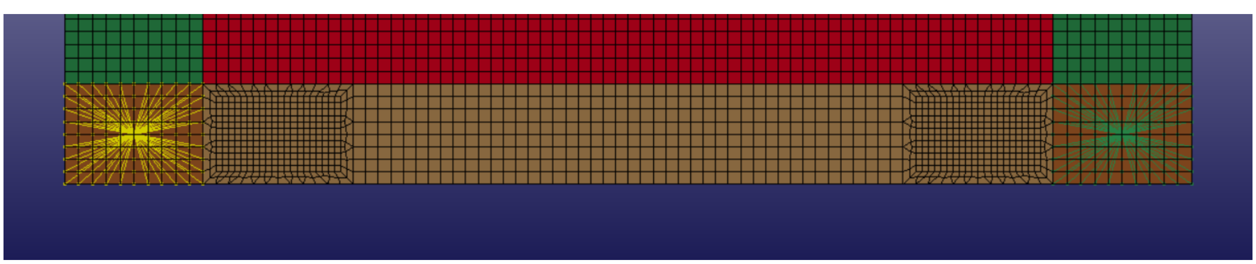

Figure 5-5 Refined mesh at the HBE ends

Figure 5-6 plots the values for material model presented previously from Table 3-1 (obtained from the coupon test in Webster et al. (2014) and converted into normalized values), which is also used in this section. The key values for different members were presented in Table 5-5.

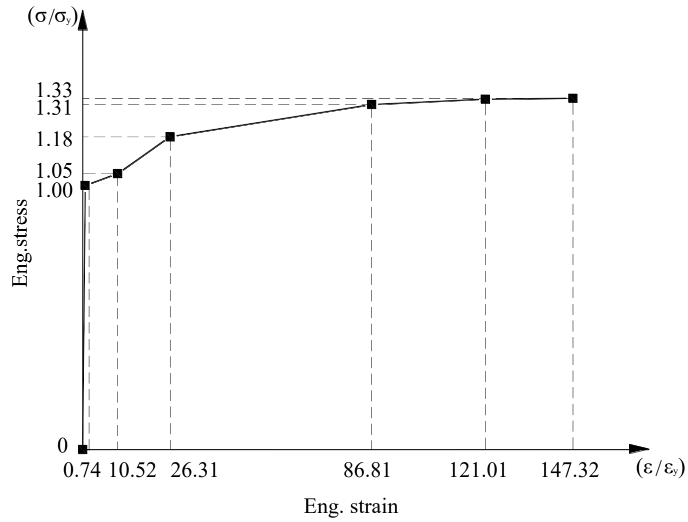

Figure 5-6 Material model from Webster et al. (2014)

Table 5-5 Material models of the real SPSW in LS-DYNA

Member		Point 1	Point 2	Point 3	Point 4	Point 5	Point 6	Point 7
Web	Eng. Strain	0	0.0008	0.0109	0.0272	0.0898	0.1252	0.1524
	Eng. Stress (ksi)	0	30.0000	31.3589	35.5401	39.1986	39.8258	39.9303
	True Strain	0	0.0008	0.0108	0.0269	0.0860	0.1179	0.1418
	True Stress (ksi)	0	30.0229	31.7002	36.5072	42.7189	44.8113	46.0156
	Effective Plastic Strain	-	0.0000	0.0101	0.0261	0.0852	0.1172	0.1411
HBE and VBE	Eng. Strain	0	0.0013	0.0181	0.0454	0.1497	0.2086	0.2540
	Eng. Stress (ksi)	0	50.0000	52.2648	59.2334	65.3310	66.3763	66.5505
	True Strain	0	0.0013	0.0180	0.0444	0.1395	0.1895	0.2263
	True Stress (ksi)	0	50.0635	53.2130	61.9201	75.1095	80.2250	83.4540
	Effective Plastic Strain	-	0.0000	0.0167	0.0431	0.1382	0.1882	0.2251

Note that node merging requires nodes from one part to share identical coordinates with those of another part. However, here, different flange widths of VBEs and HBEs resulted in different meshes, as shown by the arrows in Figure 5-7a. To simplify the modeling and avoid iterations of mesh size, the actual cross-sections were converted into equivalent cross-sections over the three-story SPSW models. Two principles were followed for that purpose: (1) As for the VBE, the equivalent section was sized to have identical height, shear, and moment capacity as the original section, in order to avoid the premature yielding of the web by shear, and; (2) The flange width of HBE was converted to align with the mesh of VBE without changing its flange area.

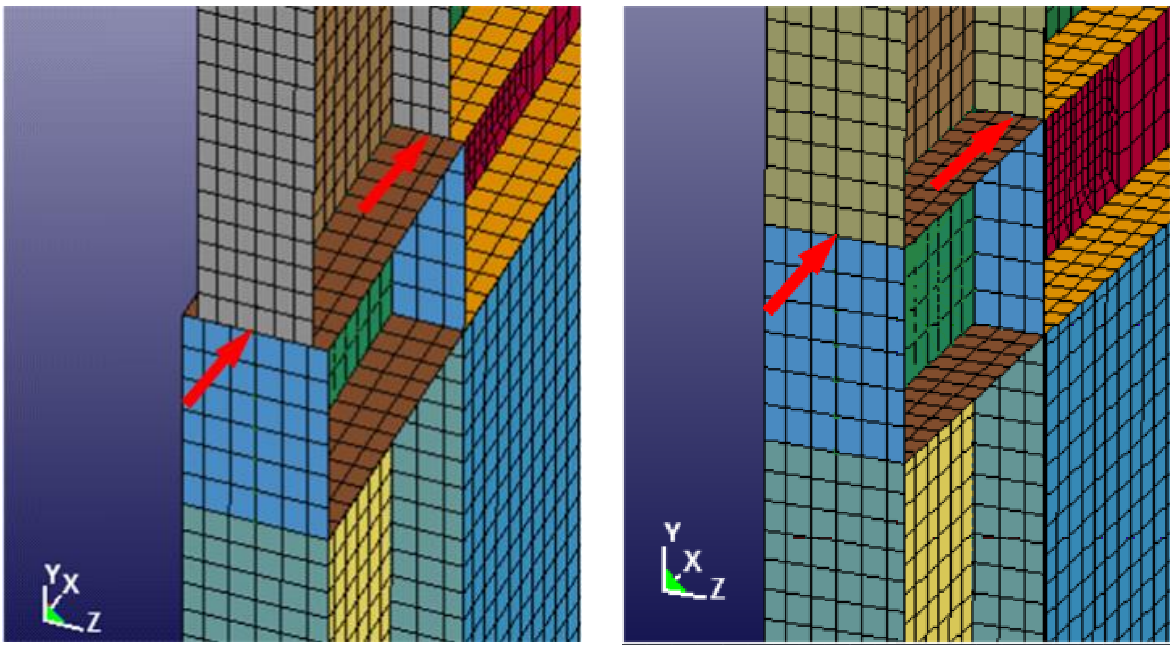

a. Before section conversion **b. After section conversion**

Figure 5-7 Section conversion applied for three-story SPSWs

Four real SPSWs were studied under monotonic loading. For the SW11, both force control and displacement control were done for comparison. In the former case, a load was applied to each node along the middle height of the top beam, while for the latter, the displacement of the nodal point in the upper right panel zone was controlled. Since the displacement-control was found to achieve a better performance on the convergence, it was eventually used for all the finite element models final analyses. These will be discussed in the following section.

5.4 Summary

Four real SPSWs with different aspect ratios and numbers of stories were designed and subjected to the same loads as those applied to a reference SPSW (called SW320) in Purba and Bruneau (2010). For these designs, the web plate thicknesses were calculated to resist 100% of their story shear force. HBE design followed the procedure in Bruneau et al (2011). Note that only the moment demand-to-capacity ratio was considered in HBE design due to the insignificant axial forces in the HBEs in these cases. Strip models were built in SAP2000 to assist the VBE design and check the sway mechanism of the whole structure.

Additionally, LS-DYNA models were developed for the additional SPSWs considered here and compared with the LS-DYNA models in Section 3 and 4. In particular, they were constructed with three-dimensional boundary elements. The mass centers of the two bottom panel zones were pin-supported on the ground and the flange plate edge nodes of the upper panel zones were fixed in the direction normal to the web plate (to laterally restrain the models). To better capture the plastic hinge performance, a refined mesh was applied to the ends of the HBE. Some cross-section simplifications were made to create both equivalent HBEs and VBEs in the three-story SPSW cases to facilitate modeling. Results from the finite element analyses conducted using the above models are presented in Section 6.

SECTION 6
ANALYSIS OF FOUR REAL SPSWS

6.1 General

This section presents and analyzes the results for SW11, SW12, SW31 and SW32 designed in Section 5, where the first number and the second number refer to the number of stories and the aspect ratio, respectively. Detailed results from the LS-DYNA analyses of these four SPSWs are presented in Sections 6.2 to 6.5, including results on inclination angles and combined moment-axial force demands. Additional information on the loading control and deformation of the top HBE of the SW11 is also included in Section 6.2. The influence of aspect ratio and the number of stories is addressed in Section 6.6. Based on these results and analyses, an optimum inclination angle is proposed for SPSW design.

6.2 Analyses of SW11

6.2.1 Force control and displacement control comparison

As mentioned in SECTION 5, both displacement control (displacing the right-most rigid panel as shown in Figure 6-1) and force control (applying a uniformly distributed load to the centerline of the HBE, as shown in Figure 6-2) were applied on SW11 to investigate the consequence of these two approaches to push-over analysis on the obtained results. The load-drift curves obtained for the different control methods are plotted in Figure 6-3. To be consistent with the analyses in SECTION 3 and SECTION 4, 6% drift was the maximum drift considered here. Though the force-control curve only could provide results up to a drift 3.2%, it almost overlaps with the displacement-control curves over the range of available results. Figure 6-4 shows that the inclination angle curves obtained from displacement control and force control also agree well. Note that a slight difference is observed from top beam curves in the early stage, which can be attributed to sequential yielding in diagonal tension field of the web plate under different loading methods. In view of above observations and its ability to provide results up to greater drifts, displacement control was deemed to be the better method and was applied for all the real SPSW finite element models.

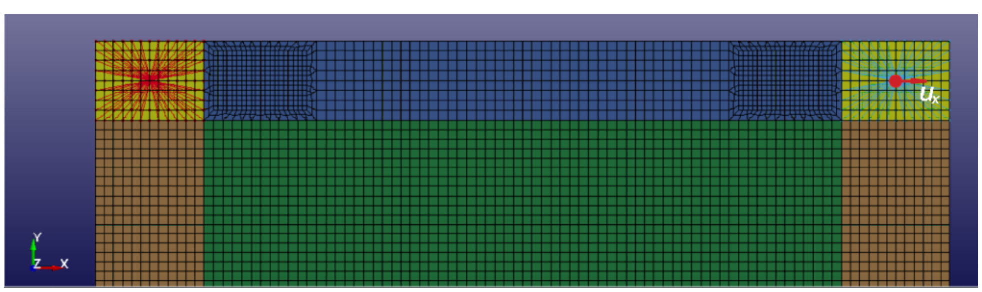

Figure 6-1 Displacement-control loading

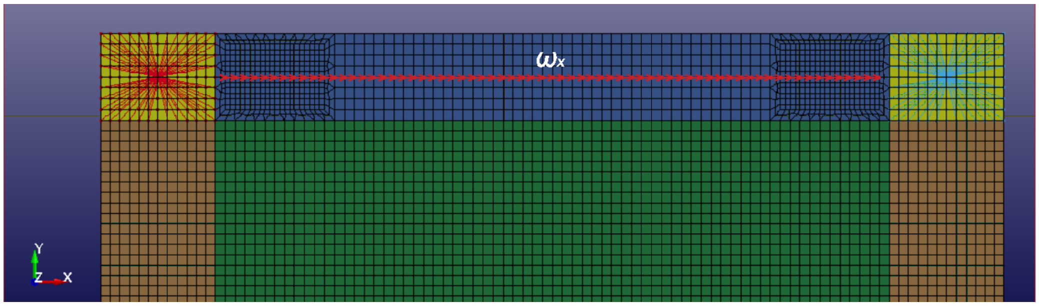

Figure 6-2 Force-control loading

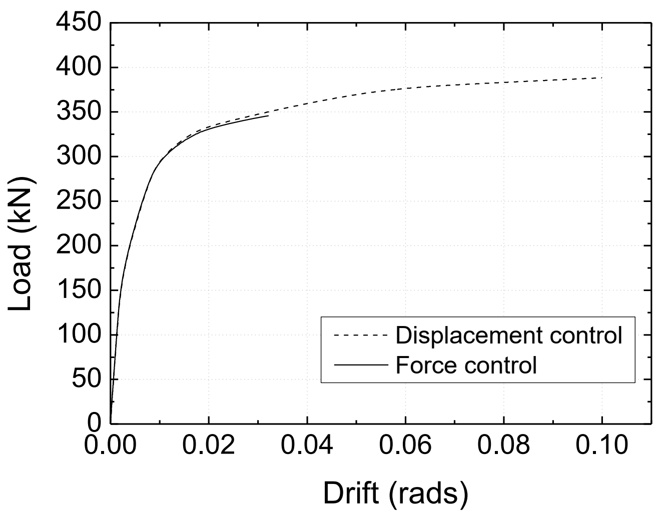

Figure 6-3 Load-drift curves comparison between force control and displacement control

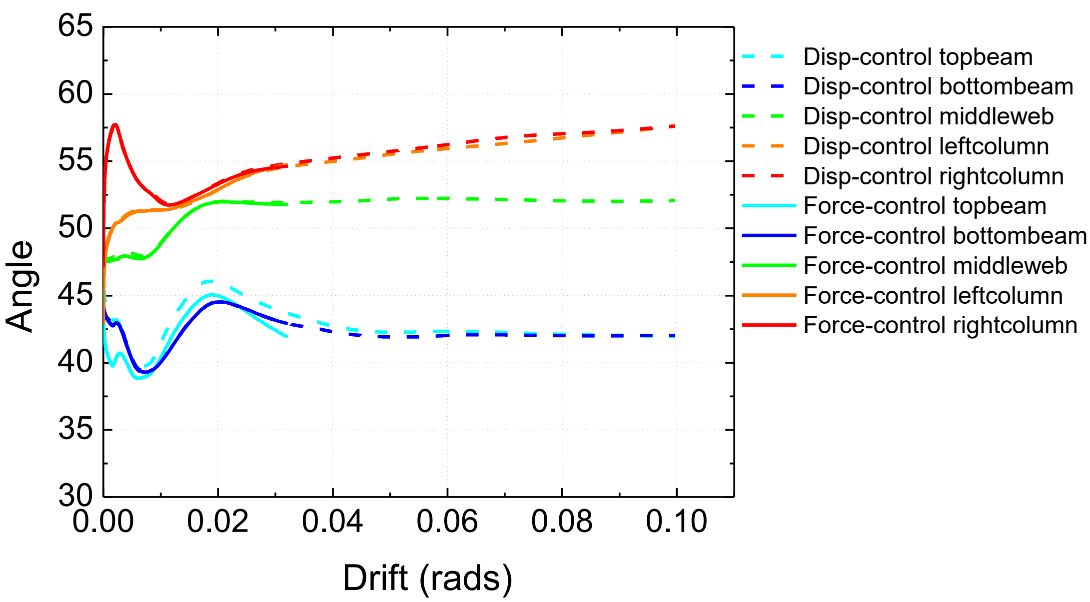

Figure 6-4 Inclination angle comparison between force control and displacement control

6.2.2 Inclination angle analysis of SW11

Figure 6-4 shows the overall trend in the variation of the inclination angle as a function of drift for SW11, which is quite similar to the inclination angle curve shape of Model B observed in Figure 4-1, but with values generally higher than those of Model B. For example, for the right column, results fluctuate noticeably for drifts lower than 2% drift, but remain higher than 50°, and at 6% drift, the inclination angle reaches 56° in SW11 compared to 50° in Model B. For web plate and beams, the average inclination angles of SW11 reach up to approximately 52° for the web plate and 42° for the beams at 6% drift, compared to the 45° for web plate and 37° for the beams in Model B. The observed fluctuations in the beam results at lower drifts were deemed to be due to the deflections of HBE; this was investigated and findings are reported in the subsequent section.

6.2.3 Deformation of the top HBE

To study the cause of the above fluctuations in results at lower drifts, a few critical drifts for response in the results obtained with the LS-DYNA model were first determined and analyzed. In view of symmetry, only results for the top beam are discussed here. Von-Mises stress contours of Model SW11 for each selected drifts are shown in Figure 6-5. It is found that these drifts correspond to the development of web yielding and plastic hinging at the right and left ends of the HBE, at around 0.2%, 0.9% and 2%, respectively.

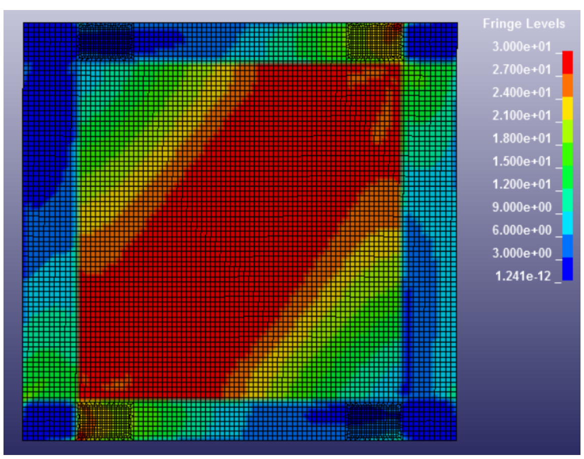

a. Von-Mises stress contour at 0.2% drift

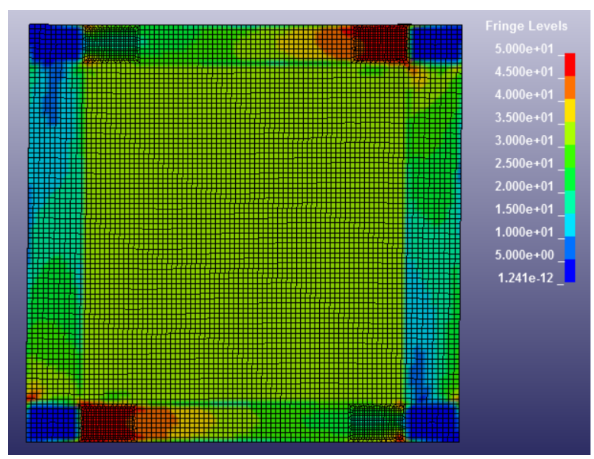

b. Von-Mises stress contour at 0.9% drift

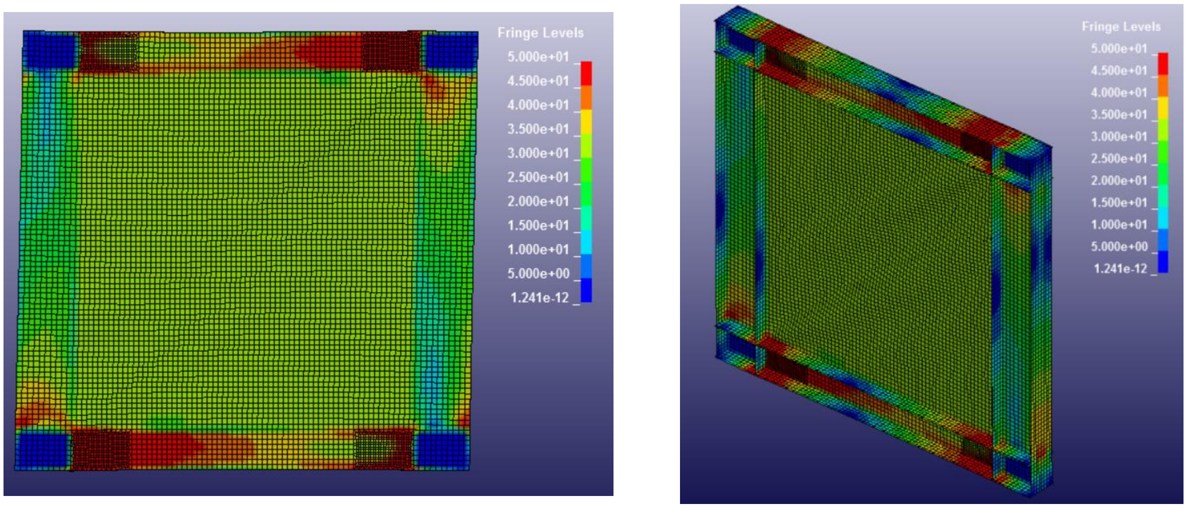

c. Von-Mises stress contour at 2.0% drift

Figure 6-5 Von-Mises stress contours of Model SW11 at three critical drifts

To investigate how those fluctuations possibly relate to the plastic response of HBE, the deflections of the HBE obtained directly from LS-DYNA at different drifts are plotted in Figure 6-7a. For comparison, also plotted in Figure 6-8a are the calculated deflections from the SAP2000 model where the HBE was deem to be a simple beam and subjected to ends moments and distributed loads obtained from the SAP2000 at the corresponding selected drifts, defined in Figure 6-6.

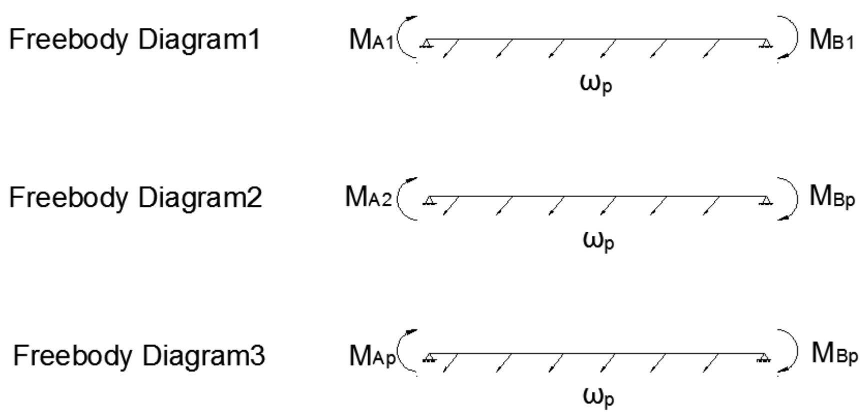

Figure 6-6 Forces in each selected drift from the SAP2000

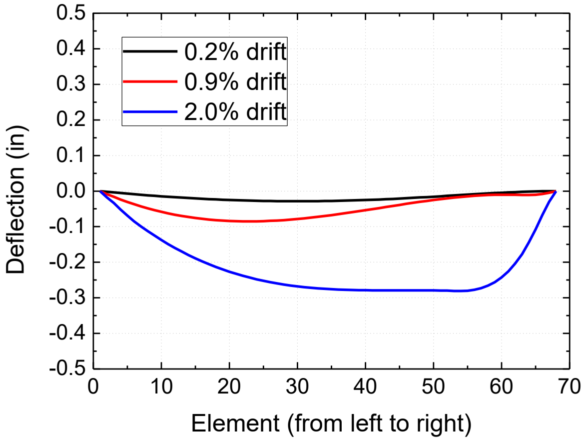

a. The deflection of top beam in LS-DYNA model

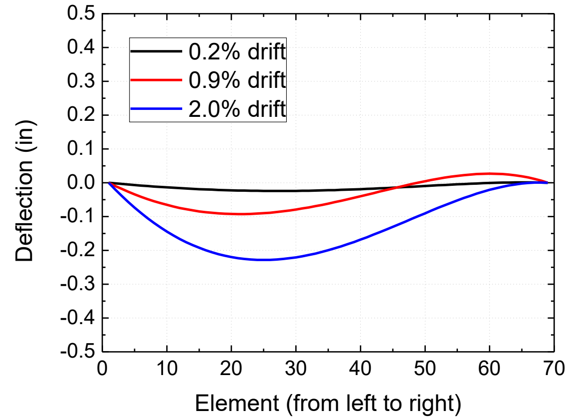

a. The deflection of top beam in SAP2000 model

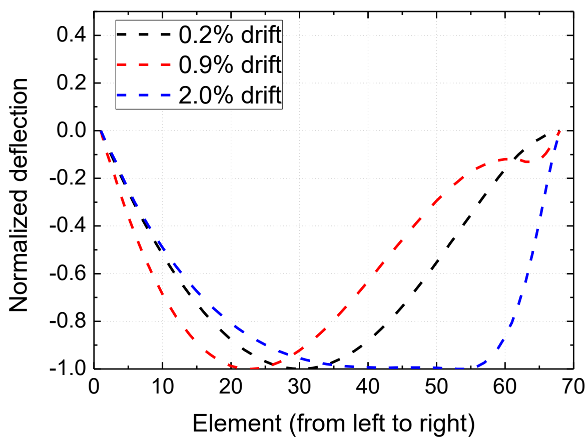

b. The normalized deflection in LS-DYNA model

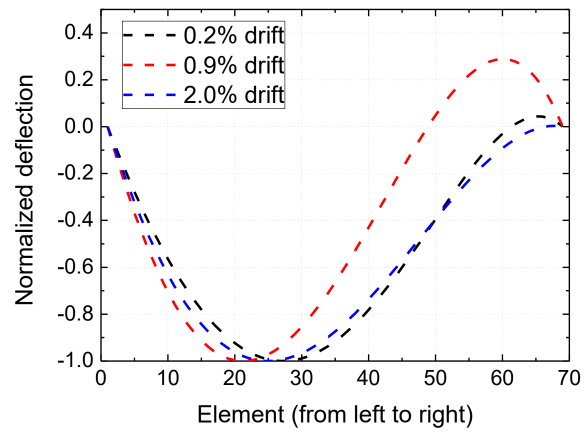

b. The normalized deflection in SAP2000 model

Figure 6-7 The real and normalized deflection of top beam for SW11 in LS-DYNA model

Figure 6-8 The real and normalized deflection of top beam for SW11 in SAP2000 model

Comparing Figure 6-7a and Figure 6-8a, the amplitudes of the deflections at drifts of 0.2% and 0.9% from LS-DYNA and SAP2000 models are close to each other, whereas the deflection at 2% drift from LS-DYNA model exhibits a larger amplitude. To better compare the curve shape, each curve was normalized by its maximum deflection, as shown in Figure 6-7b and Figure 6-8b. It is found that the normalized deflection obtained from LS-DYNA at 0.9% drift do not exhibit a positive segment near the right end of the beam, contrary to what is observed in the SAP2000 results. More significantly, though, it is observed that the maximum deflection of the curve obtained with LS-DYNA at 2% drift is located over a certain length of the HBE instead of being reached at a single point, which suggests that not only flexure but other factors may also contribute to the deflected shape.

In general, the moment, shear, and rotation of the panel zones would contribute to the total beam deflection. Given that the effect of flexure is already accounted for in the deflected shape calculated by SAP2000, the difference in results with LS-DYNA arises from the effect of shear and rotation of the panel zones. Here the panel zone was defined as rigid in LS-DYNA and the rotation of rigid panel zone in this case cannot lead to the large negative y-displacement at the HBE right end. So the shear deformation was deemed likely to be responsible for this observation. Note that inelastic shear deformations cannot be considered in SAP2000, which may explain the difference. To investigate if inelastic shear strains developed, the shear strain at several typical locations near the ends of the beam obtained from the LS-DYNA model are compared to the yield strain (in dash line) in Figure 6-9. It is observed that when drifts reach approximately 1% drift, the shell elements near the right end of the top HBE apparently reach the yield strain, which confirm the shear deformations are considerable at the right end of the beam and have contributed to the total deflection of that top HBE.

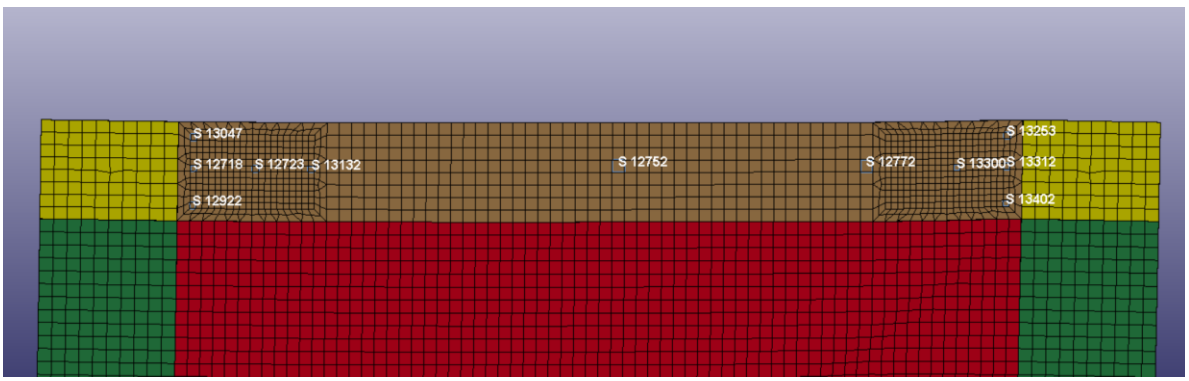

a. Locaion of shell elements for shear strain output

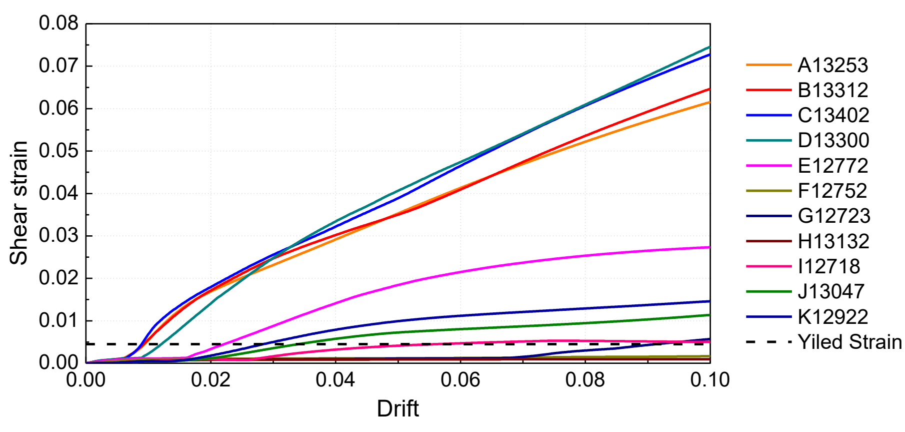

b. Shear strain-drift curve

Figure 6-9 The location and shear strain of the shell elements in the top beam

6.2.4 Combined moment-axial force demand analysis of SW11

Table 6-1 shows the combined moment-axial force demand analysis results for SW11. The shaded parts indicate those results for which the combined moment-axial force demand ratio is always conservative. Results obtained for the top HBE indicate that, when comparing demands obtained from simple analyses considering a constant angle of inclination for the strips with the actual demands obtained from finite element analysis, results obtained from an analysis considering constant angles ranging from 35° to 45° will always be conservative. It is also found that several demand ratios obtained using a constant angle of 50° are unconservative, by up to 10.6% (i.e., for top beam at 1% drift). As for design of the left VBE, none of the results using constant angles can ensure conservatism when compared to finite element results for all the drifts considered. For example, for a constant angle of 45°, two-thirds of the demand ratios for the left VBE are greater than 2 by at least 8%, with a maximum demand ratio of 2.197, which is unconservative by 9.9%. For the left VBE, using a constant angle of 50° would best match results from finite element analyses, with demands ratios exceeding 2.0 by no more than 1.1%.

Table 6-1 Combined moment-axial force demand ratio of SW11

			35 °							
SW11		**Drift**	**$M_u/M_{u-35°}$**		**$P_u/P_{u-35°}$**		**summary**			
	top beam	**1%**	0.736	*0.772*	0.910	*1.008*	1.646	-17.699%	*1.780*	*-11.017%*
		3%	0.680	*0.696*	0.922	*0.950*	1.602	-19.879%	*1.646*	*-17.710%*
		6%	0.708	*0.731*	0.950	*1.008*	1.658	-17.087%	*1.738*	*-13.075%*
	left column	**1%**	1.751	*1.778*	0.958	*1.014*	2.709	35.426%	*2.792*	*39.600%*
		3%	1.949	*1.951*	0.959	*0.971*	2.908	45.413%	*2.922*	*46.086%*
		6%	2.037	*2.034*	0.939	*0.945*	2.976	48.786%	*2.980*	*48.983%*
			40 °							
		Drift	**$M_u/M_{u-40°}$**		**$P_u/P_{u-40°}$**		**summary**			
	top beam	**1%**	0.841	*0.881*	0.868	*0.961*	1.708	-14.590%	*1.842*	*-7.883%*
		3%	0.776	*0.794*	0.877	*0.904*	1.653	-17.348%	*1.697*	*-15.136%*
		6%	0.801	*0.827*	0.842	*0.893*	1.644	-17.815%	*1.720*	*-13.978%*
	left column	**1%**	1.393	*1.415*	0.913	*0.966*	2.306	15.282%	*2.381*	*19.042%*
		3%	1.548	*1.549*	0.912	*0.924*	2.460	23.006%	*2.473*	*23.637%*
		6%	1.606	*1.604*	0.887	*0.893*	2.493	24.630%	*2.497*	*24.836%*
			45 °							
		Drift	**$M_u/M_{u-45°}$**		**$P_u/P_{u-45°}$**		**Summary**			
	top beam	**1%**	0.986	*1.034*	0.854	*0.946*	1.840	-7.980%	*1.980*	*-0.993%*
		3%	0.909	*0.930*	0.863	*0.889*	1.773	-11.365%	*1.820*	*-9.020%*
		6%	0.938	*0.968*	0.827	*0.876*	1.764	-11.792%	*1.844*	*-7.781%*
	left column	**1%**	1.150	*1.169*	0.899	*0.951*	2.049	2.464%	*2.120*	*5.991%*
		3%	1.278	*1.279*	0.898	*0.909*	2.175	8.770%	*2.188*	*9.384%*
		6%	1.322	*1.321*	0.871	*0.876*	2.193	9.648%	*2.197*	*9.864%*
			50 °							
		Drift	**$M_u/M_{u-50°}$**		**$P_u/P_{u-50°}$**		**Summary**			
	top beam	**1%**	1.194	*1.252*	0.868	*0.961*	2.062	3.076%	*2.213*	*10.640%*
		3%	1.102	*1.127*	0.877	*0.904*	1.979	-1.049%	*2.031*	*1.539%*
		6%	1.138	*1.175*	0.842	*0.893*	1.981	-0.973%	*2.068*	*3.410%*
	left column	**1%**	0.981	*0.996*	0.913	*0.966*	1.894	-5.322%	*1.962*	*-1.887%*
		3%	1.090	*1.090*	0.912	*0.924*	2.002	0.106%	*2.014*	*0.724%*
		6%	1.130	*1.129*	0.887	*0.893*	2.017	0.874%	*2.022*	*1.108%*

6.3 Analyses of SW12

6.3.1 Inclination angle analysis of SW12

Figure 6-10 shows the inclination angle variation-drift relationship for SW12. It also can be seen from this plot that fluctuations initially occur within 2% drift, after which the angles smoothly increase up to the maximum drift considered. Note that some different fluctuation patterns are observed in SW12. Both left and right columns start with a jump to approximately 58° and 62°, respectively, and decrease around 52° at 1.5% drift. The middle web curve also jump to as high as 53° and decrease, but reaches a second lower peak value at 1.5% drift by 51°. For the top and bottom beams, the curves drop until 1.5% drift, at which point the values temporarily fluctuate (i.e., increase before decreasing again). Compared to SW11, the inclination angles of the middle web and beams obtained beyond 2% drift are lower in SW12, while those in the columns have similar values.

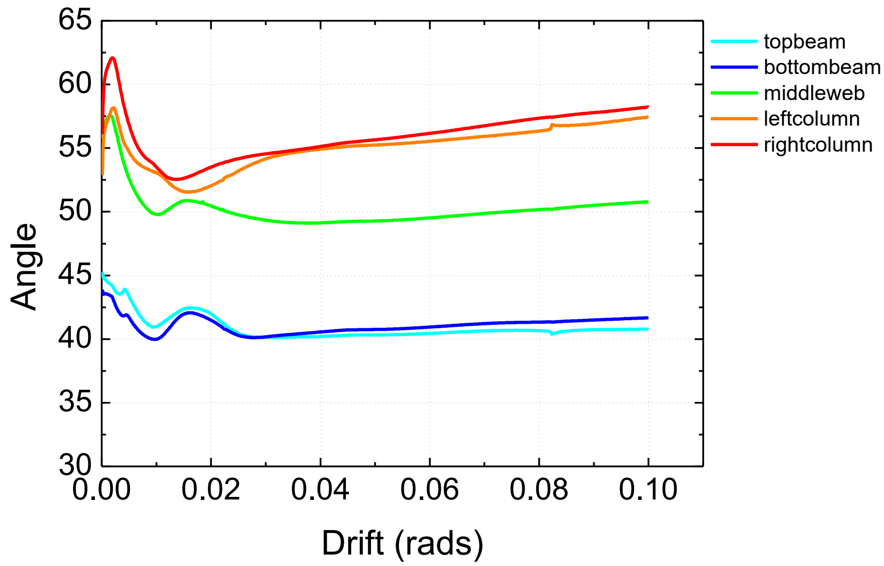

Figure 6-10 Inclination angle variation of SW12

6.3.2 Combined moment-axial force demand analysis of SW12

Results in Table 6-2 for SW12 show that using constant angles ranging from 35° to 45° would be always conservative for the design of HBEs. Using constant angle of 50° would be unconservative at all drifts, by up to 11.6% (for the top beam at 6% drift). For the VBE, using constant angles ranging from 35° to 45° would lead to unconservative designs. For example, results obtained using a constant angle of 45° are unconservative, by 3.769% to 8.823%. However, using a constant angle of 50° is almost always conservative for VBEs, with the ratio at 1% drift exceeding by 0.6%.

Table 6-2 Combined moment-axial force demand ratio of SW12

SW12			**35 °**							
		Drift	$\mathbf{M_u/M_{u-35°}}$		$\mathbf{P_u/P_{u-35°}}$		**Summary**			
	top beam	**1%**	0.724	*0.751*	0.908	*1.009*	1.632	-18.399%	*1.761*	*-11.973%*
		3%	0.781	*0.793*	0.914	*0.947*	1.695	-15.242%	*1.740*	*-12.999%*
		6%	0.792	*0.812*	0.995	*1.044*	1.787	-10.660%	*1.857*	*-7.173%*
	left column	**1%**	1.823	*1.850*	0.935	*1.024*	2.758	37.906%	*2.874*	*43.685%*
		3%	1.880	*1.864*	0.918	*0.967*	2.798	39.916%	*2.831*	*41.537%*
		6%	1.954	*1.928*	0.902	*0.938*	2.856	42.807%	*2.867*	*43.346%*
			40 °							
		Drift	$\mathbf{M_u/M_{u-40°}}$		$\mathbf{P_u/P_{u-40°}}$		**Summary**			
	top beam	**1%**	0.827	*0.858*	0.865	*0.962*	1.693	-15.368%	*1.820*	*-8.984%*
		3%	0.890	*0.904*	0.870	*0.901*	1.760	-11.988%	*1.805*	*-9.736%*
		6%	0.896	*0.919*	0.882	*0.926*	1.778	-11.092%	*1.845*	*-7.748%*
	left column	**1%**	1.450	*1.471*	0.891	*0.976*	2.341	17.073%	*2.447*	*22.375%*
		3%	1.493	*1.480*	0.874	*0.920*	2.366	18.323%	*2.400*	*19.992%*
		6%	1.540	*1.520*	0.852	*0.887*	2.393	19.630%	*2.407*	*20.339%*
			45 °							
		Drift	$\mathbf{M_u/M_{u-45°}}$		$\mathbf{P_u/P_{u-45°}}$		**Summary**			
	top beam	**1%**	0.970	*1.007*	0.852	*0.947*	1.823	-8.875%	*1.954*	*-2.295%*
		3%	1.044	*1.060*	0.856	*0.886*	1.900	-5.012%	*1.947*	*-2.661%*
		6%	1.048	*1.075*	0.866	*0.909*	1.914	-4.302%	*1.984*	*-0.802%*
	left column	**1%**	1.198	*1.215*	0.877	*0.961*	2.075	3.769%	*2.176*	*8.823%*
		3%	1.232	*1.222*	0.860	*0.905*	2.092	4.600%	*2.127*	*6.343%*
		6%	1.269	*1.252*	0.837	*0.870*	2.105	5.256%	*2.122*	*6.110%*
			50 °							
		Drift	$\mathbf{M_u/M_{u-50°}}$		$\mathbf{P_u/P_{u-50°}}$		**summary**			
	top beam	**1%**	1.175	*1.219*	0.865	*0.962*	2.040	2.013%	*2.181*	*9.054%*
		3%	1.264	*1.285*	0.870	*0.901*	2.134	6.717%	*2.185*	*9.270%*
		6%	1.273	*1.306*	0.882	*0.926*	2.155	7.740%	*2.231*	*11.572%*
	left column	**1%**	1.021	*1.036*	0.891	*0.976*	1.912	-4.385%	*2.012*	*0.607%*
		3%	1.051	*1.042*	0.874	*0.920*	1.925	-3.761%	*1.962*	*-1.902%*
		6%	1.085	*1.070*	0.852	*0.887*	1.937	-3.160%	*1.957*	*-2.153%*

6.4 Analyses of SW31

6.4.1 Inclination angle analysis of SW31

Figure 6-11a to c present inclination angle variations in different floors of SW31. Based on the results presented for the first floor of this three story SPSW, beams, columns and middle web exhibit quite different trends in the variation of inclination angle. The angle at the right column initially reaches as high as 58° before decreasing to 48° at 2% drift, and then gradually increasing up to approximately 53° at 6% drift. The angle for the left column also quickly increases within the first 1% drift, but keeps increasing afterwards without significant drop. It finally reaches about 54°, which is close to the value for the right column. In spite of some slight fluctuations before 3% drift, the inclination angle of middle web generally exhibits a smooth increase from 46° to 49°. As for the top and bottom beams, curves dramatically fluctuate within the first 4% drift, ending up with 35° and 42° at 6% drift, respectively. The asynchronous fluctuations observed in the top and bottom beams may due to the sequence of plastic hinge development, while the difference in value may be caused by the different uniform distributed load from the web plates (e.g., the bottom beam was subjected to the uniform distributed load from the web plate of only the first floor, while the top beam was subjected to the subtraction of distributed loads between the first and second floors).

In the plots showing results for the second floor, the fluctuations are again concentrated within the first 2% drift for all curves. Columns and beams even have less serious variations than those observed for the first floor. Moreover, the difference between beams is narrowed down to approximately 3°. Though the curve of middle web has an obvious fluctuation at early stage, it becomes more smooth than that of the first floor as drift increases, finally reaching a lower value of about 46° at 6% drift.

In the third floor, the fluctuations are generally occurring only within the first 1% drift, except for the top beam. The curves for the columns exhibit a similar trend as what was observed for SW11, approaching to 55° at 6% drift. There is no notable fluctuation in the curve of middle web, stabilized at about 48°. Note that the difference between the top and bottom beams is now increased, with the inclination angle of the former larger than that of the latter. This can be again explained (as was the case for the first floor) by the difference in distributed loads from the web plates.

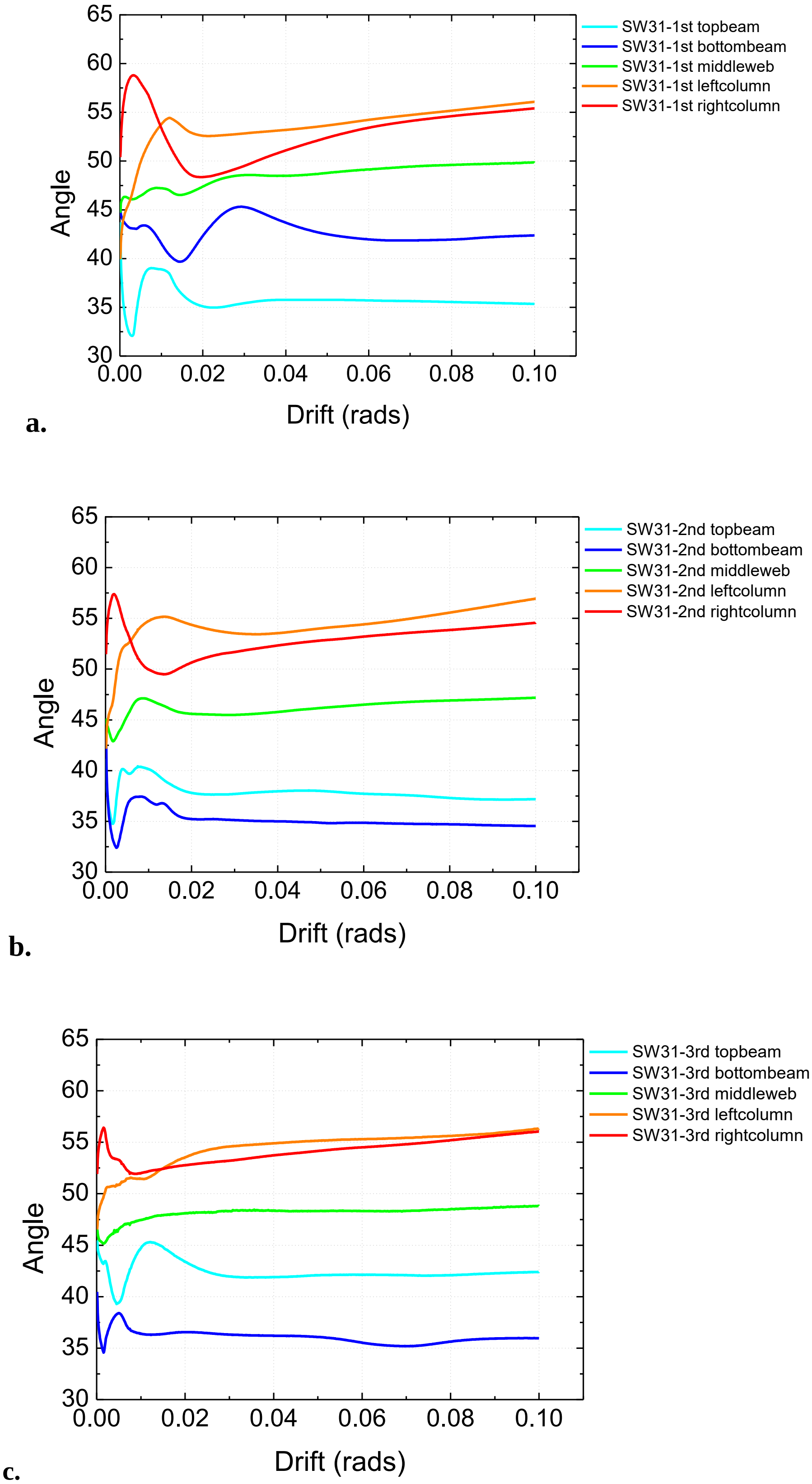

Figure 6-11 Inclination angle variation of SW31

6.4.2 Combined moment-axial force demand analysis of SW31

The combined moment-axial force demand analysis results obtained from SW31 are shown in Table 6-3 to Table 6-5. Results obtained for the top HBE at the first floor indicate that, using constant angles ranging from 35° to 45° are always conservative for the design of HBEs whereas using the angle of 50° is not. For the design of the VBEs, it is unconservative to use the constant angles of 35° and 40°, and generally conservative to use 45°, with a few of the obtained results being unconservative by no more than 5.1% (i.e., results for the left column at 6% drift). Using a constant angle of 50° is always conservative. The third floor yields similar observations as the first floor except for the results obtained for the left column using the constant angle of 45°, none of which is conservative. Unlike the first floor and third floor, the results obtained from the second floor show that using a constant angle of 45° leads to a few unconservativeness for the HBE design by 3.5% at maximum, but can ensure the conservatism for the VBE design at all drifts.

Table 6-3 Combined moment-axial force demand ratio of SW31-1st floor

SW31			**35 °**							
		Drift	$\mathbf{M_u/M_{u-35^\circ}}$		$\mathbf{P_u/P_{u-35^\circ}}$		**summary**			
	top beam	**1%**	0.789	0.826	0.858	0.910	1.647	-17.650%	1.735	-13.231%
		3%	0.827	0.841	0.830	0.899	1.656	-17.190%	1.741	-12.963%
		6%	0.847	0.855	0.924	0.977	1.772	-11.412%	1.832	-8.404%
	left column	**1%**	1.723	1.741	0.827	0.837	2.550	27.479%	2.578	28.891%
		3%	1.796	1.814	0.923	0.915	2.719	35.946%	2.729	36.472%
		6%	1.901	1.926	0.922	0.918	2.822	41.106%	2.845	42.229%
			40 °							
		Drift	$\mathbf{M_u/M_{u-40^\circ}}$		$\mathbf{P_u/P_{u-40^\circ}}$		**summary**			
	top beam	**1%**	0.901	0.943	0.818	0.867	1.719	-14.041%	1.810	-9.482%
		3%	0.943	0.959	0.789	0.856	1.732	-13.407%	1.815	-9.248%
		6%	0.959	0.968	0.819	0.866	1.779	-11.072%	1.834	-8.314%
	left column	**1%**	1.370	1.385	0.788	0.798	2.159	7.928%	2.183	9.131%
		3%	1.426	1.440	0.878	0.871	2.304	15.206%	2.311	15.564%
		6%	1.498	1.519	0.871	0.867	2.369	18.441%	2.386	19.300%
			45 °							
		Drift	$\mathbf{M_u/M_{u-45^\circ}}$		$\mathbf{P_u/P_{u-45^\circ}}$		**summary**			
	top beam	**1%**	1.057	1.107	0.805	0.854	1.863	-6.868%	1.960	-1.984%
		3%	1.105	1.125	0.777	0.842	1.882	-5.913%	1.967	-1.664%
		6%	1.122	1.132	0.804	0.850	1.926	-3.689%	1.982	-0.902%
	left column	**1%**	1.132	1.144	0.776	0.786	1.908	-4.600%	1.929	-3.529%
		3%	1.177	1.189	0.864	0.857	2.041	2.060%	2.046	2.300%
		6%	1.234	1.251	0.855	0.851	2.088	4.421%	2.102	5.104%
			50 °							
		Drift	$\mathbf{M_u/M_{u-50^\circ}}$		$\mathbf{P_u/P_{u-50^\circ}}$		**summary**			
	top beam	**1%**	1.280	1.340	0.818	0.867	2.098	4.898%	2.207	10.339%
		3%	1.339	1.362	0.789	0.856	2.128	6.400%	2.218	10.910%
		6%	1.362	1.375	0.819	0.866	2.182	9.086%	2.240	12.023%
	left column	**1%**	0.965	0.975	0.788	0.798	1.753	-12.347%	1.773	-11.356%
		3%	1.004	1.014	0.878	0.871	1.882	-5.892%	1.885	-5.745%
		6%	1.055	1.069	0.871	0.867	1.925	-3.726%	1.937	-3.168%

Table 6-4 Combined moment-axial force demand ratio of SW31-2nd floor

SW31			**35 °**							
		Drift	**$M_u/M_{u-35°}$**		**$P_u/P_{u-35°}$**		**summary**			
	top beam	**1%**	0.783	0.822	0.911	0.961	1.693	-15.338%	1.783	-10.850%
		3%	0.850	0.885	0.908	0.948	1.758	-12.118%	1.833	-8.335%
		6%	0.842	0.875	0.954	1.010	1.796	-10.179%	1.885	-5.746%
	left column	**1%**	1.768	1.775	0.827	0.870	2.595	29.752%	2.645	32.245%
		3%	1.758	1.751	0.851	0.887	2.609	30.445%	2.638	31.924%
		6%	1.781	1.775	0.831	0.846	2.612	30.595%	2.621	31.072%
			40 °							
		Drift	**$M_u/M_{u-40°}$**		**$P_u/P_{u-40°}$**		**summary**			
	top beam	**1%**	0.894	0.939	0.868	0.916	1.762	-11.898%	1.855	-7.248%
		3%	0.969	1.009	0.864	0.902	1.833	-8.364%	1.911	-4.430%
		6%	0.954	0.991	0.846	0.895	1.799	-10.042%	1.886	-5.706%
	left column	**1%**	1.406	1.412	0.789	0.829	2.195	9.740%	2.241	12.059%
		3%	1.396	1.390	0.809	0.844	2.205	10.268%	2.235	11.732%
		6%	1.404	1.400	0.785	0.799	2.189	9.443%	2.199	9.941%
			45 °							
		Drift	**$M_u/M_{u-45°}$**		**$P_u/P_{u-45°}$**		**summary**			
	top beam	**1%**	1.049	1.102	0.855	0.902	1.903	-4.827%	2.003	0.174%
		3%	1.136	1.183	0.850	0.888	1.986	-0.704%	2.071	3.549%
		6%	1.115	1.159	0.830	0.878	1.945	-2.731%	2.038	1.877%
	left column	**1%**	1.162	1.166	0.776	0.816	1.938	-3.100%	1.983	-0.863%
		3%	1.153	1.148	0.796	0.831	1.949	-2.561%	1.978	-1.076%
		6%	1.157	1.153	0.770	0.785	1.927	-3.668%	1.937	-3.142%
			50 °							
		Drift	**$M_u/M_{u-50°}$**		**$P_u/P_{u-50°}$**		**summary**			
	top beam	**1%**	1.270	1.333	0.868	0.916	2.138	6.889%	2.250	12.481%
		3%	1.376	1.433	0.864	0.902	2.240	11.995%	2.336	16.779%
		6%	1.354	1.408	0.846	0.895	2.200	9.997%	2.302	15.119%
	left column	**1%**	0.990	0.994	0.789	0.829	1.779	-11.064%	1.823	-8.831%
		3%	0.983	0.979	0.809	0.844	1.792	-10.387%	1.823	-8.840%
		6%	0.989	0.985	0.785	0.799	1.773	-11.333%	1.785	-10.766%

Table 6-5 Combined moment-axial force demand ratio of SW31-3rd floor

SW31			**35 °**							
		Drift	**$M_u/M_{u-35°}$**		**$P_u/P_{u-35°}$**		**summary**			
	top beam	**1%**	0.716	0.738	1.012	1.059	1.728	-13.606%	1.796	-10.191%
		3%	0.759	0.791	0.949	0.968	1.708	-14.593%	1.759	-12.046%
		6%	0.760	0.800	1.019	1.061	1.779	-11.062%	1.861	-6.952%
	left column	**1%**	1.733	1.765	0.940	1.027	2.673	33.664%	2.792	39.602%
		3%	1.880	1.866	0.894	0.955	2.774	38.708%	2.821	41.059%
		6%	1.906	1.882	0.874	0.920	2.780	39.023%	2.802	40.103%
			40 °							
		Drift	**$M_u/M_{u-40°}$**		**$P_u/P_{u-40°}$**		**summary**			
	top beam	**1%**	0.817	0.843	0.965	1.009	1.782	-10.880%	1.852	-7.417%
		3%	0.865	0.902	0.903	0.921	1.768	-11.576%	1.823	-8.848%
		6%	0.860	0.906	0.903	0.940	1.763	-11.838%	1.846	-7.697%
	left column	**1%**	1.379	1.404	0.896	0.979	2.275	13.739%	2.383	19.147%
		3%	1.493	1.482	0.850	0.909	2.343	17.168%	2.390	19.517%
		6%	1.503	1.483	0.826	0.869	2.329	16.430%	2.353	17.639%
			45 °							
		Drift	**$M_u/M_{u-45°}$**		**$P_u/P_{u-45°}$**		**summary**			
	top beam	**1%**	0.959	0.989	0.950	0.993	1.909	-4.548%	1.982	-0.901%
		3%	1.015	1.058	0.889	0.906	1.903	-4.840%	1.964	-1.809%
		6%	1.006	1.060	0.886	0.923	1.893	-5.374%	1.982	-0.876%
	left column	**1%**	1.139	1.160	0.882	0.963	2.021	1.053%	2.123	6.175%
		3%	1.233	1.223	0.837	0.894	2.069	3.460%	2.117	5.860%
		6%	1.237	1.222	0.811	0.853	2.048	2.414%	2.075	3.751%
			50 °							
		Drift	**$M_u/M_{u-50°}$**		**$P_u/P_{u-50°}$**		**summary**			
	top beam	**1%**	1.161	1.197	0.965	1.009	2.126	6.297%	2.206	10.288%
		3%	1.229	1.281	0.903	0.921	2.132	6.609%	2.202	10.110%
		6%	1.222	1.287	0.903	0.940	2.125	6.236%	2.227	11.344%
	left column	**1%**	0.971	0.989	0.896	0.979	1.867	-6.661%	1.967	-1.631%
		3%	1.051	1.043	0.850	0.909	1.902	-4.923%	1.952	-2.407%
		6%	1.058	1.044	0.826	0.869	1.884	-5.800%	1.914	-4.309%

6.5 Analyses of SW32

6.5.1 Inclination angle analysis of SW32

The inclination angle variations in each floor of SW32 are shown in Figure 6-12a to 6-12c. As seen from the results obtained for the first floor, the inclination angles of the right and left columns increase to about 62° at early drifts. After that, the curve for the right column decreases to below 50° and then raises again to a value of 55° at 6% drift, while the one for the left column gradually drops to a value of 55°. The inclination angle curve for the middle web has less variation, staying around 50° as the drift increases. The curves for the top and bottom beams also fluctuate within the first 4% drift, but less significantly than for the columns. The curve eventually converge towards 40°, with the value for the bottom beam being slightly higher than that of top beam.

For the beams and columns of the second floor, both the scale and amplitude of fluctuations reduce. However, the curve for the middle web has more fluctuations and eventually approaches a lower value of 48°.

On the third floor, the difference of inclination angles between the two columns reduce compared to the difference observed for the other floors, whereas the difference between the beams increase. Again, significant variations are observed at the beginning in the curves for the beams, with inclination angles of the top beam being higher than for the bottom beam, which can also be explained (as was the case for the first floor of SW31) by the difference in distributed loads from the web plates. Overall, for these three floors of SW32, a smaller difference is observed between top and bottom beam, likely attributed to a more uniform stress distribution as the aspect ratio increases.

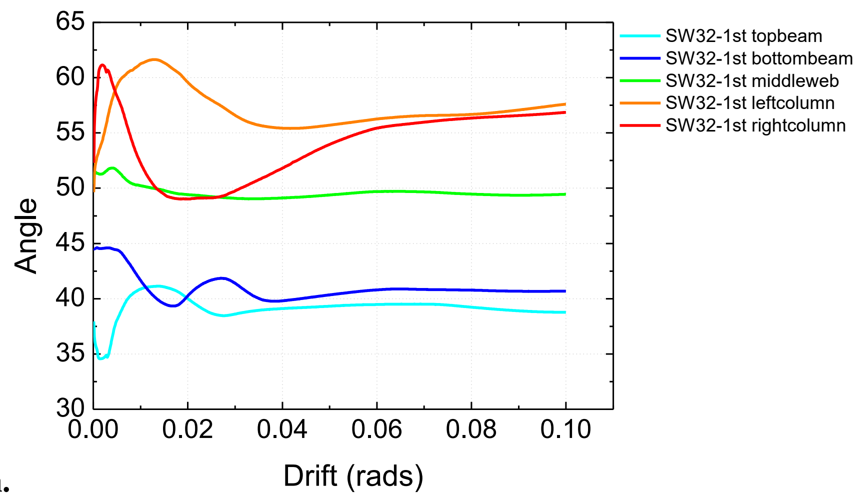

a.

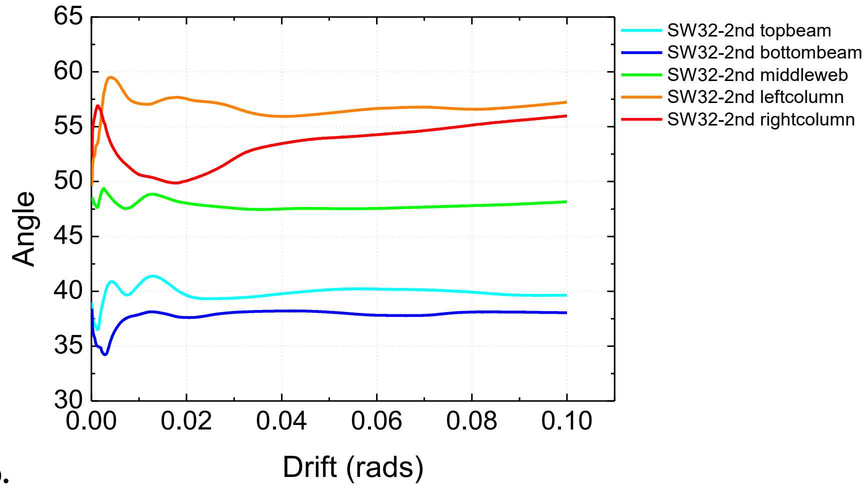

b.

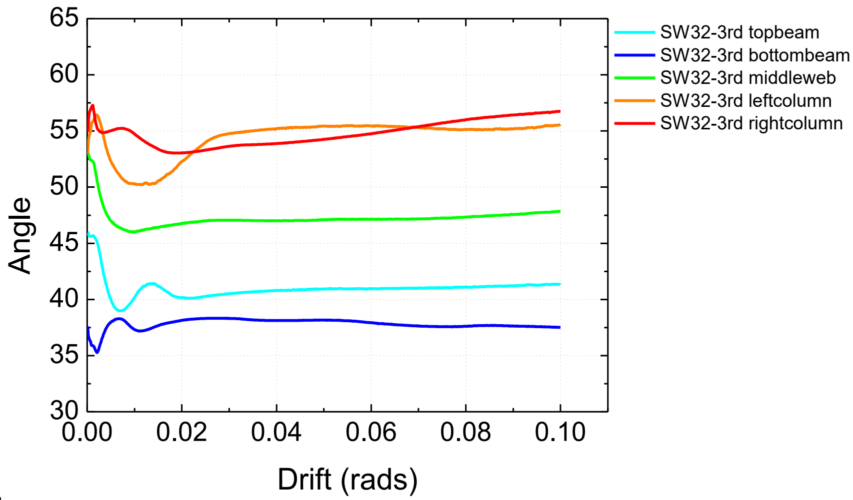

c.

Figure 6-12 Inclination angle variation of SW32

6.5.2 Combined moment-axial force demand analysis of SW32

The combined moment-axial force demand analysis results obtained from SW32 are shown in Table 6-6 to Table 6-8. Similar observations and findings can be made for SW32 as those for SW31, except for some differences observed from the second and third floor, which suggest in this case that using the constant angle of 45° is unconservative for both the HBE and VBE design.

Table 6-6 Combined moment-axial force demand ratio of SW32-1st floor

			35 °							
		Drift	$\mathbf{M}_{u}/\mathbf{M}_{u-35°}$		$\mathbf{P}_{u}/\mathbf{P}_{u-35°}$		**Summary**			
SW32	**top beam**	**1%**	0.723	*0.769*	0.871	*0.911*	1.594	-20.299%	*1.680*	*-15.991%*
		3%	0.769	*0.793*	0.862	*0.882*	1.632	-18.419%	*1.675*	*-16.263%*
		6%	0.776	*0.793*	0.946	*0.956*	1.722	-13.894%	*1.749*	*-12.539%*
	left column	**1%**	2.006	*1.985*	0.713	*0.754*	2.719	35.946%	*2.739*	*36.948%*
		3%	1.894	*1.876*	0.817	*0.828*	2.711	35.531%	*2.704*	*35.198%*
		6%	1.887	*1.882*	0.838	*0.835*	2.725	36.256%	*2.716*	*35.821%*
			40 °							
		Drift	$\mathbf{M}_{u}/\mathbf{M}_{u-40°}$		$\mathbf{P}_{u}/\mathbf{P}_{u-40°}$		**summary**			
	top beam	**1%**	0.826	*0.878*	0.830	*0.869*	1.656	-17.187%	*1.747*	*-12.650%*
		3%	0.877	*0.904*	0.821	*0.839*	1.698	-15.120%	*1.743*	*-12.841%*
		6%	0.878	*0.898*	0.839	*0.847*	1.717	-14.151%	*1.745*	*-12.738%*
	left column	**1%**	1.596	*1.579*	0.679	*0.719*	2.275	13.762%	*2.298*	*14.886%*
		3%	1.504	*1.490*	0.777	*0.788*	2.281	14.041%	*2.277*	*13.862%*
		6%	1.487	*1.483*	0.792	*0.788*	2.279	13.967%	*2.272*	*13.595%*
			45 °							
		Drift	$\mathbf{M}_{u}/\mathbf{M}_{u-45°}$		$\mathbf{P}_{u}/\mathbf{P}_{u-45°}$		**summary**			
	top beam	**1%**	0.969	*1.030*	0.817	*0.855*	1.787	-10.673%	*1.886*	*-5.716%*
		3%	1.028	*1.060*	0.807	*0.825*	1.836	-8.217%	*1.886*	*-5.716%*
		6%	1.027	*1.050*	0.823	*0.832*	1.851	-7.473%	*1.882*	*-5.903%*
	left column	**1%**	1.318	*1.304*	0.669	*0.708*	1.987	-0.644%	*2.012*	*0.598%*
		3%	1.241	*1.230*	0.765	*0.775*	2.006	0.300%	*2.005*	*0.234%*
		6%	1.225	*1.222*	0.777	*0.774*	2.002	0.115%	*1.996*	*-0.219%*
			50 °							
		Drift	$\mathbf{M}_{u}/\mathbf{M}_{u-50°}$		$\mathbf{P}_{u}/\mathbf{P}_{u-50°}$		**summary**			
	top beam	**1%**	1.174	*1.247*	0.830	*0.869*	2.004	0.177%	*2.116*	*5.807%*
		3%	1.246	*1.285*	0.821	*0.839*	2.066	3.309%	*2.123*	*6.165%*
		6%	1.247	*1.275*	0.839	*0.847*	2.086	4.305%	*2.123*	*6.128%*
	left column	**1%**	1.124	*1.112*	0.679	*0.719*	1.803	-9.851%	*1.831*	*-8.474%*
		3%	1.059	*1.049*	0.777	*0.788*	1.836	-8.206%	*1.836*	*-8.178%*
		6%	1.047	*1.044*	0.792	*0.788*	1.839	-8.039%	*1.833*	*-8.354%*

Table 6-7 Combined moment-axial force demand ratio of SW32-2nd floor

SW32			**35 °**							
		Drift	**$M_u/M_{u-35°}$**		**$P_u/P_{u-35°}$**		**summary**			
	top beam	**1%**	0.757	*0.793*	0.916	*0.979*	1.673	-16.327%	*1.772*	*-11.392%*
		3%	0.812	*0.843*	0.935	*0.936*	1.747	-12.635%	*1.779*	*-11.056%*
		6%	0.815	*0.848*	1.003	*1.021*	1.818	-9.101%	*1.869*	*-6.538%*
	left column	**1%**	1.884	*1.879*	0.813	*0.886*	2.696	34.821%	*2.765*	*38.268%*
		3%	1.900	*1.877*	0.826	*0.868*	2.726	36.312%	*2.746*	*37.278%*
		6%	1.857	*1.831*	0.816	*0.816*	2.673	33.665%	*2.647*	*32.349%*
			40 °							
		Drift	**$M_u/M_{u-40°}$**		**$P_u/P_{u-40°}$**		**summary**			
	top beam	**1%**	0.865	*0.906*	0.874	*0.934*	1.738	-13.081%	*1.839*	*-8.040%*
		3%	0.926	*0.961*	0.890	*0.891*	1.816	-9.212%	*1.852*	*-7.421%*
		6%	0.923	*0.960*	0.889	*0.905*	1.812	-9.419%	*1.865*	*-6.742%*
	left column	**1%**	1.498	*1.495*	0.775	*0.845*	2.273	13.655%	*2.340*	*16.980%*
		3%	1.509	*1.491*	0.786	*0.826*	2.295	14.732%	*2.317*	*15.832%*
		6%	1.464	*1.443*	0.771	*0.771*	2.235	11.748%	*2.214*	*10.715%*
			45 °							
		Drift	**$M_u/M_{u-45°}$**		**$P_u/P_{u-45°}$**		**summary**			
	top beam	**1%**	1.015	*1.062*	0.860	*0.919*	1.875	-6.267%	*1.982*	*-0.920%*
		3%	1.086	*1.127*	0.876	*0.876*	1.961	-1.943%	*2.003*	*0.149%*
		6%	1.080	*1.123*	0.872	*0.888*	1.952	-2.408%	*2.011*	*0.570%*
	left column	**1%**	1.238	*1.235*	0.763	*0.832*	2.000	0.023%	*2.067*	*3.327%*
		3%	1.246	*1.231*	0.773	*0.813*	2.019	0.938%	*2.043*	*2.165%*
		6%	1.206	*1.189*	0.756	*0.757*	1.962	-1.880%	*1.945*	*-2.728%*
			50 °							
		Drift	**$M_u/M_{u-50°}$**		**$P_u/P_{u-50°}$**		**summary**			
	top beam	**1%**	1.228	*1.286*	0.874	*0.934*	2.102	5.092%	*2.220*	*10.989%*
		3%	1.315	*1.365*	0.890	*0.891*	2.205	10.244%	*2.255*	*12.770%*
		6%	1.311	*1.364*	0.889	*0.905*	2.200	9.977%	*2.269*	*13.436%*
	left column	**1%**	1.055	*1.052*	0.775	*0.845*	1.830	-8.516%	*1.897*	*-5.133%*
		3%	1.062	*1.050*	0.786	*0.826*	1.848	-7.591%	*1.876*	*-6.222%*
		6%	1.031	*1.016*	0.771	*0.771*	1.802	-9.917%	*1.787*	*-10.638%*

Table 6-8 Combined moment-axial force demand ratio of SW32-3rd floor

SW32			**35 °**							
		Drift	$\mathbf{M_u/M_{u-35^\circ}}$		$\mathbf{P_u/P_{u-35^\circ}}$		**summary**			
	top beam	**1%**	0.798	*0.819*	0.962	*1.027*	1.760	-11.984%	*1.846*	*-7.702%*
		3%	0.838	*0.875*	0.983	*0.991*	1.821	-8.941%	*1.867*	*-6.671%*
		6%	0.825	*0.865*	1.034	*1.056*	1.858	-7.077%	*1.921*	*-3.938%*
	left column	**1%**	1.660	*1.689*	0.945	*1.030*	2.606	30.275%	*2.719*	*35.961%*
		3%	1.859	*1.829*	0.888	*0.939*	2.747	37.370%	*2.768*	*38.398%*
		6%	1.858	*1.820*	0.859	*0.878*	2.717	35.866%	*2.698*	*34.919%*
			40 °							
		Drift	$\mathbf{M_u/M_{u-40^\circ}}$		$\mathbf{P_u/P_{u-40^\circ}}$		**summary**			
	top beam	**1%**	0.912	*0.935*	0.917	*0.979*	1.829	-8.555%	*1.914*	*-4.279%*
		3%	0.956	*0.998*	0.935	*0.943*	1.891	-5.450%	*1.941*	*-2.939%*
		6%	0.934	*0.979*	0.916	*0.936*	1.850	-7.507%	*1.915*	*-4.229%*
	left column	**1%**	1.321	*1.343*	0.901	*0.982*	2.222	11.087%	*2.326*	*16.281%*
		3%	1.476	*1.452*	0.845	*0.893*	2.321	16.064%	*2.346*	*17.279%*
		6%	1.465	*1.435*	0.812	*0.829*	2.276	13.821%	*2.264*	*13.223%*
			45 °							
		Drift	$\mathbf{M_u/M_{u-45^\circ}}$		$\mathbf{P_u/P_{u-45^\circ}}$		**summary**			
	top beam	**1%**	1.069	*1.097*	0.903	*0.964*	1.973	-1.371%	*2.061*	*3.062%*
		3%	1.121	*1.170*	0.920	*0.928*	2.041	2.039%	*2.098*	*4.910%*
		6%	1.092	*1.146*	0.899	*0.919*	1.991	-0.430%	*2.064*	*3.218%*
	left column	**1%**	1.091	*1.110*	0.887	*0.967*	1.978	-1.096%	*2.077*	*3.836%*
		3%	1.219	*1.199*	0.832	*0.879*	2.050	2.509%	*2.078*	*3.892%*
		6%	1.206	*1.182*	0.797	*0.814*	2.003	0.149%	*1.996*	*-0.202%*
			50 °							
		Drift	$\mathbf{M_u/M_{u-50^\circ}}$		$\mathbf{P_u/P_{u-50^\circ}}$		**summary**			
	top beam	**1%**	1.295	*1.328*	0.917	*0.979*	2.212	10.600%	*2.307*	*15.371%*
		3%	1.357	*1.418*	0.935	*0.943*	2.293	14.632%	*2.361*	*18.035%*
		6%	1.326	*1.391*	0.916	*0.936*	2.242	12.115%	*2.327*	*16.353%*
	left column	**1%**	0.930	*0.946*	0.901	*0.982*	1.831	-8.451%	*1.928*	*-3.595%*
		3%	1.039	*1.022*	0.845	*0.893*	1.885	-5.774%	*1.916*	*-4.206%*
		6%	1.031	*1.010*	0.812	*0.829*	1.843	-7.853%	*1.840*	*-8.010%*

6.6 Parametric study of inclination angle for varying aspect ratio and number of stories

To investigate the variation of inclination angle trends under the different aspect ratios and number of stories considered, the figures showing the variation of inclination angle as a function of drift presented in Sections 6.2 to 6.5 were rearranged. In terms of aspect ratios, each inclination angle curve from SW*i*1 is compared with those from SW*i*2 at the same floor, where *i* refers to the number of stories (for example, SW11 and SW12, to compare the how results change as a function of aspect ratio for a single-story SPSW). While in terms of number of stories, each inclination angle curve from SW1*j* is compared to the corresponding curve of each floor from SW3*j*, where *j* refers to the aspect ratio (for example, SW13 and SW33, to compare how results change as a function of number of stories for a given aspect ratio).

Similar comparison is performed for the values provided earlier in the tables of combined moment-axial force demand analysis, to again compare response as a function of aspect ratios and number of stories. For each constant angle used, the combined moment-axial force demand ratios from SW*i*1 were plotted to compare with those of SW*i*2 per floor in the perspective of aspect ratios. Also, the combined moment-axial force demand ratios from SW1*j* were plotted to compare with those of each floor from SW3*j* in the perspective of number of stories. Each group of comparison is to investigate how much the combined moment-axial force demand ratios varies as a function of aspect ratios or number of stories, and whether the conservatism in using a certain constant angle would change or not as these parameters change. Note that, in all the combined moment-axial force demand figures presented below, the scale of vertical axis for the top beam (from 1.1 to 2.4) and left column (from 1.7 to 3.0) are respectively kept the same to allow a better comparison between results.

6.6.1 Aspect ratio analysis of Real SPSWs

Figure 6-13 compares the inclination angle variation for SPSW having different aspect ratios. For one-story SPSW, the aspect ratio has a noticeable impact on the inclination angle of middle web, with a maximum difference of 10° before 2% drift, and 3° for larger drifts. For tall SPSWs, the influence of aspect ratio is more significant on columns and beams. As seen from Figure 6-13b, the greater the aspect ratio, the more serious the fluctuation in results obtained for the columns, but this effect diminishes at higher floor, as shown in Figure 6-13c and d. The inclination angle of top beams under varying aspect ratios generally have a difference within 4°. The influence of aspect ratio on the middle web in three-story SPSW is much less significant, with observed variation focused within 2% drift.

Figure 6-14 and 6-15 were made from Table 6-1 to Table 6-8 to explicitly compare the combined moment-axial force demand ratios under different SPSW aspect ratios. In Figure 6-14a, for example, the blue and red points represent the data for SPSWs having aspect ratio of 1 and 2, respectively. The solid line connects the points obtained for moments at the end of HBEs while the dash line reflects the points obtained from the moment near the middle of the HBEs. It is shown that the red points are higher than the blue ones at 3% and 6% drifts, with a maximum absolute difference of approximately 0.2. As compared to the value of 2 (below which results are deemed conservative), both sets of points are typically either conservative or unconservative, namely either less than 2 when using the constant angle from 35° to 45° or greater than 2 when using the constant angle of 50°. Since the same observation can be made for the left column of the one-story SPSW, as shown in Figure 6-15a, the results indicate that the aspect ratio has an insignificant effect on the conservatism of results when constant angles are considered in the design of single-story SPSWs.

Regarding the results for the three-story SPSWs, it is observed that variation in the combined moment-axial force demand ratio differs from one floor to another. For example, in Figure 6-14b to 6-14d, the ratios for the HBEs of the SPWS with an aspect ratio of 2 are lower than those of the SPSW with an aspect ratio of 1 in the first floor, but the latter becomes higher than the former in higher floors. Oppositely, the combined moment-axial force demand ratios for VBEs of the SPSW with an aspect ratio of 1 are higher in the third floor. It is also found that the results for the top beam using the constant angle of 35°, 40° and those for the left column using 50° are always conservative. However, in the case of 45°, changing the aspect ratio changes the level of conservatism of the results obtained from both the top beams and left columns of the second and the third floor of tall SPSWs.

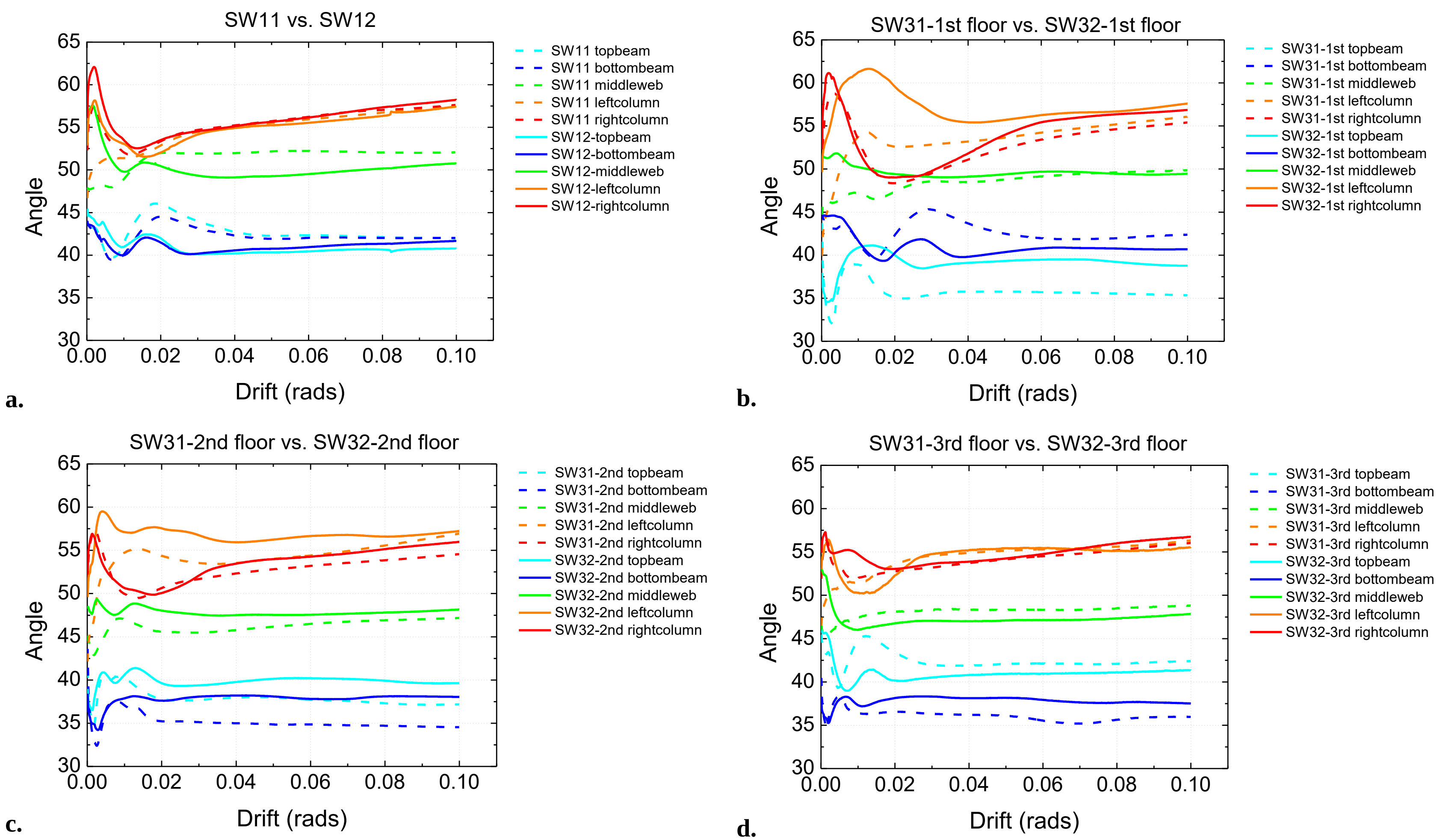

Figure 6-13 Comparison on inclination angles variation for different aspect ratios

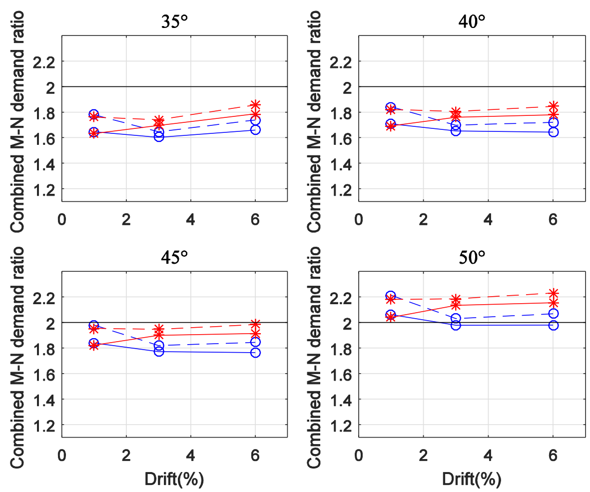

a. SW11 vs. SW12

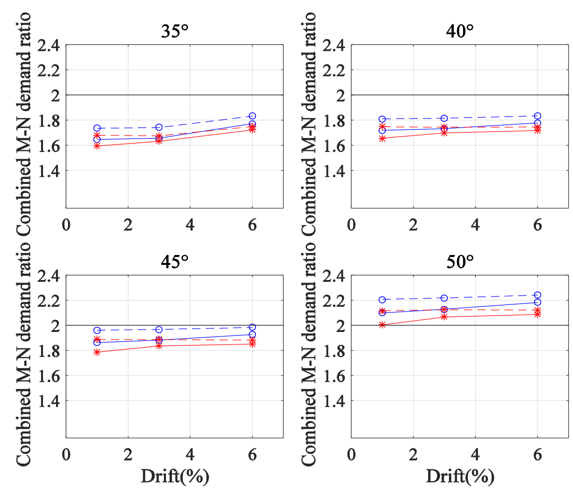

b. SW31 vs. SW32 at the 1st floor

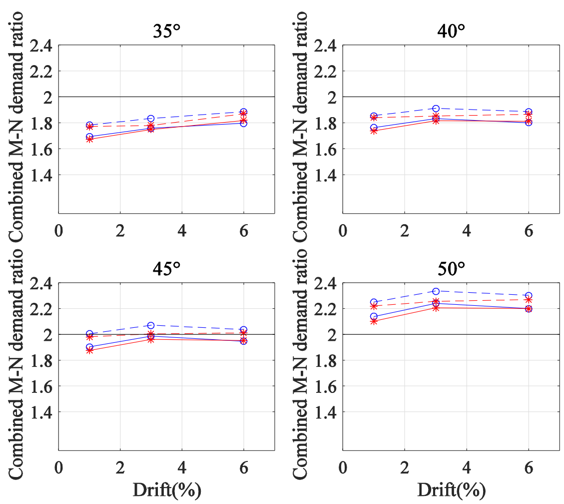

c. SW31 vs. SW32 at the 2nd floor

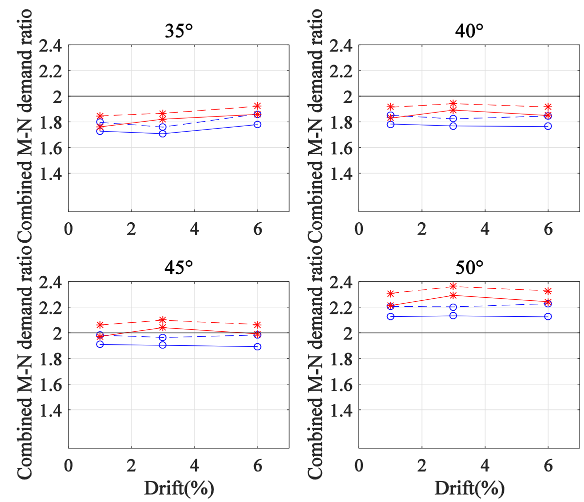

b. SW31 vs. SW32 at the 3rd floor

Data from the End w/AR=1 Data from the Middle w/AR=1 Data from the End w/AR=2 Data from the Middle w/AR=2

Figure 6-14 Comparison on combined moment and axial force demand ratio of top beam for different aspect ratios

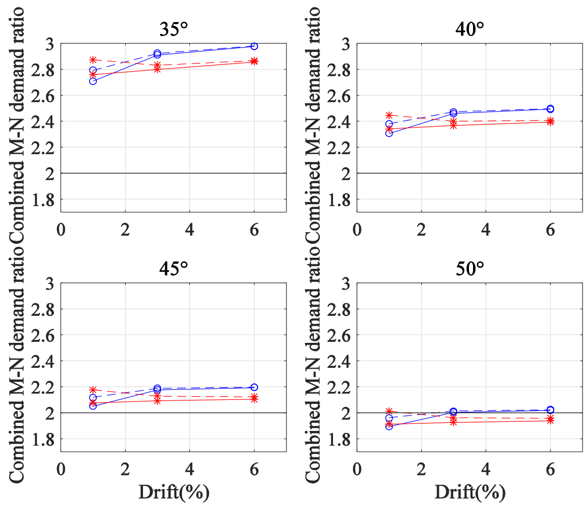

a. SW11 vs. SW12

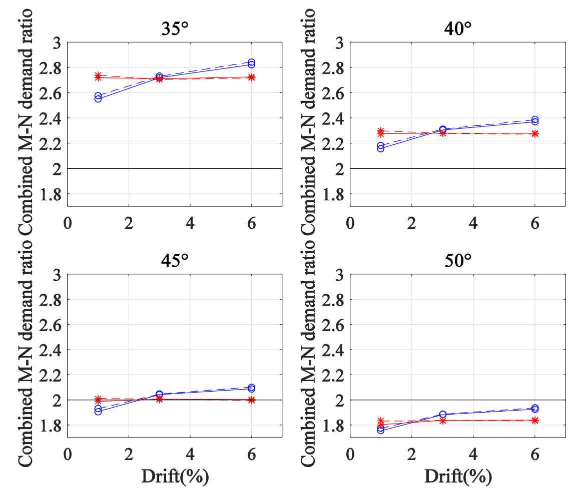

b. SW31 vs. SW32 at the 1st floor

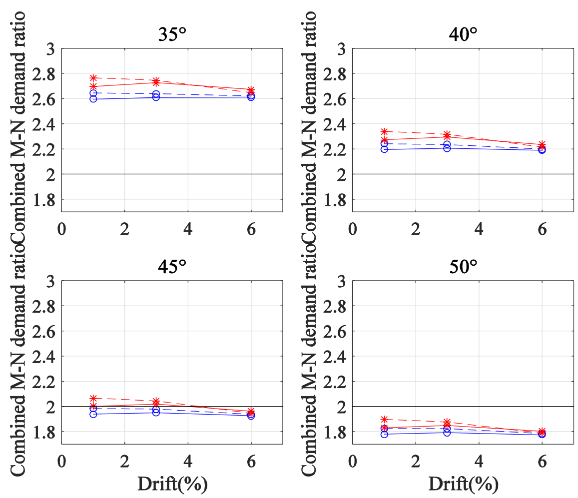

c. SW31 vs. SW32 at the 2nd floor

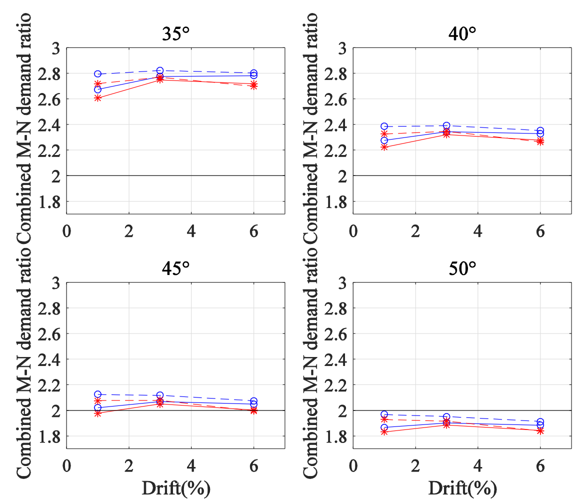

b. SW31 vs. SW32 at the 3rd floor

Data from the End w/AR=1 Data from the Middle w/AR=1 Data from the End w/AR=2 Data from the Middle w/AR=2

Figure 6-15 Comparison on combined moment and axial force demand ratio of left column for different aspect ratios

6.6.2 Number of stories analysis of Real SPSWs

The inclination angle variations for one-story SPSWs were compared to those for each floor of the corresponding three-story SPSWs having identical aspect ratio. It is seen from Figure 6-16 and Figure **6-17** that the curves for the columns of one-story SPSW are significantly different from those for the first floor of the corresponding three-story SPSW, with up to a 10° difference. However, the magnitude of the differences decreased when compared to the higher floor of three-story SPSW. As for the top and bottom beams, the curves obtained from the SPSWs with an aspect ratio of 1 show that results for the one-story SPSW do not match those on any of the floors of the corresponding three-story, with a maximum difference about 7° after 2% drift. For the SPSWs with an aspect ratio of 2, this difference is significantly reduced to approximately 3°, and the lower floor matches better with the corresponding one-story SPSW than the high floors. Similar observation can be made for the middle web.

In order to figure out the influence of number of stories on the conservatism of constant angles for the SPSW design, the data from Table 6-1 to Table 6-8 are plotted in Figure 6-18. The blue points stand for the results obtained from the one-story SPSWs while the points in other colors stand for the results obtained from the three-story SPSWs. According to Figure 6-18a and 6-18b, the combined moment-axial force demand ratios for the top beams of the one-story SPSWs are always lower than the maximum value of three-story SPSWs, while in Figure 6-18c and 6-18d, the left column exhibits an opposite trend. Also, in the case of using a constant angle of 45°, changing the number of stories from 1 to 3 would change the combined moment-axial force demand ratio for the top beams from being conservative to unconservative, as well as change those for the left columns from being unconservative to conservative.

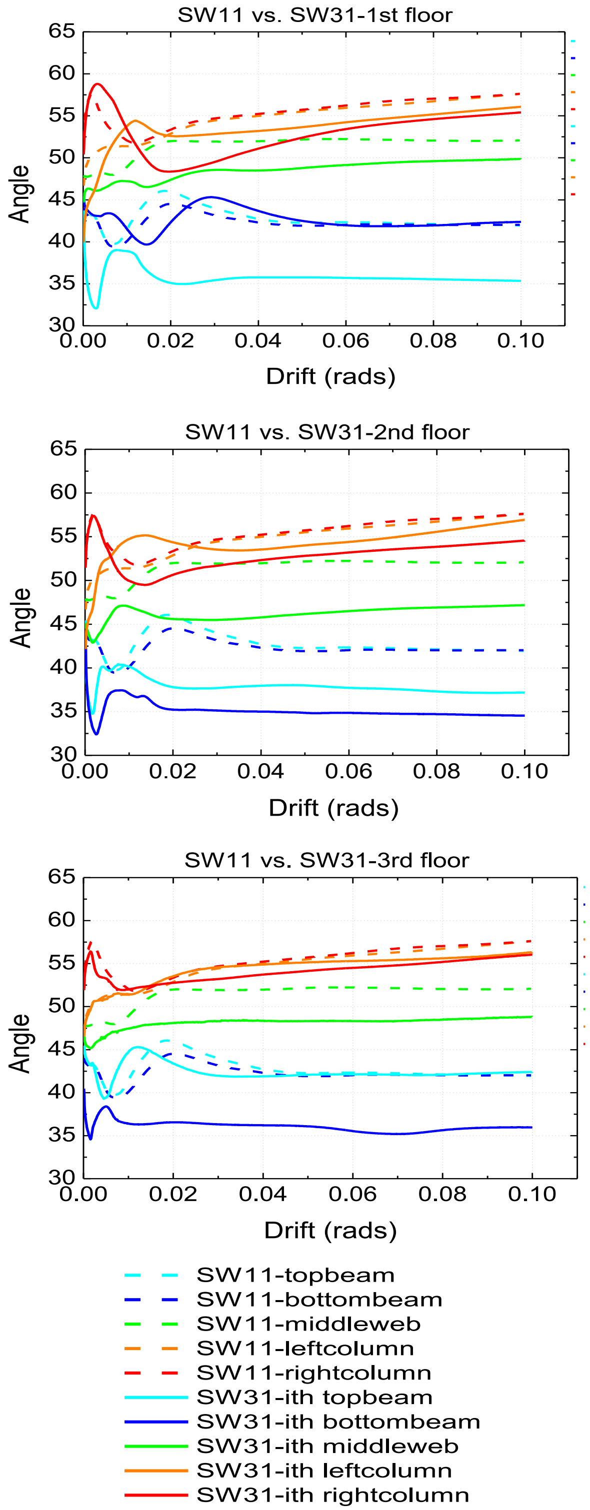

Figure 6-16 Comparison on inclination angles variation between SW11 and SW31

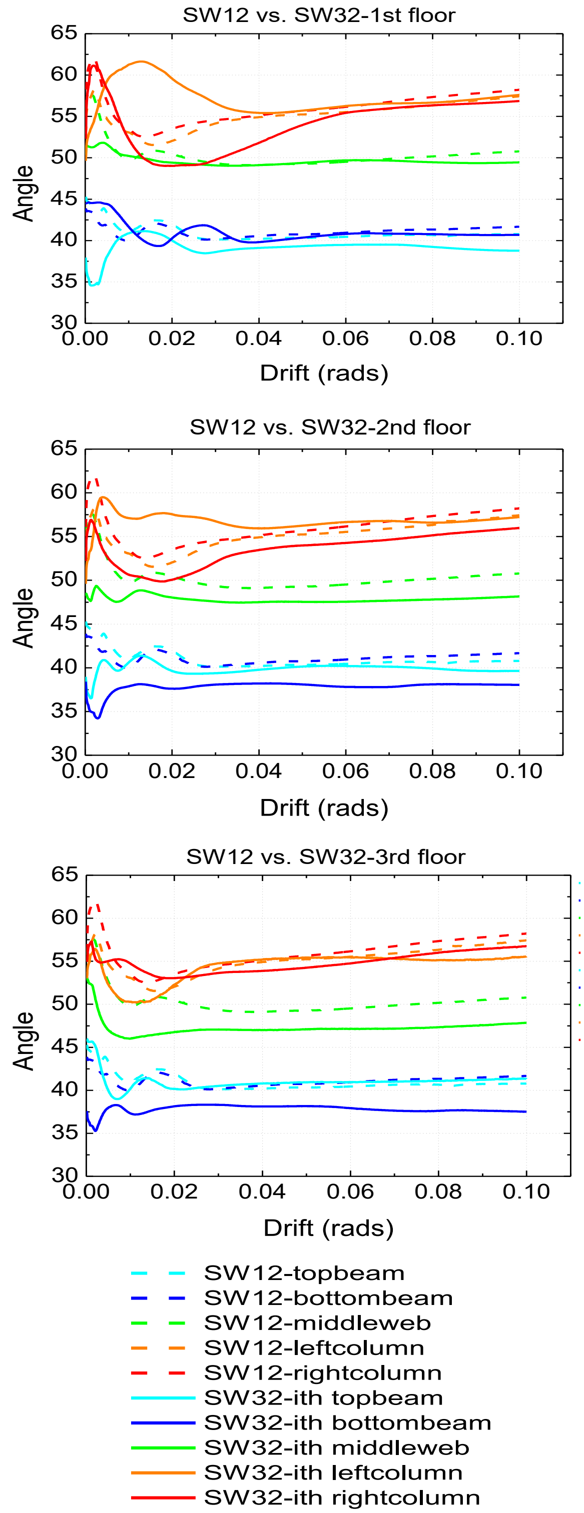

Figure 6-17 Comparison on inclination angles variation between SW12 and SW32

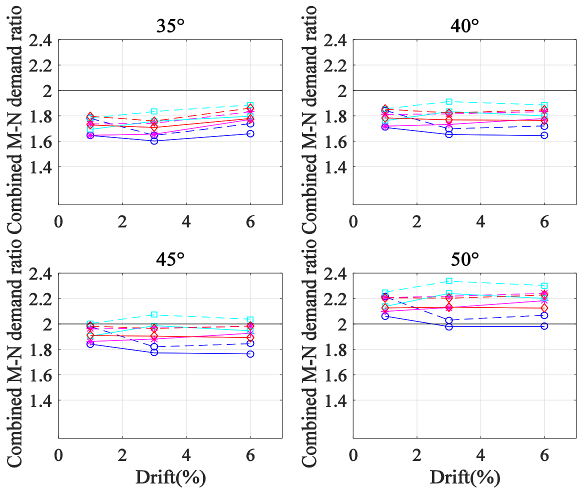

a. Top beam (with aspect ratio of 1)

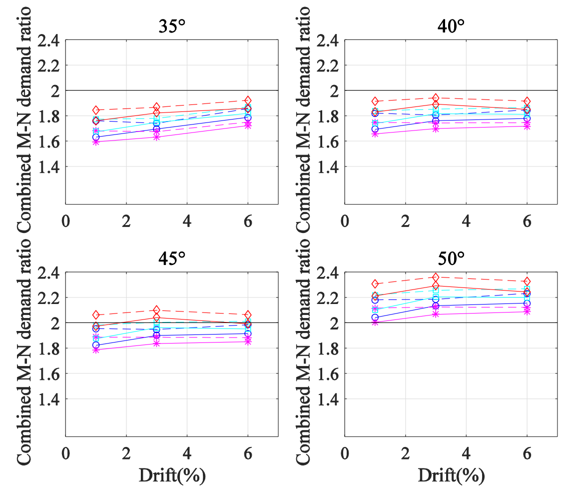

b. Top beam (with aspect ratio of 2)

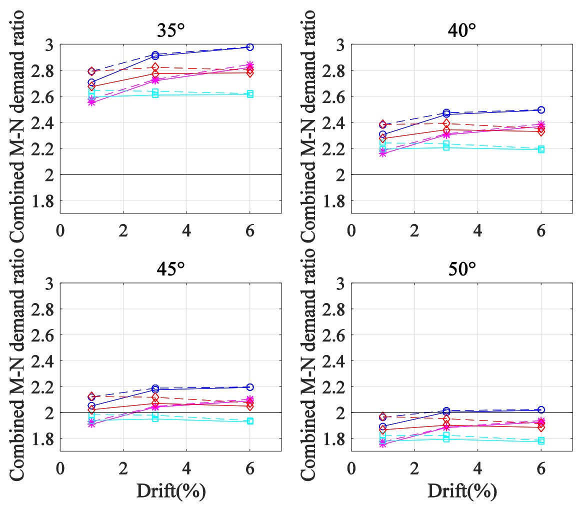

c. Left column (with aspect ratio of 1)

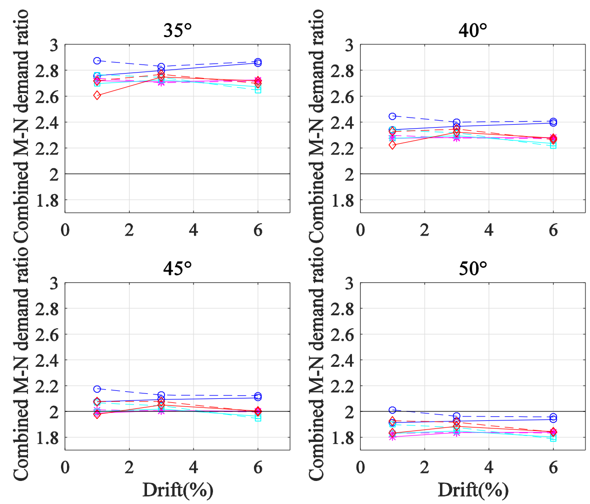

d. Left column (with aspect ratio of 2)

SW12 SW32-1st floor SW32-2nd floor SW32-3rd floor SW32 2nd floor-end SW32 2nd floor-middle SW32 3rd floor-end SW32 3rd floor-middle

Figure 6-18 Comparison on combined moment-axial force demand ratio of topbeam for different number of stories

6.6.3 Inclination angle for web plate design

As indicated in Figure 6-13, Figure 6-16, and Figure 6-17, the inclination angle of the diagonal tension field action across the middle of the web usually varies from 45° to 55° for real SPSWs. To investigate the influence of inclination angle for the web plate design, the demands in cases SW11 and SW31-2nd floor are compared; these cases are chosen here as they respectively represent the cases having the highest and lowest inclination angles. Figure 6-19 plots the shear stress distribution obtained from the LS-DYNA analyses for each element in the group of web plate at three considered drifts, compared to the design stresses calculated using 35°, 40°, and 45° (note that results for 55° and 50° are identical to those for 40° and 35°, respectively, due to the sin2α in Equation 3-10). Note that the stress distributions here are compared with the design stresses considering various design specified yield stress values.

It is shown that the shear stress distributions of SW11 at the three considered drifts and those of SW31-2nd floor at 1% drift are close to the design stresses, while the shear stresses at 3% and 6% drift of SW31-2nd floor are slightly higher than the design stress at mid-span, with a difference of approximately 1 ksi.

The above observations confirm that orienting the design stresses in the web at angles ranging from 35° to 55° is of minimal consequence because of the sin2α in Equation 3-10. Therefore, both inclination angles of 40° (currently in AISC-341) and 45° (proposed here) are conservative for the web plate design.

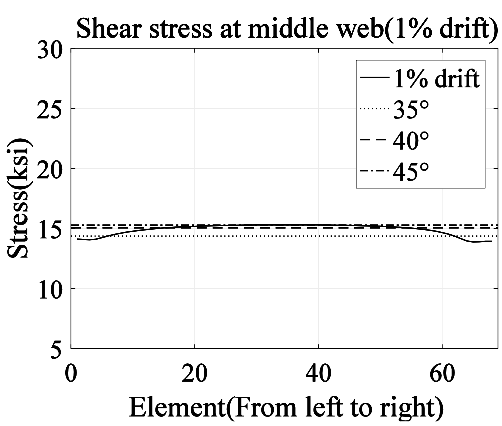

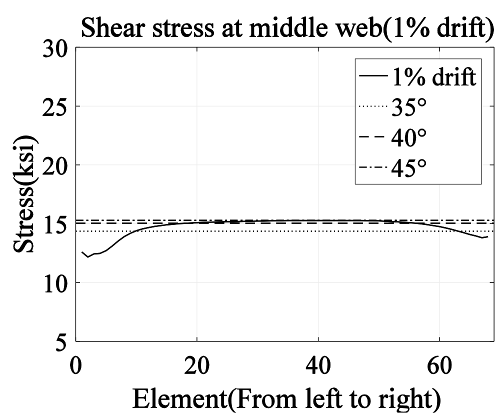

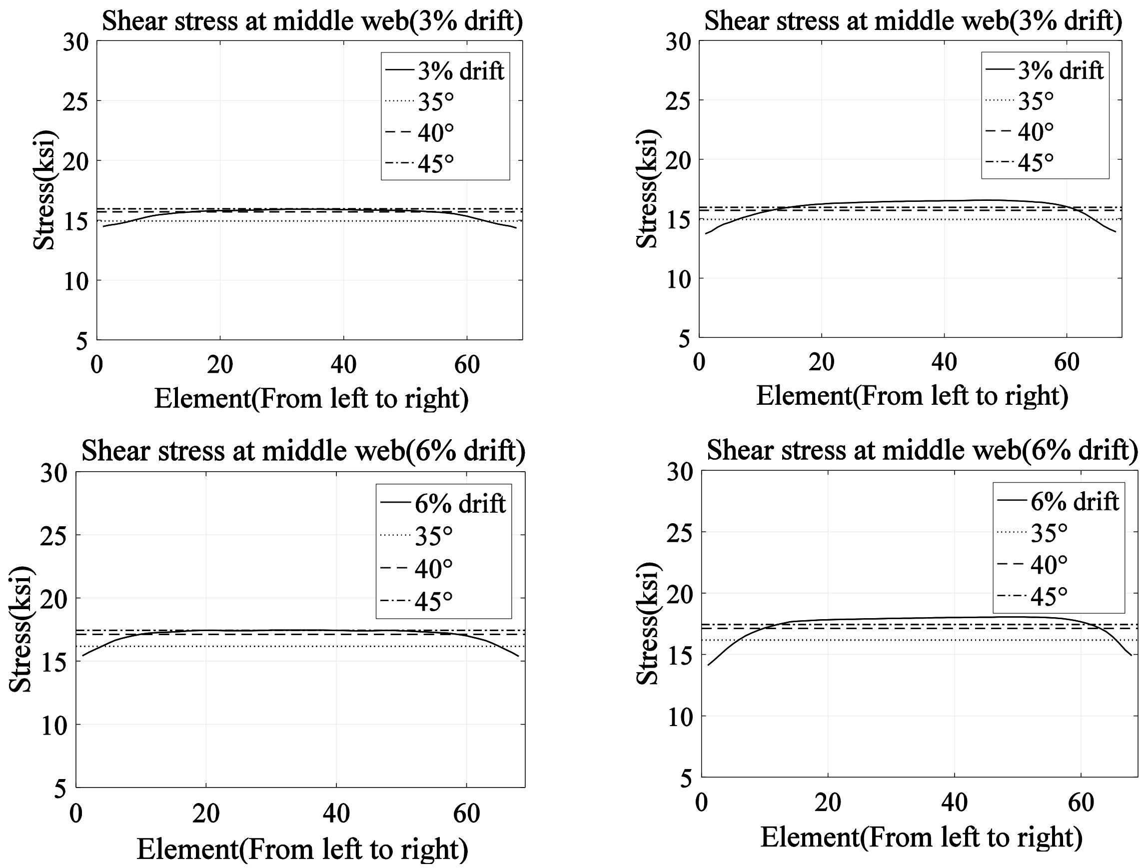

(a) SW11 **(b) SW31-2nd floor**

Figure 6-19 Comparison on shear stress of web plate shell elements (middle web)

6.6.4 Inclination angle for SPSW design

Based on the analyses above, it is observed that the inclination angle of the diagonal tension field action along the top beam, along the left column, and across the middle of the web usually varies from 35° to 45°, 45° to 65° and 45° to 55°, respectively. These ranges are higher than the corresponding inclination angle ranges presented in Section 4, in which a 2D LS-DYNA model was used without considering the plastic hinge on the HBEs.

The combined moment-axial force demand analyses resulting for all the analyses conducted as part of this study point to similar conclusions related to the conservatism of using specific constant angles for SPSW design. Generally, it would always be conservative to use a constant angle of 35° and 40° for HBE design and 50° for VBE design. Using a constant angle of 50° for HBE design could be unconservative by up to 18% while using constant angles of 35° and 40° for VBE design could be unconservative by up to 38% and 14%, respectively. However, using different inclination angles for HBEs and VBEs is not practical for design, and it is desirable to use a single constant angle for the design of all structural elements that constitute a SPSW.

The results obtained for both HBE and VBE using a constant angle of 45° are sometimes conservative, sometimes unconservative, and vary from case to case. Table 6-9 presents a summary of the maximum results obtained for HBEs and VBEs from the above case studies when compared with constant angle of 45°. The ratios greater than the value of 2 are deemed unconservative and highlighted in gray. Results in this table indicate that the maximum combined moment-axial force demand ratio was obtained for the case with aspect ratio of 1 (not exceeding the value of 2 by more than 10%). On that basis, the constant angle of 45° is deemed to be the best constant angle to use if one desires to simplify the design process by using a single angle.

Table 6-9 Classification of Boundary elements respect to conservatism using the constant angle of 45°

SPSW	Floor	Aspect ratio of 1		Aspect ratio of 2	
		Top beam	Left column	Top beam	Left column
One-story		1.980	2.197	1.984	2.176
Three-story	3	1.982	2.123	2.098	2.078
	2	2.071	1.983	2.011	2.067
	1	1.982	2.102	1.886	2.012

Note that the text in white background is conservative while in gray background is not. The value in the parenthesis shows the maximum combined moment-axial force demand ratio.

6.7 Summary

In this section, results from finite element analysis of the real SPSWs described in Section 5 were presented. First, the results obtained when using displacement control at the top of a SPSW were compared with that obtained using force control, and it was determined that both methods gave similar results. As displacement control proved more stable for analyses purposes, it was used for all subsequent SPSW finite element analyses. It was also observed from the shape of the curve that expresses how the inclination angle changes as a function of drift that three major fluctuations occurred along the curve for the beams results in SW11 (used as a case study to investigate what caused this typical fluctuation observed in most results). These fluctuations were found to how deflected shapes of the beams varied due to progressive web plate yielding and hinge development as drift increased. Furthermore, shear deformation were found to have a significant impact on those beam deflections in these cases.

The variation of the inclination angle of the diagonal tension field action and the combined moment-axial force demand were compared for SPSWs having different aspect ratios and numbers of stories. Floor-by-floor comparison of results was accomplished for SPSWs having aspect ratios of 1 and 2, as well as across all floors for the walls having the same aspect ratio. It was observed that the aspect ratio has a noticeable impact on the inclination angle for the middle web of one-story SPSW, with a maximum difference of 10° before 2% drift, and 3° for larger drifts. It also influences the curves for the columns of the tall SPSWs by inducing serious fluctuations in results, but this effect diminishes at higher floor. The inclination angle for the top beams of tall SPSWs under varying aspect ratios generally have a difference within 4°. In addition, the number of stories have influence for all curves. For the columns, the curves for the one-story SPSW differ from those for the first floor of the corresponding three-story SPSW by up to 10°. However, these differences decreased when compared to the higher floor of three-story SPSW. For the beams, the curves obtained from the one-story SPSWs seldom match those on the floors of the corresponding three-story, with a maximum difference about 7°. Similar observation can be made for the middle web.

With respect to the combined moment-axial force demands, the analyses conducted indicated that changing the aspect ratio of the walls did not change the level of conservatism in the results obtained when comparing results for the same constant angles considered in respective one-story SPSWs, but that it would change the level of conservatism for the results obtained in three-story SPSWs, most significantly when using a constant angle of 45°. The number of stories was also found to have an impact on the conservatism of the results obtained using the constant angle of 45°, as the combined moment-axial force demand ratio of the top beams changed from being conservative to unconservative as the number of stories increased, and those for the left columns changed from being unconservative to conservative as the number of stories increased.

In summary, it is was found to be always conservative to use 35° and 40° for HBE and 50° for VBE design. Using a constant angle of 50° for HBE design could be unconservative by up to 18% while using constant angles of 35° and 40° for VBE design could be unconservative by up to 38% and 14%, respectively. However, using different inclination angles for HBEs and VBEs is not practical for design, and it is desirable to use a single constant angle for the design of all structural elements that constitute a SPSW. In addition, the demand of web plate is not sensitive to the variation of inclination angle. Consequently, the single angle of 45° is recommended for the design of the entire SPSW.

SECTION 7
CONCLUSIONS

7.1 Summary

Research was conducted to study how the inclination angle of the diagonal tension field action varied across the entire web plate of SPSWs as a function of drift, and to determine the optimum constant angle value that should be used for the design of SPSWs. This was done by comparing results and demands obtained using nonlinear finite element analysis with those obtained from calculated various values of constant inclination angles. A LS-DYNA model was first built having the same geometry, material properties, loading and boundary conditions as the specimen tested and investigated using ABAQUS by Webster et al. (2014). This LS-DYNA model was validated by comparing it with the Webster experimental and analytical load-drift hysteretic curve, as well as the average inclination angles of the diagonal tension field action over the entire plate. Variations in the inclination angle, and resulting stress distributions, at five locations within the web plate were obtained and analyzed in detail.

Two new LS-DYNA models, namely Model A and B, then were built to investigate how results would change considering solid web (the web in Websters' specimen had cutout in the corners) and different HBE-to-VBE connections (i.e., rigid instead of the pin connection used by Webster's). A combined moment-axial force demand ratio was introduced as a reasonable criterion to compare both the effect of axial and flexural demands on HBEs and VBEs obtained from the finite element analyses with those calculated using constant angle models.

Similar analyses were then performed on real SPSWs designed per AISC 341. Four real SPSWs with different aspect ratios and number of stories were designed and subjected to the same loads that were applied to a reference SPSW (called SW320) in Purba and Bruneau (2010). For these designs, the web plate thicknesses were designed to resist 100% of their story shear force. The HBE design followed the capacity design procedure in Bruneau et al (2011). Strip models were built in SAP2000 to assist the VBE design and check the sway mechanism of the whole structure.

New LS-DYNA models were constructed for the analysis of these four real SPSWs, by fully modeling the HBEs and VBEs. Analyses were conducted to determine variations in the inclination angles and the resulting combined moment-axial force demands. Results obtained from all these analyses were compared to assess sensitivity of results to wall aspect ratios and number of stories. An optimum constant angles for the design of SPSW was proposed to achieve simplicity in design while ensuring adequate conservatism (or acceptable unconservatism).

7.2 Conclusion

The variation in the inclination angle of diagonal tension field action observed in the seven models considered (i.e., the validated model in Section 3, Model A and B, SW11, SW12, SW31 and SW32) indicate that significantly different average inclination angles occur at different locations of the web plate and that each of those inclination angles vary as a function of drifts, panel aspect ratio, and number of stories. For real SPSWs designed per AISC 341, the inclination angle for the top beam, left column, and web plate usually varies from 35° to 45°, 45° to 65°, and 45° to 55°, respectively. Several major fluctuations in results are observed on the curve relating the inclination angle to drifts, as a consequence of how the deflected shape of the HBEs vary as web plate yielding and HBE hinging develop as drift increases. The shear deformations of HBEs can also have an impact on those fluctuations.

Variations in inclination angles were compared for SPSWs having panel aspect ratios of 1 and 2 and for single-story and three-story SPSWs. The aspect ratio has a noticeable impact on the inclination angle for the middle web of one-story SPSWs, with a maximum difference of 10° before 2% drift, and 3° for larger drifts when comparing results for SPSWs having panel aspect ratios of 1 and 2. It also influences the curves for the columns of the tall SPSWs by inducing serious fluctuations in results, but this effect diminishes at higher floors. The inclination angle for the top beams of tall SPSWs under varying aspect ratios generally have a difference within 4°. In addition, the number of stories have influence on all curves. For the columns, the curves for the one-story SPSW differ from those for the first floor of the corresponding three-story SPSWs by up to 10°. However, these differences decreased when compared to the higher floor of three-story SPSWs. For the beams, the curves obtained from the one-story SPSWs seldom match those on the floors of the corresponding three-story, with a maximum difference about 7°. Similar observation can be made for the middle web.

With respect to the combined moment-axial force demands, the analyses conducted indicated that changing the aspect ratio of the walls did not change the level of conservatism in the results obtained when comparing results for the same constant angles considered in respective one-story SPSWs, but that it would change the level of conservatism for the results obtained in three-story SPSWs, most significantly when using a constant angle of 45°. The number of stories was also found to have an impact on the conservatism of the results obtained using the constant angle of 45°, as the combined moment-axial force demand ratio of the top beams changed from being conservative to unconservative as the number of stories increased, and those for the left columns changed from being unconservative to conservative as the number of stories increased.

Based on the results obtained for the cases analyzed in this study, and particularly when considering the combined moment-axial force demands on the HBEs and VBEs, it is was found to be always conservative to use 35° and 40° for HBE and 50° for VBE design. Using a constant angle of 50° for HBE design could be unconservative by up to 18% while using constant angles of 35° and 40° for VBE design could be unconservative by up to 38% and 14%, respectively. However, using different inclination angles for HBEs and VBEs is not practical for design, and it is desirable to use a single constant angle for the design of all structural elements that constitute a SPSW. It is found that using a constant angle of 45° is adequate for web design and provides a good compromise for both HBEs and VBEs design if one desires to simplify the design process such as to use a single angle.

7.3 Recommendations for Future Research

This research considered seven SPSWs as case studies using finite element analysis. Four of these SPSWs had boundary elements designed in compliance with AISC 341, allowing two panel aspect ratios and two different of numbers of stories to be considered. More case studies could be conducted in the future to extend the number of SPSWs considered. Such future parametric studies would be useful to further investigate and verify the trends in variation of the inclination angle as a function of aspect ratio and number of stories.

Furthermore, all evidence accumulated to date to determine the value of constant angle were conducted using either monotonic loading or cyclic analysis scenarios. This was done because SPSW web plates are typically slender and behave in a “tension-only” manner, typically not “re-engaging” in subsequent cycles of displacement before reaching anew the maximum drift previous attained during a displacement history. However, future studies could investigate how whether results obtained would change significantly under actual seismic loading scenarios, possibly due to the small compression capacity that can develop in parts of the web plates (near the corners or in particularly thicker plates)

Also, here the HBEs of real SPSWs were designed to yield in flexure. However, significant shear deformations developed at the beam ends in the LS-DYNA model during the formation of the second plastic hinge (typically starting at drifts of 1%). It was observed here that inelastic deflections of HBEs has an impact on variation of the inclination angle. Further investigation would be required to quantify the influence of the shear deformation on the variation of the inclination angle. Besides, as further model improvements, flexible panel zones could be considered, and how this and the effect of the connection to HBEs could be accomplished to diminish the effect of shear deformations.

SECTION 8
REFERENCES

AISC. (2010). "Seismic Provisions for Structural Steel Buildings." ANSI/AISC 341-10 American Institute of Steel Construction, Inc., Chicago, IL.

AISC. (2010). "Specification for Structural Steel Buildings." ANSI/AISC 360-10 American Institute of Steel Construction, Inc., Chicago, IL.

Choi, I.R. and Park, H.G. (2009). "Steel plate shear walls with various infill plate designs." *J. Struct. Eng.*, 10.1061/ (ASCE) 0733-9445(2009)135:7(785), 785-796.

Dastfan, M. and Driver, R.G. (2008). "Flexural stiffness limits for frame members of steel plate shear wall systems." *Proc., Annual Stability Conf.*, Structural Stability Research Council, Nashville, TN, 321-334.

Driver, R. G., Kulak, G. L., Kennedy, D. J. L., and Elwi, A. E. (1997). "Seismic behavior of steel plate shear walls." *Structural Engineering Rep. No. 215*, Univ. of Alberta, Edmonton, Alberta.

Elgaaly, M., Caccese, V., and Du, C. (1993). "Post-buckling behavior of steel plate shear walls under cyclic loads." *J. Struct. Eng.,* 10.1061/ (ASCE) 0733-9445(1993)119:2(588), 588-605.

Kharrazi, M. H. K. (2005). "Rational method for analysis and design of steel plate walls." Doctoral dissertation, Univ. of British Columbia, Vancouver, BC.

Lubell, A. S. (1997). "Performance of unstiffened steel plate shear walls under cyclic quasi-static loading." Master's thesis, Univ. of British Columbia, Vancouver, BC.

LSTC. (2006). "LS-DYNA Theory Manual". Livermore Software Technology Corporation, Livermore, CA.

Purba, R., and Bruneau, M. (2010). "Impact of Horizontal Boundary Elements Design on Seismic Behavior of Steel Plate Shear Walls." *Technical Report No. MCEER-10-0007*, Multidisciplinary Center for Earthquake Engineering Research, Buffalo, NY.

Rezai, M. (1999). "Seismic behavior of steel plate shear walls by shake table testing." Doctoral dissertation, Univ. of British Columbia, Vancouver, BC.

Timler, P. A., and Kulak, G. L. (1983). "Experimental study of steel plate shear walls." *Structural Engineering Rep. No. 114*, Department of Civil Engineering, University of Alberta, Edmonton, Alberta, Canada.

Webster, D.J., (2013). "The Inelastic Seismic Response of Steel Plate Shear Wall Web Plates and Their Interaction with the Vertical Boundary Members." Ph.D. Dissertation, University of Washington, Washington.

Webster, D.J., Berman, and J. W., Lowes, L. N. (2014). "Experimental Investigation of SPSW Web Plate Stress Field Development and Vertical Boundary Element Demand". *Journal of Structural Engineering*, ASCE, Vol. 140, No 6, 04014011

MCEER Technical Reports

MCEER publishes technical reports on a variety of subjects written by authors funded through MCEER. These reports are available from both MCEER Publications and the National Technical Information Service (NTIS). Requests for reports should be directed to MCEER Publications, MCEER, University at Buffalo, State University of New York, 133A Ketter Hall, Buffalo, New York 14260. Reports can also be requested through NTIS, P.O. Box 1425, Springfield, Virginia 22151. NTIS accession numbers are shown in parenthesis, if available.

NCEER-87-0001 "First-Year Program in Research, Education and Technology Transfer," 3/5/87, (PB88-134275, A04, MF-A01).

NCEER-87-0002 "Experimental Evaluation of Instantaneous Optimal Algorithms for Structural Control," by R.C. Lin, T.T. Soong and A.M. Reinhorn, 4/20/87, (PB88-134341, A04, MF-A01).

NCEER-87-0003 "Experimentation Using the Earthquake Simulation Facilities at University at Buffalo," by A.M. Reinhorn and R.L. Ketter, not available.

NCEER-87-0004 "The System Characteristics and Performance of a Shaking Table," by J.S. Hwang, K.C. Chang and G.C. Lee, 6/1/87, (PB88-134259, A03, MF-A01). This report is available only through NTIS (see address given above).

NCEER-87-0005 "A Finite Element Formulation for Nonlinear Viscoplastic Material Using a Q Model," by O. Gyebi and G. Dasgupta, 11/2/87, (PB88-213764, A08, MF-A01).

NCEER-87-0006 "Symbolic Manipulation Program (SMP) - Algebraic Codes for Two and Three Dimensional Finite Element Formulations," by X. Lee and G. Dasgupta, 11/9/87, (PB88-218522, A05, MF-A01).

NCEER-87-0007 "Instantaneous Optimal Control Laws for Tall Buildings Under Seismic Excitations," by J.N. Yang, A. Akbarpour and P. Ghaemmaghami, 6/10/87, (PB88-134333, A06, MF-A01). This report is only available through NTIS (see address given above).

NCEER-87-0008 "IDARC: Inelastic Damage Analysis of Reinforced Concrete Frame - Shear-Wall Structures," by Y.J. Park, A.M. Reinhorn and S.K. Kunnath, 7/20/87, (PB88-134325, A09, MF-A01). This report is only available through NTIS (see address given above).

NCEER-87-0009 "Liquefaction Potential for New York State: A Preliminary Report on Sites in Manhattan and Buffalo," by M. Budhu, V. Vijayakumar, R.F. Giese and L. Baumgras, 8/31/87, (PB88-163704, A03, MF-A01). This report is available only through NTIS (see address given above).

NCEER-87-0010 "Vertical and Torsional Vibration of Foundations in Inhomogeneous Media," by A.S. Veletsos and K.W. Dotson, 6/1/87, (PB88-134291, A03, MF-A01). This report is only available through NTIS (see address given above).

NCEER-87-0011 "Seismic Probabilistic Risk Assessment and Seismic Margins Studies for Nuclear Power Plants," by Howard H.M. Hwang, 6/15/87, (PB88-134267, A03, MF-A01). This report is only available through NTIS (see address given above).

NCEER-87-0012 "Parametric Studies of Frequency Response of Secondary Systems Under Ground-Acceleration Excitations," by Y. Yong and Y.K. Lin, 6/10/87, (PB88-134309, A03, MF-A01). This report is only available through NTIS (see address given above).

NCEER-87-0013 "Frequency Response of Secondary Systems Under Seismic Excitation," by J.A. HoLung, J. Cai and Y.K. Lin, 7/31/87, (PB88-134317, A05, MF-A01). This report is only available through NTIS (see address given above).

NCEER-87-0014 "Modelling Earthquake Ground Motions in Seismically Active Regions Using Parametric Time Series Methods," by G.W. Ellis and A.S. Cakmak, 8/25/87, (PB88-134283, A08, MF-A01). This report is only available through NTIS (see address given above).

NCEER-87-0015 "Detection and Assessment of Seismic Structural Damage," by E. DiPasquale and A.S. Cakmak, 8/25/87, (PB88-163712, A05, MF-A01). This report is only available through NTIS (see address given above).

NCEER-87-0016 "Pipeline Experiment at Parkfield, California," by J. Isenberg and E. Richardson, 9/15/87, (PB88-163720, A03, MF-A01). This report is available only through NTIS (see address given above).

NCEER-87-0017 "Digital Simulation of Seismic Ground Motion," by M. Shinozuka, G. Deodatis and T. Harada, 8/31/87, (PB88-155197, A04, MF-A01). This report is available only through NTIS (see address given above).

NCEER-87-0018 "Practical Considerations for Structural Control: System Uncertainty, System Time Delay and Truncation of Small Control Forces," J.N. Yang and A. Akbarpour, 8/10/87, (PB88-163738, A08, MF-A01). This report is only available through NTIS (see address given above).

NCEER-87-0019 "Modal Analysis of Nonclassically Damped Structural Systems Using Canonical Transformation," by J.N. Yang, S. Sarkani and F.X. Long, 9/27/87, (PB88-187851, A04, MF-A01).

NCEER-87-0020 "A Nonstationary Solution in Random Vibration Theory," by J.R. Red-Horse and P.D. Spanos, 11/3/87, (PB88-163746, A03, MF-A01).

NCEER-87-0021 "Horizontal Impedances for Radially Inhomogeneous Viscoelastic Soil Layers," by A.S. Veletsos and K.W. Dotson, 10/15/87, (PB88-150859, A04, MF-A01).

NCEER-87-0022 "Seismic Damage Assessment of Reinforced Concrete Members," by Y.S. Chung, C. Meyer and M. Shinozuka, 10/9/87, (PB88-150867, A05, MF-A01). This report is available only through NTIS (see address given above).

NCEER-87-0023 "Active Structural Control in Civil Engineering," by T.T. Soong, 11/11/87, (PB88-187778, A03, MF-A01).

NCEER-87-0024 "Vertical and Torsional Impedances for Radially Inhomogeneous Viscoelastic Soil Layers," by K.W. Dotson and A.S. Veletsos, 12/87, (PB88-187786, A03, MF-A01).

NCEER-87-0025 "Proceedings from the Symposium on Seismic Hazards, Ground Motions, Soil-Liquefaction and Engineering Practice in Eastern North America," October 20-22, 1987, edited by K.H. Jacob, 12/87, (PB88-188115, A23, MF-A01). This report is available only through NTIS (see address given above).

NCEER-87-0026 "Report on the Whittier-Narrows, California, Earthquake of October 1, 1987," by J. Pantelic and A. Reinhorn, 11/87, (PB88-187752, A03, MF-A01). This report is available only through NTIS (see address given above).

NCEER-87-0027 "Design of a Modular Program for Transient Nonlinear Analysis of Large 3-D Building Structures," by S. Srivastav and J.F. Abel, 12/30/87, (PB88-187950, A05, MF-A01). This report is only available through NTIS (see address given above).

NCEER-87-0028 "Second-Year Program in Research, Education and Technology Transfer," 3/8/88, (PB88-219480, A04, MF-A01).

NCEER-88-0001 "Workshop on Seismic Computer Analysis and Design of Buildings With Interactive Graphics," by W. McGuire, J.F. Abel and C.H. Conley, 1/18/88, (PB88-187760, A03, MF-A01). This report is only available through NTIS (see address given above).

NCEER-88-0002 "Optimal Control of Nonlinear Flexible Structures," by J.N. Yang, F.X. Long and D. Wong, 1/22/88, (PB88-213772, A06, MF-A01).

NCEER-88-0003 "Substructuring Techniques in the Time Domain for Primary-Secondary Structural Systems," by G.D. Manolis and G. Juhn, 2/10/88, (PB88-213780, A04, MF-A01).

NCEER-88-0004 "Iterative Seismic Analysis of Primary-Secondary Systems," by A. Singhal, L.D. Lutes and P.D. Spanos, 2/23/88, (PB88-213798, A04, MF-A01).

NCEER-88-0005 "Stochastic Finite Element Expansion for Random Media," by P.D. Spanos and R. Ghanem, 3/14/88, (PB88-213806, A03, MF-A01).

NCEER-88-0006 "Combining Structural Optimization and Structural Control," by F.Y. Cheng and C.P. Pantelides, 1/10/88, (PB88-213814, A05, MF-A01).

NCEER-88-0007 "Seismic Performance Assessment of Code-Designed Structures," by H.H-M. Hwang, J-W. Jaw and H-J. Shau, 3/20/88, (PB88-219423, A04, MF-A01). This report is only available through NTIS (see address given above).

NCEER-88-0008 "Reliability Analysis of Code-Designed Structures Under Natural Hazards," by H.H-M. Hwang, H. Ushiba and M. Shinozuka, 2/29/88, (PB88-229471, A07, MF-A01). This report is only available through NTIS (see address given above).

NCEER-88-0009 "Seismic Fragility Analysis of Shear Wall Structures," by J-W Jaw and H.H-M. Hwang, 4/30/88, (PB89-102867, A04, MF-A01).

NCEER-88-0010 "Base Isolation of a Multi-Story Building Under a Harmonic Ground Motion - A Comparison of Performances of Various Systems," by F-G Fan, G. Ahmadi and I.G. Tadjbakhsh, 5/18/88, (PB89-122238, A06, MF-A01). This report is only available through NTIS (see address given above).

NCEER-88-0011 "Seismic Floor Response Spectra for a Combined System by Green's Functions," by F.M. Lavelle, L.A. Bergman and P.D. Spanos, 5/1/88, (PB89-102875, A03, MF-A01).

NCEER-88-0012 "A New Solution Technique for Randomly Excited Hysteretic Structures," by G.Q. Cai and Y.K. Lin, 5/16/88, (PB89-102883, A03, MF-A01).

NCEER-88-0013 "A Study of Radiation Damping and Soil-Structure Interaction Effects in the Centrifuge," by K. Weissman, supervised by J.H. Prevost, 5/24/88, (PB89-144703, A06, MF-A01).

NCEER-88-0014 "Parameter Identification and Implementation of a Kinematic Plasticity Model for Frictional Soils," by J.H. Prevost and D.V. Griffiths, not available.

NCEER-88-0015 "Two- and Three- Dimensional Dynamic Finite Element Analyses of the Long Valley Dam," by D.V. Griffiths and J.H. Prevost, 6/17/88, (PB89-144711, A04, MF-A01).

NCEER-88-0016 "Damage Assessment of Reinforced Concrete Structures in Eastern United States," by A.M. Reinhorn, M.J. Seidel, S.K. Kunnath and Y.J. Park, 6/15/88, (PB89-122220, A04, MF-A01). This report is only available through NTIS (see address given above).

NCEER-88-0017 "Dynamic Compliance of Vertically Loaded Strip Foundations in Multilayered Viscoelastic Soils," by S. Ahmad and A.S.M. Israil, 6/17/88, (PB89-102891, A04, MF-A01).

NCEER-88-0018 "An Experimental Study of Seismic Structural Response With Added Viscoelastic Dampers," by R.C. Lin, Z. Liang, T.T. Soong and R.H. Zhang, 6/30/88, (PB89-122212, A05, MF-A01). This report is available only through NTIS (see address given above).

NCEER-88-0019 "Experimental Investigation of Primary - Secondary System Interaction," by G.D. Manolis, G. Juhn and A.M. Reinhorn, 5/27/88, (PB89-122204, A04, MF-A01).

NCEER-88-0020 "A Response Spectrum Approach For Analysis of Nonclassically Damped Structures," by J.N. Yang, S. Sarkani and F.X. Long, 4/22/88, (PB89-102909, A04, MF-A01).

NCEER-88-0021 "Seismic Interaction of Structures and Soils: Stochastic Approach," by A.S. Veletsos and A.M. Prasad, 7/21/88, (PB89-122196, A04, MF-A01). This report is only available through NTIS (see address given above).

NCEER-88-0022 "Identification of the Serviceability Limit State and Detection of Seismic Structural Damage," by E. DiPasquale and A.S. Cakmak, 6/15/88, (PB89-122188, A05, MF-A01). This report is available only through NTIS (see address given above).

NCEER-88-0023 "Multi-Hazard Risk Analysis: Case of a Simple Offshore Structure," by B.K. Bhartia and E.H. Vanmarcke, 7/21/88, (PB89-145213, A05, MF-A01).

NCEER-88-0024 "Automated Seismic Design of Reinforced Concrete Buildings," by Y.S. Chung, C. Meyer and M. Shinozuka, 7/5/88, (PB89-122170, A06, MF-A01). This report is available only through NTIS (see address given above).

NCEER-88-0025 "Experimental Study of Active Control of MDOF Structures Under Seismic Excitations," by L.L. Chung, R.C. Lin, T.T. Soong and A.M. Reinhorn, 7/10/88, (PB89-122600, A04, MF-A01).

NCEER-88-0026 "Earthquake Simulation Tests of a Low-Rise Metal Structure," by J.S. Hwang, K.C. Chang, G.C. Lee and R.L. Ketter, 8/1/88, (PB89-102917, A04, MF-A01).

NCEER-88-0027 "Systems Study of Urban Response and Reconstruction Due to Catastrophic Earthquakes," by F. Kozin and H.K. Zhou, 9/22/88, (PB90-162348, A04, MF-A01).

NCEER-88-0028 "Seismic Fragility Analysis of Plane Frame Structures," by H.H-M. Hwang and Y.K. Low, 7/31/88, (PB89-131445, A06, MF-A01).

NCEER-88-0029 "Response Analysis of Stochastic Structures," by A. Kardara, C. Bucher and M. Shinozuka, 9/22/88, (PB89-174429, A04, MF-A01).

NCEER-88-0030 "Nonnormal Accelerations Due to Yielding in a Primary Structure," by D.C.K. Chen and L.D. Lutes, 9/19/88, (PB89-131437, A04, MF-A01).

NCEER-88-0031 "Design Approaches for Soil-Structure Interaction," by A.S. Veletsos, A.M. Prasad and Y. Tang, 12/30/88, (PB89-174437, A03, MF-A01). This report is available only through NTIS (see address given above).

NCEER-88-0032 "A Re-evaluation of Design Spectra for Seismic Damage Control," by C.J. Turkstra and A.G. Tallin, 11/7/88, (PB89-145221, A05, MF-A01).

NCEER-88-0033 "The Behavior and Design of Noncontact Lap Splices Subjected to Repeated Inelastic Tensile Loading," by V.E. Sagan, P. Gergely and R.N. White, 12/8/88, (PB89-163737, A08, MF-A01).

NCEER-88-0034 "Seismic Response of Pile Foundations," by S.M. Mamoon, P.K. Banerjee and S. Ahmad, 11/1/88, (PB89-145239, A04, MF-A01).

NCEER-88-0035 "Modeling of R/C Building Structures With Flexible Floor Diaphragms (IDARC2)," by A.M. Reinhorn, S.K. Kunnath and N. Panahshahi, 9/7/88, (PB89-207153, A07, MF-A01).

NCEER-88-0036 "Solution of the Dam-Reservoir Interaction Problem Using a Combination of FEM, BEM with Particular Integrals, Modal Analysis, and Substructuring," by C-S. Tsai, G.C. Lee and R.L. Ketter, 12/31/88, (PB89-207146, A04, MF-A01).

NCEER-88-0037 "Optimal Placement of Actuators for Structural Control," by F.Y. Cheng and C.P. Pantelides, 8/15/88, (PB89-162846, A05, MF-A01).

NCEER-88-0038 "Teflon Bearings in Aseismic Base Isolation: Experimental Studies and Mathematical Modeling," by A. Mokha, M.C. Constantinou and A.M. Reinhorn, 12/5/88, (PB89-218457, A10, MF-A01). This report is available only through NTIS (see address given above).

NCEER-88-0039 "Seismic Behavior of Flat Slab High-Rise Buildings in the New York City Area," by P. Weidlinger and M. Ettouney, 10/15/88, (PB90-145681, A04, MF-A01).

NCEER-88-0040 "Evaluation of the Earthquake Resistance of Existing Buildings in New York City," by P. Weidlinger and M. Ettouney, 10/15/88, not available.

NCEER-88-0041 "Small-Scale Modeling Techniques for Reinforced Concrete Structures Subjected to Seismic Loads," by W. Kim, A. El-Attar and R.N. White, 11/22/88, (PB89-189625, A05, MF-A01).

NCEER-88-0042 "Modeling Strong Ground Motion from Multiple Event Earthquakes," by G.W. Ellis and A.S. Cakmak, 10/15/88, (PB89-174445, A03, MF-A01).

NCEER-88-0043 "Nonstationary Models of Seismic Ground Acceleration," by M. Grigoriu, S.E. Ruiz and E. Rosenblueth, 7/15/88, (PB89-189617, A04, MF-A01).

NCEER-88-0044 "SARCF User's Guide: Seismic Analysis of Reinforced Concrete Frames," by Y.S. Chung, C. Meyer and M. Shinozuka, 11/9/88, (PB89-174452, A08, MF-A01).

NCEER-88-0045 "First Expert Panel Meeting on Disaster Research and Planning," edited by J. Pantelic and J. Stoyle, 9/15/88, (PB89-174460, A05, MF-A01).

NCEER-88-0046 "Preliminary Studies of the Effect of Degrading Infill Walls on the Nonlinear Seismic Response of Steel Frames," by C.Z. Chrysostomou, P. Gergely and J.F. Abel, 12/19/88, (PB89-208383, A05, MF-A01).

NCEER-88-0047 "Reinforced Concrete Frame Component Testing Facility - Design, Construction, Instrumentation and Operation," by S.P. Pessiki, C. Conley, T. Bond, P. Gergely and R.N. White, 12/16/88, (PB89-174478, A04, MF-A01).

NCEER-89-0001 "Effects of Protective Cushion and Soil Compliancy on the Response of Equipment Within a Seismically Excited Building," by J.A. HoLung, 2/16/89, (PB89-207179, A04, MF-A01).

NCEER-89-0002 "Statistical Evaluation of Response Modification Factors for Reinforced Concrete Structures," by H.H-M. Hwang and J-W. Jaw, 2/17/89, (PB89-207187, A05, MF-A01).

NCEER-89-0003 "Hysteretic Columns Under Random Excitation," by G-Q. Cai and Y.K. Lin, 1/9/89, (PB89-196513, A03, MF-A01).

NCEER-89-0004 "Experimental Study of `Elephant Foot Bulge' Instability of Thin-Walled Metal Tanks," by Z-H. Jia and R.L. Ketter, 2/22/89, (PB89-207195, A03, MF-A01).

NCEER-89-0005 "Experiment on Performance of Buried Pipelines Across San Andreas Fault," by J. Isenberg, E. Richardson and T.D. O'Rourke, 3/10/89, (PB89-218440, A04, MF-A01). This report is available only through NTIS (see address given above).

NCEER-89-0006 "A Knowledge-Based Approach to Structural Design of Earthquake-Resistant Buildings," by M. Subramani, P. Gergely, C.H. Conley, J.F. Abel and A.H. Zaghw, 1/15/89, (PB89-218465, A06, MF-A01).

NCEER-89-0007 "Liquefaction Hazards and Their Effects on Buried Pipelines," by T.D. O'Rourke and P.A. Lane, 2/1/89, (PB89-218481, A09, MF-A01).

NCEER-89-0008 "Fundamentals of System Identification in Structural Dynamics," by H. Imai, C-B. Yun, O. Maruyama and M. Shinozuka, 1/26/89, (PB89-207211, A04, MF-A01).

NCEER-89-0009 "Effects of the 1985 Michoacan Earthquake on Water Systems and Other Buried Lifelines in Mexico," by A.G. Ayala and M.J. O'Rourke, 3/8/89, (PB89-207229, A06, MF-A01).

NCEER-89-R010 "NCEER Bibliography of Earthquake Education Materials," by K.E.K. Ross, Second Revision, 9/1/89, (PB90-125352, A05, MF-A01). This report is replaced by NCEER-92-0018.

NCEER-89-0011 "Inelastic Three-Dimensional Response Analysis of Reinforced Concrete Building Structures (IDARC-3D), Part I - Modeling," by S.K. Kunnath and A.M. Reinhorn, 4/17/89, (PB90-114612, A07, MF-A01). This report is available only through NTIS (see address given above).

NCEER-89-0012 "Recommended Modifications to ATC-14," by C.D. Poland and J.O. Malley, 4/12/89, (PB90-108648, A15, MF-A01).

NCEER-89-0013 "Repair and Strengthening of Beam-to-Column Connections Subjected to Earthquake Loading," by M. Corazao and A.J. Durrani, 2/28/89, (PB90-109885, A06, MF-A01).

NCEER-89-0014 "Program EXKAL2 for Identification of Structural Dynamic Systems," by O. Maruyama, C-B. Yun, M. Hoshiya and M. Shinozuka, 5/19/89, (PB90-109877, A09, MF-A01).

NCEER-89-0015 "Response of Frames With Bolted Semi-Rigid Connections, Part I - Experimental Study and Analytical Predictions," by P.J. DiCorso, A.M. Reinhorn, J.R. Dickerson, J.B. Radziminski and W.L. Harper, 6/1/89, not available.

NCEER-89-0016 "ARMA Monte Carlo Simulation in Probabilistic Structural Analysis," by P.D. Spanos and M.P. Mignolet, 7/10/89, (PB90-109893, A03, MF-A01).

NCEER-89-P017 "Preliminary Proceedings from the Conference on Disaster Preparedness - The Place of Earthquake Education in Our Schools," Edited by K.E.K. Ross, 6/23/89, (PB90-108606, A03, MF-A01).

NCEER-89-0017 "Proceedings from the Conference on Disaster Preparedness - The Place of Earthquake Education in Our Schools," Edited by K.E.K. Ross, 12/31/89, (PB90-207895, A012, MF-A02). This report is available only through NTIS (see address given above).

NCEER-89-0018 "Multidimensional Models of Hysteretic Material Behavior for Vibration Analysis of Shape Memory Energy Absorbing Devices, by E.J. Graesser and F.A. Cozzarelli, 6/7/89, (PB90-164146, A04, MF-A01).

NCEER-89-0019 "Nonlinear Dynamic Analysis of Three-Dimensional Base Isolated Structures (3D-BASIS)," by S. Nagarajaiah, A.M. Reinhorn and M.C. Constantinou, 8/3/89, (PB90-161936, A06, MF-A01). This report has been replaced by NCEER-93-0011.

NCEER-89-0020 "Structural Control Considering Time-Rate of Control Forces and Control Rate Constraints," by F.Y. Cheng and C.P. Pantelides, 8/3/89, (PB90-120445, A04, MF-A01).

NCEER-89-0021 "Subsurface Conditions of Memphis and Shelby County," by K.W. Ng, T-S. Chang and H-H.M. Hwang, 7/26/89, (PB90-120437, A03, MF-A01).

NCEER-89-0022 "Seismic Wave Propagation Effects on Straight Jointed Buried Pipelines," by K. Elhmadi and M.J. O'Rourke, 8/24/89, (PB90-162322, A10, MF-A02).

NCEER-89-0023 "Workshop on Serviceability Analysis of Water Delivery Systems," edited by M. Grigoriu, 3/6/89, (PB90-127424, A03, MF-A01).

NCEER-89-0024 "Shaking Table Study of a 1/5 Scale Steel Frame Composed of Tapered Members," by K.C. Chang, J.S. Hwang and G.C. Lee, 9/18/89, (PB90-160169, A04, MF-A01).

NCEER-89-0025 "DYNA1D: A Computer Program for Nonlinear Seismic Site Response Analysis - Technical Documentation," by Jean H. Prevost, 9/14/89, (PB90-161944, A07, MF-A01). This report is available only through NTIS (see address given above).

NCEER-89-0026 "1:4 Scale Model Studies of Active Tendon Systems and Active Mass Dampers for Aseismic Protection," by A.M. Reinhorn, T.T. Soong, R.C. Lin, Y.P. Yang, Y. Fukao, H. Abe and M. Nakai, 9/15/89, (PB90-173246, A10, MF-A02). This report is available only through NTIS (see address given above).

NCEER-89-0027 "Scattering of Waves by Inclusions in a Nonhomogeneous Elastic Half Space Solved by Boundary Element Methods," by P.K. Hadley, A. Askar and A.S. Cakmak, 6/15/89, (PB90-145699, A07, MF-A01).

NCEER-89-0028 "Statistical Evaluation of Deflection Amplification Factors for Reinforced Concrete Structures," by H.H.M. Hwang, J-W. Jaw and A.L. Ch'ng, 8/31/89, (PB90-164633, A05, MF-A01).

NCEER-89-0029 "Bedrock Accelerations in Memphis Area Due to Large New Madrid Earthquakes," by H.H.M. Hwang, C.H.S. Chen and G. Yu, 11/7/89, (PB90-162330, A04, MF-A01).

NCEER-89-0030 "Seismic Behavior and Response Sensitivity of Secondary Structural Systems," by Y.Q. Chen and T.T. Soong, 10/23/89, (PB90-164658, A08, MF-A01).

NCEER-89-0031 "Random Vibration and Reliability Analysis of Primary-Secondary Structural Systems," by Y. Ibrahim, M. Grigoriu and T.T. Soong, 11/10/89, (PB90-161951, A04, MF-A01).

NCEER-89-0032 "Proceedings from the Second U.S. - Japan Workshop on Liquefaction, Large Ground Deformation and Their Effects on Lifelines, September 26-29, 1989," Edited by T.D. O'Rourke and M. Hamada, 12/1/89, (PB90-209388, A22, MF-A03).

NCEER-89-0033 "Deterministic Model for Seismic Damage Evaluation of Reinforced Concrete Structures," by J.M. Bracci, A.M. Reinhorn, J.B. Mander and S.K. Kunnath, 9/27/89, (PB91-108803, A06, MF-A01).

NCEER-89-0034 "On the Relation Between Local and Global Damage Indices," by E. DiPasquale and A.S. Cakmak, 8/15/89, (PB90-173865, A05, MF-A01).

NCEER-89-0035 "Cyclic Undrained Behavior of Nonplastic and Low Plasticity Silts," by A.J. Walker and H.E. Stewart, 7/26/89, (PB90-183518, A10, MF-A01).

NCEER-89-0036 "Liquefaction Potential of Surficial Deposits in the City of Buffalo, New York," by M. Budhu, R. Giese and L. Baumgrass, 1/17/89, (PB90-208455, A04, MF-A01).

NCEER-89-0037 "A Deterministic Assessment of Effects of Ground Motion Incoherence," by A.S. Veletsos and Y. Tang, 7/15/89, (PB90-164294, A03, MF-A01).

NCEER-89-0038 "Workshop on Ground Motion Parameters for Seismic Hazard Mapping," July 17-18, 1989, edited by R.V. Whitman, 12/1/89, (PB90-173923, A04, MF-A01).

NCEER-89-0039 "Seismic Effects on Elevated Transit Lines of the New York City Transit Authority," by C.J. Costantino, C.A. Miller and E. Heymsfield, 12/26/89, (PB90-207887, A06, MF-A01).

NCEER-89-0040 "Centrifugal Modeling of Dynamic Soil-Structure Interaction," by K. Weissman, Supervised by J.H. Prevost, 5/10/89, (PB90-207879, A07, MF-A01).

NCEER-89-0041 "Linearized Identification of Buildings With Cores for Seismic Vulnerability Assessment," by I-K. Ho and A.E. Aktan, 11/1/89, (PB90-251943, A07, MF-A01).

NCEER-90-0001 "Geotechnical and Lifeline Aspects of the October 17, 1989 Loma Prieta Earthquake in San Francisco," by T.D. O'Rourke, H.E. Stewart, F.T. Blackburn and T.S. Dickerman, 1/90, (PB90-208596, A05, MF-A01).

NCEER-90-0002 "Nonnormal Secondary Response Due to Yielding in a Primary Structure," by D.C.K. Chen and L.D. Lutes, 2/28/90, (PB90-251976, A07, MF-A01).

NCEER-90-0003 "Earthquake Education Materials for Grades K-12," by K.E.K. Ross, 4/16/90, (PB91-251984, A05, MF-A05). This report has been replaced by NCEER-92-0018.

NCEER-90-0004 "Catalog of Strong Motion Stations in Eastern North America," by R.W. Busby, 4/3/90, (PB90-251984, A05, MF-A01).

NCEER-90-0005 "NCEER Strong-Motion Data Base: A User Manual for the GeoBase Release (Version 1.0 for the Sun3)," by P. Friberg and K. Jacob, 3/31/90 (PB90-258062, A04, MF-A01).

NCEER-90-0006 "Seismic Hazard Along a Crude Oil Pipeline in the Event of an 1811-1812 Type New Madrid Earthquake," by H.H.M. Hwang and C-H.S. Chen, 4/16/90, (PB90-258054, A04, MF-A01).

NCEER-90-0007 "Site-Specific Response Spectra for Memphis Sheahan Pumping Station," by H.H.M. Hwang and C.S. Lee, 5/15/90, (PB91-108811, A05, MF-A01).

NCEER-90-0008 "Pilot Study on Seismic Vulnerability of Crude Oil Transmission Systems," by T. Ariman, R. Dobry, M. Grigoriu, F. Kozin, M. O'Rourke, T. O'Rourke and M. Shinozuka, 5/25/90, (PB91-108837, A06, MF-A01).

NCEER-90-0009 "A Program to Generate Site Dependent Time Histories: EQGEN," by G.W. Ellis, M. Srinivasan and A.S. Cakmak, 1/30/90, (PB91-108829, A04, MF-A01).

NCEER-90-0010 "Active Isolation for Seismic Protection of Operating Rooms," by M.E. Talbott, Supervised by M. Shinozuka, 6/8/9, (PB91-110205, A05, MF-A01).

NCEER-90-0011 "Program LINEARID for Identification of Linear Structural Dynamic Systems," by C-B. Yun and M. Shinozuka, 6/25/90, (PB91-110312, A08, MF-A01).

NCEER-90-0012 "Two-Dimensional Two-Phase Elasto-Plastic Seismic Response of Earth Dams," by A.N. Yiagos, Supervised by J.H. Prevost, 6/20/90, (PB91-110197, A13, MF-A02).

NCEER-90-0013 "Secondary Systems in Base-Isolated Structures: Experimental Investigation, Stochastic Response and Stochastic Sensitivity," by G.D. Manolis, G. Juhn, M.C. Constantinou and A.M. Reinhorn, 7/1/90, (PB91-110320, A08, MF-A01).

NCEER-90-0014 "Seismic Behavior of Lightly-Reinforced Concrete Column and Beam-Column Joint Details," by S.P. Pessiki, C.H. Conley, P. Gergely and R.N. White, 8/22/90, (PB91-108795, A11, MF-A02).

NCEER-90-0015 "Two Hybrid Control Systems for Building Structures Under Strong Earthquakes," by J.N. Yang and A. Danielians, 6/29/90, (PB91-125393, A04, MF-A01).

NCEER-90-0016 "Instantaneous Optimal Control with Acceleration and Velocity Feedback," by J.N. Yang and Z. Li, 6/29/90, (PB91-125401, A03, MF-A01).

NCEER-90-0017 "Reconnaissance Report on the Northern Iran Earthquake of June 21, 1990," by M. Mehrain, 10/4/90, (PB91-125377, A03, MF-A01).

NCEER-90-0018 "Evaluation of Liquefaction Potential in Memphis and Shelby County," by T.S. Chang, P.S. Tang, C.S. Lee and H. Hwang, 8/10/90, (PB91-125427, A09, MF-A01).

NCEER-90-0019 "Experimental and Analytical Study of a Combined Sliding Disc Bearing and Helical Steel Spring Isolation System," by M.C. Constantinou, A.S. Mokha and A.M. Reinhorn, 10/4/90, (PB91-125385, A06, MF-A01). This report is available only through NTIS (see address given above).

NCEER-90-0020 "Experimental Study and Analytical Prediction of Earthquake Response of a Sliding Isolation System with a Spherical Surface," by A.S. Mokha, M.C. Constantinou and A.M. Reinhorn, 10/11/90, (PB91-125419, A05, MF-A01).

NCEER-90-0021 "Dynamic Interaction Factors for Floating Pile Groups," by G. Gazetas, K. Fan, A. Kaynia and E. Kausel, 9/10/90, (PB91-170381, A05, MF-A01).

NCEER-90-0022 "Evaluation of Seismic Damage Indices for Reinforced Concrete Structures," by S. Rodriguez-Gomez and A.S. Cakmak, 9/30/90, PB91-171322, A06, MF-A01).

NCEER-90-0023 "Study of Site Response at a Selected Memphis Site," by H. Desai, S. Ahmad, E.S. Gazetas and M.R. Oh, 10/11/90, (PB91-196857, A03, MF-A01).

NCEER-90-0024 "A User's Guide to Strongmo: Version 1.0 of NCEER's Strong-Motion Data Access Tool for PCs and Terminals," by P.A. Friberg and C.A.T. Susch, 11/15/90, (PB91-171272, A03, MF-A01).

NCEER-90-0025 "A Three-Dimensional Analytical Study of Spatial Variability of Seismic Ground Motions," by L-L. Hong and A.H.-S. Ang, 10/30/90, (PB91-170399, A09, MF-A01).

NCEER-90-0026 "MUMOID User's Guide - A Program for the Identification of Modal Parameters," by S. Rodriguez-Gomez and E. DiPasquale, 9/30/90, (PB91-171298, A04, MF-A01).

NCEER-90-0027 "SARCF-II User's Guide - Seismic Analysis of Reinforced Concrete Frames," by S. Rodriguez-Gomez, Y.S. Chung and C. Meyer, 9/30/90, (PB91-171280, A05, MF-A01).

NCEER-90-0028 "Viscous Dampers: Testing, Modeling and Application in Vibration and Seismic Isolation," by N. Makris and M.C. Constantinou, 12/20/90 (PB91-190561, A06, MF-A01).

NCEER-90-0029 "Soil Effects on Earthquake Ground Motions in the Memphis Area," by H. Hwang, C.S. Lee, K.W. Ng and T.S. Chang, 8/2/90, (PB91-190751, A05, MF-A01).

NCEER-91-0001 "Proceedings from the Third Japan-U.S. Workshop on Earthquake Resistant Design of Lifeline Facilities and Countermeasures for Soil Liquefaction, December 17-19, 1990," edited by T.D. O'Rourke and M. Hamada, 2/1/91, (PB91-179259, A99, MF-A04).

NCEER-91-0002 "Physical Space Solutions of Non-Proportionally Damped Systems," by M. Tong, Z. Liang and G.C. Lee, 1/15/91, (PB91-179242, A04, MF-A01).

NCEER-91-0003 "Seismic Response of Single Piles and Pile Groups," by K. Fan and G. Gazetas, 1/10/91, (PB92-174994, A04, MF-A01).

NCEER-91-0004 "Damping of Structures: Part 1 - Theory of Complex Damping," by Z. Liang and G. Lee, 10/10/91, (PB92-197235, A12, MF-A03).

NCEER-91-0005 "3D-BASIS - Nonlinear Dynamic Analysis of Three Dimensional Base Isolated Structures: Part II," by S. Nagarajaiah, A.M. Reinhorn and M.C. Constantinou, 2/28/91, (PB91-190553, A07, MF-A01). This report has been replaced by NCEER-93-0011.

NCEER-91-0006 "A Multidimensional Hysteretic Model for Plasticity Deforming Metals in Energy Absorbing Devices," by E.J. Graesser and F.A. Cozzarelli, 4/9/91, (PB92-108364, A04, MF-A01).

NCEER-91-0007 "A Framework for Customizable Knowledge-Based Expert Systems with an Application to a KBES for Evaluating the Seismic Resistance of Existing Buildings," by E.G. Ibarra-Anaya and S.J. Fenves, 4/9/91, (PB91-210930, A08, MF-A01).

NCEER-91-0008 "Nonlinear Analysis of Steel Frames with Semi-Rigid Connections Using the Capacity Spectrum Method," by G.G. Deierlein, S-H. Hsieh, Y-J. Shen and J.F. Abel, 7/2/91, (PB92-113828, A05, MF-A01).

NCEER-91-0009 "Earthquake Education Materials for Grades K-12," by K.E.K. Ross, 4/30/91, (PB91-212142, A06, MF-A01). This report has been replaced by NCEER-92-0018.

NCEER-91-0010 "Phase Wave Velocities and Displacement Phase Differences in a Harmonically Oscillating Pile," by N. Makris and G. Gazetas, 7/8/91, (PB92-108356, A04, MF-A01).

NCEER-91-0011 "Dynamic Characteristics of a Full-Size Five-Story Steel Structure and a 2/5 Scale Model," by K.C. Chang, G.C. Yao, G.C. Lee, D.S. Hao and Y.C. Yeh," 7/2/91, (PB93-116648, A06, MF-A02).

NCEER-91-0012 "Seismic Response of a 2/5 Scale Steel Structure with Added Viscoelastic Dampers," by K.C. Chang, T.T. Soong, S-T. Oh and M.L. Lai, 5/17/91, (PB92-110816, A05, MF-A01).

NCEER-91-0013 "Earthquake Response of Retaining Walls; Full-Scale Testing and Computational Modeling," by S. Alampalli and A-W.M. Elgamal, 6/20/91, not available.

NCEER-91-0014 "3D-BASIS-M: Nonlinear Dynamic Analysis of Multiple Building Base Isolated Structures," by P.C. Tsopelas, S. Nagarajaiah, M.C. Constantinou and A.M. Reinhorn, 5/28/91, (PB92-113885, A09, MF-A02).

NCEER-91-0015 "Evaluation of SEAOC Design Requirements for Sliding Isolated Structures," by D. Theodossiou and M.C. Constantinou, 6/10/91, (PB92-114602, A11, MF-A03).

NCEER-91-0016 "Closed-Loop Modal Testing of a 27-Story Reinforced Concrete Flat Plate-Core Building," by H.R. Somaprasad, T. Toksoy, H. Yoshiyuki and A.E. Aktan, 7/15/91, (PB92-129980, A07, MF-A02).

NCEER-91-0017 "Shake Table Test of a 1/6 Scale Two-Story Lightly Reinforced Concrete Building," by A.G. El-Attar, R.N. White and P. Gergely, 2/28/91, (PB92-222447, A06, MF-A02).

NCEER-91-0018 "Shake Table Test of a 1/8 Scale Three-Story Lightly Reinforced Concrete Building," by A.G. El-Attar, R.N. White and P. Gergely, 2/28/91, (PB93-116630, A08, MF-A02).

NCEER-91-0019 "Transfer Functions for Rigid Rectangular Foundations," by A.S. Veletsos, A.M. Prasad and W.H. Wu, 7/31/91, not available.

NCEER-91-0020 "Hybrid Control of Seismic-Excited Nonlinear and Inelastic Structural Systems," by J.N. Yang, Z. Li and A. Danielians, 8/1/91, (PB92-143171, A06, MF-A02).

NCEER-91-0021 "The NCEER-91 Earthquake Catalog: Improved Intensity-Based Magnitudes and Recurrence Relations for U.S. Earthquakes East of New Madrid," by L. Seeber and J.G. Armbruster, 8/28/91, (PB92-176742, A06, MF-A02).

NCEER-91-0022 "Proceedings from the Implementation of Earthquake Planning and Education in Schools: The Need for Change - The Roles of the Changemakers," by K.E.K. Ross and F. Winslow, 7/23/91, (PB92-129998, A12, MF-A03).

NCEER-91-0023 "A Study of Reliability-Based Criteria for Seismic Design of Reinforced Concrete Frame Buildings," by H.H.M. Hwang and H-M. Hsu, 8/10/91, (PB92-140235, A09, MF-A02).

NCEER-91-0024 "Experimental Verification of a Number of Structural System Identification Algorithms," by R.G. Ghanem, H. Gavin and M. Shinozuka, 9/18/91, (PB92-176577, A18, MF-A04).

NCEER-91-0025 "Probabilistic Evaluation of Liquefaction Potential," by H.H.M. Hwang and C.S. Lee," 11/25/91, (PB92-143429, A05, MF-A01).

NCEER-91-0026 "Instantaneous Optimal Control for Linear, Nonlinear and Hysteretic Structures - Stable Controllers," by J.N. Yang and Z. Li, 11/15/91, (PB92-163807, A04, MF-A01).

NCEER-91-0027 "Experimental and Theoretical Study of a Sliding Isolation System for Bridges," by M.C. Constantinou, A. Kartoum, A.M. Reinhorn and P. Bradford, 11/15/91, (PB92-176973, A10, MF-A03).

NCEER-92-0001 "Case Studies of Liquefaction and Lifeline Performance During Past Earthquakes, Volume 1: Japanese Case Studies," Edited by M. Hamada and T. O'Rourke, 2/17/92, (PB92-197243, A18, MF-A04).

NCEER-92-0002 "Case Studies of Liquefaction and Lifeline Performance During Past Earthquakes, Volume 2: United States Case Studies," Edited by T. O'Rourke and M. Hamada, 2/17/92, (PB92-197250, A20, MF-A04).

NCEER-92-0003 "Issues in Earthquake Education," Edited by K. Ross, 2/3/92, (PB92-222389, A07, MF-A02).

NCEER-92-0004 "Proceedings from the First U.S. - Japan Workshop on Earthquake Protective Systems for Bridges," Edited by I.G. Buckle, 2/4/92, (PB94-142239, A99, MF-A06).

NCEER-92-0005 "Seismic Ground Motion from a Haskell-Type Source in a Multiple-Layered Half-Space," A.P. Theoharis, G. Deodatis and M. Shinozuka, 1/2/92, not available.

NCEER-92-0006 "Proceedings from the Site Effects Workshop," Edited by R. Whitman, 2/29/92, (PB92-197201, A04, MF-A01).

NCEER-92-0007 "Engineering Evaluation of Permanent Ground Deformations Due to Seismically-Induced Liquefaction," by M.H. Baziar, R. Dobry and A-W.M. Elgamal, 3/24/92, (PB92-222421, A13, MF-A03).

NCEER-92-0008 "A Procedure for the Seismic Evaluation of Buildings in the Central and Eastern United States," by C.D. Poland and J.O. Malley, 4/2/92, (PB92-222439, A20, MF-A04).

NCEER-92-0009 "Experimental and Analytical Study of a Hybrid Isolation System Using Friction Controllable Sliding Bearings," by M.Q. Feng, S. Fujii and M. Shinozuka, 5/15/92, (PB93-150282, A06, MF-A02).

NCEER-92-0010 "Seismic Resistance of Slab-Column Connections in Existing Non-Ductile Flat-Plate Buildings," by A.J. Durrani and Y. Du, 5/18/92, (PB93-116812, A06, MF-A02).

NCEER-92-0011 "The Hysteretic and Dynamic Behavior of Brick Masonry Walls Upgraded by Ferrocement Coatings Under Cyclic Loading and Strong Simulated Ground Motion," by H. Lee and S.P. Prawel, 5/11/92, not available.

NCEER-92-0012 "Study of Wire Rope Systems for Seismic Protection of Equipment in Buildings," by G.F. Demetriades, M.C. Constantinou and A.M. Reinhorn, 5/20/92, (PB93-116655, A08, MF-A02).

NCEER-92-0013 "Shape Memory Structural Dampers: Material Properties, Design and Seismic Testing," by P.R. Witting and F.A. Cozzarelli, 5/26/92, (PB93-116663, A05, MF-A01).

NCEER-92-0014 "Longitudinal Permanent Ground Deformation Effects on Buried Continuous Pipelines," by M.J. O'Rourke, and C. Nordberg, 6/15/92, (PB93-116671, A08, MF-A02).

NCEER-92-0015 "A Simulation Method for Stationary Gaussian Random Functions Based on the Sampling Theorem," by M. Grigoriu and S. Balopoulou, 6/11/92, (PB93-127496, A05, MF-A01).

NCEER-92-0016 "Gravity-Load-Designed Reinforced Concrete Buildings: Seismic Evaluation of Existing Construction and Detailing Strategies for Improved Seismic Resistance," by G.W. Hoffmann, S.K. Kunnath, A.M. Reinhorn and J.B. Mander, 7/15/92, (PB94-142007, A08, MF-A02).

NCEER-92-0017 "Observations on Water System and Pipeline Performance in the Limón Area of Costa Rica Due to the April 22, 1991 Earthquake," by M. O'Rourke and D. Ballantyne, 6/30/92, (PB93-126811, A06, MF-A02).

NCEER-92-0018 "Fourth Edition of Earthquake Education Materials for Grades K-12," Edited by K.E.K. Ross, 8/10/92, (PB93-114023, A07, MF-A02).

NCEER-92-0019 "Proceedings from the Fourth Japan-U.S. Workshop on Earthquake Resistant Design of Lifeline Facilities and Countermeasures for Soil Liquefaction," Edited by M. Hamada and T.D. O'Rourke, 8/12/92, (PB93-163939, A99, MF-E11).

NCEER-92-0020 "Active Bracing System: A Full Scale Implementation of Active Control," by A.M. Reinhorn, T.T. Soong, R.C. Lin, M.A. Riley, Y.P. Wang, S. Aizawa and M. Higashino, 8/14/92, (PB93-127512, A06, MF-A02).

NCEER-92-0021 "Empirical Analysis of Horizontal Ground Displacement Generated by Liquefaction-Induced Lateral Spreads," by S.F. Bartlett and T.L. Youd, 8/17/92, (PB93-188241, A06, MF-A02).

NCEER-92-0022 "IDARC Version 3.0: Inelastic Damage Analysis of Reinforced Concrete Structures," by S.K. Kunnath, A.M. Reinhorn and R.F. Lobo, 8/31/92, (PB93-227502, A07, MF-A02).

NCEER-92-0023 "A Semi-Empirical Analysis of Strong-Motion Peaks in Terms of Seismic Source, Propagation Path and Local Site Conditions, by M. Kamiyama, M.J. O'Rourke and R. Flores-Berrones, 9/9/92, (PB93-150266, A08, MF-A02).

NCEER-92-0024 "Seismic Behavior of Reinforced Concrete Frame Structures with Nonductile Details, Part I: Summary of Experimental Findings of Full Scale Beam-Column Joint Tests," by A. Beres, R.N. White and P. Gergely, 9/30/92, (PB93-227783, A05, MF-A01).

NCEER-92-0025 "Experimental Results of Repaired and Retrofitted Beam-Column Joint Tests in Lightly Reinforced Concrete Frame Buildings," by A. Beres, S. El-Borgi, R.N. White and P. Gergely, 10/29/92, (PB93-227791, A05, MF-A01).

NCEER-92-0026 "A Generalization of Optimal Control Theory: Linear and Nonlinear Structures," by J.N. Yang, Z. Li and S. Vongchavalitkul, 11/2/92, (PB93-188621, A05, MF-A01).

NCEER-92-0027 "Seismic Resistance of Reinforced Concrete Frame Structures Designed Only for Gravity Loads: Part I - Design and Properties of a One-Third Scale Model Structure," by J.M. Bracci, A.M. Reinhorn and J.B. Mander, 12/1/92, (PB94-104502, A08, MF-A02).

NCEER-92-0028 "Seismic Resistance of Reinforced Concrete Frame Structures Designed Only for Gravity Loads: Part II - Experimental Performance of Subassemblages," by L.E. Aycardi, J.B. Mander and A.M. Reinhorn, 12/1/92, (PB94-104510, A08, MF-A02).

NCEER-92-0029 "Seismic Resistance of Reinforced Concrete Frame Structures Designed Only for Gravity Loads: Part III - Experimental Performance and Analytical Study of a Structural Model," by J.M. Bracci, A.M. Reinhorn and J.B. Mander, 12/1/92, (PB93-227528, A09, MF-A01).

NCEER-92-0030 "Evaluation of Seismic Retrofit of Reinforced Concrete Frame Structures: Part I - Experimental Performance of Retrofitted Subassemblages," by D. Choudhuri, J.B. Mander and A.M. Reinhorn, 12/8/92, (PB93-198307, A07, MF-A02).

NCEER-92-0031 "Evaluation of Seismic Retrofit of Reinforced Concrete Frame Structures: Part II - Experimental Performance and Analytical Study of a Retrofitted Structural Model," by J.M. Bracci, A.M. Reinhorn and J.B. Mander, 12/8/92, (PB93-198315, A09, MF-A03).

NCEER-92-0032 "Experimental and Analytical Investigation of Seismic Response of Structures with Supplemental Fluid Viscous Dampers," by M.C. Constantinou and M.D. Symans, 12/21/92, (PB93-191435, A10, MF-A03). This report is available only through NTIS (see address given above).

NCEER-92-0033 "Reconnaissance Report on the Cairo, Egypt Earthquake of October 12, 1992," by M. Khater, 12/23/92, (PB93-188621, A03, MF-A01).

NCEER-92-0034 "Low-Level Dynamic Characteristics of Four Tall Flat-Plate Buildings in New York City," by H. Gavin, S. Yuan, J. Grossman, E. Pekelis and K. Jacob, 12/28/92, (PB93-188217, A07, MF-A02).

NCEER-93-0001 "An Experimental Study on the Seismic Performance of Brick-Infilled Steel Frames With and Without Retrofit," by J.B. Mander, B. Nair, K. Wojtkowski and J. Ma, 1/29/93, (PB93-227510, A07, MF-A02).

NCEER-93-0002 "Social Accounting for Disaster Preparedness and Recovery Planning," by S. Cole, E. Pantoja and V. Razak, 2/22/93, (PB94-142114, A12, MF-A03).

NCEER-93-0003 "Assessment of 1991 NEHRP Provisions for Nonstructural Components and Recommended Revisions," by T.T. Soong, G. Chen, Z. Wu, R-H. Zhang and M. Grigoriu, 3/1/93, (PB93-188639, A06, MF-A02).

NCEER-93-0004 "Evaluation of Static and Response Spectrum Analysis Procedures of SEAOC/UBC for Seismic Isolated Structures," by C.W. Winters and M.C. Constantinou, 3/23/93, (PB93-198299, A10, MF-A03).

NCEER-93-0005 "Earthquakes in the Northeast - Are We Ignoring the Hazard? A Workshop on Earthquake Science and Safety for Educators," edited by K.E.K. Ross, 4/2/93, (PB94-103066, A09, MF-A02).

NCEER-93-0006 "Inelastic Response of Reinforced Concrete Structures with Viscoelastic Braces," by R.F. Lobo, J.M. Bracci, K.L. Shen, A.M. Reinhorn and T.T. Soong, 4/5/93, (PB93-227486, A05, MF-A02).

NCEER-93-0007 "Seismic Testing of Installation Methods for Computers and Data Processing Equipment," by K. Kosar, T.T. Soong, K.L. Shen, J.A. HoLung and Y.K. Lin, 4/12/93, (PB93-198299, A07, MF-A02).

NCEER-93-0008 "Retrofit of Reinforced Concrete Frames Using Added Dampers," by A. Reinhorn, M. Constantinou and C. Li, not available.

NCEER-93-0009 "Seismic Behavior and Design Guidelines for Steel Frame Structures with Added Viscoelastic Dampers," by K.C. Chang, M.L. Lai, T.T. Soong, D.S. Hao and Y.C. Yeh, 5/1/93, (PB94-141959, A07, MF-A02).

NCEER-93-0010 "Seismic Performance of Shear-Critical Reinforced Concrete Bridge Piers," by J.B. Mander, S.M. Waheed, M.T.A. Chaudhary and S.S. Chen, 5/12/93, (PB93-227494, A08, MF-A02).

NCEER-93-0011 "3D-BASIS-TABS: Computer Program for Nonlinear Dynamic Analysis of Three Dimensional Base Isolated Structures," by S. Nagarajaiah, C. Li, A.M. Reinhorn and M.C. Constantinou, 8/2/93, (PB94-141819, A09, MF-A02).

NCEER-93-0012 "Effects of Hydrocarbon Spills from an Oil Pipeline Break on Ground Water," by O.J. Helweg and H.H.M. Hwang, 8/3/93, (PB94-141942, A06, MF-A02).

NCEER-93-0013 "Simplified Procedures for Seismic Design of Nonstructural Components and Assessment of Current Code Provisions," by M.P. Singh, L.E. Suarez, E.E. Matheu and G.O. Maldonado, 8/4/93, (PB94-141827, A09, MF-A02).

NCEER-93-0014 "An Energy Approach to Seismic Analysis and Design of Secondary Systems," by G. Chen and T.T. Soong, 8/6/93, (PB94-142767, A11, MF-A03).

NCEER-93-0015 "Proceedings from School Sites: Becoming Prepared for Earthquakes - Commemorating the Third Anniversary of the Loma Prieta Earthquake," Edited by F.E. Winslow and K.E.K. Ross, 8/16/93, (PB94-154275, A16, MF-A02).

NCEER-93-0016 "Reconnaissance Report of Damage to Historic Monuments in Cairo, Egypt Following the October 12, 1992 Dahshur Earthquake," by D. Sykora, D. Look, G. Croci, E. Karaesmen and E. Karaesmen, 8/19/93, (PB94-142221, A08, MF-A02).

NCEER-93-0017 "The Island of Guam Earthquake of August 8, 1993," by S.W. Swan and S.K. Harris, 9/30/93, (PB94-141843, A04, MF-A01).

NCEER-93-0018 "Engineering Aspects of the October 12, 1992 Egyptian Earthquake," by A.W. Elgamal, M. Amer, K. Adalier and A. Abul-Fadl, 10/7/93, (PB94-141983, A05, MF-A01).

NCEER-93-0019 "Development of an Earthquake Motion Simulator and its Application in Dynamic Centrifuge Testing," by I. Krstelj, Supervised by J.H. Prevost, 10/23/93, (PB94-181773, A-10, MF-A03).

NCEER-93-0020 "NCEER-Taisei Corporation Research Program on Sliding Seismic Isolation Systems for Bridges: Experimental and Analytical Study of a Friction Pendulum System (FPS)," by M.C. Constantinou, P. Tsopelas, Y-S. Kim and S. Okamoto, 11/1/93, (PB94-142775, A08, MF-A02).

NCEER-93-0021 "Finite Element Modeling of Elastomeric Seismic Isolation Bearings," by L.J. Billings, Supervised by R. Shepherd, 11/8/93, not available.

NCEER-93-0022 "Seismic Vulnerability of Equipment in Critical Facilities: Life-Safety and Operational Consequences," by K. Porter, G.S. Johnson, M.M. Zadeh, C. Scawthorn and S. Eder, 11/24/93, (PB94-181765, A16, MF-A03).

NCEER-93-0023 "Hokkaido Nansei-oki, Japan Earthquake of July 12, 1993, by P.I. Yanev and C.R. Scawthorn, 12/23/93, (PB94-181500, A07, MF-A01).

NCEER-94-0001 "An Evaluation of Seismic Serviceability of Water Supply Networks with Application to the San Francisco Auxiliary Water Supply System," by I. Markov, Supervised by M. Grigoriu and T. O'Rourke, 1/21/94, (PB94-204013, A07, MF-A02).

NCEER-94-0002 "NCEER-Taisei Corporation Research Program on Sliding Seismic Isolation Systems for Bridges: Experimental and Analytical Study of Systems Consisting of Sliding Bearings, Rubber Restoring Force Devices and Fluid Dampers," Volumes I and II, by P. Tsopelas, S. Okamoto, M.C. Constantinou, D. Ozaki and S. Fujii, 2/4/94, (PB94-181740, A09, MF-A02 and PB94-181757, A12, MF-A03).

NCEER-94-0003 "A Markov Model for Local and Global Damage Indices in Seismic Analysis," by S. Rahman and M. Grigoriu, 2/18/94, (PB94-206000, A12, MF-A03).

NCEER-94-0004 "Proceedings from the NCEER Workshop on Seismic Response of Masonry Infills," edited by D.P. Abrams, 3/1/94, (PB94-180783, A07, MF-A02).

NCEER-94-0005 "The Northridge, California Earthquake of January 17, 1994: General Reconnaissance Report," edited by J.D. Goltz, 3/11/94, (PB94-193943, A10, MF-A03).

NCEER-94-0006 "Seismic Energy Based Fatigue Damage Analysis of Bridge Columns: Part I - Evaluation of Seismic Capacity," by G.A. Chang and J.B. Mander, 3/14/94, (PB94-219185, A11, MF-A03).

NCEER-94-0007 "Seismic Isolation of Multi-Story Frame Structures Using Spherical Sliding Isolation Systems," by T.M. Al-Hussaini, V.A. Zayas and M.C. Constantinou, 3/17/94, (PB94-193745, A09, MF-A02).

NCEER-94-0008 "The Northridge, California Earthquake of January 17, 1994: Performance of Highway Bridges," edited by I.G. Buckle, 3/24/94, (PB94-193851, A06, MF-A02).

NCEER-94-0009 "Proceedings of the Third U.S.-Japan Workshop on Earthquake Protective Systems for Bridges," edited by I.G. Buckle and I. Friedland, 3/31/94, (PB94-195815, A99, MF-A06).

NCEER-94-0010 "3D-BASIS-ME: Computer Program for Nonlinear Dynamic Analysis of Seismically Isolated Single and Multiple Structures and Liquid Storage Tanks," by P.C. Tsopelas, M.C. Constantinou and A.M. Reinhorn, 4/12/94, (PB94-204922, A09, MF-A02).

NCEER-94-0011 "The Northridge, California Earthquake of January 17, 1994: Performance of Gas Transmission Pipelines," by T.D. O'Rourke and M.C. Palmer, 5/16/94, (PB94-204989, A05, MF-A01).

NCEER-94-0012 "Feasibility Study of Replacement Procedures and Earthquake Performance Related to Gas Transmission Pipelines," by T.D. O'Rourke and M.C. Palmer, 5/25/94, (PB94-206638, A09, MF-A02).

NCEER-94-0013 "Seismic Energy Based Fatigue Damage Analysis of Bridge Columns: Part II - Evaluation of Seismic Demand," by G.A. Chang and J.B. Mander, 6/1/94, (PB95-18106, A08, MF-A02).

NCEER-94-0014 "NCEER-Taisei Corporation Research Program on Sliding Seismic Isolation Systems for Bridges: Experimental and Analytical Study of a System Consisting of Sliding Bearings and Fluid Restoring Force/Damping Devices," by P. Tsopelas and M.C. Constantinou, 6/13/94, (PB94-219144, A10, MF-A03).

NCEER-94-0015 "Generation of Hazard-Consistent Fragility Curves for Seismic Loss Estimation Studies," by H. Hwang and J-R. Huo, 6/14/94, (PB95-181996, A09, MF-A02).

NCEER-94-0016 "Seismic Study of Building Frames with Added Energy-Absorbing Devices," by W.S. Pong, C.S. Tsai and G.C. Lee, 6/20/94, (PB94-219136, A10, A03).

NCEER-94-0017 "Sliding Mode Control for Seismic-Excited Linear and Nonlinear Civil Engineering Structures," by J. Yang, J. Wu, A. Agrawal and Z. Li, 6/21/94, (PB95-138483, A06, MF-A02).

NCEER-94-0018 "3D-BASIS-TABS Version 2.0: Computer Program for Nonlinear Dynamic Analysis of Three Dimensional Base Isolated Structures," by A.M. Reinhorn, S. Nagarajaiah, M.C. Constantinou, P. Tsopelas and R. Li, 6/22/94, (PB95-182176, A08, MF-A02).

NCEER-94-0019 "Proceedings of the International Workshop on Civil Infrastructure Systems: Application of Intelligent Systems and Advanced Materials on Bridge Systems," Edited by G.C. Lee and K.C. Chang, 7/18/94, (PB95-252474, A20, MF-A04).

NCEER-94-0020 "Study of Seismic Isolation Systems for Computer Floors," by V. Lambrou and M.C. Constantinou, 7/19/94, (PB95-138533, A10, MF-A03).

NCEER-94-0021 "Proceedings of the U.S.-Italian Workshop on Guidelines for Seismic Evaluation and Rehabilitation of Unreinforced Masonry Buildings," Edited by D.P. Abrams and G.M. Calvi, 7/20/94, (PB95-138749, A13, MF-A03).

NCEER-94-0022 "NCEER-Taisei Corporation Research Program on Sliding Seismic Isolation Systems for Bridges: Experimental and Analytical Study of a System Consisting of Lubricated PTFE Sliding Bearings and Mild Steel Dampers," by P. Tsopelas and M.C. Constantinou, 7/22/94, (PB95-182184, A08, MF-A02).

NCEER-94-0023 “Development of Reliability-Based Design Criteria for Buildings Under Seismic Load,” by Y.K. Wen, H. Hwang and M. Shinozuka, 8/1/94, (PB95-211934, A08, MF-A02).

NCEER-94-0024 “Experimental Verification of Acceleration Feedback Control Strategies for an Active Tendon System,” by S.J. Dyke, B.F. Spencer, Jr., P. Quast, M.K. Sain, D.C. Kaspari, Jr. and T.T. Soong, 8/29/94, (PB95-212320, A05, MF-A01).

NCEER-94-0025 “Seismic Retrofitting Manual for Highway Bridges,” Edited by I.G. Buckle and I.F. Friedland, published by the Federal Highway Administration (PB95-212676, A15, MF-A03).

NCEER-94-0026 “Proceedings from the Fifth U.S.-Japan Workshop on Earthquake Resistant Design of Lifeline Facilities and Countermeasures Against Soil Liquefaction,” Edited by T.D. O’Rourke and M. Hamada, 11/7/94, (PB95-220802, A99, MF-E08).

NCEER-95-0001 "Experimental and Analytical Investigation of Seismic Retrofit of Structures with Supplemental Damping: Part 1 - Fluid Viscous Damping Devices," by A.M. Reinhorn, C. Li and M.C. Constantinou, 1/3/95, (PB95-266599, A09, MF-A02).

NCEER-95-0002 "Experimental and Analytical Study of Low-Cycle Fatigue Behavior of Semi-Rigid Top-And-Seat Angle Connections," by G. Pekcan, J.B. Mander and S.S. Chen, 1/5/95, (PB95-220042, A07, MF-A02).

NCEER-95-0003 "NCEER-ATC Joint Study on Fragility of Buildings," by T. Anagnos, C. Rojahn and A.S. Kiremidjian, 1/20/95, (PB95-220026, A06, MF-A02).

NCEER-95-0004 "Nonlinear Control Algorithms for Peak Response Reduction," by Z. Wu, T.T. Soong, V. Gattulli and R.C. Lin, 2/16/95, (PB95-220349, A05, MF-A01).

NCEER-95-0005 "Pipeline Replacement Feasibility Study: A Methodology for Minimizing Seismic and Corrosion Risks to Underground Natural Gas Pipelines," by R.T. Eguchi, H.A. Seligson and D.G. Honegger, 3/2/95, (PB95-252326, A06, MF-A02).

NCEER-95-0006 "Evaluation of Seismic Performance of an 11-Story Frame Building During the 1994 Northridge Earthquake," by F. Naeim, R. DiSulio, K. Benuska, A. Reinhorn and C. Li, not available.

NCEER-95-0007 "Prioritization of Bridges for Seismic Retrofitting," by N. Basöz and A.S. Kiremidjian, 4/24/95, (PB95-252300, A08, MF-A02).

NCEER-95-0008 "Method for Developing Motion Damage Relationships for Reinforced Concrete Frames," by A. Singhal and A.S. Kiremidjian, 5/11/95, (PB95-266607, A06, MF-A02).

NCEER-95-0009 "Experimental and Analytical Investigation of Seismic Retrofit of Structures with Supplemental Damping: Part II - Friction Devices," by C. Li and A.M. Reinhorn, 7/6/95, (PB96-128087, A11, MF-A03).

NCEER-95-0010 "Experimental Performance and Analytical Study of a Non-Ductile Reinforced Concrete Frame Structure Retrofitted with Elastomeric Spring Dampers," by G. Pekcan, J.B. Mander and S.S. Chen, 7/14/95, (PB96-137161, A08, MF-A02).

NCEER-95-0011 "Development and Experimental Study of Semi-Active Fluid Damping Devices for Seismic Protection of Structures," by M.D. Symans and M.C. Constantinou, 8/3/95, (PB96-136940, A23, MF-A04).

NCEER-95-0012 "Real-Time Structural Parameter Modification (RSPM): Development of Innervated Structures," by Z. Liang, M. Tong and G.C. Lee, 4/11/95, (PB96-137153, A06, MF-A01).

NCEER-95-0013 "Experimental and Analytical Investigation of Seismic Retrofit of Structures with Supplemental Damping: Part III - Viscous Damping Walls," by A.M. Reinhorn and C. Li, 10/1/95, (PB96-176409, A11, MF-A03).

NCEER-95-0014 "Seismic Fragility Analysis of Equipment and Structures in a Memphis Electric Substation," by J-R. Huo and H.H.M. Hwang, 8/10/95, (PB96-128087, A09, MF-A02).

NCEER-95-0015 "The Hanshin-Awaji Earthquake of January 17, 1995: Performance of Lifelines," Edited by M. Shinozuka, 11/3/95, (PB96-176383, A15, MF-A03).

NCEER-95-0016 "Highway Culvert Performance During Earthquakes," by T.L. Youd and C.J. Beckman, available as NCEER-96-0015.

NCEER-95-0017 "The Hanshin-Awaji Earthquake of January 17, 1995: Performance of Highway Bridges," Edited by I.G. Buckle, 12/1/95, not available.

NCEER-95-0018 "Modeling of Masonry Infill Panels for Structural Analysis," by A.M. Reinhorn, A. Madan, R.E. Valles, Y. Reichmann and J.B. Mander, 12/8/95, (PB97-110886, MF-A01, A06).

NCEER-95-0019 "Optimal Polynomial Control for Linear and Nonlinear Structures," by A.K. Agrawal and J.N. Yang, 12/11/95, (PB96-168737, A07, MF-A02).

NCEER-95-0020 "Retrofit of Non-Ductile Reinforced Concrete Frames Using Friction Dampers," by R.S. Rao, P. Gergely and R.N. White, 12/22/95, (PB97-133508, A10, MF-A02).

NCEER-95-0021 "Parametric Results for Seismic Response of Pile-Supported Bridge Bents," by G. Mylonakis, A. Nikolaou and G. Gazetas, 12/22/95, (PB97-100242, A12, MF-A03).

NCEER-95-0022 "Kinematic Bending Moments in Seismically Stressed Piles," by A. Nikolaou, G. Mylonakis and G. Gazetas, 12/23/95, (PB97-113914, MF-A03, A13).

NCEER-96-0001 "Dynamic Response of Unreinforced Masonry Buildings with Flexible Diaphragms," by A.C. Costley and D.P. Abrams," 10/10/96, (PB97-133573, MF-A03, A15).

NCEER-96-0002 "State of the Art Review: Foundations and Retaining Structures," by I. Po Lam, not available.

NCEER-96-0003 "Ductility of Rectangular Reinforced Concrete Bridge Columns with Moderate Confinement," by N. Wehbe, M. Saiidi, D. Sanders and B. Douglas, 11/7/96, (PB97-133557, A06, MF-A02).

NCEER-96-0004 "Proceedings of the Long-Span Bridge Seismic Research Workshop," edited by I.G. Buckle and I.M. Friedland, not available.

NCEER-96-0005 "Establish Representative Pier Types for Comprehensive Study: Eastern United States," by J. Kulicki and Z. Prucz, 5/28/96, (PB98-119217, A07, MF-A02).

NCEER-96-0006 "Establish Representative Pier Types for Comprehensive Study: Western United States," by R. Imbsen, R.A. Schamber and T.A. Osterkamp, 5/28/96, (PB98-118607, A07, MF-A02).

NCEER-96-0007 "Nonlinear Control Techniques for Dynamical Systems with Uncertain Parameters," by R.G. Ghanem and M.I. Bujakov, 5/27/96, (PB97-100259, A17, MF-A03).

NCEER-96-0008 "Seismic Evaluation of a 30-Year Old Non-Ductile Highway Bridge Pier and Its Retrofit," by J.B. Mander, B. Mahmoodzadegan, S. Bhadra and S.S. Chen, 5/31/96, (PB97-110902, MF-A03, A10).

NCEER-96-0009 "Seismic Performance of a Model Reinforced Concrete Bridge Pier Before and After Retrofit," by J.B. Mander, J.H. Kim and C.A. Ligozio, 5/31/96, (PB97-110910, MF-A02, A10).

NCEER-96-0010 "IDARC2D Version 4.0: A Computer Program for the Inelastic Damage Analysis of Buildings," by R.E. Valles, A.M. Reinhorn, S.K. Kunnath, C. Li and A. Madan, 6/3/96, (PB97-100234, A17, MF-A03).

NCEER-96-0011 "Estimation of the Economic Impact of Multiple Lifeline Disruption: Memphis Light, Gas and Water Division Case Study," by S.E. Chang, H.A. Seligson and R.T. Eguchi, 8/16/96, (PB97-133490, A11, MF-A03).

NCEER-96-0012 "Proceedings from the Sixth Japan-U.S. Workshop on Earthquake Resistant Design of Lifeline Facilities and Countermeasures Against Soil Liquefaction, Edited by M. Hamada and T. O'Rourke, 9/11/96, (PB97-133581, A99, MF-A06).

NCEER-96-0013 "Chemical Hazards, Mitigation and Preparedness in Areas of High Seismic Risk: A Methodology for Estimating the Risk of Post-Earthquake Hazardous Materials Release," by H.A. Seligson, R.T. Eguchi, K.J. Tierney and K. Richmond, 11/7/96, (PB97-133565, MF-A02, A08).

NCEER-96-0014 "Response of Steel Bridge Bearings to Reversed Cyclic Loading," by J.B. Mander, D-K. Kim, S.S. Chen and G.J. Premus, 11/13/96, (PB97-140735, A12, MF-A03).

NCEER-96-0015 "Highway Culvert Performance During Past Earthquakes," by T.L. Youd and C.J. Beckman, 11/25/96, (PB97-133532, A06, MF-A01).

NCEER-97-0001 "Evaluation, Prevention and Mitigation of Pounding Effects in Building Structures," by R.E. Valles and A.M. Reinhorn, 2/20/97, (PB97-159552, A14, MF-A03).

NCEER-97-0002 "Seismic Design Criteria for Bridges and Other Highway Structures," by C. Rojahn, R. Mayes, D.G. Anderson, J. Clark, J.H. Hom, R.V. Nutt and M.J. O'Rourke, 4/30/97, (PB97-194658, A06, MF-A03).

NCEER-97-0003 “Proceedings of the U.S.-Italian Workshop on Seismic Evaluation and Retrofit,” Edited by D.P. Abrams and G.M. Calvi, 3/19/97, (PB97-194666, A13, MF-A03).

NCEER-97-0004 "Investigation of Seismic Response of Buildings with Linear and Nonlinear Fluid Viscous Dampers," by A.A. Seleemah and M.C. Constantinou, 5/21/97, (PB98-109002, A15, MF-A03).

NCEER-97-0005 "Proceedings of the Workshop on Earthquake Engineering Frontiers in Transportation Facilities," edited by G.C. Lee and I.M. Friedland, 8/29/97, (PB98-128911, A25, MR-A04).

NCEER-97-0006 "Cumulative Seismic Damage of Reinforced Concrete Bridge Piers," by S.K. Kunnath, A. El-Bahy, A. Taylor and W. Stone, 9/2/97, (PB98-108814, A11, MF-A03).

NCEER-97-0007 "Structural Details to Accommodate Seismic Movements of Highway Bridges and Retaining Walls," by R.A. Imbsen, R.A. Schamber, E. Thorkildsen, A. Kartoum, B.T. Martin, T.N. Rosser and J.M. Kulicki, 9/3/97, (PB98-108996, A09, MF-A02).

NCEER-97-0008 "A Method for Earthquake Motion-Damage Relationships with Application to Reinforced Concrete Frames," by A. Singhal and A.S. Kiremidjian, 9/10/97, (PB98-108988, A13, MF-A03).

NCEER-97-0009 "Seismic Analysis and Design of Bridge Abutments Considering Sliding and Rotation," by K. Fishman and R. Richards, Jr., 9/15/97, (PB98-108897, A06, MF-A02).

NCEER-97-0010 "Proceedings of the FHWA/NCEER Workshop on the National Representation of Seismic Ground Motion for New and Existing Highway Facilities," edited by I.M. Friedland, M.S. Power and R.L. Mayes, 9/22/97, (PB98-128903, A21, MF-A04).

NCEER-97-0011 "Seismic Analysis for Design or Retrofit of Gravity Bridge Abutments," by K.L. Fishman, R. Richards, Jr. and R.C. Divito, 10/2/97, (PB98-128937, A08, MF-A02).

NCEER-97-0012 "Evaluation of Simplified Methods of Analysis for Yielding Structures," by P. Tsopelas, M.C. Constantinou, C.A. Kircher and A.S. Whittaker, 10/31/97, (PB98-128929, A10, MF-A03).

NCEER-97-0013 "Seismic Design of Bridge Columns Based on Control and Repairability of Damage," by C-T. Cheng and J.B. Mander, 12/8/97, (PB98-144249, A11, MF-A03).

NCEER-97-0014 "Seismic Resistance of Bridge Piers Based on Damage Avoidance Design," by J.B. Mander and C-T. Cheng, 12/10/97, (PB98-144223, A09, MF-A02).

NCEER-97-0015 “Seismic Response of Nominally Symmetric Systems with Strength Uncertainty,” by S. Balopoulou and M. Grigoriu, 12/23/97, (PB98-153422, A11, MF-A03).

NCEER-97-0016 “Evaluation of Seismic Retrofit Methods for Reinforced Concrete Bridge Columns,” by T.J. Wipf, F.W. Klaiber and F.M. Russo, 12/28/97, (PB98-144215, A12, MF-A03).

NCEER-97-0017 “Seismic Fragility of Existing Conventional Reinforced Concrete Highway Bridges,” by C.L. Mullen and A.S. Cakmak, 12/30/97, (PB98-153406, A08, MF-A02).

NCEER-97-0018 “Loss Asssessment of Memphis Buildings,” edited by D.P. Abrams and M. Shinozuka, 12/31/97, (PB98-144231, A13, MF-A03).

NCEER-97-0019 “Seismic Evaluation of Frames with Infill Walls Using Quasi-static Experiments,” by K.M. Mosalam, R.N. White and P. Gergely, 12/31/97, (PB98-153455, A07, MF-A02).

NCEER-97-0020 “Seismic Evaluation of Frames with Infill Walls Using Pseudo-dynamic Experiments,” by K.M. Mosalam, R.N. White and P. Gergely, 12/31/97, (PB98-153430, A07, MF-A02).

NCEER-97-0021 “Computational Strategies for Frames with Infill Walls: Discrete and Smeared Crack Analyses and Seismic Fragility,” by K.M. Mosalam, R.N. White and P. Gergely, 12/31/97, (PB98-153414, A10, MF-A02).

NCEER-97-0022 "Proceedings of the NCEER Workshop on Evaluation of Liquefaction Resistance of Soils," edited by T.L. Youd and I.M. Idriss, 12/31/97, (PB98-155617, A15, MF-A03).

MCEER-98-0001 "Extraction of Nonlinear Hysteretic Properties of Seismically Isolated Bridges from Quick-Release Field Tests," by Q. Chen, B.M. Douglas, E.M. Maragakis and I.G. Buckle, 5/26/98, (PB99-118838, A06, MF-A01).

MCEER-98-0002 "Methodologies for Evaluating the Importance of Highway Bridges," by A. Thomas, S. Eshenaur and J. Kulicki, 5/29/98, (PB99-118846, A10, MF-A02).

MCEER-98-0003 "Capacity Design of Bridge Piers and the Analysis of Overstrength," by J.B. Mander, A. Dutta and P. Goel, 6/1/98, (PB99-118853, A09, MF-A02).

MCEER-98-0004 "Evaluation of Bridge Damage Data from the Loma Prieta and Northridge, California Earthquakes," by N. Basoz and A. Kiremidjian, 6/2/98, (PB99-118861, A15, MF-A03).

MCEER-98-0005 "Screening Guide for Rapid Assessment of Liquefaction Hazard at Highway Bridge Sites," by T. L. Youd, 6/16/98, (PB99-118879, A06, not available on microfiche).

MCEER-98-0006 "Structural Steel and Steel/Concrete Interface Details for Bridges," by P. Ritchie, N. Kauhl and J. Kulicki, 7/13/98, (PB99-118945, A06, MF-A01).

MCEER-98-0007 "Capacity Design and Fatigue Analysis of Confined Concrete Columns," by A. Dutta and J.B. Mander, 7/14/98, (PB99-118960, A14, MF-A03).

MCEER-98-0008 "Proceedings of the Workshop on Performance Criteria for Telecommunication Services Under Earthquake Conditions," edited by A.J. Schiff, 7/15/98, (PB99-118952, A08, MF-A02).

MCEER-98-0009 "Fatigue Analysis of Unconfined Concrete Columns," by J.B. Mander, A. Dutta and J.H. Kim, 9/12/98, (PB99-123655, A10, MF-A02).

MCEER-98-0010 "Centrifuge Modeling of Cyclic Lateral Response of Pile-Cap Systems and Seat-Type Abutments in Dry Sands," by A.D. Gadre and R. Dobry, 10/2/98, (PB99-123606, A13, MF-A03).

MCEER-98-0011 "IDARC-BRIDGE: A Computational Platform for Seismic Damage Assessment of Bridge Structures," by A.M. Reinhorn, V. Simeonov, G. Mylonakis and Y. Reichman, 10/2/98, (PB99-162919, A15, MF-A03).

MCEER-98-0012 "Experimental Investigation of the Dynamic Response of Two Bridges Before and After Retrofitting with Elastomeric Bearings," by D.A. Wendichansky, S.S. Chen and J.B. Mander, 10/2/98, (PB99-162927, A15, MF-A03).

MCEER-98-0013 "Design Procedures for Hinge Restrainers and Hinge Sear Width for Multiple-Frame Bridges," by R. Des Roches and G.L. Fenves, 11/3/98, (PB99-140477, A13, MF-A03).

MCEER-98-0014 "Response Modification Factors for Seismically Isolated Bridges," by M.C. Constantinou and J.K. Quarshie, 11/3/98, (PB99-140485, A14, MF-A03).

MCEER-98-0015 "Proceedings of the U.S.-Italy Workshop on Seismic Protective Systems for Bridges," edited by I.M. Friedland and M.C. Constantinou, 11/3/98, (PB2000-101711, A22, MF-A04).

MCEER-98-0016 "Appropriate Seismic Reliability for Critical Equipment Systems: Recommendations Based on Regional Analysis of Financial and Life Loss," by K. Porter, C. Scawthorn, C. Taylor and N. Blais, 11/10/98, (PB99-157265, A08, MF-A02).

MCEER-98-0017 "Proceedings of the U.S. Japan Joint Seminar on Civil Infrastructure Systems Research," edited by M. Shinozuka and A. Rose, 11/12/98, (PB99-156713, A16, MF-A03).

MCEER-98-0018 "Modeling of Pile Footings and Drilled Shafts for Seismic Design," by I. PoLam, M. Kapuskar and D. Chaudhuri, 12/21/98, (PB99-157257, A09, MF-A02).

MCEER-99-0001 "Seismic Evaluation of a Masonry Infilled Reinforced Concrete Frame by Pseudodynamic Testing," by S.G. Buonopane and R.N. White, 2/16/99, (PB99-162851, A09, MF-A02).

MCEER-99-0002 "Response History Analysis of Structures with Seismic Isolation and Energy Dissipation Systems: Verification Examples for Program SAP2000," by J. Scheller and M.C. Constantinou, 2/22/99, (PB99-162869, A08, MF-A02).

MCEER-99-0003 "Experimental Study on the Seismic Design and Retrofit of Bridge Columns Including Axial Load Effects," by A. Dutta, T. Kokorina and J.B. Mander, 2/22/99, (PB99-162877, A09, MF-A02).

MCEER-99-0004 "Experimental Study of Bridge Elastomeric and Other Isolation and Energy Dissipation Systems with Emphasis on Uplift Prevention and High Velocity Near-source Seismic Excitation," by A. Kasalanati and M. C. Constantinou, 2/26/99, (PB99-162885, A12, MF-A03).

MCEER-99-0005 "Truss Modeling of Reinforced Concrete Shear-flexure Behavior," by J.H. Kim and J.B. Mander, 3/8/99, (PB99-163693, A12, MF-A03).

MCEER-99-0006 "Experimental Investigation and Computational Modeling of Seismic Response of a 1:4 Scale Model Steel Structure with a Load Balancing Supplemental Damping System," by G. Pekcan, J.B. Mander and S.S. Chen, 4/2/99, (PB99-162893, A11, MF-A03).

MCEER-99-0007 "Effect of Vertical Ground Motions on the Structural Response of Highway Bridges," by M.R. Button, C.J. Cronin and R.L. Mayes, 4/10/99, (PB2000-101411, A10, MF-A03).

MCEER-99-0008 "Seismic Reliability Assessment of Critical Facilities: A Handbook, Supporting Documentation, and Model Code Provisions," by G.S. Johnson, R.E. Sheppard, M.D. Quilici, S.J. Eder and C.R. Scawthorn, 4/12/99, (PB2000-101701, A18, MF-A04).

MCEER-99-0009 "Impact Assessment of Selected MCEER Highway Project Research on the Seismic Design of Highway Structures," by C. Rojahn, R. Mayes, D.G. Anderson, J.H. Clark, D'Appolonia Engineering, S. Gloyd and R.V. Nutt, 4/14/99, (PB99-162901, A10, MF-A02).

MCEER-99-0010 "Site Factors and Site Categories in Seismic Codes," by R. Dobry, R. Ramos and M.S. Power, 7/19/99, (PB2000-101705, A08, MF-A02).

MCEER-99-0011 "Restrainer Design Procedures for Multi-Span Simply-Supported Bridges," by M.J. Randall, M. Saiidi, E. Maragakis and T. Isakovic, 7/20/99, (PB2000-101702, A10, MF-A02).

MCEER-99-0012 "Property Modification Factors for Seismic Isolation Bearings," by M.C. Constantinou, P. Tsopelas, A. Kasalanati and E. Wolff, 7/20/99, (PB2000-103387, A11, MF-A03).

MCEER-99-0013 "Critical Seismic Issues for Existing Steel Bridges," by P. Ritchie, N. Kauhl and J. Kulicki, 7/20/99, (PB2000-101697, A09, MF-A02).

MCEER-99-0014 "Nonstructural Damage Database," by A. Kao, T.T. Soong and A. Vender, 7/24/99, (PB2000-101407, A06, MF-A01).

MCEER-99-0015 "Guide to Remedial Measures for Liquefaction Mitigation at Existing Highway Bridge Sites," by H.G. Cooke and J. K. Mitchell, 7/26/99, (PB2000-101703, A11, MF-A03).

MCEER-99-0016 "Proceedings of the MCEER Workshop on Ground Motion Methodologies for the Eastern United States," edited by N. Abrahamson and A. Becker, 8/11/99, (PB2000-103385, A07, MF-A02).

MCEER-99-0017 "Quindío, Colombia Earthquake of January 25, 1999: Reconnaissance Report," by A.P. Asfura and P.J. Flores, 10/4/99, (PB2000-106893, A06, MF-A01).

MCEER-99-0018 "Hysteretic Models for Cyclic Behavior of Deteriorating Inelastic Structures," by M.V. Sivaselvan and A.M. Reinhorn, 11/5/99, (PB2000-103386, A08, MF-A02).

MCEER-99-0019 "Proceedings of the 7th U.S.- Japan Workshop on Earthquake Resistant Design of Lifeline Facilities and Countermeasures Against Soil Liquefaction," edited by T.D. O'Rourke, J.P. Bardet and M. Hamada, 11/19/99, (PB2000-103354, A99, MF-A06).

MCEER-99-0020 "Development of Measurement Capability for Micro-Vibration Evaluations with Application to Chip Fabrication Facilities," by G.C. Lee, Z. Liang, J.W. Song, J.D. Shen and W.C. Liu, 12/1/99, (PB2000-105993, A08, MF-A02).

MCEER-99-0021 "Design and Retrofit Methodology for Building Structures with Supplemental Energy Dissipating Systems," by G. Pekcan, J.B. Mander and S.S. Chen, 12/31/99, (PB2000-105994, A11, MF-A03).

MCEER-00-0001 "The Marmara, Turkey Earthquake of August 17, 1999: Reconnaissance Report," edited by C. Scawthorn; with major contributions by M. Bruneau, R. Eguchi, T. Holzer, G. Johnson, J. Mander, J. Mitchell, W. Mitchell, A. Papageorgiou, C. Scaethorn, and G. Webb, 3/23/00, (PB2000-106200, A11, MF-A03).

MCEER-00-0002 "Proceedings of the MCEER Workshop for Seismic Hazard Mitigation of Health Care Facilities," edited by G.C. Lee, M. Ettouney, M. Grigoriu, J. Hauer and J. Nigg, 3/29/00, (PB2000-106892, A08, MF-A02).

MCEER-00-0003 "The Chi-Chi, Taiwan Earthquake of September 21, 1999: Reconnaissance Report," edited by G.C. Lee and C.H. Loh, with major contributions by G.C. Lee, M. Bruneau, I.G. Buckle, S.E. Chang, P.J. Flores, T.D. O'Rourke, M. Shinozuka, T.T. Soong, C-H. Loh, K-C. Chang, Z-J. Chen, J-S. Hwang, M-L. Lin, G-Y. Liu, K-C. Tsai, G.C. Yao and C-L. Yen, 4/30/00, (PB2001-100980, A10, MF-A02).

MCEER-00-0004 "Seismic Retrofit of End-Sway Frames of Steel Deck-Truss Bridges with a Supplemental Tendon System: Experimental and Analytical Investigation," by G. Pekcan, J.B. Mander and S.S. Chen, 7/1/00, (PB2001-100982, A10, MF-A02).

MCEER-00-0005 "Sliding Fragility of Unrestrained Equipment in Critical Facilities," by W.H. Chong and T.T. Soong, 7/5/00, (PB2001-100983, A08, MF-A02).

MCEER-00-0006 "Seismic Response of Reinforced Concrete Bridge Pier Walls in the Weak Direction," by N. Abo-Shadi, M. Saiidi and D. Sanders, 7/17/00, (PB2001-100981, A17, MF-A03).

MCEER-00-0007 "Low-Cycle Fatigue Behavior of Longitudinal Reinforcement in Reinforced Concrete Bridge Columns," by J. Brown and S.K. Kunnath, 7/23/00, (PB2001-104392, A08, MF-A02).

MCEER-00-0008 "Soil Structure Interaction of Bridges for Seismic Analysis," I. PoLam and H. Law, 9/25/00, (PB2001-105397, A08, MF-A02).

MCEER-00-0009 "Proceedings of the First MCEER Workshop on Mitigation of Earthquake Disaster by Advanced Technologies (MEDAT-1), edited by M. Shinozuka, D.J. Inman and T.D. O'Rourke, 11/10/00, (PB2001-105399, A14, MF-A03).

MCEER-00-0010 "Development and Evaluation of Simplified Procedures for Analysis and Design of Buildings with Passive Energy Dissipation Systems, Revision 01," by O.M. Ramirez, M.C. Constantinou, C.A. Kircher, A.S. Whittaker, M.W. Johnson, J.D. Gomez and C. Chrysostomou, 11/16/01, (PB2001-105523, A23, MF-A04).

MCEER-00-0011 "Dynamic Soil-Foundation-Structure Interaction Analyses of Large Caissons," by C-Y. Chang, C-M. Mok, Z-L. Wang, R. Settgast, F. Waggoner, M.A. Ketchum, H.M. Gonnermann and C-C. Chin, 12/30/00, (PB2001-104373, A07, MF-A02).

MCEER-00-0012 "Experimental Evaluation of Seismic Performance of Bridge Restrainers," by A.G. Vlassis, E.M. Maragakis and M. Saiid Saiidi, 12/30/00, (PB2001-104354, A09, MF-A02).

MCEER-00-0013 "Effect of Spatial Variation of Ground Motion on Highway Structures," by M. Shinozuka, V. Saxena and G. Deodatis, 12/31/00, (PB2001-108755, A13, MF-A03).

MCEER-00-0014 "A Risk-Based Methodology for Assessing the Seismic Performance of Highway Systems," by S.D. Werner, C.E. Taylor, J.E. Moore, II, J.S. Walton and S. Cho, 12/31/00, (PB2001-108756, A14, MF-A03).

MCEER-01-0001 "Experimental Investigation of P-Delta Effects to Collapse During Earthquakes," by D. Vian and M. Bruneau, 6/25/01, (PB2002-100534, A17, MF-A03).

MCEER-01-0002 "Proceedings of the Second MCEER Workshop on Mitigation of Earthquake Disaster by Advanced Technologies (MEDAT-2)," edited by M. Bruneau and D.J. Inman, 7/23/01, (PB2002-100434, A16, MF-A03).

MCEER-01-0003 "Sensitivity Analysis of Dynamic Systems Subjected to Seismic Loads," by C. Roth and M. Grigoriu, 9/18/01, (PB2003-100884, A12, MF-A03).

MCEER-01-0004 "Overcoming Obstacles to Implementing Earthquake Hazard Mitigation Policies: Stage 1 Report," by D.J. Alesch and W.J. Petak, 12/17/01, (PB2002-107949, A07, MF-A02).

MCEER-01-0005 "Updating Real-Time Earthquake Loss Estimates: Methods, Problems and Insights," by C.E. Taylor, S.E. Chang and R.T. Eguchi, 12/17/01, (PB2002-107948, A05, MF-A01).

MCEER-01-0006 "Experimental Investigation and Retrofit of Steel Pile Foundations and Pile Bents Under Cyclic Lateral Loadings," by A. Shama, J. Mander, B. Blabac and S. Chen, 12/31/01, (PB2002-107950, A13, MF-A03).

MCEER-02-0001 "Assessment of Performance of Bolu Viaduct in the 1999 Duzce Earthquake in Turkey" by P.C. Roussis, M.C. Constantinou, M. Erdik, E. Durukal and M. Dicleli, 5/8/02, (PB2003-100883, A08, MF-A02).

MCEER-02-0002 "Seismic Behavior of Rail Counterweight Systems of Elevators in Buildings," by M.P. Singh, Rildova and L.E. Suarez, 5/27/02. (PB2003-100882, A11, MF-A03).

MCEER-02-0003 "Development of Analysis and Design Procedures for Spread Footings," by G. Mylonakis, G. Gazetas, S. Nikolaou and A. Chauncey, 10/02/02, (PB2004-101636, A13, MF-A03, CD-A13).

MCEER-02-0004 "Bare-Earth Algorithms for Use with SAR and LIDAR Digital Elevation Models," by C.K. Huyck, R.T. Eguchi and B. Houshmand, 10/16/02, (PB2004-101637, A07, CD-A07).

MCEER-02-0005 "Review of Energy Dissipation of Compression Members in Concentrically Braced Frames," by K.Lee and M. Bruneau, 10/18/02, (PB2004-101638, A10, CD-A10).

MCEER-03-0001 "Experimental Investigation of Light-Gauge Steel Plate Shear Walls for the Seismic Retrofit of Buildings" by J. Berman and M. Bruneau, 5/2/03, (PB2004-101622, A10, MF-A03, CD-A10).

MCEER-03-0002 "Statistical Analysis of Fragility Curves," by M. Shinozuka, M.Q. Feng, H. Kim, T. Uzawa and T. Ueda, 6/16/03, (PB2004-101849, A09, CD-A09).

MCEER-03-0003 "Proceedings of the Eighth U.S.-Japan Workshop on Earthquake Resistant Design f Lifeline Facilities and Countermeasures Against Liquefaction," edited by M. Hamada, J.P. Bardet and T.D. O'Rourke, 6/30/03, (PB2004-104386, A99, CD-A99).

MCEER-03-0004 "Proceedings of the PRC-US Workshop on Seismic Analysis and Design of Special Bridges," edited by L.C. Fan and G.C. Lee, 7/15/03, (PB2004-104387, A14, CD-A14).

MCEER-03-0005 "Urban Disaster Recovery: A Framework and Simulation Model," by S.B. Miles and S.E. Chang, 7/25/03, (PB2004-104388, A07, CD-A07).

MCEER-03-0006 "Behavior of Underground Piping Joints Due to Static and Dynamic Loading," by R.D. Meis, M. Maragakis and R. Siddharthan, 11/17/03, (PB2005-102194, A13, MF-A03, CD-A00).

MCEER-04-0001 "Experimental Study of Seismic Isolation Systems with Emphasis on Secondary System Response and Verification of Accuracy of Dynamic Response History Analysis Methods," by E. Wolff and M. Constantinou, 1/16/04 (PB2005-102195, A99, MF-E08, CD-A00).

MCEER-04-0002 "Tension, Compression and Cyclic Testing of Engineered Cementitious Composite Materials," by K. Kesner and S.L. Billington, 3/1/04, (PB2005-102196, A08, CD-A08).

MCEER-04-0003 "Cyclic Testing of Braces Laterally Restrained by Steel Studs to Enhance Performance During Earthquakes," by O.C. Celik, J.W. Berman and M. Bruneau, 3/16/04, (PB2005-102197, A13, MF-A03, CD-A00).

MCEER-04-0004 "Methodologies for Post Earthquake Building Damage Detection Using SAR and Optical Remote Sensing: Application to the August 17, 1999 Marmara, Turkey Earthquake," by C.K. Huyck, B.J. Adams, S. Cho, R.T. Eguchi, B. Mansouri and B. Houshmand, 6/15/04, (PB2005-104888, A10, CD-A00).

MCEER-04-0005 "Nonlinear Structural Analysis Towards Collapse Simulation: A Dynamical Systems Approach," by M.V. Sivaselvan and A.M. Reinhorn, 6/16/04, (PB2005-104889, A11, MF-A03, CD-A00).

MCEER-04-0006 "Proceedings of the Second PRC-US Workshop on Seismic Analysis and Design of Special Bridges," edited by G.C. Lee and L.C. Fan, 6/25/04, (PB2005-104890, A16, CD-A00).

MCEER-04-0007 "Seismic Vulnerability Evaluation of Axially Loaded Steel Built-up Laced Members," by K. Lee and M. Bruneau, 6/30/04, (PB2005-104891, A16, CD-A00).

MCEER-04-0008 "Evaluation of Accuracy of Simplified Methods of Analysis and Design of Buildings with Damping Systems for Near-Fault and for Soft-Soil Seismic Motions," by E.A. Pavlou and M.C. Constantinou, 8/16/04, (PB2005-104892, A08, MF-A02, CD-A00).

MCEER-04-0009 "Assessment of Geotechnical Issues in Acute Care Facilities in California," by M. Lew, T.D. O'Rourke, R. Dobry and M. Koch, 9/15/04, (PB2005-104893, A08, CD-A00).

MCEER-04-0010 "Scissor-Jack-Damper Energy Dissipation System," by A.N. Sigaher-Boyle and M.C. Constantinou, 12/1/04 (PB2005-108221).

MCEER-04-0011 "Seismic Retrofit of Bridge Steel Truss Piers Using a Controlled Rocking Approach," by M. Pollino and M. Bruneau, 12/20/04 (PB2006-105795).

MCEER-05-0001 "Experimental and Analytical Studies of Structures Seismically Isolated with an Uplift-Restraint Isolation System," by P.C. Roussis and M.C. Constantinou, 1/10/05 (PB2005-108222).

MCEER-05-0002 "A Versatile Experimentation Model for Study of Structures Near Collapse Applied to Seismic Evaluation of Irregular Structures," by D. Kusumastuti, A.M. Reinhorn and A. Rutenberg, 3/31/05 (PB2006-101523).

MCEER-05-0003 "Proceedings of the Third PRC-US Workshop on Seismic Analysis and Design of Special Bridges," edited by L.C. Fan and G.C. Lee, 4/20/05, (PB2006-105796).

MCEER-05-0004 "Approaches for the Seismic Retrofit of Braced Steel Bridge Piers and Proof-of-Concept Testing of an Eccentrically Braced Frame with Tubular Link," by J.W. Berman and M. Bruneau, 4/21/05 (PB2006-101524).

MCEER-05-0005 "Simulation of Strong Ground Motions for Seismic Fragility Evaluation of Nonstructural Components in Hospitals," by A. Wanitkorkul and A. Filiatrault, 5/26/05 (PB2006-500027).

MCEER-05-0006 "Seismic Safety in California Hospitals: Assessing an Attempt to Accelerate the Replacement or Seismic Retrofit of Older Hospital Facilities," by D.J. Alesch, L.A. Arendt and W.J. Petak, 6/6/05 (PB2006-105794).

MCEER-05-0007 "Development of Seismic Strengthening and Retrofit Strategies for Critical Facilities Using Engineered Cementitious Composite Materials," by K. Kesner and S.L. Billington, 8/29/05 (PB2006-111701).

MCEER-05-0008 "Experimental and Analytical Studies of Base Isolation Systems for Seismic Protection of Power Transformers," by N. Murota, M.Q. Feng and G-Y. Liu, 9/30/05 (PB2006-111702).

MCEER-05-0009 "3D-BASIS-ME-MB: Computer Program for Nonlinear Dynamic Analysis of Seismically Isolated Structures," by P.C. Tsopelas, P.C. Roussis, M.C. Constantinou, R. Buchanan and A.M. Reinhorn, 10/3/05 (PB2006-111703).

MCEER-05-0010 "Steel Plate Shear Walls for Seismic Design and Retrofit of Building Structures," by D. Vian and M. Bruneau, 12/15/05 (PB2006-111704).

MCEER-05-0011 "The Performance-Based Design Paradigm," by M.J. Astrella and A. Whittaker, 12/15/05 (PB2006-111705).

MCEER-06-0001 "Seismic Fragility of Suspended Ceiling Systems," H. Badillo-Almaraz, A.S. Whittaker, A.M. Reinhorn and G.P. Cimellaro, 2/4/06 (PB2006-111706).

MCEER-06-0002 "Multi-Dimensional Fragility of Structures," by G.P. Cimellaro, A.M. Reinhorn and M. Bruneau, 3/1/06 (PB2007-106974, A09, MF-A02, CD A00).

MCEER-06-0003 "Built-Up Shear Links as Energy Dissipators for Seismic Protection of Bridges," by P. Dusicka, A.M. Itani and I.G. Buckle, 3/15/06 (PB2006-111708).

MCEER-06-0004 "Analytical Investigation of the Structural Fuse Concept," by R.E. Vargas and M. Bruneau, 3/16/06 (PB2006-111709).

MCEER-06-0005 "Experimental Investigation of the Structural Fuse Concept," by R.E. Vargas and M. Bruneau, 3/17/06 (PB2006-111710).

MCEER-06-0006 "Further Development of Tubular Eccentrically Braced Frame Links for the Seismic Retrofit of Braced Steel Truss Bridge Piers," by J.W. Berman and M. Bruneau, 3/27/06 (PB2007-105147).

MCEER-06-0007 "REDARS Validation Report," by S. Cho, C.K. Huyck, S. Ghosh and R.T. Eguchi, 8/8/06 (PB2007-106983).

MCEER-06-0008 "Review of Current NDE Technologies for Post-Earthquake Assessment of Retrofitted Bridge Columns," by J.W. Song, Z. Liang and G.C. Lee, 8/21/06 (PB2007-106984).

MCEER-06-0009 "Liquefaction Remediation in Silty Soils Using Dynamic Compaction and Stone Columns," by S. Thevanayagam, G.R. Martin, R. Nashed, T. Shenthan, T. Kanagalingam and N. Ecemis, 8/28/06 (PB2007-106985).

MCEER-06-0010 "Conceptual Design and Experimental Investigation of Polymer Matrix Composite Infill Panels for Seismic Retrofitting," by W. Jung, M. Chiewanichakorn and A.J. Aref, 9/21/06 (PB2007-106986).

MCEER-06-0011 "A Study of the Coupled Horizontal-Vertical Behavior of Elastomeric and Lead-Rubber Seismic Isolation Bearings," by G.P. Warn and A.S. Whittaker, 9/22/06 (PB2007-108679).

MCEER-06-0012 "Proceedings of the Fourth PRC-US Workshop on Seismic Analysis and Design of Special Bridges: Advancing Bridge Technologies in Research, Design, Construction and Preservation," Edited by L.C. Fan, G.C. Lee and L. Ziang, 10/12/06 (PB2007-109042).

MCEER-06-0013 "Cyclic Response and Low Cycle Fatigue Characteristics of Plate Steels," by P. Dusicka, A.M. Itani and I.G. Buckle, 11/1/06 06 (PB2007-106987).

MCEER-06-0014 "Proceedings of the Second US-Taiwan Bridge Engineering Workshop," edited by W.P. Yen, J. Shen, J-Y. Chen and M. Wang, 11/15/06 (PB2008-500041).

MCEER-06-0015 "User Manual and Technical Documentation for the REDARS^{TM} Import Wizard," by S. Cho, S. Ghosh, C.K. Huyck and S.D. Werner, 11/30/06 (PB2007-114766).

MCEER-06-0016 "Hazard Mitigation Strategy and Monitoring Technologies for Urban and Infrastructure Public Buildings: Proceedings of the China-US Workshops," edited by X.Y. Zhou, A.L. Zhang, G.C. Lee and M. Tong, 12/12/06 (PB2008-500018).

MCEER-07-0001 "Static and Kinetic Coefficients of Friction for Rigid Blocks," by C. Kafali, S. Fathali, M. Grigoriu and A.S. Whittaker, 3/20/07 (PB2007-114767).

MCEER-07-0002 "Hazard Mitigation Investment Decision Making: Organizational Response to Legislative Mandate," by L.A. Arendt, D.J. Alesch and W.J. Petak, 4/9/07 (PB2007-114768).

MCEER-07-0003 "Seismic Behavior of Bidirectional-Resistant Ductile End Diaphragms with Unbonded Braces in Straight or Skewed Steel Bridges," by O. Celik and M. Bruneau, 4/11/07 (PB2008-105141).

MCEER-07-0004 "Modeling Pile Behavior in Large Pile Groups Under Lateral Loading," by A.M. Dodds and G.R. Martin, 4/16/07(PB2008-105142).

MCEER-07-0005 "Experimental Investigation of Blast Performance of Seismically Resistant Concrete-Filled Steel Tube Bridge Piers," by S. Fujikura, M. Bruneau and D. Lopez-Garcia, 4/20/07 (PB2008-105143).

MCEER-07-0006 "Seismic Analysis of Conventional and Isolated Liquefied Natural Gas Tanks Using Mechanical Analogs," by I.P. Christovasilis and A.S. Whittaker, 5/1/07, not available.

MCEER-07-0007 "Experimental Seismic Performance Evaluation of Isolation/Restraint Systems for Mechanical Equipment – Part 1: Heavy Equipment Study," by S. Fathali and A. Filiatrault, 6/6/07 (PB2008-105144).

MCEER-07-0008 "Seismic Vulnerability of Timber Bridges and Timber Substructures," by A.A. Sharma, J.B. Mander, I.M. Friedland and D.R. Allicock, 6/7/07 (PB2008-105145).

MCEER-07-0009 "Experimental and Analytical Study of the XY-Friction Pendulum (XY-FP) Bearing for Bridge Applications," by C.C. Marin-Artieda, A.S. Whittaker and M.C. Constantinou, 6/7/07 (PB2008-105191).

MCEER-07-0010 "Proceedings of the PRC-US Earthquake Engineering Forum for Young Researchers," Edited by G.C. Lee and X.Z. Qi, 6/8/07 (PB2008-500058).

MCEER-07-0011 "Design Recommendations for Perforated Steel Plate Shear Walls," by R. Purba and M. Bruneau, 6/18/07, (PB2008-105192).

MCEER-07-0012 "Performance of Seismic Isolation Hardware Under Service and Seismic Loading," by M.C. Constantinou, A.S. Whittaker, Y. Kalpakidis, D.M. Fenz and G.P. Warn, 8/27/07, (PB2008-105193).

MCEER-07-0013 "Experimental Evaluation of the Seismic Performance of Hospital Piping Subassemblies," by E.R. Goodwin, E. Maragakis and A.M. Itani, 9/4/07, (PB2008-105194).

MCEER-07-0014 "A Simulation Model of Urban Disaster Recovery and Resilience: Implementation for the 1994 Northridge Earthquake," by S. Miles and S.E. Chang, 9/7/07, (PB2008-106426).

MCEER-07-0015 "Statistical and Mechanistic Fragility Analysis of Concrete Bridges," by M. Shinozuka, S. Banerjee and S-H. Kim, 9/10/07, (PB2008-106427).

MCEER-07-0016 "Three-Dimensional Modeling of Inelastic Buckling in Frame Structures," by M. Schachter and AM. Reinhorn, 9/13/07, (PB2008-108125).

MCEER-07-0017 "Modeling of Seismic Wave Scattering on Pile Groups and Caissons," by I. Po Lam, H. Law and C.T. Yang, 9/17/07 (PB2008-108150).

MCEER-07-0018 "Bridge Foundations: Modeling Large Pile Groups and Caissons for Seismic Design," by I. Po Lam, H. Law and G.R. Martin (Coordinating Author), 12/1/07 (PB2008-111190).

MCEER-07-0019 "Principles and Performance of Roller Seismic Isolation Bearings for Highway Bridges," by G.C. Lee, Y.C. Ou, Z. Liang, T.C. Niu and J. Song, 12/10/07 (PB2009-110466).

MCEER-07-0020 "Centrifuge Modeling of Permeability and Pinning Reinforcement Effects on Pile Response to Lateral Spreading," by L.L Gonzalez-Lagos, T. Abdoun and R. Dobry, 12/10/07 (PB2008-111191).

MCEER-07-0021 "Damage to the Highway System from the Pisco, Perú Earthquake of August 15, 2007," by J.S. O'Connor, L. Mesa and M. Nykamp, 12/10/07, (PB2008-108126).

MCEER-07-0022 "Experimental Seismic Performance Evaluation of Isolation/Restraint Systems for Mechanical Equipment – Part 2: Light Equipment Study," by S. Fathali and A. Filiatrault, 12/13/07 (PB2008-111192).

MCEER-07-0023 "Fragility Considerations in Highway Bridge Design," by M. Shinozuka, S. Banerjee and S.H. Kim, 12/14/07 (PB2008-111193).

MCEER-07-0024 "Performance Estimates for Seismically Isolated Bridges," by G.P. Warn and A.S. Whittaker, 12/30/07 (PB2008-112230).

MCEER-08-0001 "Seismic Performance of Steel Girder Bridge Superstructures with Conventional Cross Frames," by L.P. Carden, A.M. Itani and I.G. Buckle, 1/7/08, (PB2008-112231).

MCEER-08-0002 "Seismic Performance of Steel Girder Bridge Superstructures with Ductile End Cross Frames with Seismic Isolators," by L.P. Carden, A.M. Itani and I.G. Buckle, 1/7/08 (PB2008-112232).

MCEER-08-0003 "Analytical and Experimental Investigation of a Controlled Rocking Approach for Seismic Protection of Bridge Steel Truss Piers," by M. Pollino and M. Bruneau, 1/21/08 (PB2008-112233).

MCEER-08-0004 "Linking Lifeline Infrastructure Performance and Community Disaster Resilience: Models and Multi-Stakeholder Processes," by S.E. Chang, C. Pasion, K. Tatebe and R. Ahmad, 3/3/08 (PB2008-112234).

MCEER-08-0005 "Modal Analysis of Generally Damped Linear Structures Subjected to Seismic Excitations," by J. Song, Y-L. Chu, Z. Liang and G.C. Lee, 3/4/08 (PB2009-102311).

MCEER-08-0006 "System Performance Under Multi-Hazard Environments," by C. Kafali and M. Grigoriu, 3/4/08 (PB2008-112235).

MCEER-08-0007 "Mechanical Behavior of Multi-Spherical Sliding Bearings," by D.M. Fenz and M.C. Constantinou, 3/6/08 (PB2008-112236).

MCEER-08-0008 "Post-Earthquake Restoration of the Los Angeles Water Supply System," by T.H.P. Tabucchi and R.A. Davidson, 3/7/08 (PB2008-112237).

MCEER-08-0009 "Fragility Analysis of Water Supply Systems," by A. Jacobson and M. Grigoriu, 3/10/08 (PB2009-105545).

MCEER-08-0010 "Experimental Investigation of Full-Scale Two-Story Steel Plate Shear Walls with Reduced Beam Section Connections," by B. Qu, M. Bruneau, C-H. Lin and K-C. Tsai, 3/17/08 (PB2009-106368).

MCEER-08-0011 "Seismic Evaluation and Rehabilitation of Critical Components of Electrical Power Systems," S. Ersoy, B. Feizi, A. Ashrafi and M. Ala Saadeghvaziri, 3/17/08 (PB2009-105546).

MCEER-08-0012 "Seismic Behavior and Design of Boundary Frame Members of Steel Plate Shear Walls," by B. Qu and M. Bruneau, 4/26/08 . (PB2009-106744).

MCEER-08-0013 "Development and Appraisal of a Numerical Cyclic Loading Protocol for Quantifying Building System Performance," by A. Filiatrault, A. Wanitkorkul and M. Constantinou, 4/27/08 (PB2009-107906).

MCEER-08-0014 "Structural and Nonstructural Earthquake Design: The Challenge of Integrating Specialty Areas in Designing Complex, Critical Facilities," by W.J. Petak and D.J. Alesch, 4/30/08 (PB2009-107907).

MCEER-08-0015 "Seismic Performance Evaluation of Water Systems," by Y. Wang and T.D. O'Rourke, 5/5/08 (PB2009-107908).

MCEER-08-0016 "Seismic Response Modeling of Water Supply Systems," by P. Shi and T.D. O'Rourke, 5/5/08 (PB2009-107910).

MCEER-08-0017 "Numerical and Experimental Studies of Self-Centering Post-Tensioned Steel Frames," by D. Wang and A. Filiatrault, 5/12/08 (PB2009-110479).

MCEER-08-0018 "Development, Implementation and Verification of Dynamic Analysis Models for Multi-Spherical Sliding Bearings," by D.M. Fenz and M.C. Constantinou, 8/15/08 (PB2009-107911).

MCEER-08-0019 "Performance Assessment of Conventional and Base Isolated Nuclear Power Plants for Earthquake Blast Loadings," by Y.N. Huang, A.S. Whittaker and N. Luco, 10/28/08 (PB2009-107912).

MCEER-08-0020 "Remote Sensing for Resilient Multi-Hazard Disaster Response – Volume I: Introduction to Damage Assessment Methodologies," by B.J. Adams and R.T. Eguchi, 11/17/08 (PB2010-102695).

MCEER-08-0021 "Remote Sensing for Resilient Multi-Hazard Disaster Response – Volume II: Counting the Number of Collapsed Buildings Using an Object-Oriented Analysis: Case Study of the 2003 Bam Earthquake," by L. Gusella, C.K. Huyck and B.J. Adams, 11/17/08 (PB2010-100925).

MCEER-08-0022 "Remote Sensing for Resilient Multi-Hazard Disaster Response – Volume III: Multi-Sensor Image Fusion Techniques for Robust Neighborhood-Scale Urban Damage Assessment," by B.J. Adams and A. McMillan, 11/17/08 (PB2010-100926).

MCEER-08-0023 "Remote Sensing for Resilient Multi-Hazard Disaster Response – Volume IV: A Study of Multi-Temporal and Multi-Resolution SAR Imagery for Post-Katrina Flood Monitoring in New Orleans," by A. McMillan, J.G. Morley, B.J. Adams and S. Chesworth, 11/17/08 (PB2010-100927).

MCEER-08-0024 "Remote Sensing for Resilient Multi-Hazard Disaster Response – Volume V: Integration of Remote Sensing Imagery and VIEWS^{TM} Field Data for Post-Hurricane Charley Building Damage Assessment," by J.A. Womble, K. Mehta and B.J. Adams, 11/17/08 (PB2009-115532).

MCEER-08-0025 "Building Inventory Compilation for Disaster Management: Application of Remote Sensing and Statistical Modeling," by P. Sarabandi, A.S. Kiremidjian, R.T. Eguchi and B. J. Adams, 11/20/08 (PB2009-110484).

MCEER-08-0026 "New Experimental Capabilities and Loading Protocols for Seismic Qualification and Fragility Assessment of Nonstructural Systems," by R. Retamales, G. Mosqueda, A. Filiatrault and A. Reinhorn, 11/24/08 (PB2009-110485).

MCEER-08-0027 "Effects of Heating and Load History on the Behavior of Lead-Rubber Bearings," by I.V. Kalpakidis and M.C. Constantinou, 12/1/08 (PB2009-115533).

MCEER-08-0028 "Experimental and Analytical Investigation of Blast Performance of Seismically Resistant Bridge Piers," by S.Fujikura and M. Bruneau, 12/8/08 (PB2009-115534).

MCEER-08-0029 "Evolutionary Methodology for Aseismic Decision Support," by Y. Hu and G. Dargush, 12/15/08.

MCEER-08-0030 "Development of a Steel Plate Shear Wall Bridge Pier System Conceived from a Multi-Hazard Perspective," by D. Keller and M. Bruneau, 12/19/08 (PB2010-102696).

MCEER-09-0001 "Modal Analysis of Arbitrarily Damped Three-Dimensional Linear Structures Subjected to Seismic Excitations," by Y.L. Chu, J. Song and G.C. Lee, 1/31/09 (PB2010-100922).

MCEER-09-0002 "Air-Blast Effects on Structural Shapes," by G. Ballantyne, A.S. Whittaker, A.J. Aref and G.F. Dargush, 2/2/09 (PB2010-102697).

MCEER-09-0003 "Water Supply Performance During Earthquakes and Extreme Events," by A.L. Bonneau and T.D. O'Rourke, 2/16/09 (PB2010-100923).

MCEER-09-0004 "Generalized Linear (Mixed) Models of Post-Earthquake Ignitions," by R.A. Davidson, 7/20/09 (PB2010-102698).

MCEER-09-0005 "Seismic Testing of a Full-Scale Two-Story Light-Frame Wood Building: NEESWood Benchmark Test," by I.P. Christovasilis, A. Filiatrault and A. Wanitkorkul, 7/22/09 (PB2012-102401).

MCEER-09-0006 "IDARC2D Version 7.0: A Program for the Inelastic Damage Analysis of Structures," by A.M. Reinhorn, H. Roh, M. Sivaselvan, S.K. Kunnath, R.E. Valles, A. Madan, C. Li, R. Lobo and Y.J. Park, 7/28/09 (PB2010-103199).

MCEER-09-0007 "Enhancements to Hospital Resiliency: Improving Emergency Planning for and Response to Hurricanes," by D.B. Hess and L.A. Arendt, 7/30/09 (PB2010-100924).

MCEER-09-0008 "Assessment of Base-Isolated Nuclear Structures for Design and Beyond-Design Basis Earthquake Shaking," by Y.N. Huang, A.S. Whittaker, R.P. Kennedy and R.L. Mayes, 8/20/09 (PB2010-102699).

MCEER-09-0009 "Quantification of Disaster Resilience of Health Care Facilities," by G.P. Cimellaro, C. Fumo, A.M Reinhorn and M. Bruneau, 9/14/09 (PB2010-105384).

MCEER-09-0010 "Performance-Based Assessment and Design of Squat Reinforced Concrete Shear Walls," by C.K. Gulec and A.S. Whittaker, 9/15/09 (PB2010-102700).

MCEER-09-0011 "Proceedings of the Fourth US-Taiwan Bridge Engineering Workshop," edited by W.P. Yen, J.J. Shen, T.M. Lee and R.B. Zheng, 10/27/09 (PB2010-500009).

MCEER-09-0012 "Proceedings of the Special International Workshop on Seismic Connection Details for Segmental Bridge Construction," edited by W. Phillip Yen and George C. Lee, 12/21/09 (PB2012-102402).

MCEER-10-0001 "Direct Displacement Procedure for Performance-Based Seismic Design of Multistory Woodframe Structures," by W. Pang and D. Rosowsky, 4/26/10 (PB2012-102403).

MCEER-10-0002 "Simplified Direct Displacement Design of Six-Story NEESWood Capstone Building and Pre-Test Seismic Performance Assessment," by W. Pang, D. Rosowsky, J. van de Lindt and S. Pei, 5/28/10 (PB2012-102404).

MCEER-10-0003 "Integration of Seismic Protection Systems in Performance-Based Seismic Design of Woodframed Structures," by J.K. Shinde and M.D. Symans, 6/18/10 (PB2012-102405).

MCEER-10-0004 "Modeling and Seismic Evaluation of Nonstructural Components: Testing Frame for Experimental Evaluation of Suspended Ceiling Systems," by A.M. Reinhorn, K.P. Ryu and G. Maddaloni, 6/30/10 (PB2012-102406).

MCEER-10-0005 "Analytical Development and Experimental Validation of a Structural-Fuse Bridge Pier Concept," by S. El-Bahey and M. Bruneau, 10/1/10 (PB2012-102407).

MCEER-10-0006 "A Framework for Defining and Measuring Resilience at the Community Scale: The PEOPLES Resilience Framework," by C.S. Renschler, A.E. Frazier, L.A. Arendt, G.P. Cimellaro, A.M. Reinhorn and M. Bruneau, 10/8/10 (PB2012-102408).

MCEER-10-0007 "Impact of Horizontal Boundary Elements Design on Seismic Behavior of Steel Plate Shear Walls," by R. Purba and M. Bruneau, 11/14/10 (PB2012-102409).

MCEER-10-0008 "Seismic Testing of a Full-Scale Mid-Rise Building: The NEESWood Capstone Test," by S. Pei, J.W. van de Lindt, S.E. Pryor, H. Shimizu, H. Isoda and D.R. Rammer, 12/1/10 (PB2012-102410).

MCEER-10-0009 "Modeling the Effects of Detonations of High Explosives to Inform Blast-Resistant Design," by P. Sherkar, A.S. Whittaker and A.J. Aref, 12/1/10 (PB2012-102411).

MCEER-10-0010 "L'Aquila Earthquake of April 6, 2009 in Italy: Rebuilding a Resilient City to Withstand Multiple Hazards," by G.P. Cimellaro, I.P. Christovasilis, A.M. Reinhorn, A. De Stefano and T. Kirova, 12/29/10.

MCEER-11-0001 "Numerical and Experimental Investigation of the Seismic Response of Light-Frame Wood Structures," by I.P. Christovasilis and A. Filiatrault, 8/8/11 (PB2012-102412).

MCEER-11-0002 "Seismic Design and Analysis of a Precast Segmental Concrete Bridge Model," by M. Anagnostopoulou, A. Filiatrault and A. Aref, 9/15/11.

MCEER-11-0003 'Proceedings of the Workshop on Improving Earthquake Response of Substation Equipment," Edited by A.M. Reinhorn, 9/19/11 (PB2012-102413).

MCEER-11-0004 "LRFD-Based Analysis and Design Procedures for Bridge Bearings and Seismic Isolators," by M.C. Constantinou, I. Kalpakidis, A. Filiatrault and R.A. Ecker Lay, 9/26/11.

MCEER-11-0005 "Experimental Seismic Evaluation, Model Parameterization, and Effects of Cold-Formed Steel-Framed Gypsum Partition Walls on the Seismic Performance of an Essential Facility," by R. Davies, R. Retamales, G. Mosqueda and A. Filiatrault, 10/12/11.

MCEER-11-0006 "Modeling and Seismic Performance Evaluation of High Voltage Transformers and Bushings," by A.M. Reinhorn, K. Oikonomou, H. Roh, A. Schiff and L. Kempner, Jr., 10/3/11.

MCEER-11-0007 "Extreme Load Combinations: A Survey of State Bridge Engineers," by G.C. Lee, Z. Liang, J.J. Shen and J.S. O'Connor, 10/14/11.

MCEER-12-0001 "Simplified Analysis Procedures in Support of Performance Based Seismic Design," by Y.N. Huang and A.S. Whittaker.

MCEER-12-0002 "Seismic Protection of Electrical Transformer Bushing Systems by Stiffening Techniques," by M. Koliou, A. Filiatrault, A.M. Reinhorn and N. Oliveto, 6/1/12.

MCEER-12-0003 "Post-Earthquake Bridge Inspection Guidelines," by J.S. O'Connor and S. Alampalli, 6/8/12.

MCEER-12-0004 "Integrated Design Methodology for Isolated Floor Systems in Single-Degree-of-Freedom Structural Fuse Systems," by S. Cui, M. Bruneau and M.C. Constantinou, 6/13/12.

MCEER-12-0005 "Characterizing the Rotational Components of Earthquake Ground Motion," by D. Basu, A.S. Whittaker and M.C. Constantinou, 6/15/12.

MCEER-12-0006 "Bayesian Fragility for Nonstructural Systems," by C.H. Lee and M.D. Grigoriu, 9/12/12.

MCEER-12-0007 "A Numerical Model for Capturing the In-Plane Seismic Response of Interior Metal Stud Partition Walls," by R.L. Wood and T.C. Hutchinson, 9/12/12.

MCEER-12-0008 "Assessment of Floor Accelerations in Yielding Buildings," by J.D. Wieser, G. Pekcan, A.E. Zaghi, A.M. Itani and E. Maragakis, 10/5/12.

MCEER-13-0001 "Experimental Seismic Study of Pressurized Fire Sprinkler Piping Systems," by Y. Tian, A. Filiatrault and G. Mosqueda, 4/8/13.

MCEER-13-0002 "Enhancing Resource Coordination for Multi-Modal Evacuation Planning," by D.B. Hess, B.W. Conley and C.M. Farrell, 2/8/13.

MCEER-13-0003 "Seismic Response of Base Isolated Buildings Considering Pounding to Moat Walls," by A. Masroor and G. Mosqueda, 2/26/13.

MCEER-13-0004 "Seismic Response Control of Structures Using a Novel Adaptive Passive Negative Stiffness Device," by D.T.R. Pasala, A.A. Sarlis, S. Nagarajaiah, A.M. Reinhorn, M.C. Constantinou and D.P. Taylor, 6/10/13.

MCEER-13-0005 "Negative Stiffness Device for Seismic Protection of Structures," by A.A. Sarlis, D.T.R. Pasala, M.C. Constantinou, A.M. Reinhorn, S. Nagarajaiah and D.P. Taylor, 6/12/13.

MCEER-13-0006 "Emilia Earthquake of May 20, 2012 in Northern Italy: Rebuilding a Resilient Community to Withstand Multiple Hazards," by G.P. Cimellaro, M. Chiriatti, A.M. Reinhorn and L. Tirca, June 30, 2013.

MCEER-13-0007 "Precast Concrete Segmental Components and Systems for Accelerated Bridge Construction in Seismic Regions," by A.J. Aref, G.C. Lee, Y.C. Ou and P. Sideris, with contributions from K.C. Chang, S. Chen, A. Filiatrault and Y. Zhou, June 13, 2013.

MCEER-13-0008 "A Study of U.S. Bridge Failures (1980-2012)," by G.C. Lee, S.B. Mohan, C. Huang and B.N. Fard, June 15, 2013.

MCEER-13-0009 "Development of a Database Framework for Modeling Damaged Bridges," by G.C. Lee, J.C. Qi and C. Huang, June 16, 2013.

MCEER-13-0010 "Model of Triple Friction Pendulum Bearing for General Geometric and Frictional Parameters and for Uplift Conditions," by A.A. Sarlis and M.C. Constantinou, July 1, 2013.

MCEER-13-0011 "Shake Table Testing of Triple Friction Pendulum Isolators under Extreme Conditions," by A.A. Sarlis, M.C. Constantinou and A.M. Reinhorn, July 2, 2013.

MCEER-13-0012 "Theoretical Framework for the Development of MH-LRFD," by G.C. Lee (coordinating author), H.A Capers, Jr., C. Huang, J.M. Kulicki, Z. Liang, T. Murphy, J.J.D. Shen, M. Shinozuka and P.W.H. Yen, July 31, 2013.

MCEER-13-0013 "Seismic Protection of Highway Bridges with Negative Stiffness Devices," by N.K.A. Attary, M.D. Symans, S. Nagarajaiah, A.M. Reinhorn, M.C. Constantinou, A.A. Sarlis, D.T.R. Pasala, and D.P. Taylor, September 3, 2014.

MCEER-14-0001 "Simplified Seismic Collapse Capacity-Based Evaluation and Design of Frame Buildings with and without Supplemental Damping Systems," by M. Hamidia, A. Filiatrault, and A. Aref, May 19, 2014.

MCEER-14-0002 "Comprehensive Analytical Seismic Fragility of Fire Sprinkler Piping Systems," by Siavash Soroushian, Emmanuel "Manos" Maragakis, Arash E. Zaghi, Alicia Echevarria, Yuan Tian and Andre Filiatrault, August 26, 2014.

MCEER-14-0003 "Hybrid Simulation of the Seismic Response of a Steel Moment Frame Building Structure through Collapse," by M. Del Carpio Ramos, G. Mosqueda and D.G. Lignos, October 30, 2014.

MCEER-14-0004 "Blast and Seismic Resistant Concrete-Filled Double Skin Tubes and Modified Steel Jacketed Bridge Columns," by P.P. Fouche and M. Bruneau, June 30, 2015.

MCEER-14-0005 "Seismic Performance of Steel Plate Shear Walls Considering Various Design Approaches," by R. Purba and M. Bruneau, October 31, 2014.

MCEER-14-0006 "Air-Blast Effects on Civil Structures," by Jinwon Shin, Andrew S. Whittaker, Amjad J. Aref and David Cormie, October 30, 2014.

MCEER-14-0007 "Seismic Performance Evaluation of Precast Girders with Field-Cast Ultra High Performance Concrete (UHPC) Connections," by G.C. Lee, C. Huang, J. Song, and J. S. O'Connor, July 31, 2014.

MCEER-14-0008 "Post-Earthquake Fire Resistance of Ductile Concrete-Filled Double-Skin Tube Columns," by Reza Imani, Gilberto Mosqueda and Michel Bruneau, December 1, 2014.

MCEER-14-0009 "Cyclic Inelastic Behavior of Concrete Filled Sandwich Panel Walls Subjected to In-Plane Flexure," by Y. Alzeni and M. Bruneau, December 19, 2014.

MCEER-14-0010 "Analytical and Experimental Investigation of Self-Centering Steel Plate Shear Walls," by D.M. Dowden and M. Bruneau, December 19, 2014.

MCEER-15-0001 "Seismic Analysis of Multi-story Unreinforced Masonry Buildings with Flexible Diaphragms," by J. Aleman, G. Mosqueda and A.S. Whittaker, June 12, 2015.

MCEER-15-0002 "Site Response, Soil-Structure Interaction and Structure-Soil-Structure Interaction for Performance Assessment of Buildings and Nuclear Structures," by C. Bolisetti and A.S. Whittaker, June 15, 2015.

MCEER-15-0003 "Stress Wave Attenuation in Solids for Mitigating Impulsive Loadings," by R. Rafiee-Dehkharghani, A.J. Aref and G. Dargush, August 15, 2015.

MCEER-15-0004 "Computational, Analytical, and Experimental Modeling of Masonry Structures," by K.M. Dolatshahi and A.J. Aref, November 16, 2015.

MCEER-15-0005 "Property Modification Factors for Seismic Isolators: Design Guidance for Buildings," by W.J. McVitty and M.C. Constantinou, June 30, 2015.

MCEER-15-0006 "Seismic Isolation of Nuclear Power Plants using Sliding Bearings," by Manish Kumar, Andrew S. Whittaker and Michael C. Constantinou, December 27, 2015.

MCEER-15-0007 "Quintuple Friction Pendulum Isolator Behavior, Modeling and Validation," by Donghun Lee and Michael C. Constantinou, December 28, 2015.

MCEER-15-0008 "Seismic Isolation of Nuclear Power Plants using Elastomeric Bearings," by Manish Kumar, Andrew S. Whittaker and Michael C. Constantinou, December 29, 2015.

MCEER-16-0001 "Experimental, Numerical and Analytical Studies on the Seismic Response of Steel-Plate Concrete (SC) Composite Shear Walls," by Siamak Epackachi and Andrew S. Whittaker, June 15, 2016.

MCEER-16-0002 "Seismic Demand in Columns of Steel Frames," by Lisa Shrestha and Michel Bruneau, June 17, 2016.

MCEER-16-0003 "Development and Evaluation of Procedures for Analysis and Design of Buildings with Fluidic Self-Centering Systems" by Shoma Kitayama and Michael C. Constantinou, July 21, 2016.

MCEER-16-0004 "Real Time Control of Shake Tables for Nonlinear Hysteretic Systems," by Ki Pung Ryu and Andrei M. Reinhorn, October 22, 2016.

MCEER-16-0006 "Seismic Isolation of High Voltage Electrical Power Transformers," by Kostis Oikonomou, Michael C. Constantinou, Andrei M. Reinhorn and Leon Kemper, Jr., November 2, 2016.

MCEER-16-0007 "Open Space Damping System Theory and Experimental Validation," by Erkan Polat and Michael C. Constantinou, December 13, 2016.

MCEER-16-0008 "Seismic Response of Low Aspect Ratio Reinforced Concrete Walls for Buildings and Safety-Related Nuclear Applications," by Bismarck N. Luna and Andrew S. Whittaker.

MCEER-16-0009 "Buckling Restrained Braces Applications for Superstructure and Substructure Protection in Bridges," by Xiaone Wei and Michel Bruneau, December 28, 2016.

MCEER-16-0010 "Procedures and Results of Assessment of Seismic Performance of Seismically Isolated Electrical Transformers with Due Consideration for Vertical Isolation and Vertical Ground Motion Effects," by Shoma Kitayama, Michael C. Constantinou and Donghun Lee, December 31, 2016.

MCEER-17-0001 "Diagonal Tension Field Inclination Angle in Steel Plate Shear Walls," by Yushan Fu, Fangbo Wang and Michel Bruneau, February 10, 2017.

MCEER
EARTHQUAKE ENGINEERING TO EXTREME EVENTS
University at Buffalo, The State University of New York
133A Ketter Hall ▪ Buffalo, New York 14260-4300
Phone: (716) 645-3391 ▪ Fax: (716) 645-3399
Email: *mceer@buffalo.edu* ▪ Web: *http://mceer.buffalo.edu*
University at Buffalo *The State University of New York*

ISSN 1520-295X